Mechanisms of appendicular dermal bone loss and endochondral bone expansion during the fin-to-limb transition

Robert Lalonde

Thesis submitted to the University of Ottawa
in partial fulfillment of the requirements for the
Doctor of Philosophy in Biology

Department of Biology
Faculty of Science
University of Ottawa

Thèse soumise à l'Université d'Ottawa
envers la réalization partielle des éxigeances du
Doctorat en Philosophie en Biologie

Département de Biologie
Faculté des Sciences
Université d'Ottawa

ABSTRACT

The evolution of the tetrapod limb from paired fish fins involved drastic changes to the appendicular dermal and endochondral skeleton. Fish fin rays were lost, and the endochondral bone was modified and elaborated to form three distinct segments common to all tetrapod limbs: the stylopod, the zeugopod, and the autopod. Identifying the molecular mechanisms that contributed to these morphological changes presents a unique insight into our own evolutionary history. Chapter II of this thesis focuses on the *actinodin* gene family and how their disappearance from the tetrapod genome during the fin-to-limb transition may have contributed to the loss of dermal fin rays. The *actinodin* genes code for structural proteins in the actinotrichia, rigid fibers being the first exoskeletal elements formed during zebrafish fin development. We have identified tisse-specific c*is*-acting regulatory elements responsible for *actinodin1* activation in the fin fold ectoderm and mesenchyme. These elements are only partially functional in transgenic reporter mouse limbs. We therefore propose that changes to *actinodin* gene regulation contributed to the loss of the *actinodin* genes during limb evolution. The actinotrichia also serve as a scaffold for the migration of cells from the distal fin mesenchyme, which has been shown to differentiate into fin ray osteoblasts. In fact, both actinotrichia and distal fin mesenchyme migration defects have been proposed as events that may lead to the loss of dermal bone during the fin-to-limb transition. Chapter III of this thesis tests the effects of distal fin mesenchyme ablation on larval and adult zebrafish fin development. Following the chemo/genetic ablation of these cells, zebrafish display actinotrichia, fin fold, and fin ray defects supporting the hypothesis the defects in distal fin mesenchyme may have contributed to the loss of dermal fin rays during tetrapod evolution. Previous research has shown that changes in the regulation of the 5'*HoxA/D* genes may have had consequences for both *actinodin* regulation and the migration of distal fin fold mesenchyme.

Chapter IV of this thesis examines the contributions of *Hoxa11* regulatory changes to the evolution of the pentadactyl, or five-digit state, in tetrapods. Through a novel tetrapod-specific enhancer, *Hoxa11* is repressed from the presumptive limb autopod region in mice. In fish, *hoxa11b* is expressed distally and ectopic expression of *Hoxa11* in the distal limb bud produces mice with polydactyly (extra digits), an ancestral tetrapod character state.

In conclusion, we have provided evidence that actinotrichia defects (potentially though changes in *actinodin* regulation) and fin fold mesenchyme defects may have contributed to the loss of fin dermal bone during the fin-to-limb transition. Our data also shows these two events may have been linked as fin fold mesenchyme require actinotrichia to migrate correctly, while actinotrichia maintenance relies on Actinodin secretion from fin fold mesenchyme. Furthermore, we have also contributed to the growing body of evidence that proposes changes in *5'HoxA/D* regulation during the fin-to-limb transition underlie changes in appendicular dermal and endochondral bone. Therefore, it is possible that modifications in shared gene regulatory networks underlie both dermal and endochondral bone evolution during the fin-to-limb transition.

RÉSUMÉ

L'évolution des membres des tétrapodes à partir des nageoires des poissons a impliqué des changements drastiques du squelette appendiculaire dermique et endochondral. Les rayons des nageoires ont été perdus et les os endochondraux ont été modifiés puis sont devenus plus élaborés pour former trois segments osseux distincts communs aux membres de chaque espèce de tétrapode : le stylopode, le zeugopode et l'autopode. L'identification des mécanismes moléculaires qui ont contribué à ces changements morphologiques présente une unique perspective dans notre propre histoire évolutive. Le Chapitre II de cette thèse se concentre sur la famille de gènes *actinodine* et comment la disparition de cette famille du génome des tétrapodes au cours de la transition nageoire-à-membre a pu contribuer à la perte des rayons. Les gènes *actinodine* codent pour des protéines structurales des actinotriches, fibres rigides, qui constituent les premiers éléments de l'exosquelette à se former au cours du développement embryonnaire des nageoires du poisson zèbre. Nous avons identifié des éléments de régulation agissant en *cis* responsables pour l'activation de l'expression tissu-spécifique du gène *actinodine1* dans l'ectoderme et les cellules mésenchymateuses du repli distal de la nageoire. Ces éléments sont partiellement fonctionnels dans les membres de souris transgéniques.

Nous proposons que les changements de la régulation des gènes *actinodine* ont pu contribuer à la disparition de ces gènes au cours de l'évolution des membres. Les actinotriches servent aussi de guide pour la migration du mésenchyme distal des nageoires, qui va se différencier en ostéoblastes des rayons osseux. Par conséquent, l'ensemble des défauts des actinotriches et de la migration des cellules mésenchymateuses distales a été proposé comme ayant contribué à la perte des os dermiques durant la transition nageoire-à-membre. Dans le Chapitre III, j'ai testé l'effet de l'ablation des cellules mésenchymateuses distales sur le développement des nageoires du poisson zèbre au stade larvaire et adulte. Après l'ablation de ces cellules à l'aide d'une méthode

chimio/génétique, les poissons zèbres présentent des défauts au niveau des actinotriches, du repli de la nageoire et des rayons qui supportent l'hypothèse que des défauts dans les cellules mésenchymateuses distales ont peut-être contribué à la perte des rayons durant l'évolution des tétrapodes. Des études antérieures ont montré que des changements dans la régulation des gènes *5'HoxA/D* ont eu des conséquences sur la régulation des gènes *actinodin* et sur la migration des cellules mésenchymateuses distales. Dans le Chapitre IV, j'ai examiné les contributions des changements de la régulation du gène *Hoxa11* à l'évolution de l'état pentadactyl ou « cinq-doigts », observé dans les tétrapodes actuels. Un nouvel élément de régulation, unique aux tétrapodes, cause la répression de l'expression d'*Hoxa11* de la région distale de l'autopode présomptif chez l'embryon de souris. Chez les poissons, le gène *hoxa11b* est exprimé dans la région distale des nageoires et l'expression ectopique d'*Hoxa11* dans les régions distales des membres de souris cause la polydactylie (doigts supplémentaires), un caractère morphologique des tétrapodes ancestraux.

En conclusion, nous avons montré que les défauts au niveau des actinotriches (peut-être dûs à des changements de régulation des gènes d'*actinodine*) et des défauts au niveau des cellules mésenchymateuses distales de la nageoire ont pu contribuer à la perte des os dermiques de la nageoire durant la transition nageoire-à-membre. Nos résultats montrent que ces deux évènements sont peut-être liés car la migration des cellules mésenchymateuses distales requiert les actinotriches et, le maintien des actinotriches nécessite la sécrétion de l'Actinodine des cellules mésenchymateuses distales. Nos résultats contribuent aussi au nombre grandissant de données qui suggèrent que les changements de régulation des gènes *5'HoxA/D* ont conduit à des modifications des os appendiculaires de type dermique et endochondral durant la transition nageoire-au-membre. Donc, il est possible que des modifications dans les réseaux de régulation en commun a

conduit à l'évolution des os dermiques et endochondraux pendant la transition nageoire-à-membre.

ACKNOWLEDGMENTS

I would first like to thank my supervisor Dr. Marie-Andrée Akimenko for her immense support and encouragement over the past six years. She possesses a never ending pool of research ideas and objectives, and her innate nature to strive for high quality research is infectious. I would like to thank her for acknowledging and celebrating my scientific successes as well as providing stability and positivity during more challenging times.

I would also like to thank the members of my thesis advisory committee, Dr. Marc Ekker, Dr. Linda Bonen, and Dr. Iain McKinnel. Your support and critical feedback has been essential throughout this entire process. I am also extremely appreciative of the endless reference letters you have provided.

I would like to thank our lab technician extraordinaire Jing Zhang. She consistently provides unwavering emotional and technical support. She possesses seemingly limitless patience and a photographic memory. Her ability to recall the location of a midi prep or primer is second to none and she provides a much needed level of organization and peace to the lab.

I would like to thank Vishal Saxena, Bill Fletcher, Christine Archer and the entire ACVS team for providing excellent zebrafish care and overall maintenance of the entire aquatics facility. Without you, the fish room would surely descend into chaos and anarchy. I have personally witnessed drastic improvements to overall fish health and fish room organization in the past 5 years. We could not do our research without all the services you provide, keep up the great work!

I would also like to thank all of the Akimenko and Ekker lab members, past and present. In addition to providing me with endless opportunities to discuss results and troubleshoot, you guys and gals have provided emotional stability day in and day out. The lab is like a second home to all of us and you are like a second family. Never cease to support one another. Specifically, I would

like to thank all of the UROP, Honours, International and NSERC students would have contributed to the success of my various projects. In addition to contributing to research advancement, you have taught me the joys of being a supervisor. Success is ever more rewarding when it can be shared.

I would like to thank our collaborators at the IRCM in Montreal, namely Dr. Yacine Kherdjemil and Dr. Marie Kmita. It was an immense pleasure working with you both and I'd like to express my gratitude for having the confidence in me to contribute to such a significant and impactful research project.

Finally, I would not be where I am without my friends and family. I am fortunate to have been supported by four amazing parents, four sets of grandparents, step siblings, and many aunts, uncles and cousins. I am inspired daily by your shining examples of hard work, success, and overall character. I appreciate your consistent interest in my research despite the subject matter not being extremely familiar to you, and how you didn't frequently ask me when I would get an actual job. I believe staying in Ottawa for my Doctorate was one of the best decisions of my life because of how much time we have been able to spend together. For my friends, I cannot say enough about the importance of strong friendships throughout this process, you have all meant a great deal to me. I truly believe there needs to be a life outside of the lab, and you guys and gals have been with me through thick and thin. You have helped me to celebrate the victories, both big and small, and have always been there to help pull me back out of the depths of research despair. I am forever grateful.

Finally, funding for this research was provided by the Natural Science and Engineering Council

(NSERC) to Dr. Marie-Andrée Akimenko and the Ontario Government Scholarship (OGS) and permissions to include published manuscripts in this thesis was granted by Elsevier, Nature Publishing Group, and PLoS ONE.

TABLE OF CONTENTS

.

LIST OF FIGURES & TABLES

Chapter 1

Chapter 2

Chapter 4

Chapter 5

LIST OF ABBREVIATIONS

2P – 2kb *actinodin1* promoting region

AC – Actinotrichia

AER – Apical ectodermal ridge

Alx4 - Aristaless-like homeobox 4

And1-4 – Actinodin1-4

as - antisense

A-P – Anterior-Posterior

BMP – Bone morphogenetic protein

B.p. (bp) – Base pairs

CCAC – Canadian Council on Animal Care

cDNA – Complementary deoxyribonucleic acid

CDX-2 – Caudal type homeobox 2

ChIP – Chromatin immunoprecipitation

Cmlc2 – Cardiac myosin light-chain 2

CMV - Cytomegalovirus

CRE – *cis*-acting regulatory element

CRISPR – Clustered regularly interspaced palindromic repeats

Cryaa – Crystallin Alpha A

DAPI - 4′,6-diamidino-2-phenylindole

Dlx – Distal-less homeobox

DMSO – Dimethyl sulfoxide

DNA – Deoxyribonucleic acid

DSD – Developmental systems drift

DR – Distal radial

D-V – Dorsoventral

E9.5-E17 – Embryonic day 9.5 - 17

ED – Endochondral disc, Endoskeletal disc

eGFP – Enhancer green fluorescent protein

ELCR – Early limb control region

ES – Embryonic Stem

FF – Fin fold

FGF – Fibroblast growth factor

FW – Forward primer

FP – Floor plate

GCR – Global control region

GLI3A/R – Glioma-associated oncogene 3 activator/repressor

Grem – Gremlin 1

gRNA – Guide Ribonucleic Acid

Hand2 - Heart and neural crest derivatives expressed 2

HBB – Human beta-globin minimal promoter (β-globin)

Hh – Hedgehog

Hhip – Hedgehog interaction protein

Hox – Homeobox containing gene

Hpf – Hours post fertilization

IHC – Immunohistochemistry

INDEL – Insertion/deletion

ISH – *in situ* hybridization

Kr19 – KillerRed19

LP – Lepidotrichia

lncRNA – Long non-coding RNA

Mes - Mesenchyme

m-Inta11 – Mouse Intron Hoxa11

MMC – Migrating mesenchymal cell

MFF – Median fin fold

mm - millimetres

mRNA – Messenger Ribonucleic Acid

MTF-1 – Metal regulatory transcription factor 1

MTZ – Metronidazole

Ng - Nanograms

NHEJ – Non-homologous end joining

NTC - Notochord

NTR – Nitroreductase

Osr2 – Odd-skipped related 2

P-D – Proximal-Distal

PAM – Protospacer adjacent motif

Pax9 - Paired box gene 9

PCR – Polymerase chain reaction

PFA – Paraformaldehyde

PFF – Pectoral fin fold

PGK – Phosphoglycerate kinase

PR – Proximal radial

Prrx1 – Paired related homeobox 1

Ptch2 – Patched 2

PZ – Progress zone

Rev – Reverse primer

RT – Room temperature

SHH – Sonic Hedgehog

Smad3 – Mothers against decapentaplegic homolog 3

SNP – Single nucleotide polymorphisms

sub-TAD – sub-topological domain

TCF – T-cell factor

TF – Transcription factor

TUNEL – Terminal uDTP nick end labeling

UTR – Untranslated region

WGD – Whole genome duplication

WT – Wildtype

YFP – Yellow fluorescent protein

ZPA – Zone of polarizing activity

WORD ON NOMEMCLATURE

Zebrafish

Gene: *hoxa13a*
Protein: Hoxa13a

Mouse

Gene: *Hoxa13*
Protein HOXA13

Chicken/Human

Gene: *HOXA13*
Protein: HOXA13

CHAPTER 1

General Introduction

1.1. Fin-to-limb transition

Four-limbed animals, also known as tetrapods, evolved from lobe-finned fish (sarcopterygian) between 400 & 365 million years ago (Ahlberg et al. 2005; Clack 2007, 2009; Daeschler et al. 2006). This major evolutionary transition facilitated the terrestrialization of vertebrates leading to rapid rates of morphological diversification (Ruta et al. 2006). Fossils of extinct lobe-finned fish and transitional tetrapod species such as *eusthenopteron, panderichthys, tiktaalik, acanthostega,* and *ichthyostega* have provided us with amazing insight into some of the physical characterics likely shared in the common ancestors of all tetrapods during their evolution from fish (Boisvert et al. 2008; Clack 2009; Coates & Clack 1990; Coates & Clack 1991; Daeschler et al. 2006; Shubin et al. 2006; Vorobyeva et al. 1991) (Fig. 1.1). One crucial innovation during the transition onto land was the tetrapod limb, which evolved from paired fish fins (pectoral & pelvic), an event described as the fin-to-limb transition (Shubin et al. 2006). While the aquatic origins of tetrapods are still debated (marine or freshwater), it is generally agreed that limbs evolved while these animals were still fully aquatic to help navigate and survive in shallow underwater environments (Clack 2002; George & Blieck 2011; Romer 1958). Analysis of fin morphology in the closest living tetrapod relatives (lobe-finned fish) has provided limited information regarding this evolutionary event (Ahlberg 1992; Johanson et al. 2007; Jude et al. 2014; King et al. 2011; Nulens et al. 2010; Yano & Tamura 2012) (Fig. 1.1). Extant lobe-finned fish consist of two groups: lungfish and coelacanths; however lungfish possess a highly derived fin skeleton, and housing coelacanths is not possible as they live at great ocean depths (Ahlberg 1992; Johanson et al. 2007; Jude et al. 2014; King et al. 2011; Nulens et al. 2010; Yano & Tamura 20012). Instead we return to the fossil record where examination of extinct lobe-finned fish and transitional tetrapod fossils has provided clues to the major appendicular bone modifications

required in producing a limb, as well as other skeletal changes necessary for terrestrial life (reinforced pectoral and pelvic girdles, expanded rib cage, loss of neck bony elements, etc.) (Ahlberg et al. 2005; Clack 2009; Daeschler et al. 2006; Shubin et al. 2006 ; Standen et al. 2014). The evolution of the limb skeleton is characterized by a complete loss of fin exoskeletal elements, including dermal fin rays and actinotrichia fibrils, and an expansion/elaboration of limb endochondral bones to form three distinct segments: the stylopod, the zeugopod and the autopod (from proximal to distal) (Shubin et al. 2004; Shubin et al. 2006; Shubin et al. 2014) (Fig. 1.1). Shared traits in extinct transitional tetrapod species and extant tetrapods provide information on when these traits evolved and whether they existed in their last common ancestor (Fig. 1.1). A recognizable stylopod (single proximal bone of the limb) is proposed to have evolved prior to the split of extant lobe-finned fish and tetrapods, as both the coelacanth and lungfish possess this trait (Onimaru et al. 2015; Tanaka 2016). The evolution of digits and the loss of fin rays occurred prior to the split of acanthostega, and modern tetapods (Fig. 1.1) (Clack 2009), with "early tetrapods" displaying polydactyly. The evolution of the pentadactyl or five digit state evolved in the lineage leading to extant tetrapods (Clack 2009; Kherdjemil et al. 2016) (Fig. 1.1). Coupled with limb skeletal changes, were drastic changes to appendicular musculature, nervous and vasculature systems (Cole & Currie 2012; Diogo et al. 2011; Murakami & Tanaka 2011; Standen et al. 2014). Using genomic, molecular, and developmental data from a phylogenetically-broad range of fish species, in comparison with existing tetrapod models, researchers are now focused on identifying the molecular mechanisms that contributed to the evolution of limbs from fish fins (Fromental-Ramain et al. 1996; Nakamura et al. 2016; Scotti et al. 2015; Shubin et al. 1997; Standen et al. 2014; Tulenko et al. 2017; Zakany & Duboule 2007). Using zebrafish and mouse models, this thesis aims to explore some of the regulatory and morphological changes that contributed to fin

dermal bone loss and endochondral bone expansion during the fin-to-limb transition. Zebrafish are members of the teleost family of ray finned fish (actinopterygii) which split from lobe-finned fish around 450 million years ago (Braasch et al. 2016) (Fig. 1.1). Although more phylogenetically distant to tetrapods than basal ray-finned fish such as the *polypterus* or spotted gar, zebrafish remain a powerful fish model for fin-to-limb transition studies (Braasch et al. 2015) (Fig. 1.1). This thesis will also discuss some advantages and disadvantages of working with zebrafish, while highlighting how in certain cases limited conclusions can be drawn when working with such a phylogenetic distant fish species. The next two sections of this introduction will provide a morphological overview of zebrafish fin and tetrapod limb development to highlight early developmental similarities which give rise to drastically diverged adult fin and limb morphologies (Fig. 1.2.). The following sections will then provide an in depth description of the signalling pathways during early fin and limb development.

1.2. Fin Skeletal Morphology and Development

Embryonic and Early Larval Development

Zebrafish pectoral fin development begins with the formation of a bud at 28 hours post fertilization (hpf). The bud mesenchyme is derived from lateral plate mesoderm, and is covered by an ectodermal layer (Grandel & Schulte-Merker 1998) (Fig. 1.2A). Specifcally, lineage-tracing experiments have revealed lateral plate mesoderm adjacent to somites 1-4, but not somite 5, contribute to the pectoral fin bud (Wyngaarden et al. 2010). At the distal most region of the bud lies a thickening of ectoderm known as the apical ectodermal ridge (AER), which contributes to proximal-distal (P-D) development through interactions with the underlying mesenchyme. Morphologically similar to the tetrapod AER, functional homology was confirmed via expression analysis and amputation experiments (Heude et al. 2014; Mercader 2007; Yano et al. 2012) (Fig.

1.2A, D). At the posterior margin of the bud mesenchyme lies the zone of polarizing activity (ZPA), which contributes to anterior-posterior (A-P). An in-depth description of AER and ZPA activity, along with the contributions of 5'*hoxA/D* expression to the maintenance of these fin/limb signalling centres, will be provided in upcoming sections. Starting around 48-50hpf, the AER begins to extend and fold, transitioning into a structure known as the apical fin fold (Grandel & Schulte-Merker 1998) (Fig. 1.2A-B, 1.3A). The fin fold is supported by two rows of rigid fibrils known as actinotrichia, which are visible beginning at 50-52hpf (Géraudie et al. 1977, 1985; Zhang et al. 2010). Actinotrichia are considered the first exoskeletal elements formed during fin development and are composed of collagen and structural proteins called Actinodins (Duran et al. 2011; Zhang et al. 2010) (Fig. 1.3B). Interestingly, antibodies raised again dogfish ceratotrichia, a collagenous fin structure unique to cartilaginous fish, labels teleost actinotrichia highlighting similarities in composition (Duran et al. 2011; Santamaria et al. 1996). At 52hpf, distal fin fold mesenchyme will invade the fin fold, migrating distally using the existing actinotrichia as a scaffold (Wood & Thorogood 1984; Lalonde et al. 2016) (Fig. 1.3B). This process has been observed *in vivo* using time-lapse imaging in killifish, and reveals that as the mesenchymeal cells migrate, more cellular processes are formed and these processes become aligned with the actinotrichia (Wood & Thorogood 1984). At around 56hpf, the mesenchyme in the proximal region of the pectoral fin bud will condense and differentiate into chondrocytes, which will secrete cartilage matrix and form the endoskeletal disc (Fig. 1.2B, 1.4A) (Grandel & Schulte-Merker 1998). The disc then grows by cellular expansion along all three axes (Grandel & Schulte-Merker 1998). Embryonic and larval zebrafish also possess a median fin, a structure which extends from the 8th somite to the end of trunk. Initially visible at 18hpf, fin fold and actinotrichia formation,

followed by fin fold mesenchyme migration occurs in a manner similar to pectoral fin development (Abe et al. 2007; Kimmel et al. 1995).

Late larval development to Adulthood

At around standard length (defined as the measurement from tip of snout to the posterior end of the trunk) 7.5mm, the endoskeletal disc will separate into four distinct presumptive proximal radials, a process known as cartilaginous decomposition (Dewitt et al. 2011; Grandel & Schulte-Merker 1998) (Fig. 1.4B-C; 1.6D). This process is presumed to occur through chondrocyte dedifferentiation, as no evidence of cell death has been detected (Dewitt et al. 2011). Beginning at the anterior edge of the disc and then continuing posteriorly, *de novo* cartilaginous condensations within the distal rim mesenchyme will become the distal radial bones (Dewitt et al. 2011; Grandel & Schulte-Merker 1998) (Fig. 1.4B; 1.6D). Initially composed of cartilage, the proximal and distal radials will then undergo endochondral ossification to make up the proximal skeleton of the pectoral fin. Simultaneously, the pectoral fin fold mesenchyme begins to condense, forming the lepidotrichia adjacent to each presumptive distal radial bone (Fig. 1.4B-C). Lepidotrichia are the bones of the fish fin rays. The lepidotrichia, which consist of two concave symmetric hemirays underneath the epithelium, are then calcified through intramembranous ossification (Fig. 1.2C, 1.4C). Briefly, the displacement of the mesenchyme causes the epidermal basement membrane to bulge and form a semi-circular mold (one for each hemiray) for bony matrix deposition (Grandel & Schulte-Merker 1998; Mari-Beffa & Murciano 2010). Fin fold mesenchyme continues to reorganize and forms the connective tissue between the two hemirays. At this stage, actinotrichia fibrils are now completely absent from the proximal regions of the fin fold and are instead restricted distally to each lepidotrichia (Grandel & Schulte-Merker 1998; Zhang et al. 2010) (Fig. 1.4C). The caudal fin, derived from the embryonic median fin, forms

lepidotrichia in a similar manner, starting ventrally and progressing dorsally. The caudal fin rays are supported by hypural bones which are modified from the posterior-most vertebrae (Bird & Mabee 2003; Doosey & Domke 2014; Wiley et al. 2015).

1.3. Limb Skeletal Development and Morphology

Mouse forelimb development starts with the formation of a bud at embryonic day 9.5 (E9.5). The bud contains mesenchymal cells derived from the lateral plate mesoderm and is covered by the ectoderm (Fig. 1.2D, 1.5A). Mouse hindlimb development proceeds with a half day delay (E10). Very similar to the zebrafish pectoral fin, early limb development is governed by two signalling centres: the AER and the ZPA, which pattern the P-D and A-P axis, respectively (Duboule 1994; Tickle & Eichele 1994) (Fig. 1.2D). In contrast to fin development, however, where the AER transitions into the apical fin fold, the AER persists in the mouse forelimb until E14 ultimately regressing to form a layer of flattened cuboidal cells (Lu et al. 2008; Martin 1990; Wanek et al. 1989) (Fig. 1.5C). Limb bud outgrowth occurs through distal mesenchymal proliferation, which underlies the AER, in a region known as the progress zone (PZ) (Dealy et al. 1997; Martin 1998; Summerbell et al. 1973). By embryonic day 11.5 (E11.5) cartilage elements for the presumptive humerus bone (femur in hindlimb) are detected in the proximal core of the limb bud (Fig. 1.2D, 1.5B). Cartilage elements are formed when mesenchymal cells condense and differentiate into chondrocytes, cells that will secrete cartilage matrix (Kronenberg 2006). By E12.5 cartilage condensations are observed for the stylopod (humerus), zeugopod (ulna & radius), and proximal autopod (wrist & middle digits) (Martin 1990; Wanek et al. 1989). By E14.5 all elements in the mouse forelimb are detected by cartilage staining, including the distal most phalanges (Fig. 5D). Also around E14, separation of the digits occurs through interdigital mesenchymal cell death, and retraction of the interdigital epithelium (Martin 1990) (Fig. 1.2E).

The bones of the stylopod, zeugopod, and autopod are formed through endochondral ossification (Fig. 1.2E-F; 1.6A). In contrast to intramembranous ossification, endochondral bone begins with a cartilaginous template (extracellular cartilage matrix) secereted from chondrocytes. Following chondrocyte death, osteoclasts (bone-resorbing cells) and pre-osteoblasts (bone-forming cells) invade and regulate matrix removal and bone deposition (Kronenberg 2006; Mackie et al. 2008; Martin 1990; Ortega et al. 2004). Ossification begins around E15 in the stylopod, and zeugopod and E17 in the autopod and finishes 2 weeks postnatal (Patton & Kaufman 1995).

1.4. Actinotrichia and *actinodin* genes

One of the earliest morphological differences between fin and limb development is the transition of the AER into the apical fin fold in fish and the formation of actinotrichia supporting the fold (Fig 1.2A-B). This section will first describe the composition and function of these structures during fish fin development and regeneration. As these fibrils are crucial for proper fin development and are absent in tetrapods, it was proposed their disappearance may in fact have contributed to the fin-to-limb transition. This second part of this section will highlight the structural component of the actinotrichia, Actinodin proteins, and the potential contributions of both actinotrichia and Actinodin proteins to fin dermal bone loss during the fin-to-limb transition.

Actinotrichia formation during development and regeneration

Actinotrichia form as two arrays in the embryonic fin fold of fish (Bouvet 1974; Géraudie et al. 1977, 1985). Importantly, these fibrils do not form during tetrapod limb development (Martin 1990). Actinotrichia are composed of Collagen type I and II, and Actinodin, a structural protein that is secreted from both the fin fold ectoderm and fin fold mesenchyme (Duran et al. 2011; Zhang et al. 2010). Immunofluorescence of Collagen type I and II label the actinotrichia while *col1a1a* and *col2a1b* were both found to be expressed in actinotrichia forming cells (Duran

et al. 2011). During fin development, the actinotrichia support the fin fold and act as scaffold for the distal migration of mesenchyme (Géraudie et al. 1977, 1985; Wood & Thorogood 1984; Zhang et al. 2010). Morpholino-mediated knockdown of *col2a1b* resulted in collaspsed embryonic and larval fin folds, while *col1a1a* knockdown showed a mild reduction in fin fold size (Duran et al. 2011). Well formed actinotrichia are first visible in the pectoral fin around 50-52hpf, and the median fin at 36hpf and are adjacent to the fin fold ectoderm (Duran et al. 2011). This observation supports the hypothesis that actinotrichia have an ectodermal origin (Wood & Thorogood 1984). As the fin mesenchyme invades the fin fold, the actinotrichia continue to grow despite being physically separated from the ectoderm (Fig. 1.3). It is proposed the mesenchymal cells are now contributing to the elongation and thickness of the actinotrichia during fin fold extension (Duran et al. 2011). In adult zebrafish fins, the actinotrichia are restricted to the tip of each lepidotrichia, and their role in intact fins is not fully understood (Duran et al. 2011; König et al. 2017; Zhang et al. 2010). During zebrafish fin regeneration, actinotrichia assemble at the amputation plane prior to lepidotrichia regeneration suggesting they may help to organize tissues during blastema formation (Duran et al. 2011; König et al. 2017). The fibrils are distributed evenly in the newly formed tissue including the interray regions and may recapitulate processes that occur during larval fin development (König et al. 2017).

The *actinodin* gene family and the fin-to-limb transition

Along with collagen proteins, actinotrichia are also composed of actinodins. Antibodies raised against actinodins have been shown to label the actinotrichia during fin regeneration (Konig et al. 2017; Zhang et al. 2010). There are four actinodin-encoding genes in zebrafish *actinodin1-4 (and1-4*), two long paralogs and two short paralogs. During embryonic fin development, all four *actinodin* genes are expressed in the fin fold ectoderm and the distal fin mesenchyme; an

important exception being the distal most ectodermal cells of the pectoral fin, and the cleft cells of the median fin (Zhang et al. 2010). The expression of *actinodin* correlates with the formation of actinotrichia in both the median and pectoral fin. Chapter II of this thesis focuses on *actinodin1*, one of the long paralogs, which though sequence and syntenic analysis is more representative of the single ancestral long *actinodin* gene. At 36hpf *actinodin1* expression begins in the ectoderm that overlies the boundary between the proximal fin bud and the AER, where the future actinotrichia will form (Zhang et al. 2010). At 52hpf, *actinodin* expression starts in the distal mesenchyme that will migrate through the fin fold. *In situ* hybridization on pectoral fin cross sections reveals timing of tissue-specific *actinodin* expression during development (Zhang et al. 2010). It has been proposed that Actinodins are the structural component of the actinotrichia, serving as a crosslinking agent for the collagen fibres (Duran et al. 2011). The proteins encoded by the *actinodin* genes contain a signal peptide, and two potential convertase cleavage sites, providing evidence they are secreted and most likely processed. Additionally, the And1 and And2 proteins contain eight and ten repeats, respectively, of the nine-amino-acid motif C(N/D)PXXDPXC with And3 and And4 proteins predicted to encode fewer repeats. It is suggested that each repeat forms a loop and that the repeats stack to form an elongated domain (Zhang et al. 2010). Lobe-finned fish (sarcopterygian) have two *actinodin* genes, one long and one short paralog, and one incomplete *and*-like sequence has been identified in the chondricthyan elephant shark genome (Amemiya et al. 2013; Nikaido et al. 2013; Zhang et al. 2010) (Fig. 1.1). Actinotrichia are present in lobe-finned fish and their structure has been examined in lungfish and coelacanth revealing similarities with teleost actinotrichia (Géraudie & Meunier 1980; Géraudie & Meunier 1984; Géraudie 1984). Cartilagenous fish possess collagenous structures known as ceratotrichia which may be homologous to actinotrichia on the basis of composition and function

(Géraudie 1985). The *actinodin* gene family is absent from all tetrapod genomes, however syntenic analysis reveals surrounding gene organization is conserved (Moses unpublished). It is therefore proposed that this gene family was lost during the fin-to-limb transition. Chapter 3 of this thesis explores the hypothesis that changes in regulation of the *actinodin* genes contributed to their loss from the tetrapod genome. In fish, transient knockdown of both *and1/2* using morpholino oligonucleotides (MO) results in the absence of actinotrichia, fin fold collapse and disrupted migration of fin fold mesenchyme, suggesting these genes are crucial for embryonic fin development (Zhang et at. 2010). Knockdown of either *and1* or *and2* alone does not produce any phenotypic effects, suggesting redundancy between paralogs. Furthermore, these experiments reveal that functional short paralogs *and3* and *and4* are not sufficient to ensure proper actinotrichia formation (Zhang et al. 2010). Due to the transient nature of MOs and the lack of *and1/2* mutants, the effects of *and1/2* knockdown on adult fin development have not been observed. It is predicted that disrupted fin fold mesenchyme migration, resulting from actinotrichia defects, could lead to mispatterned fin rays, as it has been shown that fin fold mesenchyme contribute to fin ray fibroblasts and osteoblasts (Lee et al. 2013; Nakamura et al. 2016). In fact, it has been proposed that actinotrichia defects may have contributed to the loss of dermal bone during the fin-to-limb transition (Zhang et al. 2010).

1.5. Apical Ectodermal Ridge and FGF-signalling

As discussed in the morphological overview of fin and limb development (**Section 1.2 and 1.3**), the apical ectodermal ridge is conserved in early fin and limb development (Fig. 1.2A, D). This section will first provide a detailed description of the functions of this signalling centre, with an emphasis on limb development. The second part will then discuss the potential contributions of AER-FGF signalling to endochondral bone expansion during the fin-to-limb transition.

Contribution to appendicular development

The apical ectodermal ridge (AER) is a morphologically distinct thickening of ectoderm at the distal most tip of the fin and limb bud. This signalling centre contributes to bud outgrowth, proximal-distal patterning, and activation of the zone of polarizing activity. Manipulation experiments in the chick have shown that the removal of the AER halts limb outgrowth (Saunders 1948; Summerbell 1974). AER function is carried out by FGF signalling, which provides communication between the AER and the underlying mesenchyme, a region known as the progress zone. FGF10 is initially secreted by the lateral plate mesoderm, and induces the formation of the AER, which responds in turn by producing and secreting FGF8 (Heikinheimo et al. 1994; Ohuchi et al. 1997) (Fig. 1.6). A positive feedback loop between these two proteins maintains the AER, and the proliferative state in the progress zone, resulting in distal limb outgrowth (Martin 1998; Tickle & Eichele 1994) (Fig. 1.6). As limb development continues, cells in the more proximal regions of the limb will then leave the progress zone, leading to a halt in cell proliferation (Martin 1998; Tickle & Eichele 1994). The implantation of FGF beads at the distal limb bud in the chick can completely substitute for AER function and implantation along the flank in chick embryos can produce an extra limb (Cohn et al. 1995; Niswander et al. 1993; Tanaka et al. 1995). The AER expresses four other *Fgfs* (F*gf2, Fgf4, Fgf9, Fgf17*), known collectively as AER-FGFs; however each individual *Fgf* is not essential for normal limb development. Homozygous mutant mice for *Fgf2, Fgf9,* and *Fgf*17 produce normal limbs (Mariani et al. 2008; Martin 1998), providing the possibility of redundancy between the various FGF proteins. In the absence of both FGF4 and FGF activity in the mouse, limb developmental fails (Sun et al. 2002). Conditional AER-specific *Fgf8* knockout mice show mild limb skeletal abnormalities, however in combination, the loss of function of multiple *Fgf* genes leads to increasingly severe distal skeletal

truncation (Mariani et al. 2008; Sun et al. 2002). FGF4 signalling from the AER is also required for activation of the ZPA and the expression of *Shh,* forming another positive feedback loop that contributes to AER maintenance (Hirashima et al. 2008; Niswander 2002; Martin 1998; Zeller et al. 2009) (Fig. 1.6). Finally, FGF signalling has also been shown to be involved in early and late phase *5'HoxA/D* expression (Sheth et al. 2013). Early *HoxA/D* expression is involved in the maintenance of AER-FGF signalling, which then ensures the expression of FGF-dependent late phase *HoxA/D* expression (Sheth et al. 2013) (Fig. 1.6). The contributions of ZPA activity and *5'HoxA/D* expression to fin/limb development will be covered in the upcoming sections.

Contribution to the fin-to-limb transition

Based on the AER manipulation experiments performed in chicken embryos, there is evidence of a correlation between AER signalling and the proportion of limb bone that forms. If the AER is removed early in limb development, less bone will form compared to AER removal later in limb development (Saunders 1948; Summerbell 1974). The removal of the AER results in the disruption of FGF signalling to the mesenchyme in the progress zone, leading to a halt of proliferation (Martin 1998). Based on this observation, it has been proposed that the persistence of the AER during limb development may have been a contributor to increased endochondral bone elements during limb evolution, a hypothesis termed the 'Clock model' (Thorogood 1991; Yano & Tamura 2013). During zebrafish pectoral fin development, the AER transitions into the fin fold early and therefore results in reduced endochondral bone elements. Lobe-finned fish & extinct transitional tetrapod species are predicted to have/have had a delay in in the AER-fin fold transition, resulting in prolonged FGF signalling and an intermediated amount of endochondral bone. This model is supported by manipulation experiments in zebrafish that have shown the repeated removal of the fin fold leads to AER persistence and expanded endoskeletal disc

proportion (Yano et al. 2012). Contrastingly, recent developmental data from the paddlefish and catshark show conserved transcriptional activity between the fin fold and the AER in tetrapods, including FGF signalling (Tulenko et al. 2017). This suggests that during fin development "AER-signalling" is maintained despite the transition into the fin fold, and therefore the expansion of endochondral bone during limb evolution may not be linked to AER persistence in tetrapods (Tulenko et al. 2017).

1.6. Zone of Polarising Activity and SHH-signalling

As discussed in the morphological overview of fin and limb development (**Section 1.2 and 1.3**), the zone of polarizing activity and SHH-signalling is conserved in early fin and limb development. This section will first provide a detailed description of the functions of this signalling centre, with an emphasis on limb development. The second part will then discuss the potential contributions of ZPA-SHH signalling to the evolution of tetrapod stylopod during the fin-to-limb transition.

Contribution to appendicular development

The zone of polarising activity (ZPA) is a region of mesoderm located at the posterior edge of the early fin/limb bud (Tickle & Eichele 1994). The ZPA provides positional information required for anterior-posterior patterning, digit identity, and also contributions to the maintenance of the AER (Harfe et al. 2004; Harfe 2011; Suzuki 2013). Signalling from the ZPA is achieved through the morphogen SHH (Riddle et al. 1993; Tickle & Eichele 1994) (Fig. 1.6). Transplantation of an ectopic ZPA or a SHH bead to the anterior mesoderm of the chick limb bud results in a mirror-image duplication of the autopod, supporting the role of the ZPA in digit patterning (Anderson et al. 2012; Lopez-Martinez et al. 1995; MacCabe et al. 1973; Saunders 1972). A proposed model of digit identity states that digits 3, 4, and 5 are composed of *Shh*-

expressing cells, with digit 5 (posterior-most) receiving the highest exposure to SHH signalling. Digit 2 receives the lowest exposure to SHH signalling, and digit 1(anterior-most) is specified independently of SHH (Baduga et al. 2012; Harfe et al. 2004; Riddle et al. 1993; Suzuki 2013). Inhibition of SHH signalling in the chick using cyclopamine treatments results in anteriorization of digit identity (Scherz et al. 2007), and *Shh*-/- mice only form digit 1 in the hindlimb (Kraus et al. 2001). This initial contribution of SHH to digit identity is followed by a second phase of *Shh* function that is responsible for promoting digit growth (Suzuki 2013). The downstream effector proteins of SHH signalling are the transcriptional factors GLI1, 2, and 3, with GLI3 required for digit identity. When SHH is bound to its receptor PTCH1, GLI3 is maintained in its active form, GLI3A, and induces downstream target gene expression (Litingtung et al. 2002). When SHH is absent, GLI3 is converted to its repressor form GLI3R (Wang et al. 2000) (Fig. 1.6). Interestingly, neither *Shh* nor *Gli3* are required for digit formation, as *Shh*-/-, *Gli3* -/-double mutant mice show polydactylous limbs with no observable digit identity (Litingtung et al. 2002). Instead, it is proposed that the default state of the limb is to produce many digits, with *Shh* and *Gli3* regulating digit number and identity through the GLI3A:GLI3R ratio (Hill et al. 2009; Litingtung et al. 2002; Robert & Lallemand 2006). The ZPA and *Shh* are induced and maintained by FGF4 from the AER (Zeller et al. 2009) (Fig. 1.6). SHH signalling then in turn contributes to AER maintenance through a feedback loop involving Gremlin and BMP proteins, and to the maintenance of *5'HoxA/D* expression, through the action of the GLI3A transcriptional activator (Litingtung et al. 2002; Hirashima et al. 2008; Sheth et al. 2013) (Fig. 1.6).

Contribution to the fin-to-limb transition

Much of current research focuses on the distal expansion and elaboration of endoskeletal bone during limb evolution, however molecular and fossil data propose there was also a reduction

in endoskeletal bone in the proximal region of the limb along the anterior-posterior axis (Tanaka 2016). Several chondricthyan and basal actinopterygian species have at least three proximal bones at the base of their fins, named pro-, meso-, and metapterygium (from anterior to posterior (Coates 2003; Tanaka 2016) (Fig. 1.7A). Comparatively, the tetrapod stylopod consists of a single bone, thought to be derived from the ancestral metapterygium (Fig. 1.7B). It has been proposed that during the fin-to-limb transition, the pro- and mesopterygium were lost due to shifts in anterior-posterior polarity. Several anterior-posterior patterning genes in the SHH-GLI3 pathway were compared between catshark (chondricthyes) fins and mouse limbs: *Alx4*, and *Pax9*, which pattern anterior structures, and *Hand2*, which patterns posterior structures (Onimaru et al. 2015). Based on expression differences, it is proposed there was a major shift in positional identity in tetrapod limbs, becoming more "posteriorized", and this may have contributed to the loss of anterior structures (Onimaru et al. 2015; Tanaka 2016). During early limb development, HAND2 and GLI3 mutually repress one another, while HAND2 and SHH have a positive feedback loop, with HAND2 contributing to the initial activation of *Shh* (Fernandez-Teran et al. 2000; teWelscher et al. 2002) (Fig. 1.6). During basal fish fin development, *Gli3* is expressed in the entire anterior-posterior length of the fin. This is a marked difference compared to limb development, where *Gli3* is restricted anteriorly due to HAND2 activity. Therefore, it is suggested that the mutually antagonistic activity between GLI3 and HAND2 is weak or non-existent in basal fish (Tanaka 2016). There is also a delay in timing and a reduction in length of SHH activity during basal fish fin development (Sakamoto et al. 2009). As a reminder, SHH prevents the conversion of GLI3 to GLI3R and the ratio of GLI3R:GLI3A establishes anterior-posterior identity (Litingtung et al. 2002; Wang et al. 2000) (Fig. 1.6). It is proposed that lower levels of 5'*HoxD* transcripts, and decreased HAND2 contribute to differences in SHH activity in basal fish

(Fernandez-Teran et al. 2000; Sakamoto et al. 2009). In summary, *Gli3* expression in the entire anterior-posterior length of the fin, and the failure of SHH to prevent the conversion of GLI3 to GLI3R in the posterior half of the fin, would lead to an increased anterior identity in the fins of basal fish (Onimaru et al. 2015; Tanaka 2016).

1.7. 5'HoxA/D-signalling

This section will first summarize what is known about the regulation of *Hox* genes during fin and limb development, followed by a summary of the contributions of 5'HoxA/D signalling to fin and limb patterning including the activation and maintenance of the AER and ZPA. The second part of this section will discuss the potential contributions of 5'HoxA/D signalling to endochondral bone expansion and the evolution of the autopod during the fin-to-limb transition.

Contribution to appendicular development

Homeobox (*Hox*) genes code for transcription factors that contribute to axial patterning of many structures (Burke et al. 1995; Kessel and Gruss 1991; Krumlauf 1994). They are arranged sequentially forming clusters. Non-teleost vertebrates have four *Hox* clusters: *HoxA, HoxB, HoxC,* and *HoxD* and teleost fish have seven *Hox* clusters: *hoxAa, hoxAb, hoxBa, HoxBb, hoxCa, hoxCb,* and *hoxDa*, owing to a whole-genome duplication event that occurred, followed by a loss of the entire *hoxDb* cluster. The spatial and temporal expression of these genes correlates with their position on the chromosome, with those located at the telomeric (3') side being expressed earlier and more anteriorly/proximally than those at the centromeric (5') side of the cluster (Zakany et al. 2004; Zakany & Duboule 2007). Patterning identity is then governed by the specific set of *Hox* genes being expressed, termed the *Hox* code. Patterning of the fin and limb is regulated by the set of *Hox* genes located at the centromeric side of the *HoxA,* and *HoxD* clusters (*Hoxa9-13, Hoxd9-13*), termed 5'*HoxA/D* genes collectively (Ahn & Ho 2008; Freitas & Zhang 2007; Woltering et

al. 2014; Zakany et al. 2004). During fin and limb development 5'*HoxD* genes have two distinct waves, or phases, of expression that are controlled by regulatory landscapes on either side of the *Hox* clusters (Ahn & Ho 2008; Freitas & Zhang 2007; Woltering et al. 2014; Zakany et al. 2004). The first phase is controlled by enhancer elements located on the telomeric side of the cluster, known as the early limb control region (ELCR), and the second or "late" phase is regulated by enhancer elements on the centromeric side of the cluster, called the global control region (GCR) (Tarchini & Duboule 2006; Zakany et al. 2004). All *5'HoxA* limb enhancers are located on the telomeric side of the cluster interspersed between neighbouring genes (Berlivet et al. 2013; Gehrke et al. 2015). As with patterning of the entire larvae, each fin/limb segment along the proximal-distal axis is determined by a distinct *Hox* code (Zakany & Duboule 2007). The mutation of the *Hox13* genes (*Hoxd13, Hoxa13*) results in a loss of distal most fin/limb structures: fin rays in fish, and the autopod in mice (Fromental-Romain et al. 1996; Nakamura et al. 2016). Mice lacking *Hox11* genes form a severely truncated zeugopod and the removal of the entire *HoxA* and *HoxD* clusters halt limb growth mid-stylopod (Davis et al. 1995; Kmita et al. 2005). The 5'*HoxA/D* genes also contribute to the activation and maintenance of the ZPA and AER (Fig. 1.6). Ectopic expression of *Hoxd11-13* in the anterior portion of the limb bud activates *Shh* expression, while deletion of both *HoxA/D* clusters results in an absence of *Shh* expression in the normal posterior limb domain (Kmita et al. 2005; Zakany et al. 2004). First phase *5'HoxA/D* expression contributes to the activation and function of *Hand2*, which governs *Shh* activation in the ZPA (Galli et al. 2010; Xu & Wellik 2011) (Fig. 1.6). Second phase 5*'HoxA/D* expression then relies on SHH inhibiting the formation of GLI3R from GLI3 (Litingtung et al. 2002) (Fig. 1.6). AER function is also impaired in *HoxA/D* null mice, as *Fgf8* expression is disrupted (Sheth et al. 2013). It was found that first phase 5'*HoxA/D* expression is required for *Fgf8* activation in

the AER through their regulation of *Grem1* and *Fgf10* in the limb bud mesenchyme (Sheth et al. 2013) (Fig. 1.6). Finally, the anterior expansion of *Grem1* required for AER-FGF maintenance also depends upon *5'HoxA/D* genes, independent of their role in *Shh* activation (Sheth et al. 2013). The AER-FGFs then in turn contribute to the activation of late-phase *5'HoxA/D* expression (Niswander et al. 1994; Sheth et al. 2013) (Fig. 1.6).

Contribution to the fin-to-limb transition

Due to their contribution to ZPA and AER activation and maintenance and their role in proximal-distal appendicular patterning, the 5'*HoxA/D* genes have been a major focus for researchers hoping to elucidate some of the molecular mechanisms that contributed to the fin-to-limb transition (Shubin et al. 1997; Sordino et al. 1995; Yano & Tamura 2013). Specifically, it is proposed that changes in the regulation of these genes contributed to the evolution of the tetrapod autopod, and the loss of anterior proximal bones in basal fish. To identify enhancer elements responsible for the activation of the *5'HoxA/D* genes in mice and fish, the telomeric and centromeric regulatory landscapes have been probed using chromatin signature assays (ATAC-seq, H3K27ac, 4C etc.) and sequence conservation analysis (Amemiya et al. 2015; Berlivet et al. 2013; Gerhke et al. 2015; Gonzalez et al. 2007; Schneider et al. 2011; Sheth et al. 2016; Spitz et al. 2003). Putative enhancer elements are then tested for transcriptional activity by creating transgenic reporter animals (Amemiya et al. 2015; Berlivet et al. 2013; Gerhke et al. 2015; Gonzalez et al. 2007; Schneider et al. 2011; Sheth et al. 2016; Spitz et al. 2003). Transgenic swap experiments are performed to test differential enhancer activity between fish and mice and elucidate potential *5'HoxA/D* regulatory changes during the fin-to-limb transition (Gehrke & Shubin 2016; Gordon & Ruvinsky 2012). 5'*HoxA/D* regulatory conservation and

divergence and their implications for the fin-to-limb transition will be extensively covered in the discussion of this thesis.

An expansion or increase in *5'HoxA/D* transcripts has been linked with several aspects of limb evolution, including the evolution of the autopod, and the reduction of anterior proximal fin bones. During the early stages of limb development, first phase *5'HoxA/D* expression promotes SHH signalling, through the activation of *Hand2* (Onimaru et al. 2015; Tanaka 2016).During limb evolution, increased *Hand2* and *Shh* activity through changes in regulation of early phase *5'HoxA/D* genes, would lead to anterior-restricted *Gli3* expression, and the inhibition of GLI3R formation in the posterior limb field. This is predicted to have led to an increased posterior positional identity in the fin, and a loss of anterior proximal fin structures (pro- and mesopterygium) (Onimaru et al. 2015; Tanaka 2016). During later stages of limb development, a feedback loop is established directly between *Shh* and late phase*5'HoxA/D*. It has been shown that *Shh* activation occurs through the binding of HOXD proteins in a dose-dependent manner (Capellini et al. 2006; Sagai et al. 2005). Prolonged activation of *Shh* and late phase 5'*HoxA/D* genes is predicted to have contributed to anterior-posterior positional identity during autopod evolution (Tanaka 2016; Sheth et al. 2012; Sheth et al. 2013).

Autopod evolution has also been linked to a change in regulation of *Hoxa11* during the fin-to-limb transition (Metscher et al. 2005; Sordino & Duboule 1996; Tanaka 2016; Woltering et al. 2014; Yano & Tamura 2013). During mouse limb development, *Hoxa11* is restricted proximally in the limb bud following the activation of *Hoxa13*. The *Hoxa11* locus is known to interact with distal limb enhancers, and *Hoxa10* is expressed distally (Woltering et al. 2014). *Hoxa13/Hoxd13* null mutant mice show a distal extension of *Hoxa11* to the autopod region and in fish species, *hoxa11* (*hoxa11b* in zebrafish) and *hoxa13* (*hoxa13a* & *hoxa13b* in zebrafish) have largely

overlapping domains of expression in the distal fin regions (Ahn & Ho 2008; Metscher et al. 2005; Sheth et al. 2014). This suggests that changes in regulation of *Hoxa11*, with potential contributions from Hoxa13 and Hoxd13, may have contributed to autopod evolution during the fin-to-limb transition. Additionally, antisense long non-coding RNAs (lncRNAs) have been identified at the *Hoxa11* locus, that display complementary expression with *Hoxa11* in the limb bud and overlapping expression with *Hoxa13* in the autopod (Hsieh-Li et al. 1995). The contributions of these lncRNAs should also be investigated to determine if they contribute to changes in regulation of *Hoxa11* in tetrapods. Chapter 5 of this thesis discusses the mechanisms of *Hoxa11* distal repression in tetrapod limbs and the implications for limb development and evolution.

Finally, modulation of 5'*HoxA/D* expression has been linked to endochondral bone expansion through a shift in distal mesenchymal cell fate during the fin-to-limb transition (Ahn & Ho 2008; Nakamura et al. 2016; Paço & Freitas 2017). During zebrafish fin development, late phase *hoxa13*-expressing distal fin mesenchyme contributes to dermal fin rays (Nakamura et al. 2016). In mice, *Hoxa13*-expressing cells contribute to the endochondral bone of the autopod, suggesting a shift in distal mesenchymal cell fate from dermal to endochondral bone progenitors (Scotti et al. 2015). Furthermore, *hox13* (*hoxa13a, hoxa13b, hoxd13a*) null zebrafish mutants show an absence of dermal fin rays, while also displaying an expansion of endochondral bone elements (Nakamura et al. 2016). It is proposed that in the absence of 5'*HoxA/D* expression, distal fin mesenchyme fails to migrate through the fin fold and remains proximally restricted in the fin bud (Nakamura et al. 2016). This would lead to simultaneous restriction in the distal fin dermal skeleton, and an expansion of proximal endochondral bone. More evidence is required to confirm a link between 5'*HoxA/D* regulatory changes and defects to fin mesenchyme migration.

Furthermore, the consequences of fin mesenchyme migration defects on dermal fin ray development need to be determined. Chapter 4 of this thesis explores the consequences of fin mesenchyme defects on fin fold, actinotrichia, and fin ray formation.

1.8. Zebrafish as a model for fin-to-limb transition studies

For this thesis we have used the zebrafish as our experimental fish model to explore the molecular and morphological changes during the fin-to-limb transition. This section will summarize the well known advantages of this model as well as apparent morphological and genomic shortcomings of this derived teleost fish.

Advantages

The zebrafish is a frequently used model organism for developmental, molecular and cell biology (among others) (Nüsslein-Volhard and Dahm, 2002). It is estimated that over 3250 institutes throughout 100 countries utilize this freshwater teleost species for research purposes (Lidster et al. 2017). As fish paired fins are homologous to tetrapod limbs, zebrafish are also being used to investigate the molecular mechanisms that contributed to the evolution of limbs from fins. The use of zebrafish for fin-limb evolution studies offers the same research advantages as many other fields of biology. In terms of physiology, zebrafish are small, easy to maintain, develop rapidly, and have transparent embryos. Like other fish, zebrafish use external fertilization and can produce upwards of 300 embryos per breeding, facilitating the observation of early developmental stages. In terms of genomics, the zebrafish genome has been fully sequenced and shares a large number of orthologous genes with other terrestrial vertebrate genomes (Howe et al. 2013). The zebrafish genome is easily amenable to genetic manipulation, with the generation of transgenic and mutant animals being one of the greatest assets of zebrafish research.

Transgenic zebrafish are produced by microinjection of a plasmid containing a transgene of interest into 1-cell stage zebrafish embryos. Transgene integration efficiency has been greatly improved with the development of the *Tol2* system (Kawakami 2007). *Tol2* is an autonomous transposable element originally identified in the Medaka (Kawakami 2007). Briefly, Tol2 arms (150-200bp) flank the transgene in the plasmid, which is then coinjected with the transposase mRNA from the original *Tol2* gene. The transposase catalyzes the transposition of the transgene into the genome using a "cut & paste" method. Multiple single copy insertions are observed, which is beneficial to avoid transgene silencing (Kawakami 2007). Tandem insertions have been reported to result in *in vivo* silencing, resulting in an absence of transgene expression (Kawakmi 2007). Some negative aspects of this system include so-called positioronal effects, where the transgene may have impacts on surrounding genes or vice-versa resulting in variable transgene expression between animals or disruption of endogenous gene function (Roberts et al. 2014). Other methods are being developed in order to maintain consistency of transgene integration sites between animals, including the PhiC-31-based integration system (Roberts et al. 2014). The practical applications of transgenic zebrafish are virtually limitless. Research groups are using transgenic zebrafish for gain- and loss-of-function studies, cell-lineage tracing & cell ablation experiments, regulatory element identification & analysis, and finally, fluorescent animals are also simply used to highlight and study specific developmental processes (Kawakami 2007; Lin 2000; Mathias et al. 2014; Mosimann et al. 2011). The development of transgenic reporter lines to identify and study regulatory elements and transgenic lines for cell ablation purposes are relevant to this thesis.

The discovery of the CRISPR/cas9 system for genome manipulation has greatly facilitated the generation of mutant zebrafish lines (Doudna & Charpentier 2014; Gaj et al. 2013; Hwang et

al. 2013; Li et al. 2016). Originally from bacteria, CRISPR sequences are used to protect host bacteria against the invasion of viral DNA. Is system has since been coopted for genome modification purposes (Rath et al. 2015; Sontheimer Barrangou 2015). This system can be used to produce single nucleotide polymorphisms (SNPs), insertion/deletions (INDELs), large scale deletions, or to introduce specific sequences, at any given locus of choice (Li et al. 2016; Sander & Juong 2014). The most frequent application of this technique is gain- and loss-of-function studies. The CRISPR/cas9 system involves two components: the synthetic guideRNA (gRNA) and the cas9 endonuclease. The gRNA is designed from your locus of interest, and directs the cas9 endonuclease to your target sequence, which is then cleaved. The target sequence must be followed by a protospacer adjacent motif (PAM), typically a 5'–NGG–3', or cas9 will not bind to or cleave the DNA (Doudna & Charpentier 2014; Gaj et al. 2013; Hwang et al. 2013; Li et al. 2016. CRISPR/cas9 zebrafish mutants are produced by microinjecting guideRNA(s) (specific to a locus of interest) and cas9 mRNA/protein together into 1-cell stage embryos. The gRNA/cas9 complex will produce double stranded DNA breaks at your locus of interest, which are then repaired by means of non-homologous end joining (NHEJ) (Li et al. 2016; Sander & Juong 2014). NHEJ is an imperfect system for DNA repair and can produce SNPs as well as relatively small INDELs which may result in frameshift errors and premature stops in protein translation. Coinjection of multiple gRNAs simultaneously can produce large scale deletions between target sites, and specific sequences can be inserted by providing template DNA in the form of plasmid or single stranded DNA (Albadri et al. 2017; Xiao & Zhang 2016). For insertions, homology arms are required on the template DNA which triggers homology-directed repair instead of NHEJ following double stranded DNA breaks by the Cas9 protein (Albadri et al. 2017; Li et al. 2016).

With regards to this thesis, the generation of CRISPR/cas9 mutants for multiple projects is considered ongoing work and is addressed in the discussion section.

Disadvantages

Despite all the tools that make zebrafish a fantastic model organism, the highly derived fin morphology and the duplicated genome are traits that make zebrafish less desirable for studying the evolutionary transition from fins to limbs. To gain a better understanding of appendicular endochondral bone expansion and elaboration during limb evolution, researchers must first be preview to the ancestral state of the fin endochondral bone. Furthermore, investigating the molecular mechanisms that are representative of ancestral fish fin development would help dissect tetrapod-specific changes that contributed to the fin-to-limb transition. The fin of chondrichthyan species (catshark), basal and derived actinopterygian species (paddlefish and zebrafish), and tetrapod limbs have been compared to known transitional fossil samples (Fig. 1.7) (Coates 2003; Davis 2013; Mabee & Noordsy 2004; Tanaka 2016). The comparison reveals a truncation in the proximal endochondral bones along the anterior-posterior axis, and an expansion and elaboration of the distal most bones (Shubin et al. 2004; Shubin et al. 2006; Shubin et al. 2014; Tanaka 2016). The loss of anterior segments pro- and mesopterygium during limb evolution has previously been discussed in this introduction (Fig. 1.7A-C) (Onimaru et al. 2015; Tanaka 2016). The presence of the pro- and mesopterygium in the paddlefish fin suggests they were lost uniquely in the sarcopterygian lineage (Fig. 1.7C) (Tanaka 2016). The zebrafish fin endochondral bone consists of four proximal radials and 10-12 distal radials, having lost the posterior-most proximal bone, the metapterygium, which is still retained in the paddlefish fin (Fig. 1.7B-C) (Coates 1994; Coates & Cohn 1998; Grandel & Schulte-Merker 1998). Taken together, it presents a step-wise truncation in fin endochondral bone from the catshark to the zebrafish, revealing a highly derived fin structure

that seems to lack any homologous element to that of the tetrapod stylopod (Fig. 1.7B-D). Instead, basal actinopterygian species like the paddlefish may represent a more accurate representation of the ancestral fish fin state prior to the fin-to-limb transition (Fig. 1.7C). Indeed, the paddlefish fin endochondral bone appears to be an attractive intermediate between the catshark fin, and the tetrapod limb (Fig. 1.7A-C). Thus, investigating the molecular mechanisms that contribute to zebrafish fin development may not be an accurate baseline to highlight differences with tetrapod limb development. Researchers have now expanded their analyses to include a phylogenetically broad range of fish species (including the catshark and paddlefish) to attain a more complete picture of the molecular mechanisms that contributed to fin development in ancestral fish species (Onimaru et al. 2015; Tanaka 2016; Tulenko et al. 2016; Tulenko et al. 2017).

Many researchers are focused on identifying the molecular mechanisms that contributed to the fin-to-limb transition. Simplified, this can consist of first identifying genes important for fin and limb development, determining if orthologs of these genes exist between fish and tetrapods, and then testing for any relevant divergence in gene functionality. This can be somewhat difficult when considering the phylogenetic gap between telelosts (which include zebrafish) and tetrapods. To make matters worse, the teleost genome has undergone three whole genome duplication events (WGD), two common to all vertebrates and one unique to teleosts (Dehal & Boore 2005; Howe et al. 2013; Taylor et al. 2003). It is well known that ohnologs/paralogs experience high sequence and functional divergence following gene duplication events (Brookfield 2003; De smet et al. 2017; Warren et al. 2014). Paralogs are the descendent genes following a gene duplication event, whereas ohnologs are the descendent genes specifically from a whole genome duplication event (Singh et al. 2015). Finally, it has been determined that teleosts uniquely have rapid rates of sequence evolution (Amemiya et al. 2013; Venkatesh et al. 2014). In summary, ortholog

identification is not always possible between zebrafish and tetrapods, and it can be extremely challenging to discern if regulatory or coding sequence divergence contributed to relevant functional differences during the fin-to-limb transition or are simply derived teleost-specific modifications. To that end, the genomes of the spotted gar and the coelacanth have been sequenced, two fish who share a more recent common ancestor with tetrapods than the zebrafish. The spotted gar is a ray-finned fish whose lineage split prior to teleost evolution, and whose genome remains in an unduplicated state, and the coelacanth is deep sea dwelling lobe-finned fish whose form has remained virtually unchanged in 360 million years (Amemiya et al. 2013; Braasch et al. 2016). Comparing the genomes of these fish to the tetrapod genome can provide, with more certainty, that instances of tetrapod-specific gene loss/sequence divergence and of differential gene regulation may have had functional relevance during the fin-to-limb transition. Unfortunately neither of these fish are practical for laboratory use, and the molecular tools are not yet available to produce transgenic or mutant animals. Therefore, zebrafish are still the gold standard fish for performing gene and regulatory element functional assays to test predictions from spotted gar and coelacanth genomic analysis (Amemiya et al. 2013; Braasch et al. 2016; Gehrke et al. 2015).

1.9. Transgenic swap experiments

While the comparison of fish and tetrapod genomes has revealed a promising list of candidate genes that have been lost during the fin-to-limb transition, it is predicted in many instances that regulatory evolution is a major contributor to morphological changes during limb evolution (Amemiya et al. 2013; Prud'Homme et al. 2007; Zhang et al. 2010). In fact, it is also predicted that regulatory evolution can lead to gene loss (Lalonde et al. 2016). Gene regulation relies on two main components: the transcription factor (TF) (*trans* regulation) and the TF-binding

domain (*cis* regulation), with both elements being susceptible to evolution (Gordon & Ruvinsky 2012; Wittkopp et al. 2004). Epigenetics and chromatin accessibility can also influence the binding of transcription factors to regulatory elements (Li et al. 2011). A common way of testing enhancer functionality is to place the *cis*-acting regulatory element(s) (CRE) upstream of a minimal promoter and a reporter gene (eGFP, mCherry, LacZ etc.) and then creating a transgenic reporter animal. The organism that provides the enhancer element is considered the donor, and the organism where the enhancer element is being tested is considered the host (Gehrke & Shubin 2017; Gordon & Ruvinsky 2012). To uncover events of regulatory evolution researchers use transgenic swap experiments, where the donor and host organisms do not match. To uncover instances of regulatory evolution during the fin-to-limb transition fish (donor) enhancer elements are tested in mice (host), and vice-versa. A summary of these experiments is provided in the discussion of this thesis. When a CRE is tested in its native *trans* environment (host and donor match), the interpretation of enhancer functionality is straightforward, however when the host and donor organisms do not match there can be limitations to the interpretation of the results (Gehrke & Shubin 2017; Gordon & Ruvinsky 2012). A frequent problem is that donor CRE functionality is unknown in its native *trans* environment due to limitations of the organism (ie. the molecular tools are not available to create transgenic animals). In this case, negative results when the CRE is tested in a non-native *trans* environment do not yield any conclusions (Gehrke & Shubin 2017; Gordon & Ruvinsky 2012). To partially circumvent this problem, CREs can be tested in a closely related host model organism (ie. testing spotted gar enhancers in zebrafish) prior to being tested in a phylogenetically distant host organism (ie. testing spotted gar enhancers in mice) (Amemiya et al. 2013; Braasch et al. 2016; Gehrke et al. 2015; Gehrke & Shubin 2017; Gordon & Ruvinsky 2012). Another limitation to transgenic swap experiments is that donor CRE may fail to elicit

expression in host organisms for reasons independent of events of regulatory evolution. In a process known as developmental systems drift (DSD), both the donor and the host organisms can experience evolution in *cis* and *trans* that results in an inability of the host's *trans* system to decode the donor *cis* sequence. It is predicted that the bigger the phylogenetic gap between host and donor species, the higher the potential for DSD (Gehrke & Shubin 2017; Gordon & Ruvinsky 2012; True and Haag 2001) (Fig. 1.1). For example, it has been shown that zebrafish CREs (donor) are not always functional in mice (host), however orthologous spotted gar CREs (donor) are functional (Gehrke et al. 2015). In this case the phylogenetic gap between the spotted gar and the mouse is smaller than that between the zebrafish and the mouse. As previously discussed, teleosts have experienced rapid sequence divergence and have undergone an additional genome duplication event, and thus the zebrafish (donor) likely experienced instances of CRE evolution which render it no longer recognisable by the *trans* system in the mouse (host) (Braasch et al. 2016; Gehrke et al. 2015; Gehrke & Shubin 2017).

1.10. Nitroreductase/Metronidazole cell ablation system

This section describes in detail the system that was utilized for zebrafish fin fold mesenchyme ablation in Chapter IV. Cell ablation is a common *in vivo* strategy in development biology to identify cell lineage relationships, study cellular function, and observe regenerative processes (Grégoire & Kmita 2004). The nitroreductase (NTR)/metronidazole (MTZ) system is an inducible method that allows for spatial and temporal control of cell ablation (Clark et al. 1997; Curado et al. 2007). To ensure cell specificity, the gene encoding the *E. coli* NTR can be expressed in a tissue-specific manner using *cis*-acting regulatory elements. In the presence of the NTR enzyme, the prodrug MTZ is converted into a cytotoxic DNA cross-linking agent that results in cell ablation by apoptosis (Curado et al. 2007; Lalonde & Akimenko 2018; Mathias et al. 2014)

(Fig. 1.8). This system yields no bystander effect as only cells expressing the NTR-encoding gene will be ablated, leaving neighbouring cells unharmed. For zebrafish use, the MTZ can be readily dissolved in the embryo media or adult system water (with 1% DMSO) (Curado et al. 2007; Mathias et al. 2014), allowing for precise temporal control. To facilitate NTR visualization in transgenic zebrafish, the NTR-encoding gene can be coupled with a fluorescent reporter gene. Following MTZ exposure, the loss of fluorescence is good evidence the ablation system is functional, however cell death should be confirmed via cell death assays (Lalonde & Akimenko 2018). One major negative aspect to this system is the inherent toxicity of the MTZ prodrug at high concentrations or with long exposure times (Mathias et al. 2014). There is no standard MTZ treatment as distinct cell types require varying exposure concentrations and lengths. Personalized treatment protocols should be established after consulting published literature (Mathias et al. 2014). In order to ensure observed defects are in fact due to cell ablation, and not inherent MTZ toxicity or development defects within the transgenic line, treatments should be conducted in parallel with controls. There are two suggested (required) controls: NTR-transgenic fish exposed to DMSO only (vehicle for MTZ), and WT fish exposed to equal concentrations of MTZ. Both controls should yield similar or identical results, confirming any effect in the experimental group is due to cell ablation. Finally, to minimize the effects of MTZ toxicity, a triple mutant variant of the NTR enzyme has been developed specifically for zebrafish use that yields higher ablation efficiency at lower MTZ exposure concentrations and lengths (Mathias et al. 2014). This NTR variant was used for the ablation studies described in chapter IV.

1.11. General Objectives

Our goal was to investigate and elucidate some of the molecular and morphological changes that may have contributed to appendicular dermal and endochondral bone changes during

the fin-to-limb transition. In chapter II, we explored the mechanisms of *actinodin* regulatory evolution. The *actinodin* gene family is absent from all tetrapod genomes, suggesting it was lost during limb evolution. We predict changes in regulation of the *actinodin* genes likely contributed to their loss; therefore, we set out to identify and characterize the *cis*-acting regulatory elements of *actinodin1* in zebrafish. To test for changes in regulation during tetrapod evolution, we then observed the functionality of the *actinodin1* zebrafish regulatory elements in mice. We predict changes in the regulation of *actinodin1* would have had consequences on actinotrichia formation and distal fin mesenchyme migration.

Both actinotrichia and distal fin mesenchyme defects have been proposed as events that may have led to the loss of fin dermal bone during limb evolution. In chapter III, we used the NTR/MTZ system to ablate the distal fin mesenchyme during early and late larval zebrafish development. Our goal was to directly test the effects of distal fin mesenchyme defects on fin development. We were specifically interested in elucidating the role of these cells in fin fold, actinotrichia, and fin ray formation.

Changes in regulation of *5'HoxA/D* genes have also been consistently linked to morphological changes during the fin-to-limb transition. We have highlighted how they may in fact have had consequences for *actinodin* regulatory evolution, while others have suggested their contributions to changes in the capacity of distal fin mesenchyme to migrate correctly. Chapter IV explores how changes in regulation of *Hoxa11* in tetrapods may have contributed to autopod evolution, particularly digit number. We sought to identiy a novel tetrapod-specific regulatory element in mice that contributes to the distal repression of *Hoxa11* during limb development. Using zebrafish, we then wished to confirm such regulatory element does not exist in bony fish.

1.12. Figures

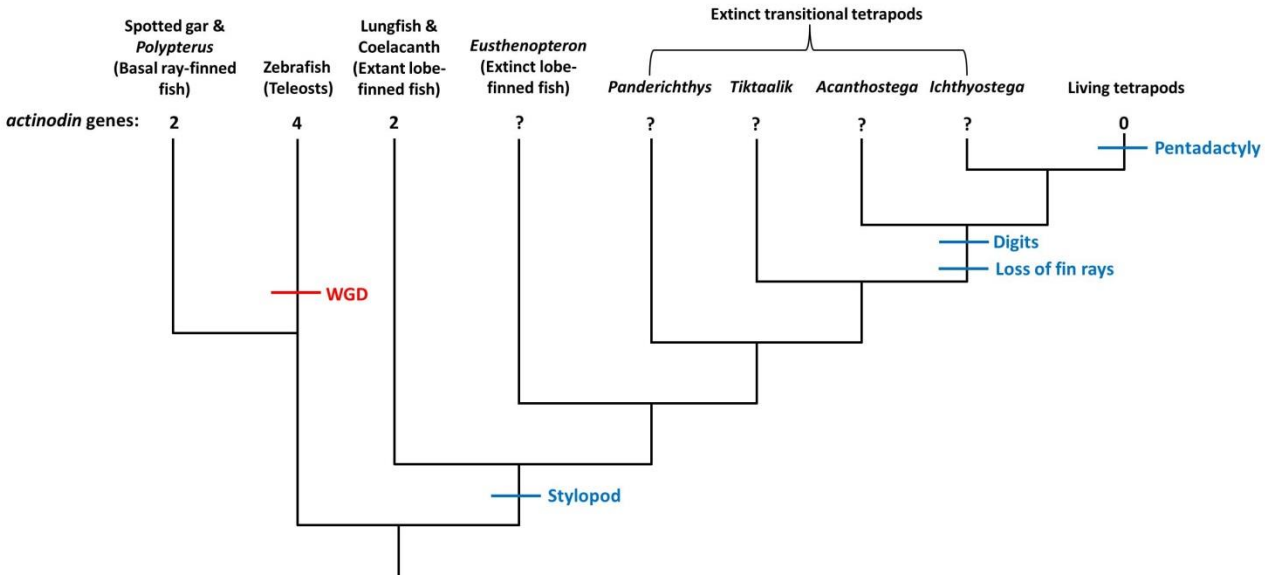

Figure 1.1. Phylogenetic tree of representative extinct and extant ray-, lobe-finned fish, and transitional and non-transitional tetrapods. Spotted gar and *polypterus* are representative basal ray-finned fish that split from teleosts prior to the whole-genome duplication (WGD). Lungfish and Coelacanth are the only remaining extant lobe-finned fish, whose lineage split from ray-finned fish around 450 million years ago. As lobe-finned fish possess only a single proximal fin bone similar to the tetrapod limb, some consider the stylopod evolved after the split from ray-finned fish. *Eusthenopteron, Panderichthys, Tiktaalik, Acanthostega, Ichthyostega* are extinct lobe-finned fish and transitional tetrapod species identified from fossils. Loss of fin rays and evolution of digits occurred prior to the split of *Acanthostega* and living tetrapods. The pentadactyl, or 5-digit state evolved in the lineage leading to extant tetrapods. Number of identified *actinodin* genes is presented. WGD = Whole genome duplication.

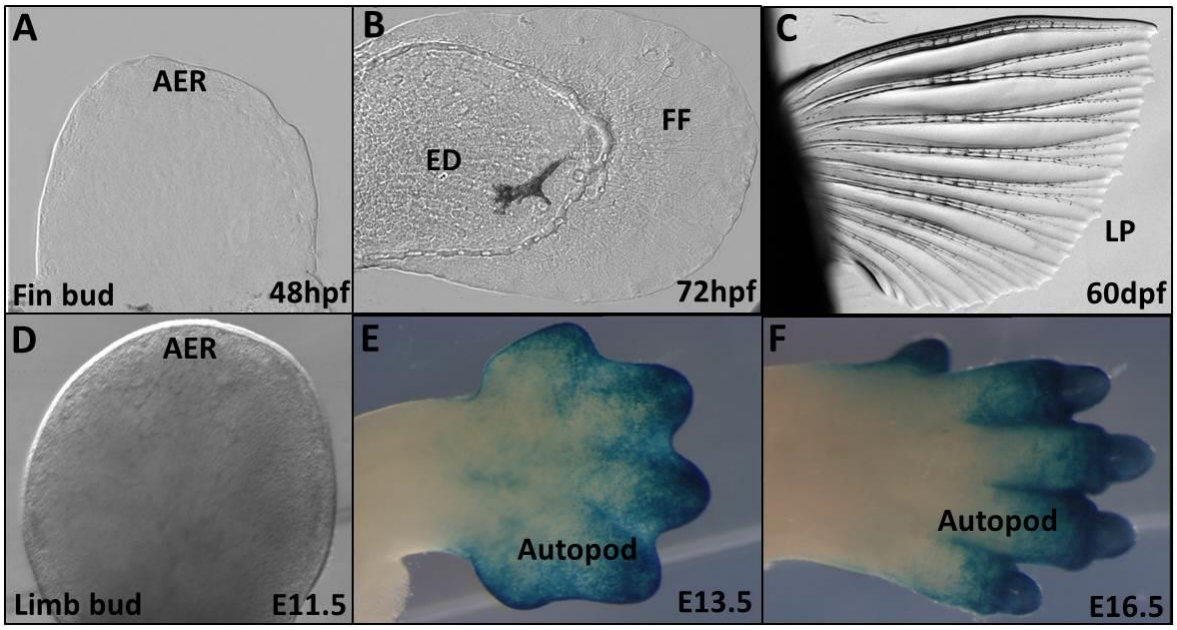

Figure 1.2. Morphological overview of zebrafish fin and mouse limb development. Fin and limb development starts with the formation of a bud made up of mesenchymal cells derived from the lateral plate mesoderm covered in ectoderm (A, D). The distal most ectoderm thickens to form a signalling centre known as the apical ectodermal ridge (AER) (A, D). During fin development, the AER will fold and elongate transitioning into the fin fold. The proximal mesenchyme will condense and chondrify to form the endoskeletal disc (B). Lepidotrichia, the bones of the fin rays, form via intramembranous ossification (C), and the proximal and distal radials (not pictured, see figure 1.3.) will form via endochondral ossification. The bones of the mouse limb will form entirely through endochondral ossification (E, F). The autopod, which consists of the hand and wrist elements, is highlighted with LacZ staining (E, F). AER = Apical ectodermal ridge, ED = Endoskeletal disc, FF = Fin fold, LP = Lepidotrichia.

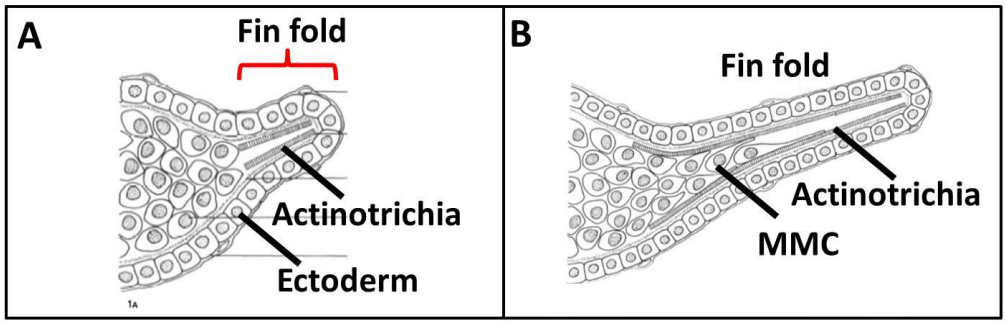

Figure 1.3. Fin fold and actinotrichia formation in zebrafish pectoral fin. The distal ectoderm (formerly AER) folds and extends to form the pectoral fin fold (A). Two rows of actinotrichia support the fold as fin fold extension proceeds (A, B). Migrating mesenchyme will then invade the fin fold, using the actinotrichia as a scaffold (B). MMC = migrating mesenchymal cell. Figure adapted from Wood & Thorogood 1984.

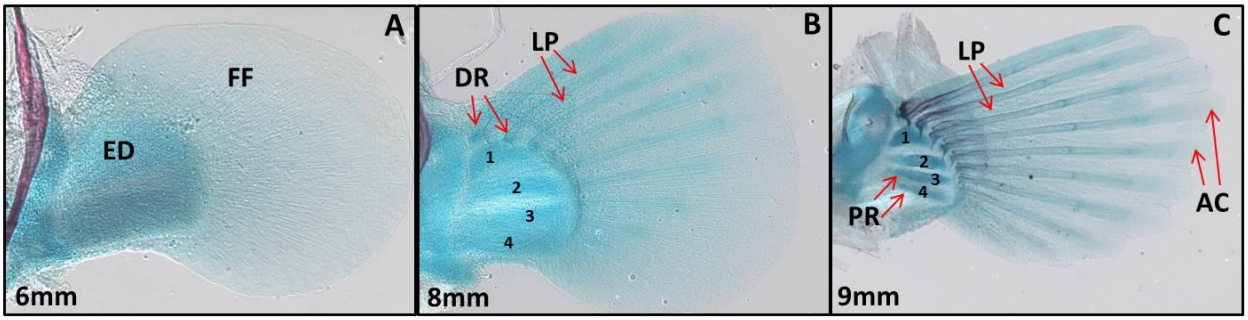

Figure 1.4. Dermal and Endochondral bone formation in zebrafish pectoral fin. The endoskeletal disc undergoes cartilaginous decomposition to form the four proximal radial bones (A-C). Distal radials are formed from *de novo* condensations within the distal rim mesenchyme starting anteriorly (B-C). Lepidotrichia first appear in the anterior fin fold as condensations of alcian-blue stained proteoglycans (B). Fin rays are formed via intramembranous ossification from proximal to distal. Actinotrichia are now located distal to each fin ray (C). The standard length of the fish is indicated in the bottom right corner of each panel. Numbers 1-4 are lebeling the presumptive proximal radials. AC = actinotrichia, DR = distal radial, ED = endoskeletal disc, FF = fin fold, LP = lepidotrichia, PR = proximal radial.

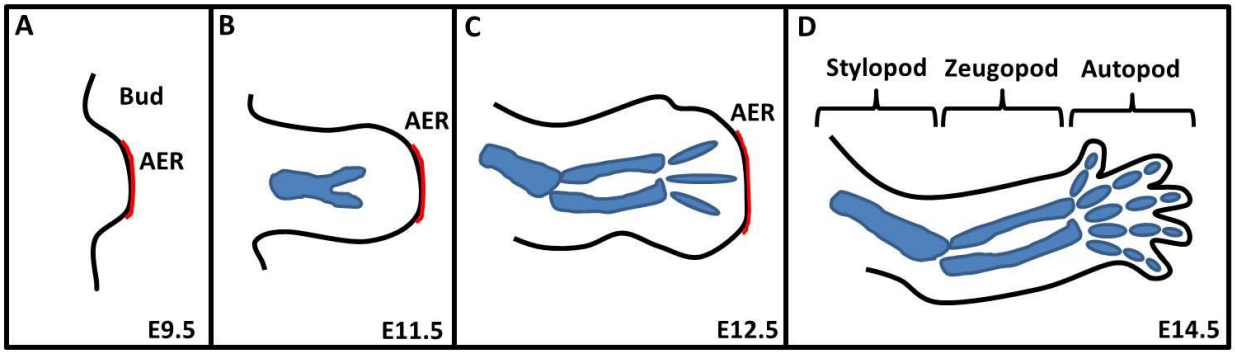

Figure 1.5. Endochondral bone formation in mouse forelimb. The AER of the mouse forelimb persists until just after E12.5 (A-C). By E11.5, stylopod cartilage condensations are observed in the proximal part of the developing limb (B). By E12.5, cartilage condensations are observed for all three distinct segments (stylopod, zeugopod & autopod), however not all digits are present (C). By E14.5, all cartilage elements are present and distinct digits are visible following interdigital cell death and retraction (D). AER = apical ectodermal ridge.

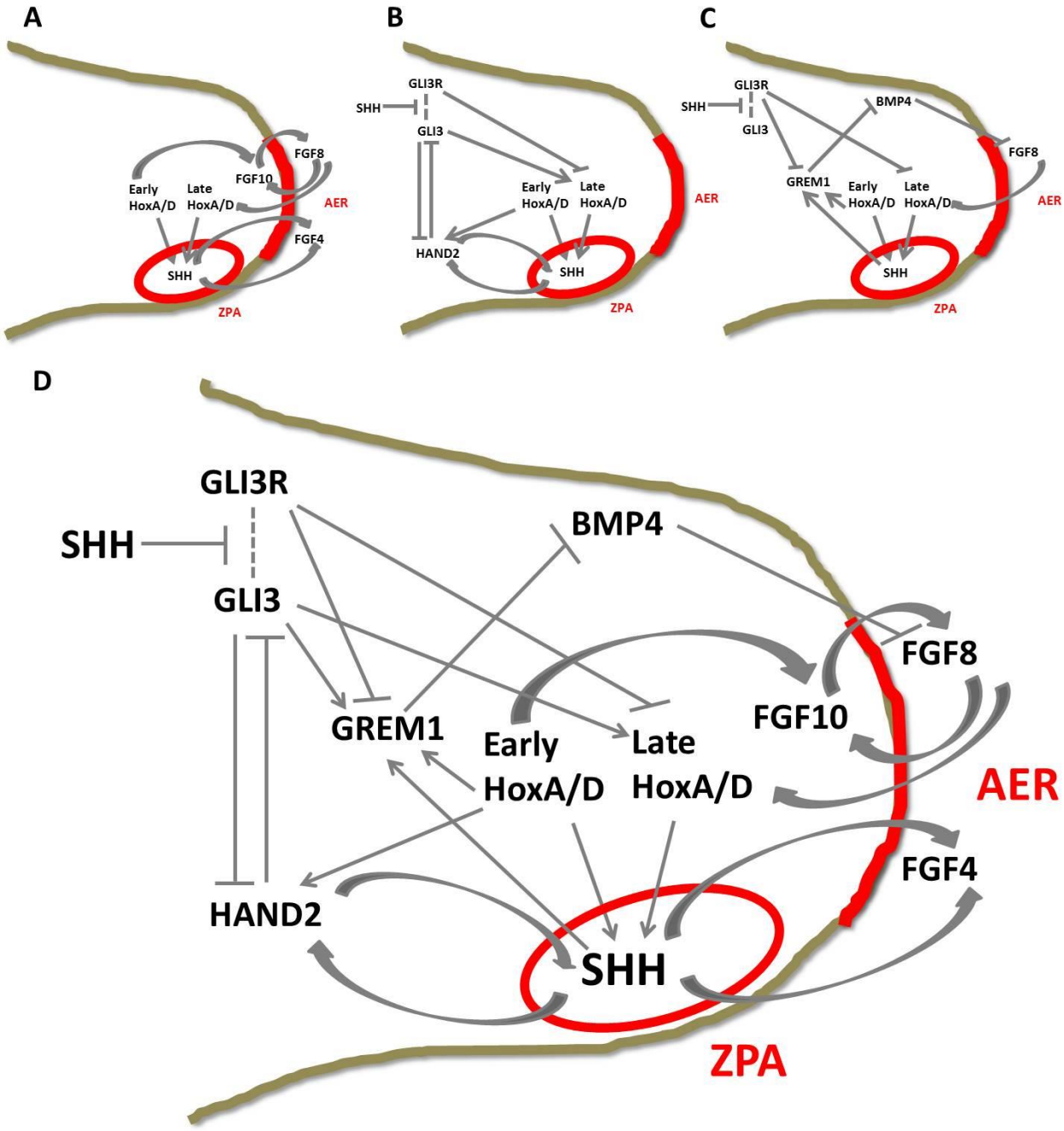

Figure 1.6. Overview of early fin & limb signalling pathways. (A-D) Schematic representation of AER-FGF, ZPA-SHH, and 5'HoxA/D signalling pathways. Partial pathays depicted (A-C), and combined image (D). Contributions to early fin and limb development are detailed in the text (Chapters 1.5, 1.6, and 1.7). AER = Apical ectodermal ridge, ZPA = Zone of Polarizing activity.

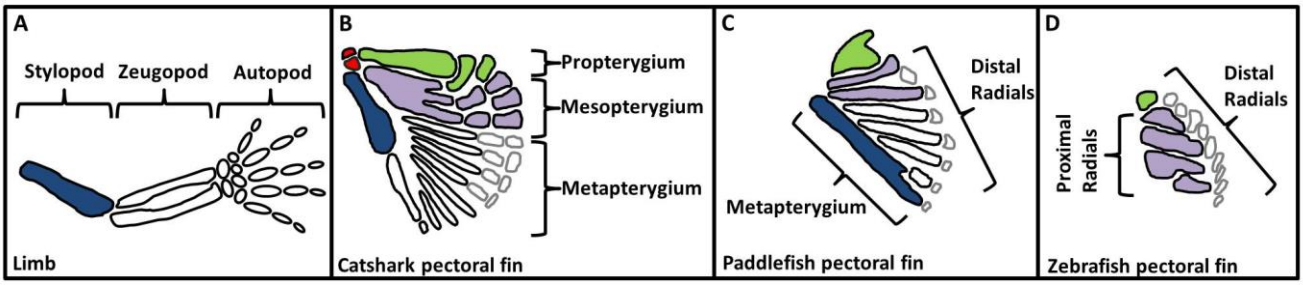

Figure 1.7. Appendicular bone/cartilage structure in tetrapods, catshark, paddlefish, and zebrafish. The tetrapod stylopod is thought to be homologous to the metapterygium present in the catshark and paddlefish pectoral fin (blue) (A-C). The tetrapod limb has lost the pro- and mesopterygium that is present in the catshark, paddlefish, and zebrafish pectoral fin (green, and purple) (A-C). Zebrafish have lost the posterior-most proximal endochondral bone (metapterygium) (D).

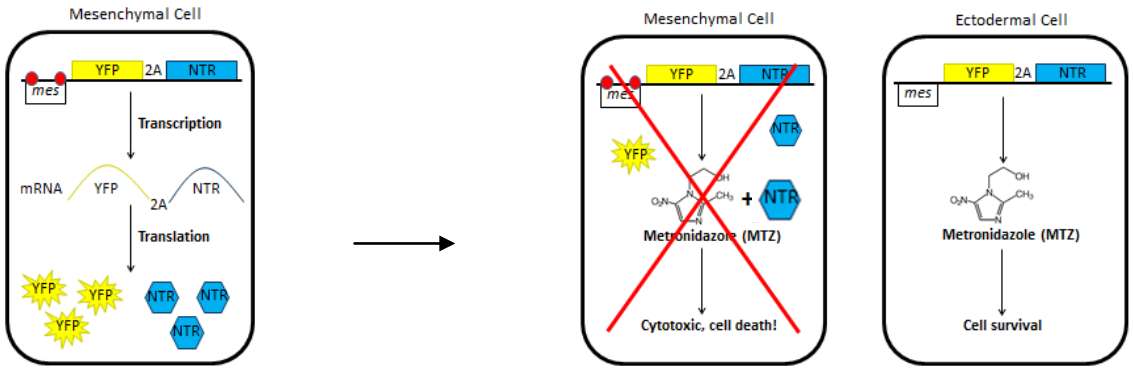

Figure 1.8. Nitroreductase/metronidazole cell ablation system. The nitroreductase-encoding gene is linked to the yellow fluorescent protein via the "2A" self-cleavable peptide. Under the control of mesenchymal-specific *cis*-acting regulatory elements, the transgene is transcribed and translated in only mesenchymal cells. Upon addition of the MTZ prodrug, NTR will convert the MTZ to a cytotoxic DNA cross-linking agent, resulting in mesenchymal cell ablation. In neighbouring cells, NTR is not produced, MTZ is not converted to a cytotoxic form and cell ablation does not occur. Mes = mesenchymal regulatory element, NTR = nitroreductase, YFP = yellow fluorescent protein.

CHAPTER 2

Differential *actinodin* regulation in zebrafish and mouse appendages

2.1. Notes on Chapter

The present chapter has been published in Developmental Biology as per the following citation:

Lalonde RL, Moses D, Zhang J, Cornell N, Ekker M, Akimenko MA. Differential *actinodin1* regulation in zebrafish and mouse appendages. Developmental Biology. 2016; 417(1):91–103.

Author contributions

R.L.L. amplified and cloned the majority of the genomic fragments to identify tissue-specific enhancer elements as well as the promoting region. R.L.L. performed transient analysis including rates of eGFP positive embryos, and percentages of fin fold fluorescence coverage. R.L.L. obtained and analysed all transgenic reporter lines in order to visualize the order of *and1* activation during fin fold development. R.L.L. identified smaller regions (22bp and 20bp) within our enhancer fragments, critical for reporter activation in the epithelial and mesenchymal cells respectively. D.M., N.C., cloned some of the original truncated ectodermal constructs and performed preliminary injection statistics. J.Z. collected and analyzed the transgenic mouse embryos. M.E. supervised the transgenic mouse generation and provided critical reading of the manuscript; M.-A.A. conceived the project and directed the study. R.L.L and M.-A.A. wrote the manuscript.

Project Introduction & Objectives

Mechanisms of *actinodin* regulatory evolution; contributions to fin dermal bone loss

Actinotrichia are crucical for proper fin fold formation, and the invasion of fin mesenchyme through the fold and defects in actinotrichia have been proposed as a mechanism of fin dermal bone loss during the fin-to-limb transition. Furthermore, this gene family is absent from all tetrapod genomes suggesting their loss may have contributed to the fin-to-limb transition.

Objective 1: Identify zebrafish *actinodin1 cis*-acting regulatory elements and test their functionality in tetrapods (Chapter II)

We propose that changes in *actinodin* regulation preceded their disappearance from the tetrapod genome. We therefore set out to identify and characterize the fin-specific *actinodin1 cis*-acting regulatory elements in zebrafish using transgenic fluorescent constructs. To provide evidence to a change in regulation during tetrapod evolution (*trans* evolution), we then tested the functionality of *actinodin1 cis*-acting regulatory elements in limbs using transgenic reporter mice.

2.2. Abstract

The fin-to-limb transition is an important evolutionary step in the colonization of land and diversification of all terrestrial vertebrates. We previously identified a gene family in zebrafish, termed *actinodin*, which codes for structural proteins crucial for the formation of actinotrichia, rigid fibrils of the teleost fin. Interestingly, this gene family is absent from all tetrapod genomes examined to date, suggesting that it was lost during limb evolution. To shed light on the disappearance of this gene family, and the consequences on fin-to-limb transition, we characterized *actinodin* regulatory elements. Using fluorescent reporters in transgenic zebrafish, we identified tissue-specific *cis*-acting regulatory elements responsible for *actinodin1 (and1)* expression in the ectodermal and mesenchymal cell populations of the fins, respectively. Mutagenesis of potential transcription factor binding sites led to the identification of one binding site crucial for *and1* expression in ectodermal cells. We show that these regulatory elements are partially functional in mouse limb buds in a tissue-specific manner. Indeed, the zebrafish regulatory elements target expression to the dorsal and ventral ectoderm of mouse limb buds. Absence of expression in the apical ectodermal ridge is observed in both mouse and zebrafish. However, cells of the mouse limb bud mesoderm do not express the transgene, in contrast to zebrafish. Altogether these results hint for a change in regulation of *and1* during evolution that led to the downregulation and eventual loss of this gene from tetrapod genomes.

2.3. Introduction

The terrestrialization of tetrapods was a major evolutionary achievement and was the basis for the diversification of all future land vertebrates (Ahlberg and Clack, 2006; Ahlberg and Milner, 1994; Daeschler et al., 2006). Among the most important innovations was the tetrapod limb. Tetrapod fore- and hindlimbs evolved from the pectoral and pelvic fins of ancestral lobbed-

finned fish (sarcopterygiians) (George and Blieck, 2011; Shubin et al., 1997). Alterations in fin endoskeleton, exoskeleton, and musculature were required in producing limbs capable of land locomotion (Yano and Tamura, 2013). Most notably, the dermal fin rays and rigid fin fibrils common to all fish species disappeared during limb evolution. By analysing and comparing early fin and limb development we hope to provide insights into the molecular and morphological changes that occurred during the evolutionary transition from fins to limbs (Ahn and Ho, 2008; Freitas et al., 2012; Shubin et al., 1997; Yano and Tamura, 2013).

Early pectoral fin formation in teleost embryos bares many morphological similarities to early limb development in tetrapods. Both structures originate as an outgrowth of lateral plate mesoderm known as a bud (Johnson and Tabin, 1997; Tickle, 2003; Wakahara et al., 2007). Limb axes are established by two important signalling centres: the apical ectodermal ridge (AER) (proximal-distal axis), and the zone of polarizing activity (ZPA) (anterior-posterior axis) (Lewandoski et al., 2000; Martin, 1998). The AER is a distal thickening of ectodermal cells in the distal bud and is responsible for mesenchymal survival, proliferation and fin/limb outgrowth (Johnson and Tabin, 1997; Grandel and Schulte-Merker, 1998; Lewandoski et al., 2000; Sun et al., 2002; Yano et al., 2012; Yano and Tamura, 2013) via FGF signalling. The AER also assists in maintaining the ZPA through the activation of *Shh* signalling, an important morphogen for creating anterior-posterior limb patterning and digit identity (Litingtung et al., 2002; Martin, 1998). One of the first major differences between fin and limb development is the fate of the AER (Wood and Thorogood, 1984; Yano et al., 2012; Yano and Tamura, 2013). In mouse limb development the AER regresses via program cell death around E12–13, and flattens to become simple ectodermal cells (Lu et al., 2008). In teleost fish the AER folds on itself and forms a structure known as the pectoral fin fold (PFF), which will extend distally (Grandel and Schulte-

Merker, 1998; Yano et al., 2012). The fin fold consists of two sheets of ectodermal cells and is maintained by two rows of rigid non-calcified fibres called actinotrichia forming within the fold (Duran et al., 2011; Geraudie, 1977; Geraudie and Meunier, 1980; Grandel and Schulte-Merker, 1998). Actinotrichia are the first exoskeletal elements formed during fin development and act as a scaffold for the migration of mesenchymal cells into the fin fold (Wood and Thorogood, 1984). In adult zebrafish fins, actinotrichia are mostly restricted to the distal domain of the dermal fin rays, known as lepidotrichia (Geraudie and Meunier, 1980). These fibres are also present in the median fin fold (MFF), a structure extending from the 8th somite to the end of the trunk and which will later become the dorsal, caudal and anal fins of the adult zebrafish (Abe et al., 2007; Kimmel et al.,1995; van den Boogaart et al., 2012).

Actinotrichia are composed of a material termed elastoidin, which is made up of collagen components and of recently characterized non-collagenous proteins called actinodins (Duran et al., 2011; Gross and Dumsha, 1958; Sastry and Ramachan, 1965). Four *actinodin* genes have been identified in zebrafish (*actinodin 1, 2, 3* and 4 (*and1, and2, and3, and 4)*) (Padhi et al., 2004; Zhang et al., 2010). Spatial and temporal expression of *and* genes correlate with the development of actinotrichia within both the MFF and PFF (Zhang et al., 2010). During embryonic development *and* expression is observed in the overlying ectodermal cells with the exception of the AER/cleft cells and the migrating mesenchymal cells in the PFF and MFF respectively (Zhang et al., 2010). Gene knockdown analyses using *and1/2* morpholinos have shown that the absence of these proteins results in the loss of actinotrichia and aberrant migratory patterns of the mesenchymal cells within the fin fold. Individual knockdown of *and1* or *and2* yield no phenotypic effects, suggesting compensatory mechanisms between these paralogs. No functional analysis

of *and3* and *and4* has been done, however both genes are expressed in the same fin fold tissue types as *and1/and2* (Zhang et al., 2010).

While *actinodin* orthologues have been identified in other fish species, including multiple actinopterygians and the lobe-finned coelacanth (*Latimeria chalumnae)*, none have been identified in any tetrapod genome examined to date (Amemiya et al., 2013; Nishidate et al., 2007; Zhang et al., 2010). During limb evolution selection pressures would have eliminated the fin fold and with it the calcified lepidotrichia rays and actinotrichia fibres (Yano and Tamura, 2013). Two distinct *and* orthologs have been identified in the coelacanth genome and thus likely existed in the common ancestral lobe-finned fish. Therefore, two separate *and*genes were lost during tetrapod evolution. While several evolutionary possibilities exist, including gene deletion events and protein coding mutations, a parsimonious event is that all *and* genes were silenced simultaneously through modification in their regulation. Following gene silencing, the ancestral *and* genes then likely disappeared from the tetrapod genome through accumulation of mutations. We identified and characterized the *cis*-acting regulatory elements necessary for the expression of the *and1* gene in the embryonic fins. To assess modifications to *and1* regulation in tetrapods, we then tested their functionality in mice. Any differences in *cis*-regulatory activity between zebrafish and tetrapods could highlight potential mechanisms of the loss of the *and* gene family, specifically through a modification of their regulation.

Using transgenic zebrafish fluorescent reporter assays, we have identified one *and1* promoter, as well as multiple tissue-specific enhancers responsible for *and1*expression in the ectodermal and mesenchymal cell populations, respectively, during embryonic fin development. To test the functionality of these enhancers in tetrapod species, we produced transgenic reporter mice. In contrast to transgenic zebrafish, reporter expression is only visible in

the dorsal and ventral ectoderm of the developing limb buds and not in the mesenchyme. These data suggest that while the *and1* gene has been lost in tetrapod species, the regulatory elements responsible for ectodermal expression in teleosts are still able to respond to upstream activators in the mouse. Absence of reporter expression in the limb bud mesenchyme reveals that the upstream activator for *and1* mesenchymal expression may have also been lost during limb evolution or are unable to recognize the zebrafish regulatory element. We propose that this absence of mesenchymal expression may be at the origin of the loss of *actinodin* gene loss in tetrapod species.

2.4. Results

The 2P*and1* regulatory element recapitulates *and1* expression in zebrafish median and pectoral fins

To identify upstream *cis*-acting regulatory elements of *and1*, a genomic fragment of approximately 2 kb (position 1941-1 base pairs (b.p.)) upstream of the first non-coding exon of *and1* was cloned into an eGFP reporter construct (Fig. 2.1A). This fragment was titled 2P (because it is a *2* kb fragment and contains a *p*romoter "P"). We focused our analysis on this 2 kb fragment due to a long series of tandem repeats further upstream. We also originally included the first exon and intron, however the inclusion of these fragments yield no differences in embryonic reporter expression (data not shown). Three independent transgenic lines *Tg(2Pand1:eGFP)* were generated and showed that the 2P fragment is sufficient to drive reporter expression in the overlying ectodermal cells and the migrating mesenchymal cells in the MFF and PFF beginning at 24 h post fertilization (h.p.f.), and 36 h.p.f. respectively (Fig. 2.9A–E). Although mesenchymal expression in the transgenic embryos is partially masked by ectodermal expression, it is visible during transient expression due to the mosaic properties of a reporter construct following injection

in zebrafish embryos (Fig. 2.10) or with confocal microscopy (Fig. 2.11). Reporter expression is absent from the cleft cells of the MFF (36 h.p.f) (Fig. 2.8B–E), and from the early PFF (48 h.p.f) (Fig. 2.1C–E). The AER transitions into a PFF at 36–38 h.p.f (Yano et al., 2012), and the cleft cells transition into the MFF at 27–30 h.p.f (Webb et al., 2007). At 48 h.p.f reporter expression is present in the entire MFF except the distal most ectodermal cells and only the proximal domain of the PFF (Fig. 2.1B–H). In contrast, by 3 days post fertilization (d.p.f) reporter expression is present in the entire PFF and MFF except the distal most ectodermal cells (Fig. 2.1I–O). Expression in the developing fins persists during larval stages (7 d.p.f) (Fig. 2.8F–L). Altogether, eGFP expression recapitulates endogenous *and1* expression during embryonic fin development in zebrafish (Zhang et al., 2010) and these results suggest that an *and1* promoter and potentially multiple tissue-specific enhancers are present within 2P. Identifying these regulatory elements is crucial for uncovering potential changes in *and1* regulation during the fin-to-limb transition.

The 2P*and1* regulatory element is only capable of driving reporter expression in mouse limb ectoderm

To test the functionality of the zebrafish 2P regulatory element in tetrapods, three independent LacZ reporter mouse transgenic lines were created, titled *Tg(2Pand1:lacZ*). Similar to the transgenic zebrafish, reporter expression is observed in the mouse forelimb ectoderm beginning at E10.5 (Fig. 2.12A–C). At E11.5, expression is observed in the forelimb and hindlimb distal ectoderm but is absent from the AER (Fig. 2.2A, E–J). Sections of the limb buds confirm these observations (Fig. 2.2F, G, I, J). The expression of *lacZ* appears to be concentrated at the distal portion of the limb bud, with no expression in the proximal region. Furthermore, in all the lines analyzed, the expression in the ectoderm is mosaic; the number of *lacZ*-expressing cells seems to decrease in a graded manner in more proximal part of the limb buds. At E13.5, following

AER regression in the forelimb (Fig. 2.2C, D, K–M), there is no longer a gap in *lacZ* expression in the ectoderm. Staining is present throughout the entire ectoderm of the autopodal domain of the forelimb (Fig. 2.2K–M). At the same stage, the AER is still present in the hindlimb and *lacZ*-expression in the ectoderm is still excluded from the AER (Fig. 2.2N–P). At E16.5, expression becomes essentially restricted to the digits (Fig. 2.12D–G). In contrast to the transgenic zebrafish, reporter expression is absent from the mesenchymal cell population at all developmental stages (E10.5–E16.5) (Fig. 2.2, 2.8). These results suggest that although the *and* gene family has been lost in tetrapods, the upstream activator necessary for *and1* ectodermal expression remains present and can recognize the zebrafish enhancer element. In contrast, the upstream activator required for mesenchymal expression has either been lost or is not expressed in the mouse limb bud or can no longer recognize the zebrafish regulatory sequence.

The 200-1*and1* fragment can function as a promoter

To identify the *and1* promoter region two 200 b.p. fragments immediately upstream of the first *and1* exon were tested using transgenesis in zebrafish. These fragments were titled 400-200*and1* and 200-1*and1* according to their positions upstream of the 1st base of the 1st exon (Fig. 2.3A). Both fragments were cloned into eGFP reporter constructs containing the previously described *shha* arC enhancer element (Muller et al., 1999). The arC enhancer drives reporter expression in the floor plate and notochord regions of zebrafish embryos only in the presence of a promoter (Muller et al., 1999). The construct *Tg(shha arC+200-1and1:eGFP)* was capable of driving reporter expression transiently in both the notochord and floor plate cells of zebrafish embryos at 3 d.p.f. (Fig. 2.3A–D). 35.2% of injected embryos (N=54, where N equals total number of viable injected embryos) displayed notochord and floor plate expression with the *Tg(shha arC+200-1and1:eGFP)*, compared to 2.22% (n=45) with the *Tg(shha arC+400-*

200and1:eGFP) (Fig. 2.3A). When the activity of the 400-1 fragment alone was tested with the *Tg(400-1and1:eGFP)* construct, 10% of embryos displayed very few positive GFP cells in the MFF, but no expression was observed in either the floor plate or notochord regions (Fig. 2.16A). This result suggests that the *and1*promoter lies in the 200 b.p. region immediately upstream of the first exon.

The 1117-975P*and1* fragment can drive reporter expression in the ectodermal cells of the zebrafish median and pectoral fin fold

Using deletion analysis, a series of reporter constructs were created to identify and isolate the enhancers responsible for driving *and1* expression in the MFF and PFF. Three different truncated 2P elements were created: 1279-1*and1*, 1117-1*and1*, and 876-1*and1* and inserted in the eGFP reporter vector (Fig. 2.4A). Percentage of GFP positive embryos and % MFF fluorescence coverage for each construct are summarized in the Fig. 4A. The % MFF fluorescence value represents the MFF coverage using the fluorescence threshold, and % area functions of ImageJ. The *Tg(1279-1and1:eGFP)* and *Tg(1117-1and1:eGFP)* constructs had similar percentages of GFP positive embryos (87.7% and 87.3% respectively) to the *Tg(2Pand1:eGFP)* construct (87.4%) and similar percentage of MFF coverage value at 2 d.p.f. In contrast, the *Tg(876-1and1: eGFP)* construct showed that further truncation of the 2P fragment led to a decrease percentage of embryos with fluorescent cells (24.4%) and an almost absence of fluorescent cells in the MFF in the injected embryos (Fig. 2.4A). Absence of ectodermal reporter expression with the *Tg(876-1and1:eGFP)* construct led us to test a smaller region 1117-967 b.p. with the human β-globin minimal promoter. This construct was capable of driving reporter expression in the ectodermal cells with the same efficiency as the full 2P*and1* element (Fig. 2.4A). We made transgenic lines from embryos injected with this construct, named *Tg(epi+β-globin:eGFP)* (Fig. 2.4B–H). The

expression patterns observed in three independent transgenic lines confirmed that the 1117-967 b.p. fragment can spatially and temporally recapitulate the ectodermal expression observed with the *2Pand1* fragment. Confocal microscopy confirmed the absence of mesenchymal reporter expression (Fig. 2.11). This suggests that an *and1*ectodermal enhancer lies within the 150 b.p. and we titled this region Epi, for ectodermal enhancer. This element is functional in mice, and therefore the upstream activating factor should be conserved in tetrapods as well.

Multiple enhancers within 2P*and1* are required for mesenchymal cell reporter expression in the zebrafish median and pectoral fin fold

To characterize the regulatory regions responsible for *and1* expression in the mesenchymal cells of the PFF and MFF, the Epi fragment was simply removed from the 2P fragment. The resulting fragment titled *2P*Δ*epi* was then inserted into a reporter construct and tested by transient transgenesis (Fig. 2.5A). The regulatory elements of *2P*Δ*epi* were capable of driving reporter expression in the migrating mesenchymal cells spatially, and temporally similar to that of the full 2P*and1*element (Fig. 2.5A). At 60 h.p.f., there is symmetrical reporter expression of the distal rim mesenchymal cells of the pectoral fin bud (Fig. 2.14). These cells are contained within the proximal domain of the fin fold prior to migration. By 72 h.p.f., despite the uniform migration of mesenchymal cells distally through the fin fold, we see a larger number of eGFP-positive cells migrating in the posterior half the fin fold (Fig. 2.5). The transient expression pattern was confirmed with five independent transgenic lines (Fig. 2.5B–H). To assess the location of the mesenchymal enhancer(s), fragments 1941-1117*and1* and 967-1*and1* were tested separately. A β-globin minimal promoter was included in the construct with the 1941-1117*and1*fragment. Neither constructs could recapitulate the full *Tg(2P*Δ*epi:eGFP)*expression (Fig. 2.5A, 2.16). Percentage of GFP positive embryos and average number of mesenchymal cells for each construct are

summarized in the Fig. 2.5A. Mesenchymal cells were simply counted in three representative embryos. In comparison to percentage of GFP embryos of *Tg(2PΔepi:eGFP)* (83.8%), *Tg(1941-1117and1:eGFP) and Tg(*967-1*and1:eGFP)* displayed drastically reduced percentages at 11.6%, and 9.25% respectively. The number of mesenchymal cells also drastically decreased with these two constructs. This suggests that enhancer elements are present in each fragment and both are required simultaneously to drive *and1* expression in the mesenchymal cells. These elements are not functional in mice, and therefore present a potential change in *and1* regulation during tetrapod evolution.

***Actinodin1* expression is activated in ectodermal cell populations prior to mesenchymal cells**

To assess the timeline of *and1* expression in the ectodermal and mesenchymal cell populations during MFF development, *in situ hybridization* (ISH) experiments were previously performed on embryonic fin sections (Zhang et al., 2010). Despite the difficulties of getting good ISH on cryosections due to the thinness of the tissue, the results suggested that ectodermal expression is beginning prior to mesenchymal expression (Zhang et al., 2010). In order to confirm these results and test more specifically the temporal expression patterns of our reporter lines, we produced a double transgenic line *Tg(2Pand1:eGFP; 2PΔepi*:*mCherry*) (Fig. 2.6A–D). Despite the presence of mesenchymal expression within *Tg(2Pand1:eGFP)*, this line was used to assess ectodermal reporter expression to ensure all potential *cis*-regulatory elements are included. We also simply examined age-matched individuals of the mesenchyme or ectodermal transgenic lines (Fig. 2.13). We observed a delay in mesenchymal reporter expression compared to ectodermal expression. By 48 h.p.f, both ectodermal and mesenchymal reporter expression is present in the MFF (Fig. 2.6I–L), however only ectodermal expression is visible in the PFF at this stage (Fig.

2.6E–H). Mesenchymal reporter expression begins around 52 h.p.f in the pectoral fin (data not shown). By 72 h.p.f, both tissues display strong expression in the MFF and PFF (Fig. 2.15).

Removal of a 23 b.p. fragment within the Epi region results in a large decrease in ectodermal reporter expression

To identify putative binding sites within the ectodermal enhancer, we analyzed our ectodermal enhancer sequences using TRANSFAC transcription factor identification software (Fig. 2.17). Based on these results, we identified four clusters of potential consensus binding sites for transcription factors including sites for smad3 (Jonk et al., 1998), CDX-2 (Nishiyama et al., 2009), Osr2 (Kawai et al., 2007), MTF-1 (Wang et al., 2004), TCF-4 (Henderson et al., 2012) and multiple sites for Dlx proteins (Feledy et al., 1999). To test the enhancer activity of these clusters, we used site-directed mutagenesis to delete these regions from our *Tg(2Pand1:eGFP)* reporter construct. Three mutations consisted of deletions (Ectodermal (epi) mutation 1–3) and one consisted of a 2 b.p. substitution (epi mutation 4) (Fig. 2.7C). GFP reporter constructs carrying each of the mutations were analyzed by transient transgenesis and the effect of each mutation on ectodermal expression was compared to *Tg(2Pand1:eGFP)* transient expression. For rate of GFP positive embryos, only embryos with visible ectodermal expression were counted, and embryos with only mesenchymal expression were not counted. The mutation at epi site 3 yielded a decrease in GFP positive embryos from 87.4% obtained with the full *Tg(2Pand1:eGFP)* to 50.9% (Fig. 2.7H). The number of GFP positive ectodermal cells decreased as well, allowing the visualization of higher number of fluorescent mesenchymal cells (Fig. 2.7I). In contrast, mutations at epi sites 1, 2, and 4 yielded a percentage of GFP positive embryos very similar to the 87.4% obtained with the *Tg(2Pand1:eGFP)* at 2 d.p.f. (Fig. 2.7A, D, F, J). Furthermore, the coverage of the median fin fold with GFP-positive cells was very similar for the three mutant constructs and

the WT construct (Fig. 2.7B, E, G, K). Mutations of the epi sites 1 and 3 were combined in order to test any synergistic effects, however no additional decrease in GFP positive embryos or levels of ectodermal expression was observed compared to the epi 3 mutation alone (Fig. 2.7L, M). Finally, epi site 3 was also mutated in the *Tg(Epi+β-globin:eGFP)* construct and yielded a drastic decrease in both GFP positive embryos (6.25%) and transient ectodermal expression (Fig. 2.7N, O). To confirm the importance of epi site 3 to ectodermal reporter expression, a transgenic line was made: *Tg(2Pand1Epi3mut:eGFP)* (Fig. 2.8A–G). This line displays a complete loss of ectodermal reporter expression, while revealing mesenchymal reporter expression similar to the *Tg(2PΔepi:eGFP)* transgenic line (Fig. 2.5B–H). At 3 d.p.f., mesenchymal reporter expression is observed in the MFF (Fig. 2.8E–G), and the PFF (Fig. 2.8B–D), with more eGFP-expressing cells being observed in the posterior half of the PFF (Fig. 2.8C, D). Overall these results suggest that an important element for ectodermal enhancer function is located within epi site 3; however there may be additional weaker ectodermal enhancers outside of the epi 3 fragment as suggested by the low levels of remaining transient ectodermal expression.

2.5. Discussion

We have identified tissue-specific *cis*-acting regulatory elements and a promoter responsible for driving *and1* expression in the overlying ectodermal cells and the migrating mesenchymal cells of the MFF and PFF during embryonic development. The promoter is located in the 200 b.p. immediately upstream of the first non-coding exon. The ectodermal enhancer is mainly located within epi site 3, a 23 b.p. region within the "epi" fragment. In contrast, there appear to be multiple mesenchymal enhancers required simultaneously for *and1* expression in mesenchymal cell populations. Double transgenic reporter fish lines to visualize ectodermal vs. mesenchymal expression revealed an earlier onset of ectodermal expression, which may support

the initial ectodermal origin of actinotrichia proposed by Wood and Thorogood (1984). It is important to note that there may be additional enhancer elements required to fully recapitulate *and1* expression. Using the zebrafish regulatory region to make a transgenic mouse reporter construct, we observed, despite the absence of the gene family from tetrapods, a remarkable recapitulation of the reporter expression in the ectoderm of the mouse limb buds but no expression in the limb mesoderm. Ectodermal expression is restricted to the developing autopod domain in the mouse limb, the distal portion of the limb bud, as in the zebrafish pectoral fin bud. The graded mosaic ectodermal expression within the developing mouse limbs may suggest the action of a morphogen type activating factor with higher concentrations being present in the distal most tissues. Our reporter expression provides evidence to a potential homology between pectoral fin fold ectoderm and the autopodal ectoderm of tetrapod limb buds. Interestingly, Gehrke et al. (2015) have recently implied a homology between the migrating mesenchymal cells of the zebrafish pectoral fin fold, and the autopodal mesenchyme domain of the mouse limb bud using spotted gar enhancer activity data. Orthologues of previously characterized tetrapod *5'hoxA/D* autopodal enhancers were identified in the spotted gar genome. Several spotted gar enhancers were tested in zebrafish and were shown to drive reporter expression in the distal rim mesenchyme during pectoral fin fold development. When the gar enhancers were tested in mice, they were shown to drive reporter expression in the autopodal mesenchyme nearly identical to the tetrapod orthologues. Based on these results, it is possible that a change in the regulation of *and1* during the fin-to-limb transition led to the downregulation of *and1* expression and subsequent loss of this gene from the tetrapod genome.

Candidate activators/repressors of *and1*

We showed that mutation of the Epi site 3 leads to an important decrease in ectodermal expression. The Epi site 3 contains putative binding sites for Osr2, MTF-1, and TCF-4 (Henderson et al., 2012; Kawai et al., 2007; Matys et al., 2006; Wang et al., 2004) (Fig. 2.16). Despite *osr2* morphants showing a reduction in pectoral fin size (Lam et al., 2013; Neto et al., 2012), *osr2* expression appears to be confined to the fin fold mesoderm and is therefore an unlikely candidate for *and1* ectodermal activation. While *TCF-4* is not expressed in the developing PFF and MFF ectoderm (Faro et al., 2009; Rai, 2010), other members of the *TCF* family are, including *TCF1*, *TC7*, and *TCF-12* (Li, 2009; Thisse and Thisse, 2005; Rai, 2010). Expression data is not available for *MTF-1* at these developmental stages; however it is highly expressed at the cleavage stage during early development (Hong, 2010).

Putative binding sites for multiple *hox* and *dlx* genes (Feledy et al., 1999; Knosp et al., 2007; Salsi et al., 2008) are present in the 2P sequence (Matys et al., 2006) (Fig. 2.17 and 2.18). The *hox* and *dlx* gene clusters are homeodomain transcription factors important for embryonic patterning, including the developing fin/limb. The *5′hoxA/D* (9–13) genes are sequentially expressed in a proximal-distal manner during fin/limb development (*hoxa11* being an exception in limb formation) and are involved in endoskeletal bone formation (Ahn and Ho, 2008; Freitas et al., 2012; Woltering et al., 2014; Yano and Tamura, 2013). The *Dlx3-7/5*-6 bi-gene clusters are expressed in the apical ectodermal ridge during limb development and they likely play a role in its maintenance (Beanan and Sargent, 2000; Heude et al., 2014; Robledo et al., 2002; Sumiyama and Ruddle, 2003). The expression pattern of *Dlx3-7* also extends to surrounding ectodermal tissue in the fin/limb bud (Beanan and Sargent, 2000; Sumiyama and Ruddle, 2003).

The epi 4 site contains a putative binding site for *dlx3*: (A/C/G)TAATT(G/A)(C/G) (Feledy et al., 1999; Matys et al., 2006) (Fig. 2.17). Expression of *dlx3b* has been observed in the ectodermal layers of the median and pectoral fin of zebrafish similar to *and* expression; however it appears to be additionally present in the AER/cleft cells (Ellies et al., 1997; Heude et al., 2014; Thisse and Thisse, 2005; Zerucha and Ekker, 2000). *Dlx3* expression is restricted to the ectodermal cells in developing limbs, and *Tg(dlx3::LacZ)* reporter lines mimic our 2P:LacZ mouse lines (Beanan and Sargent, 2000; Sumiyama and Ruddle, 2003), with the important exception being the expression of *Dlx3* within the AER. To test if *dlx3* activates *and1* in the ectodermal tissues we mutated the binding domain (AT→GC substitution, Epi 4 mutation), however we saw no difference from the original *Tg(2Pand1:eGFP)* construct. It is therefore unlikely that *dlx3* activates *and1*.

And1 expression is present in the mesenchymal cells migrating through the fin fold as well as the distal rim mesenchyme adjacent to the endoskeletal disc. According to reporter expression from the *(Tg2PΔepi:eGFP)* transgenic lines, there is also a larger number of eGFP-positive cells in the posterior half of the pectoral fin fold at 3 d.p.f. The *hoxd13a* gene has a distinct posterior expression during zebrafish pectoral fin development as well, and their overlapping expression patterns within the fin fold posterior mesenchyme may present a possible regulatory link (Ahn and Ho, 2008). Using previously identified Hox binding sites consensus sequences (Ibrahim et al., 2013; Knosp et al., 2007; Salsi et al., 2008), six potential *hoxa13* binding sites: TATAAA, ATAAAA (3), AATAAAA, (consensus sequence being AATAAA (Knosp et al., 2007)) were identified, as well as one *hoxd13* binding site: CCCATAAAATC (consensus sequence being (T/C)(A/C)AT(A/T)AAA) (Ibrahim et al., 2013; Salsi et al., 2008), and one *hoxa11* binding site: ATTTTATGGGC (consensus sequence being GGGTTT(T/A)ACGAC) (Matys et al., 2006; Shen et al., 1996) (Fig. 2.18). Both *hoxa13a* and *hoxa13b*, as well as *hoxa11b*, are expressed in the

distal rim mesenchymal cell populations during pectoral fin development and are good candidates for *and1* activation (Ahn and Ho, 2008).

Loss of the *actinodin* gene family

Analysis of the *Tg(2Pand1::LacZ)* transgenic mouse line provides some clues on the potential mechanism of *and1* down regulation during tetrapod evolution. Ectodermal reporter expression in the limb buds at stages E10.5–E16.5 reveals that the *and1*ectodermal activator in zebrafish remains present in tetrapods and is able to recognize the fish enhancer sequence. In contrast, the absence of mesenchymal expression in the limb buds at all developmental stages may be the result of different evolutionary scenarios. First, *and1* expression in the mesenchymal cells may be activated by a fish specific transcription factor that was also lost during tetrapod evolution. Recent analysis of the lobe-finned coelacanth (*Latimeria chalumnae)* identified more than 50 genes lost in tetrapods, including 13 different fin development genes (Amemiya et al., 2013). Analysis of the zebrafish orthologues would prove useful to assess the contributions of these genes to the fin-to-limb transition.

Second, the fish enhancer sequence may no longer be recognized by the mouse transcription factor (s). The genome of the spotted gar (*Lepisosteus oculatus*) was recently examined for 5′*hoxA/D* distal fin/limb enhancer activity (Gehrke et al., 2015). The gar was chosen because it is a member of the ray-finned fish which branched off prior to the teleost whole genome duplication event. Interestingly, while many gar enhancers were functional in mice, the orthologous zebrafish versions were not functional. It is proposed that the teleost genome duplication event and subsequent sequence divergence may be responsible for altered enhancer activity when tested in mice (Gehrke et al., 2015). In fact, our proposed *and1* regulatory regions

showed no conservation with *and1* upstream regions of other teleost species (medaka, stickleback) or the spotted gar (data not shown).

Third, the population of fin fold mesenchyme in zebrafish may be distinct from limb bud mesenchyme. Evidence has suggested fin fold mesenchyme may be derived from either neural crest cells (Smith et al., 1994), or paraxial mesoderm (Lee et al., 2013); however limb mesenchyme is exclusively derived from lateral plate mesoderm (Hayashi and Ozawa, 1995). Such differences in embryonic origin of these cell populations could explain differences in transcription factor presence/absence and thus enhancer activation. Although, as previously discussed, spotted gar 5′*hoxA/D* enhancer activity is conserved between zebrafish fin fold mesenchyme and tetrapod autopod mesenchyme (Gehrke et al., 2015). Alternatively, fin fold *and1* mesenchymal expression may also be a teleost-specific derived trait. Although *actinodin* genes have been identified in lobe-finned fish, there is no evidence to date that shows tissue-specific *and* expression is conserved (Amemiya et al., 2013).

The last possibility is that during limb evolution, alterations to the expression pattern of key upstream *and1* activator/repressor coding genes resulted in the downregulation and eventual silencing of this gene. We propose changes in *and* regulation during tetrapod evolution as a parsimonious mechanism for the loss of two distinct orthologs from the ancestral lobe-finned fish genome. Recent research has focused on differences in 5′ *HoxA/D* expression patterns between early fin and limb development and assessed their implications on limb evolution (Ahn and Ho, 2008; Freitas et al., 2012; Yano and Tamura, 2013). Multiple 5′*HoxA/D* genes appear to be good candidates for *and1* regulation in zebrafish. *Hoxa11b* is expressed in the proximal and distal tissues during zebrafish early pectoral fin development; however *Hoxa11* is proximally restricted during mouse limb bud development (Woltering et al., 2014). The downregulation of *Hoxa11* in

the distal tissues during limb evolution is a plausible mechanism for the downregulation of *and1* in the distal mesenchymal cells of the pectoral fin. Additionally, *hoxa13a* and *hoxa13b* are also expressed in the distal migrating cells of the pectoral fin fold and may be *and1* positive regulators, although their expression pattern mimics the distal expression of *Hoxa13* during limb development (Ahn and Ho, 2008; Woltering et al., 2014). Finally, the expansion of "late phase" *Hoxd13* expression has been linked to increased endoskeletal bone elements during limb evolution. *Hoxd13a* overexpression experiments in zebrafish yielded greater endoskeletal disc proportions and decreases of *and1* expression suggesting it may be a negative regulator (Freitas et al., 2012). *And1* mesenchymal reporter expression displays increased numbers of eGFP-positive cells in the posterior half of the pectoral fin fold in our *Tg(2PΔepi:eGFP)* transgenic line, mimicking *hoxd13a* expression, and suggesting a potential positive regulatory link.

In conclusion, we show that, despite the disappearance of the actinodin genes from the tetrapod genome, the regulation of *and1* in the ectodermal cells in the embryonic appendages of fish and mice is conserved. In contrast, there is an absence of regulatory conservation between fish and tetrapods in the mesenchymal cells. We propose that changes to activating factors of *and1* in the mesenchymal tissues contributed to the downregulation of this gene during limb evolution. Interestingly, the mesenchymal regulatory region contains putative binding domains for multiple 5′HoxA/D (9−13) proteins that have acquired novel expression patterns in tetrapods compared to zebrafish. These changes may represent a mechanism for the downregulation of *and1* and the subsequent loss of this gene during tetrapod evolution.

2.6. Methods

Animal care

All fish are bred and raised in the D' Iorio, University of Ottawa, zebrafish facility. Wild-type zebrafish stock has been bred in the laboratory for several years. The fish facility is maintained at 28 °C, with a photo-period of 14 h of light and 10 h of darkness (Westerfield, 2000). Animal care and experiments were performed according to the CCAC guidelines.

Plasmid construction

Zebrafish

All cloning and subcloning was performed following standard procedures (Sambrook and Russell, 2001). The original vector used was *pEGFP-N1*. The CMV regulatory regions were removed and Tol2 arms were inserted between the *AseI* and *NheI* (left arm) and *AflII* (right arm). Zebrafish genomic fragments were amplified using the following primers:

1941-

1and1 **FW** 5′ GGTACCTTACAGCTTTAAGACACCTCTAG 3'

Rev 5′ CCATGGCTGTTGAGAACCTGG 3'

1279-

1and1 **FW** 5′ GATCTGCAGTCACGAAGACGACAAA 3'

Rev 5′ GGCGGATCCCTGTTGAGAACCTGG 3'

1117-

1and1 **FW** 5′ GCTAGCTTTCGGAAACCCCAGAC 3'

Rev 5′ GGCGGATCCCTGTTGAGAACCTGG 3'

876-

1and1 **FW** 5′ GCTAGCAAACGGCTTTTAATCTGTA 3'

Rev 5′ GGCGGATCCCTGTTGAGAACCTGG 3'

Epi Fragment **FW** 5′ GCTAGCTTTCGGAAACCCCAGAC 3’

Rev 5′ GAATCCGGCCAATCGCATGTG 3’

1941-

1117 **FW** 5′ GCTAGCGGTGAATTACAGCTTTAAGAC 3’

and1 **Rev** 5′ GGTACCAAAAATGTGGAAACATCTGG 3’

967-

1and1 **FW** 5′ GGTACCTTAACATAAAGCACAGATGT 3’

Rev 5′ GGATCCGAGAACCTGGCCACAATTTA 3’

876-

680and1 **FW** 5′ GCTAGCAAACGGCTTTTAATCTGTA 3’

Rev 5′ GAATTCCTTCATTTACTGAATATTGTGTC 3’

680-

400and1 **FW** 5′ GAATTCGACACAATATTCAGTAAATGAAG 3’

Rev 5′ GGATCCGGCATCCGCTGCGTAAAACA 3’

400-

1and1 **Fw** 5′ GGCATCCGCTGCGTAAAACAT 3’

Rev 5′ CCATGGCTGTTGAGAACCTGG 3’

400-

200and1 **Fw** 5′ GGCATCCGCTGCGTAAAACAT 3’

Rev 5′ GGTACCTGTAAGGAACTAACATTA 3’

200-1and1 **FW** 5′ GGTACCTCATTGTTTGTTTTCGAA 3’

Rev 5′ CCATGGCTGTTGAGAACCTGG 3’

Side-directed mutagenesis was performed using the following oligonucleotides to create specific deletions/mutations of choice:

Epi 1 **FW** 5′ TACTCAAAAGTTGGAATTATTATAAA 3’

Rev 5′ TTCCGAAAAAAATGTGGAAACATCTG 3`

Epi 2 **FW** 5′ GCTTTTTTCCCTAGGCTGAAATCT 3’

Rev 5′ AACTTTTGAGTAGGAATGTCTGGG 3’

Epi 3 **FW** 5′ GTAAAGGGTGTATAATTACACATG 3’

Rev 5′ GCCTACAATCAGCACTCGAAACAG 3’

Epi 4 **FW** 5′ AGGGTGTATACGTACACATGCGAT 3’

Rev 5′ TTACAGGTGTGCAGGAATGTGCGA 3’

All fragments were cloned into *pDrive* (Qiagen) Cloning vector before being subcloned into the eGFP Tol2 reporter vector.

The human beta-globin minimal promoter was isolated from the *p1230* vector and amplified using the following primers:

FW 5′ GGATCCCTGGGCATAAAAGTCAG 3′,

Rev 5′ ACCGGTTCTGCTTCTGGAAGGCT 3′.

The *shha* arC fragment was isolated from the 2.2*shh:GFP-ABC* construct obtained from the U. Strähle laboratory and amplified using the following primers:

FW 5′ GAATTCGACTGCTCTAATTAAAAACC 3′,

Rev 5′ GCTAGCGTTTTTCTCATTCTATAAGT 3′.

Mouse

The 2P*and1* element was removed from *pEGFP-N1* (Clontech) with *KpnI* and *BamHI* (blunted), and inserted in the *p1230* LacZ reporter vector between the *KpnI* and *NcoI* (blunted).

Microinjection in zebrafish embryos

Reporter constructs (final concentration of 100 ng/µL) are co-injected with transposase RNA (final concentration of 50 ng/µL) mixed with RNAse-free water and 0.5% phenol red in one cell-stage zebrafish embryos.

TRANSFAC sequence analysis

Sequences were analyzed using TRANSFAC software. "Match – search for TF binding sites" analysis method was used with the vertebrate profile matrices.

Transient expression analysis

Transient median fin expression was analyzed at 2 d.p.f. in the three best representative fish. Ectodermal fluorescent coverage was calculated using the % area and threshold functions in ImageJ. Mesenchymal cells were simply counted.

Transgenic zebrafish

Transgenic lines were identified via fluorescence microscopy and the expression patterns were confirmed with 3–5 lines per construct. Expression analysis was performed from 24 h.p.f to7 d.p.f.

Transgenic mice

Transgenic mice were created by the Transgenic Core Service at the University of Ottawa and were confirmed via PCR. Whole mount X-Gal staining was performed as previously described (Zerucha et al., 2000). X-Gal stained embryos were cryo-sectioned to a thickness of 20 µm.

2.6. Author Contributions

R.L.L. made most of the zebrafish constructs, all the zebrafish transgenic lines, and analyzed the data. D.M., N.C., made some of the original truncated ectodermal constructs and performed preliminary injection statistics. J.Z. collected and analyzed the transgenic mouse embryos. M.E. supervised the transgenic mouse generation and provided critical reading of the manuscript; M.-A.A. conceived the project and directed the study. R.L.L and M.-A.A. wrote the manuscript.

Acknowledgements

We thank Gary Hatch, Danielle Guay, Carolyne Cléroux, Will Wu, Helena Bleeker, Pierre Peynichou, Hombline Poullain, Andie Godo and Marissa Northorp for their technical contribution. This work was supported by the Natural Sciences and Engineering Research Council of Canada (#155817-2012) and to M.-A.A.

2.8 Figures

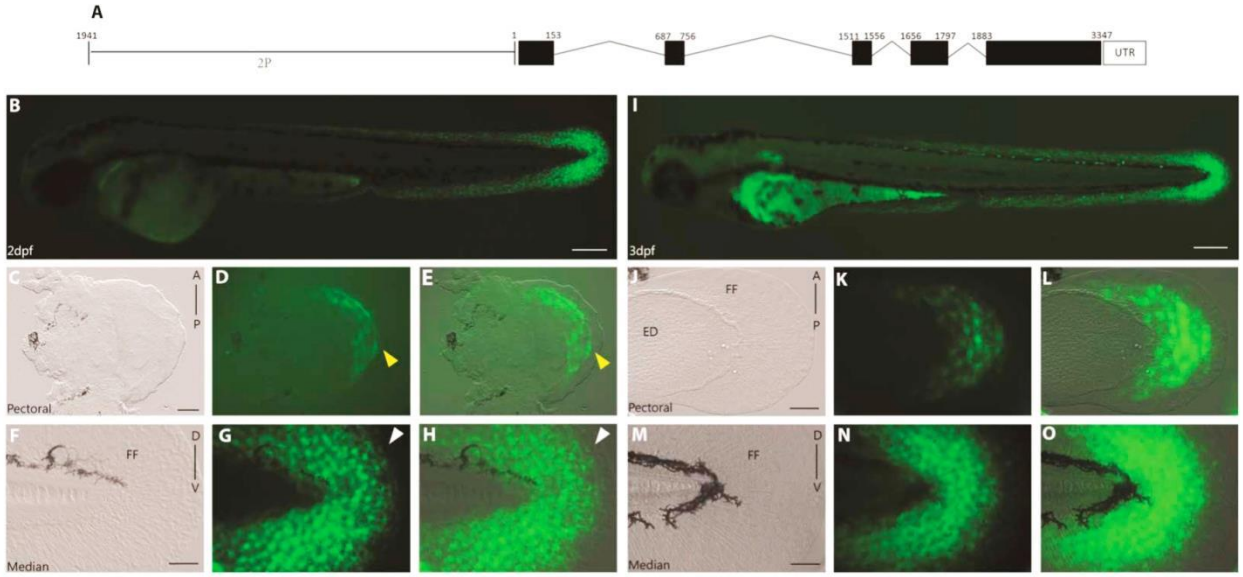

Figure 2.1. A 2 kb genomic fragment upstream of the first exon of *and1* (2P) is sufficient to recapitulate endogenous *and1* expression in zebrafish embryonic fin folds. (A) *Actinodin1*gene organization, 2P*and1* element (1941-1 b.p.) on left, black boxes represent exons, lines represent introns and 5′ upstream genomic region. (B–H) 2 d.p.f. and (I–O) 3 d.p.f. *Tg(2Pand1:eGFP)* transgenic reporter line. Pectoral (C–E, J–L) and median (F–H, M–O) fin fold display reporter expression in the ectodermal and mesenchymal cell populations. Note the absence of expression in the early pectoral fin fold at 2 d.p.f. (indicated by the yellow arrowheads) (D, E). Expression is also absent from the distal most cells of the median fin fold (indicated by the white arrowheads) (G–H). Note GFP expression in ectodermal cells masks GFP expression in the mesenchymal cells. GFP expression in mesenchymal cells is best observed with transient expression highlighted in Fig. S10 or with confocal imaging. Brightfield, (C, F, J, M), fluorescence (B, D, G, I, K, N), and brightfield/fluorescence merged images (E, H, L, O). FF, Fin Fold; ED, Endoskeletal Disc; A, Anterior; P, Posterior; D, Dorsal; V, Ventral. Scale bars: 200 µm in B, I; 50 µm in C–H, J–O.

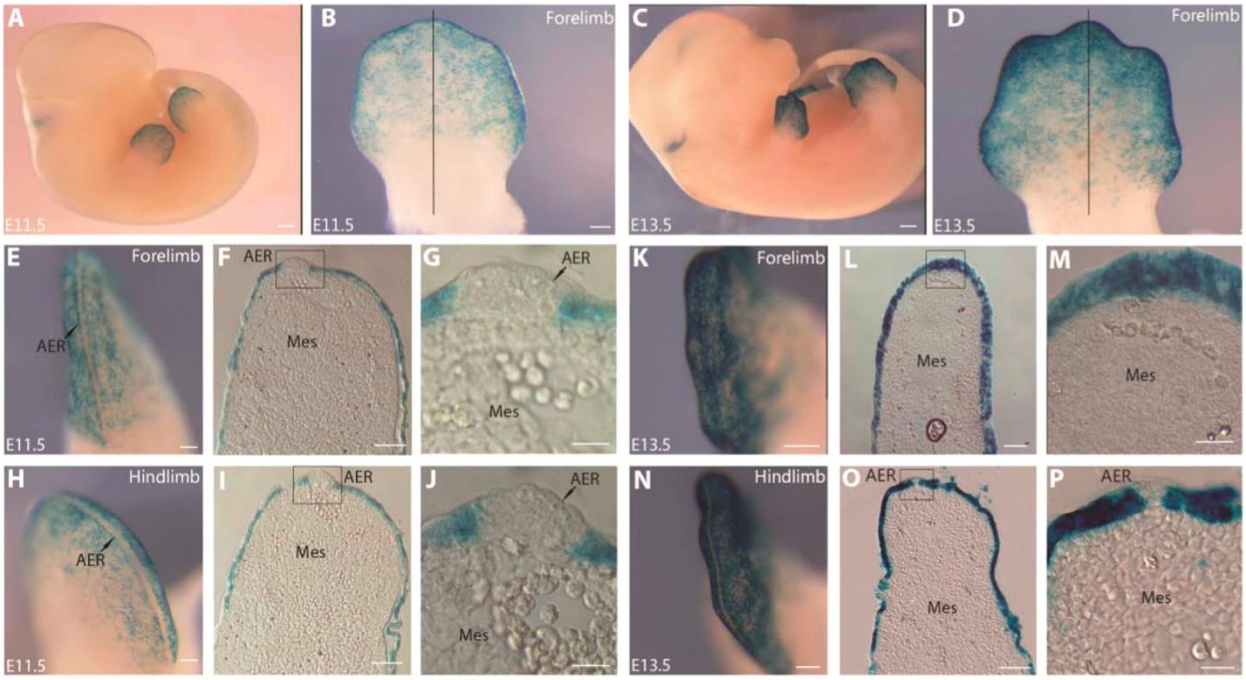

Figure 2.2. The zebrafish 2P element drives *lacZ* reporter expression in the ectodermal cells only of the mouse fore- and hindlimb buds. (A, B, E–J) E11.5, (C, D, K–P) E13.5 *Tg*(*2Pand1::LacZ*) transgenic mouse embryos. Fore- (B, E–G, K–M) and hindlimb (D, H–J, N–P) buds are presented for E11.5 and E13.5. Ventral close up of forelimb at E11.5 (B) and E13.5 (D). Limbs were sectioned along the proximal distal axis indicated by the black line (B, D). Note the presence of reporter expression in the ectodermal cells only. Note both limbs show an absence of expression in the AER at E11.5 (indicated by the yellow arrowheads) (E–G, H–J). In contrast, at E13.5, *lacZ* expression is present in the entire distal ectoderm of the forelimb bud (K–M), visualizing AER regression. Cross sections of fore- (F–G, L–M) and hindlimb (I-J, O–P) bud reveal an absence of reporter expression in the mesenchymal tissues at all stages. Note: Brain expression (A, C) is limited to this transgenic line, and is likely ectopic due to the transgene insertion site. AER, Apical Ectodermal Ridge, Mes, Mesenchyme. Scale bars: 1000 µm in A, D; 320µm in B, D; 200 µm in E, H; 400 µm in K; 500 µm in N; 100 µm in F, I; 30 µm in G, J; 100 µm in L; 60 µm in O; 50 µm in M; 30 µm in P.

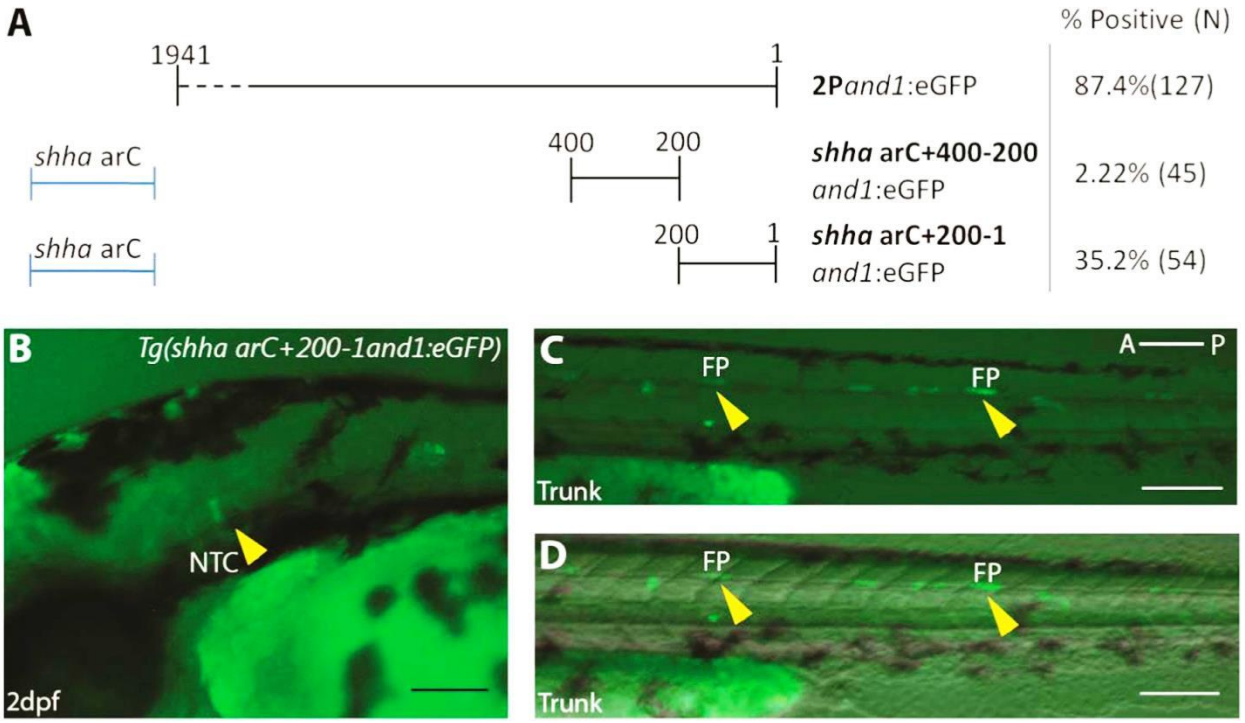

Figure 2.3. Upstream fragment 200-1*and1* contains a promoter. (A) Identification of the promoter region. Two 200 b.p. regions (200-1*and1* and 400-200*and1*) were tested for promoter activity using the *shha* ar-C enhancer region. % Positive represents percentage of embryos with notochord or floor plate expression, N=Number of total viable injected embryos. (B–D) transient expression of *Tg*(*shha ar-C+200-1and1:eGFP)* in embryos at 2 d.p.f. Notochord (B) and floor plate cells (C, D) (indicated by yellow arrowheads) display reporter expression at 2 d.p.f. Fluorescence (B, C), and brightfield/fluorescence merged images (D). NTC, Notochord; FP, Floor Plate; A, Anterior; P, Posterior. Scale bars: 200 µm in B–F.

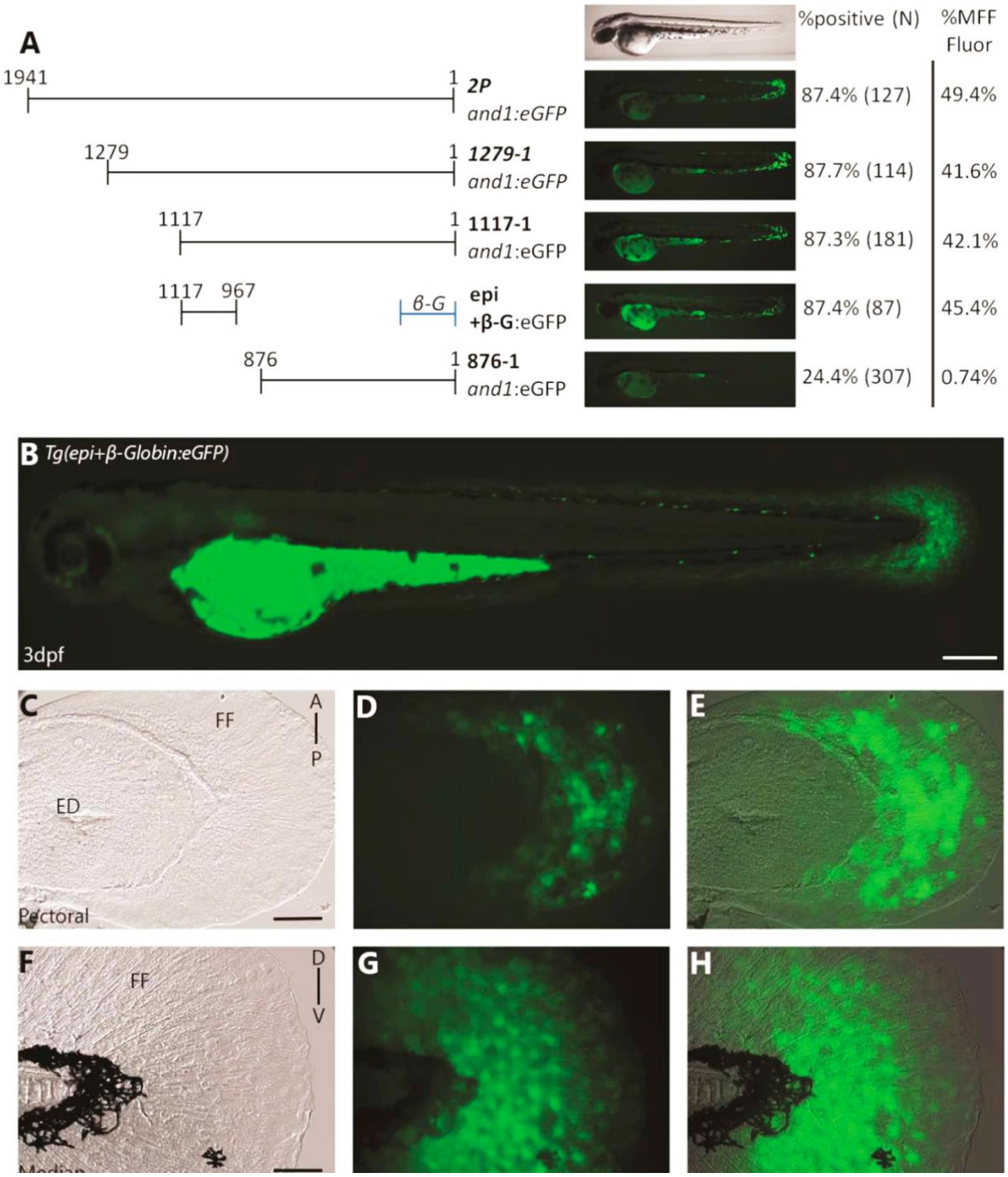

Figure 2.4. Epi fragment contains an ectodermal enhancer sufficient to recapitulate *and1* expression in epithelium of embryonic fin folds. (A) Analysis of truncated *2Pand1* reporter constructs. Constructs were tested for ectodermal enhancer activity. Percentage of eGFP positive

embryos during injections, and an average % MFF transient fluorescence coverage are presented on the right (N=Number of total viable injected embryos). Note that the 150 b.p. region 1117-967*and1* mimics transient ectodermal enhancer activity of full 2P*and1* element, when tested with the *β-globin* minimal promoter. Note the reduced percentages for *Tg(876and1:eGFP)* suggesting the absence of the ectodermal enhancer. (B–H) *Tg*(*epi+β-globin:eGFP*) transgenic reporter line at 3 d.p.f. Median (F–H) and pectoral fin fold (C–E) display reporter expression in the ectodermal cells only. Absence of mesenchymal expression is best observed using confocal microscopy. Brightfield (C, F), fluorescence (B, D, G), and brightfield/fluorescence merged images (E, H). ED, Endoskeletal Disc; FF, Fin Fold; A, Anterior; P, Posterior; D, Dorsal; V, Ventral. Scale bars: 200 μm in B; 50 μm in C–H.

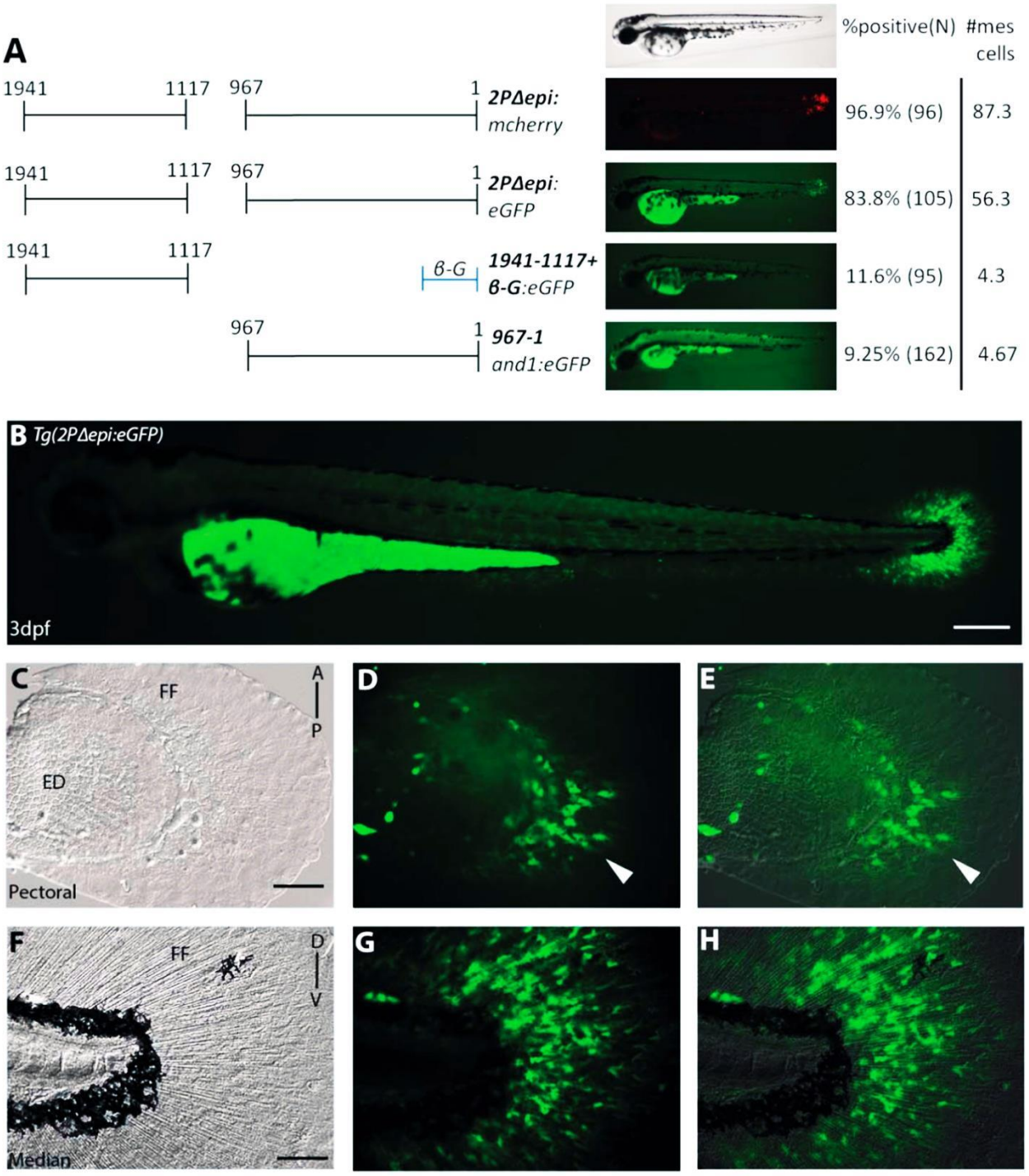

Figure 2.5. Multiple mesenchymal enhancers exist and are required simultaneously to recapitulate *and1* expression in mesenchymal cells of embryonic fin folds. (A) Analysis of truncated *2Pand1* reporter constructs. Constructs were tested for mesenchymal enhancer activity.

Percentage of eGFP positive embryos during injections, and an average number of mesenchymal cells are presented on the right (N=Number of total viable injected embryos). Note the reduced percentages with *Tg(1941-1117+β-globin:eGFP)* and *Tg(967and1:eGFP)*constructs suggesting both fragments are required for full mesenchymal expression. (B–H) T*g*(*2P*Δ*epi:eGFP*) transgenic reporter line at 3 d.p.f. Median (F–H) and pectoral fin fold (C–E) display reporter expression in the mesenchymal cells only using the 1941-1117*and1* and 967and1 fragments simultaneously. Note the higher number of eGFP-positive cells in the posterior half of the pectoral fin (D), indicated by the white arrowhead. Brightfield (C, F), fluorescence (B, D, G), and brightfield/fluorescence merged images (E, H). ED, Endoskeletal Disc; FF, Fin Fold; A, Anterior; P, Posterior; D, Dorsal; V, Ventral. Scale bars: 200 µm in B; 50 µm in C–H.

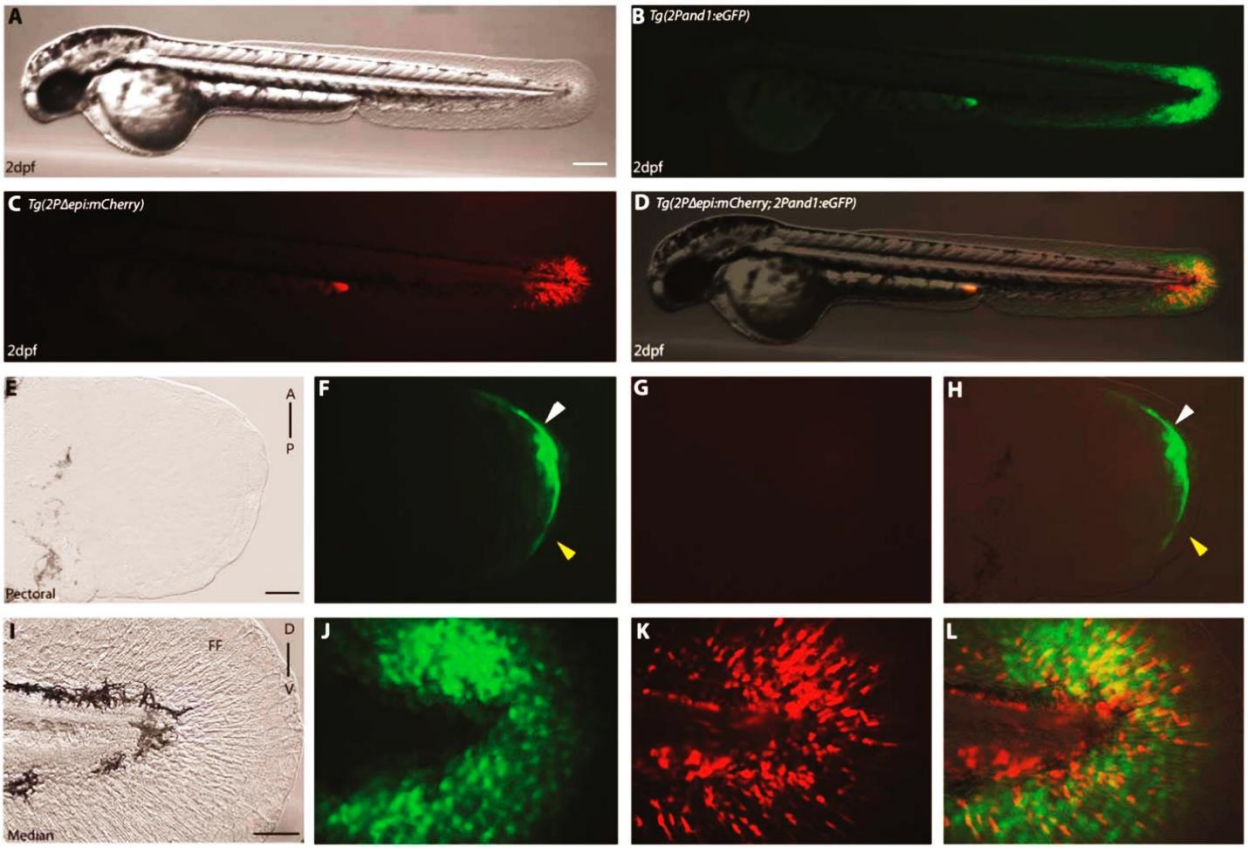

Figure 2.6. Reporter expression begins in ectodermal cells prior to mesenchymal cells in the pectoral fin folds. (A–L) double transgenic reporter line *Tg(2Pand1:eGFP; 2PΔepi:mCherry)* at 2 d.p.f., allowing visualization of the ectodermal- and mesenchymal-expressing cells simultaneously. Despite the presence of mesenchymal expression within *Tg(2Pand1:eGFP)*, this line was used to assess ectodermal reporter expression to ensure all potential *cis*-regulatory elements are included. *Tg(2Pand1:eGFP)* reporter expression in ectodermal cells and mesenchymal cells are presented in green (B, F, J), *Tg(2PΔepi:mCherry)* reporter expression in mesenchymal cells are presented in red (C, G, K). Ectodermal and mesenchymal images are merged (D, H, L) to visualize ectodermal eGFP and mesenchymal mCherry expression simultaneously. Reporter expression in ectodermal (J, L) and mesenchymal (K, L) cells is present in the median fin fold at 2 d.p.f. In contrast, the pectoral fin fold displays reporter expression in

the epithelium only at 2 d.p.f. (indicated by the white arrowheads) (F–H). Note again, the absence of reporter expression in the early pectoral fin fold (indicated by the yellow arrowheads) (F, H). Tip of the yolk sac extension displays autofluorescence (B–D). A, Anterior; P, Posterior; D, Dorsal; V, Ventral. Scale bars: 300 μm in A–D; 30 μm in E–H; 50 μm in I–L.

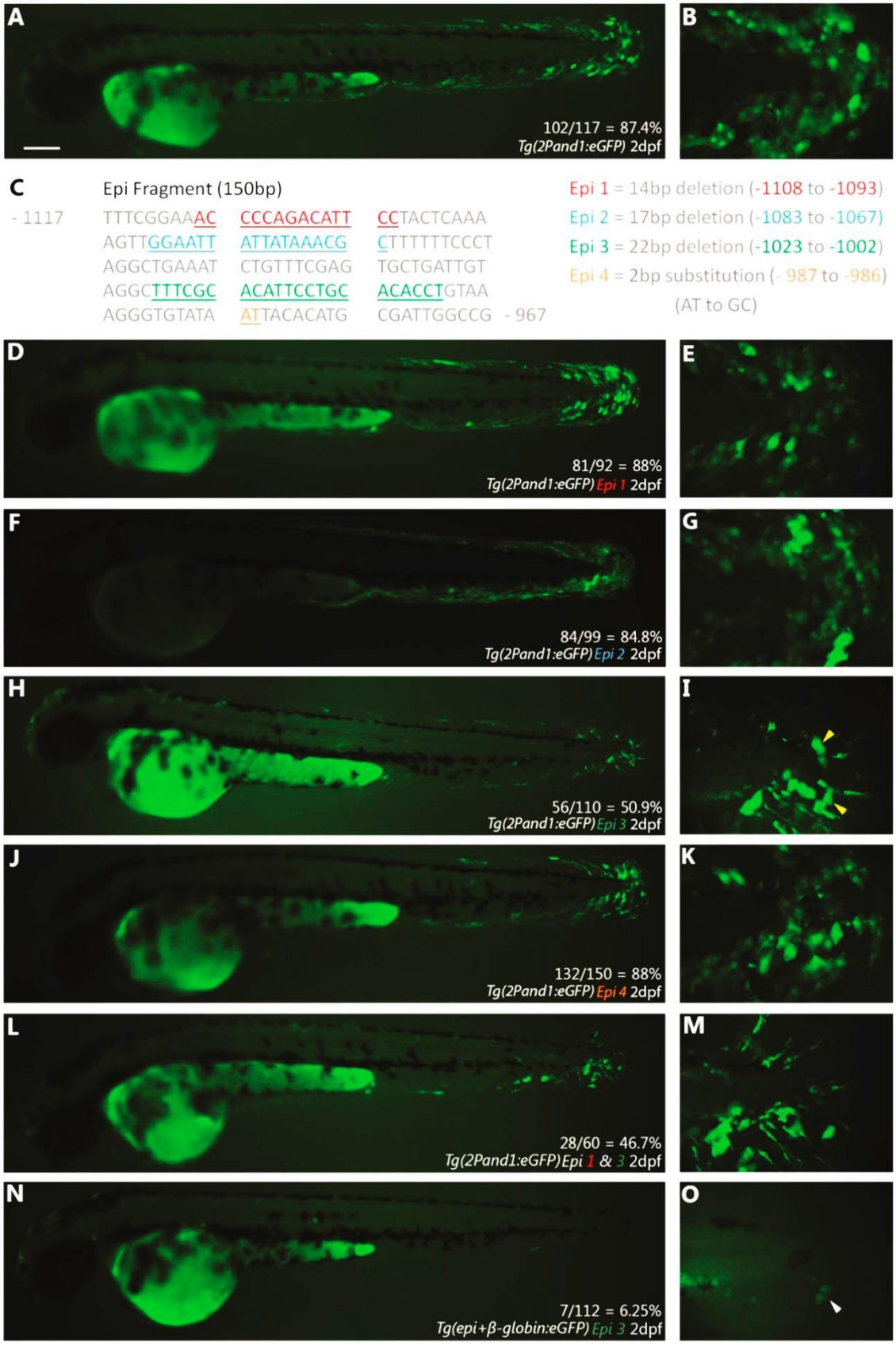
A
102/117 = 87.4%
Tg(2Pand1:eGFP) 2dpf
B
C
Epi Fragment (150bp)
- 1117
TTTCGGAAAC CCCAGACATT CCTACTCAAA
AGTTGGAATT ATTATAAACG CTTTTTTCCCT
AGGCTGAAAT CTGTTTCGAG TGCTGATTGT
AGGCTTTCGC ACATTCCTGC ACACCTGTAA
AGGGTGTATA ATTACACATG CGATTGGCCG - 967
Epi 1 = 14bp deletion (-1108 to -1093)
Epi 2 = 17bp deletion (-1083 to -1067)
Epi 3 = 22bp deletion (-1023 to -1002)
Epi 4 = 2bp substitution (- 987 to -986)
(AT to GC)
D
81/92 = 88%
Tg(2Pand1:eGFP) Epi 1 2dpf
E
F
84/99 = 84.8%
Tg(2Pand1:eGFP) Epi 2 2dpf
G
H
56/110 = 50.9%
Tg(2Pand1:eGFP) Epi 3 2dpf
I
J
132/150 = 88%
Tg(2Pand1:eGFP) Epi 4 2dpf
K
L
28/60 = 46.7%
Tg(2Pand1:eGFP) Epi 1 & 3 2dpf
M
N
7/112 = 6.25%
Tg(epi+β-globin:eGFP) Epi 3 2dpf
O

Figure 2.7. Epi site 3 contains important sequences for ectodermal reporter expression in embryonic fin folds. (A, B) unmutated *Tg(2Pand1:eGFP)* transient expression at 2 d.p.f. The rate of GFP positive embryos is indicated (A), and higher magnification of the median fin fold of representative fish is shown (B). (C) Four different mutations were tested within the Epi fragment for ectodermal enhancer activity to identify candidate ectodermal enhancer sites. Mutation locations are colour coded, and the mutation details are described on the right. Only embryos with visible ectodermal expression were counted as "GFP positive". (D–O) GFP expression observed with the mutated constructs. Epi mutations 1 (D,E), 2 (F,G), and 4 (J,K) display similar rates of GFP positive embryos and levels of ectodermal expression in the median fin fold compared to unmutated *Tg(2Pand1:eGFP)* injections. Epi mutation 3 (H, I) yields a decreased rate of GFP positive embryos (50.9%), and lower levels of ectodermal expression in the median fin fold (indicated by yellow arrowheads) (I). Epi mutations 1 and 3 tested in combination (L, M) yield no synergistic effects. (N–O) Epi 3 mutation was tested in the *Tg(epi+β-globin:eGFP)* construct and displayed a drastic decrease in GFP positive embryos (6.25%), and a nearly complete loss of ectodermal reporter expression (indicated by the white arrowhead) (O). Scale bars: 200 µm in A, D, F, H, J, L, N; 20 µm in B, E, G, I, K, M, O.

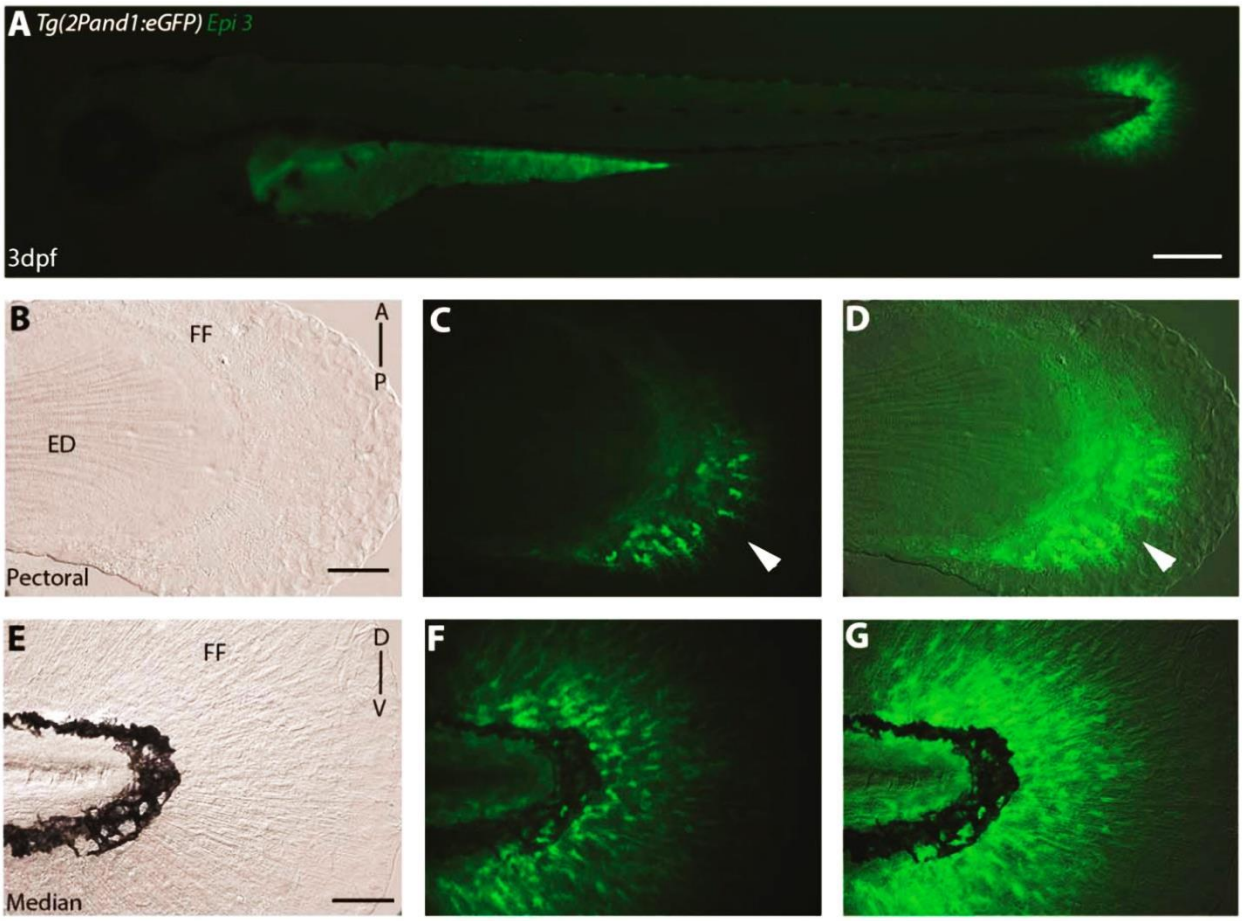

Figure 2.8. Epi site 3 required for epithelial reporter expression in *Tg(2Pand1:eGFP)*. (A–G) 3 d.p.f. *Tg(2Pand1:eGFP) epi site 3* transgenic reporter line. Ectodermal expression is completely lost with the removal of the epi site 3 23 b.p. fragment (A–G). Median (E–G) and pectoral fin fold (B–D) display reporter expression in the mesenchymal cells identical to *Tg(2PΔepi:eGFP)* transgenic line. Note the higher number of eGFP-positive cells in the posterior half of the pectoral fin fold (B, C). Brightfield (B, E), fluorescence (A, C, F), and brightfield/fluorescence merged images (D, G). ED, Endoskeletal Disc; FF, Fin Fold; A, Anterior; P, Posterior; D, Dorsal; V, Ventral. Scale bars: 200 µm in A; 50 µm in B–G.

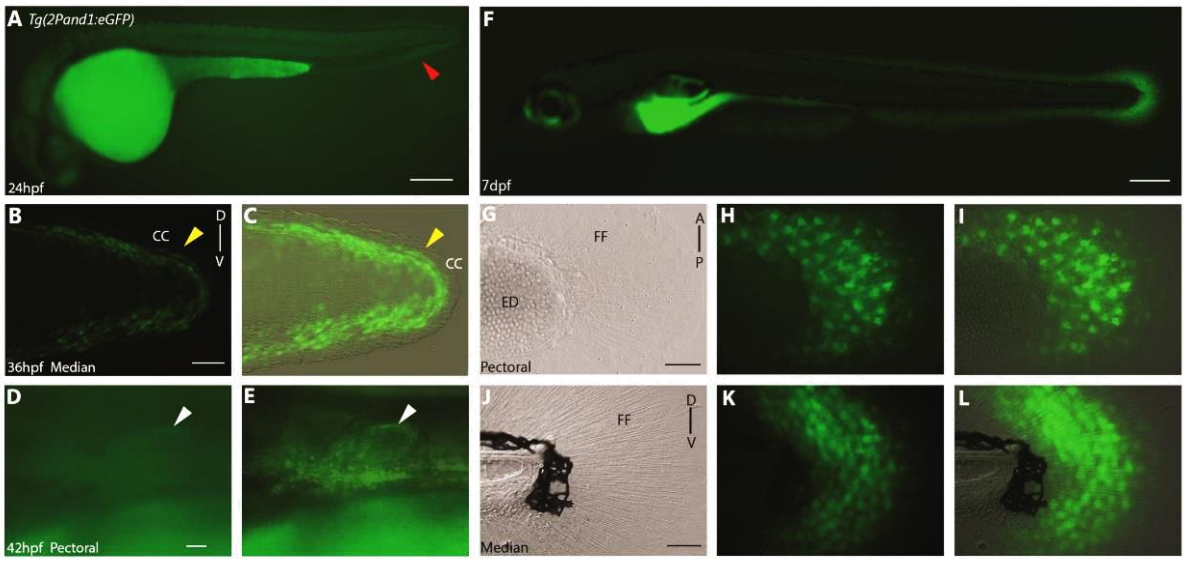

Figure 2.9. A 2 kb genomic fragment upstream of the first exon of and1 (2P) is sufficient to recapitulate endogenous *and1* expression zebrafish embryonic fin folds.

24 h.p.f., **(B, C)** 36 h.p.f, **(D-E)** 42 h.p.f, **(F-L)** 7d.p.f. *Tg(2Pand1:eGFP)* transgenic reporter line. Median fin fold displays reporter expression in the ectodermal cells beginning around 24 h.p.f. (indicated by the red arrowhead) (A). The pectoral fin fold displays reporter expression in the ectodermal cells beginning around 42 h.p.f. (indicated by the white arrowheads) (D-E). 7 d.p.f. transgenic larvae display reporter expression in both ectodermal and mesenchymal cells (F-L). Note the absence of reporter expression in the cleft cells of the median fin fold at 36 h.p.f. (indicated by yellow arrowheads) (B, C). Reminder, mesenchymal GFP expression is masked by ectodermal GFP expression, refer to Fig. 2.10 or Mov. S1. Brightfield (G, J), fluorescence (A, B, D, F, H, K), and brightfield/fluorescence merged images (C, E, I, L). CC, Cleft Cells; FF, Fin Fold; ED, Endoskeletal Disc; A, Anterior; P, Posterior; D, Dorsal; V, Ventral. Scale bars: 200µm in A; 50µm in B, C; 200µm in F; 50µm in G-I, J-L.

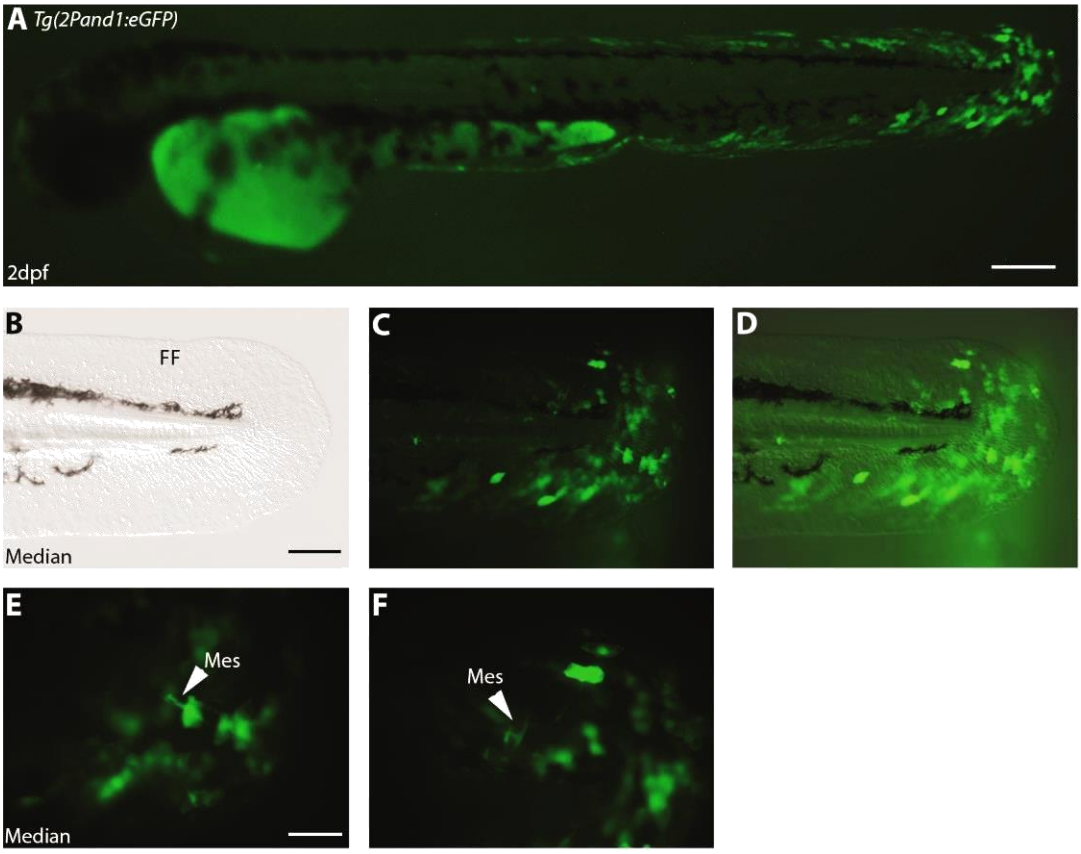

Figure 2.10. Mosaic ectodermal expression in *Tg(2Pand1:eGFP)* injected embryos reveal mesenchymal expression. (A-F) *Tg(2Pand1:eGFP)* transient expression in injected embryos at 2 d.p.f.. Following injection of a DNA construct in zebrafish embryo, expression of the transgene is always mosaic. This allows to visualize GFP expression in some mesenchymal cells (indicated by white arrowheads) due to the mosaic GFP expression in the overlaying ectodermal cells (E, F). Brightfield (B), fluorescence (A, C, E, F), and brightfield/fluorescence merged images (D). FF, Fin fold; Epi , Ectodermal cells; Mes, Mesenchymal cells. Scale bars: 200µm in A; 100µm in B-D; 50µm in E, F.

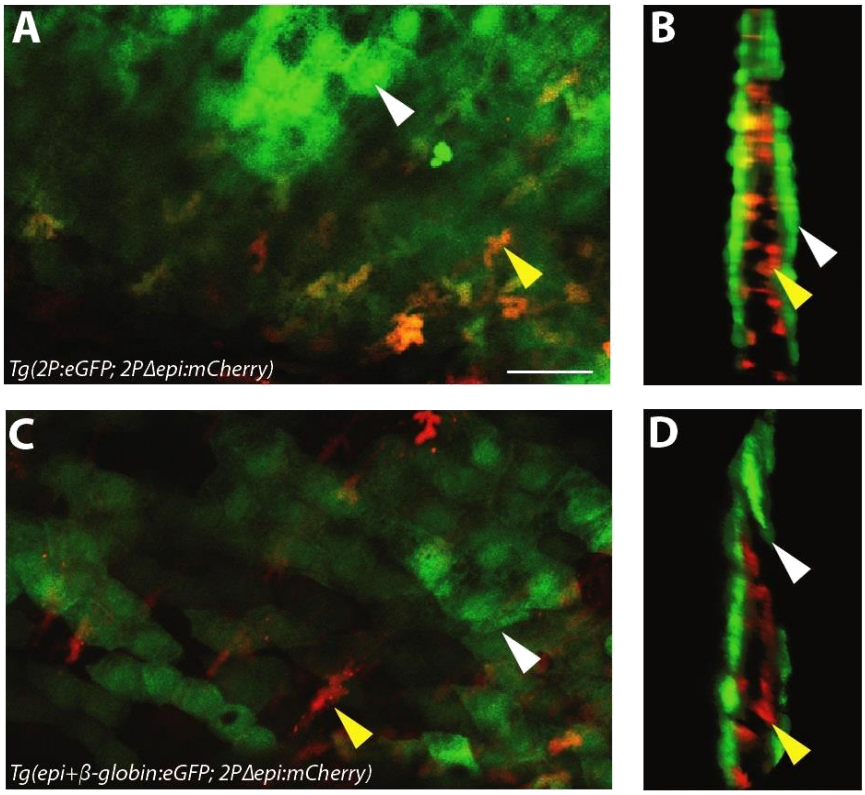

Figure 2.11. Tg(2Pand1:eGFP) displays epithelial and mesenchymal reporter expression, Tg(epi+β-globin:eGFP) displays only epithelial reporter expression. (A-B) *Tg(2P:eGFP; 2PΔepi:mCherry)* and **(C-D)** *Tg(epi+β-globin:eGFP; 2PΔepi:mCherry)* 3 d.p.f. median fin fold using confocal microscopy. Z-stack (A, C) and 3D reconstruction (B, D) images are shown. *Tg(2P:eGFP; 2PΔepi:mCherry)* double transgenic line displays eGFP in both ectodermal and mesenchymal cells (A-B). Note the orange/yellow colour of all mesenchymal cells, indicating co-expression of eGFP and mCherry (A-B). *Tg(epi+β-globin:eGFP; 2PΔepi:mCherry)* double transgenic line displays eGFP in ectodermal cells only (C-D). Note the red colour of all mesenchymal cells, indicating absence of any eGFP expression (C-D). Representative ectodermal cells are highlighted by the white arrow (A-D), and representative mesenchymal cells are highlighted by the yellow arrow (A-D). Scale bars: 25µm in A-D.

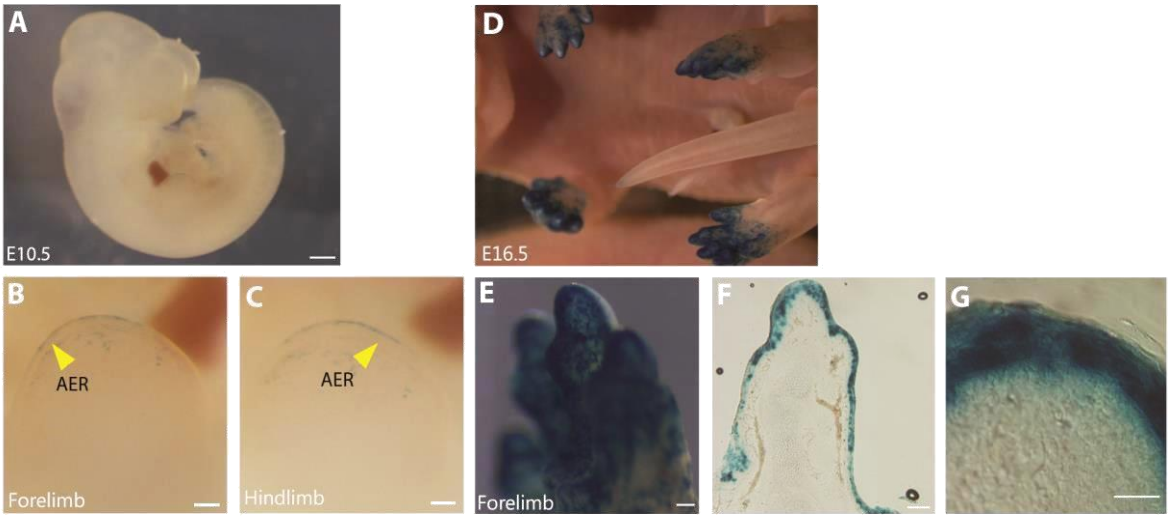

Figure 2.12. The 2P*and1* regulatory element is driving reporter expression in mouse limb ectoderm. (A-C) E10.5 and **(D-G)** E16.5 *Tg(2Pand1::LacZ)* transgenic mouse embryos. Whole embryos are presented at E10.5, and E16.5 (A, D). Whole limbs are included for E10.5, and E16.5 (B-C, E), sections are presented for E16.5 (F-G). Reporter expression is visible in the distal ectoderm of the fore- and hindlimb beginning at E10.5, with the exception of the AER (indicated by the yellow arrowheads) (A-C). By E16.5, reporter expression is presented in the entire distal ectoderm (D-G). Note the absence of reporter expression in the mesenchymal tissues at all developmental stages (B-C, F-G). AER, Apical Ectodermal Ridge. Scale bars: 1000µm in A, D; 200µm in B, C; 200µm in E; 200µm in F; 50µm in G.

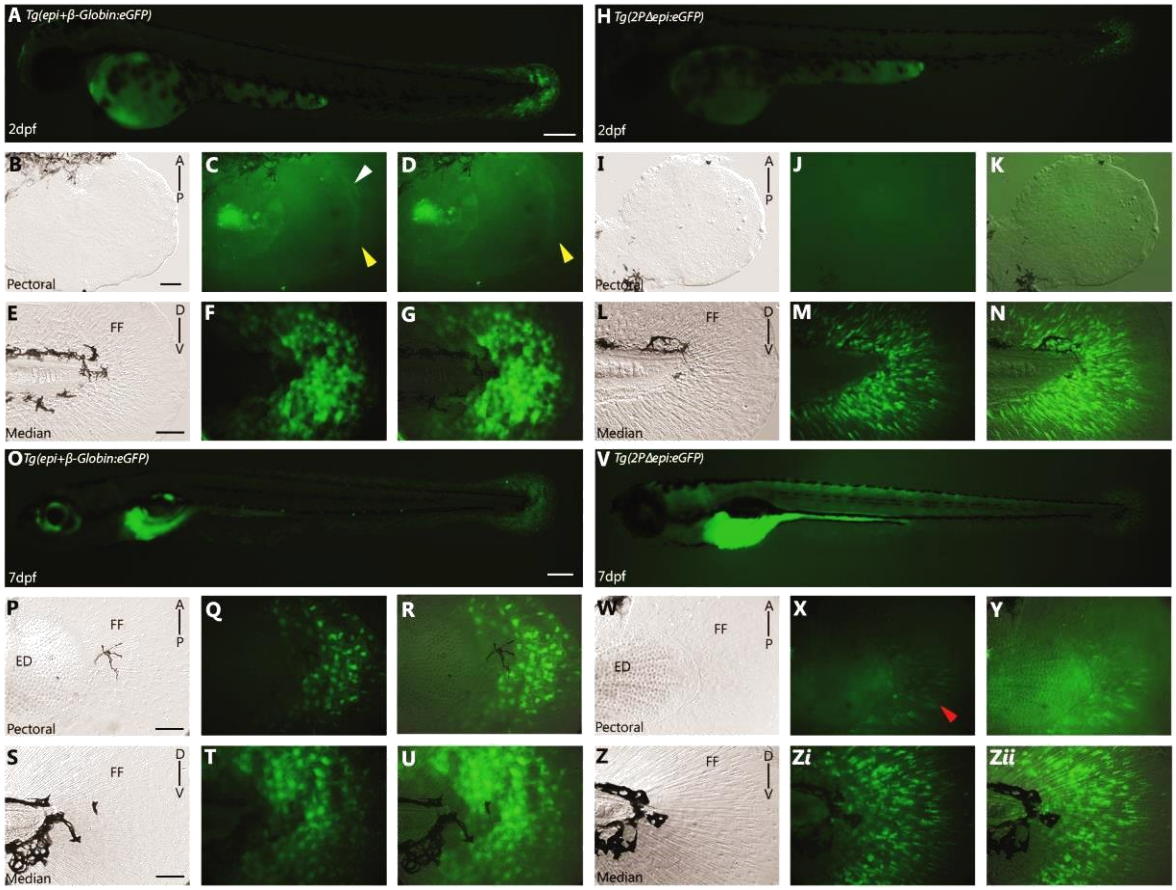

Figure 2.13. ***Tg(epi+β-globin:eGFP)*** **and** ***Tg(2PΔepi:eGFP)*** **together recapitulate endogenous** ***and1*** **expression zebrafish embryonic fin folds. (A-G)** 2 d.p.f., **(O-U)** 7 d.p.f. *Tg(epi+β-globin:eGFP)* transgenic reporter line. **(H-N)** 2 d.p.f , **(V-*Zii*)** 7 d.p.f *Tg(2PΔepi:eGFP)* transgenic reporter line. Ectodermal (E-G) and mesenchymal (L-M) expression is present in the median fin fold at 2 d.p.f.. Only ectodermal expression is present in the pectoral fin fold at 2 d.p.f. (indicated by the white arrowhead) (C). Note again, the absence of ectodermal expression in the early pectoral fin fold (indicated by the yellow arrowhead) (B-D). Ectodermal (P-U) and mesenchymal (W-Z*ii*) reporter expression is present in the pectoral and median fin fold at 7 d.p.f.. Together these two lines recapitulate *and1* expression. Note the stronger mesenchymal expression in the posterior half of the pectoral fin fold (indicated by the red arrowhead) (X).

Brightfield (B, E, I, L, P, S, W, Z), fluorescence (A, C, F, H, J, M, O, Q, T, V, X, Z*i*), and brightfield/fluorescence merged images (D, G, K, N, R, U, Y, Z*ii*). FF, Fin Fold; ED, Endoskeletal Disc; A, Anterior; P, Posterior; D, Dorsal; V, Ventral. Scale bars: 200µm in A, H, O, V; 30µm in B-D, I-K; 50µm in P-R, W-Y, E-G, L-N, S-U, Z-Z*ii*.

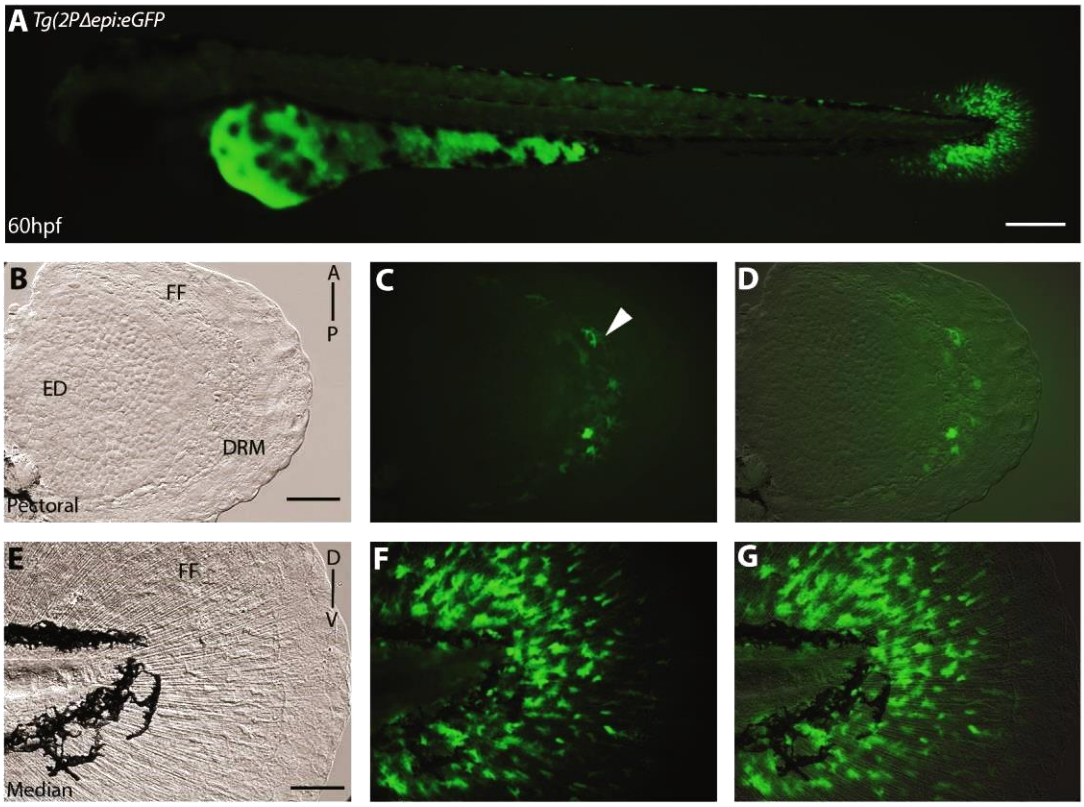

Figure 2.14. Symmetrical GFP-expressing cells in distal rim mesenchyme at 60 h.p.f. (A-G) 60 h.p.f. in *Tg(2PΔepi:eGFP)* transgenic reporter line. Mesenchymal expression is present in both the median fin fold (E-G) and the pectoral fin fold (B-D) at 60 h.p.f.. The distal rim mesenchyme of the pectoral fin bud symmetrical reporter expression (C-D). Brightfield (B, E), fluorescence (C-F), and brightfield/fluorescence (D-G) merged images. FF, Fin Fold; ED, Endoskeletal Disc, A, Anterior; P, Posterior; D, Dorsal; V, Ventral. Scale bars: 200µm in A, 50µm in B-G.

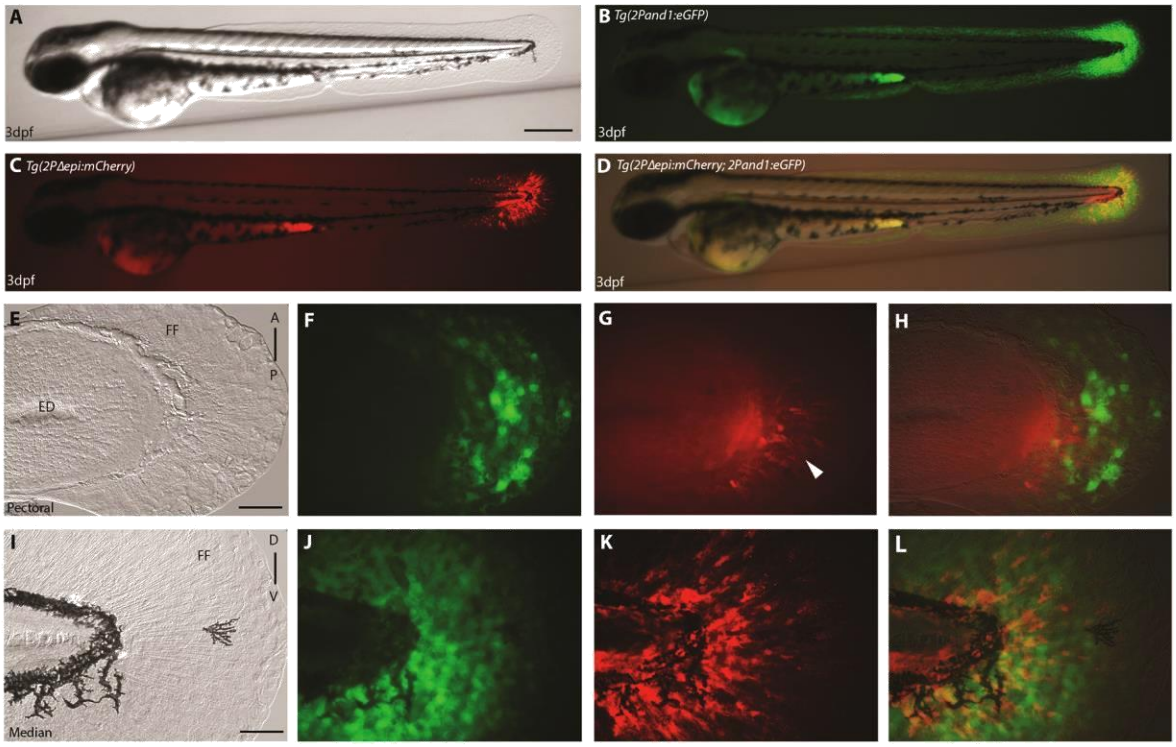

Figure 2.15. Reporter expression present in ectodermal and mesenchymal tissues in 3 d.p.f median and pectoral fin folds. (A-L) Double transgenic reporter line *Tg(2Pand1:eGFP; 2PΔepi:mCherry)* at 3 d.p.f., allowing visualization of the ectodermal- and mesenchymal-expressing cells simultaneously. Despite the presence of mesenchymal expression within *Tg(2Pand1:eGFP)*, this line was used to assess ectodermal reporter expression to ensure all potential *cis*-regulatory elements are included. *Tg(2Pand1:eGFP)* reporter expression in ectodermal cells and mesenchymal cells are presented in green (B, F, J), *Tg(2PΔepi:mCherry)* reporter expression in mesenchymal cells are presented in red (C, G, K). Ectodermal and mesenchymal images are merged (D, H, L). Ectodermal and mesenchymal images are merged (D, H, L) to visualize ectodermal eGFP and mesenchymal mCherry expression simultaneously. By 3 d.p.f, ectodermal and mesenchymal expression is present in the median and pectoral fin fold (A-L). Note the stronger mesenchymal expression in the posterior half of the pectoral fin

fold (indicated by the white arrowhead) (G). Tip of the yolk sac extension displays autofluorescence (B-D). ED, Endoskeletal Disc; FF, Fin Fold; A, Anterior; P, Posterior; D, Dorsal; V, Ventral. Scale bars: 300µm in A-D, 50µm in E-L.

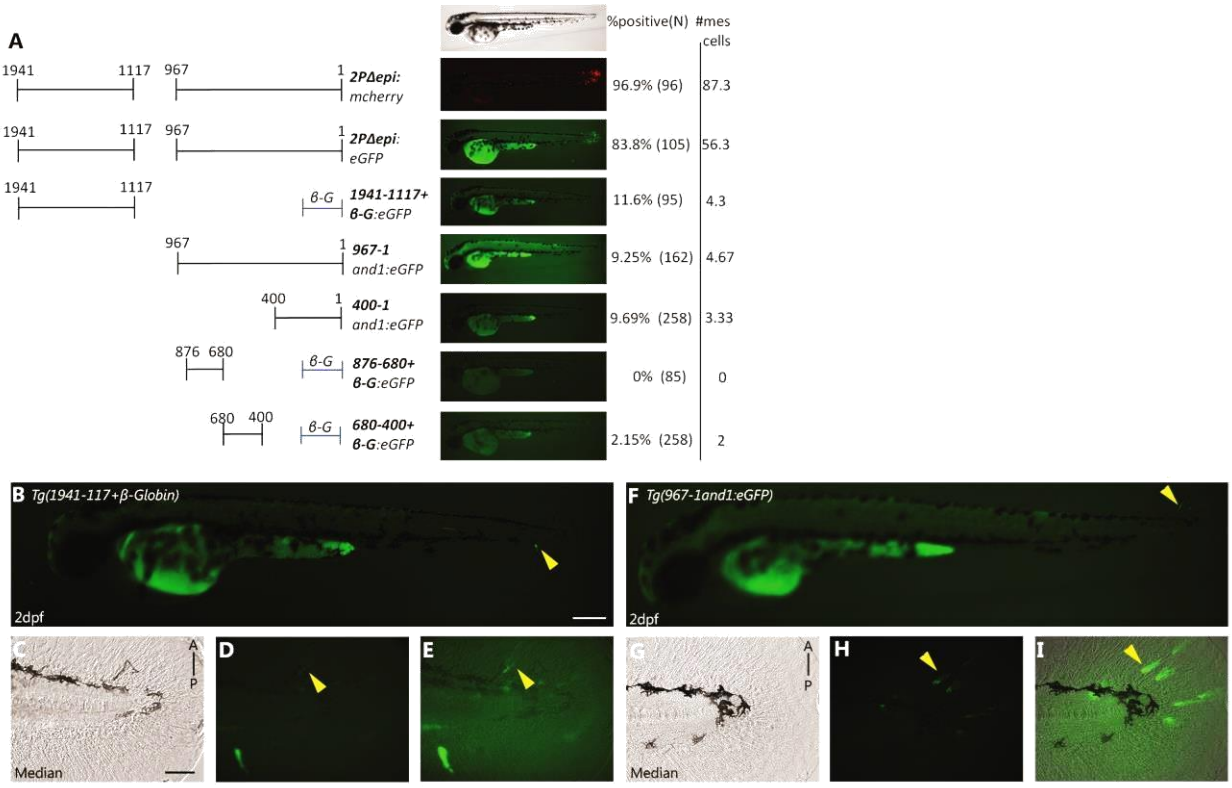

Figure 2.16. Full analysis for mesenchymal enhancer activity: multiple mesenchymal enhancers exist and are required simultaneously to recapitulate *and1* mesenchymal cells in embryonic fin folds. (**A**) Transient expression analysis of truncated *2Pand1* reporter constructs in injected embryos. Constructs were tested for mesenchymal enhancer activity. Percentage of GFP positive embryos during injections, and an average number of mesenchymal cells are presented on the right (N = Number of total viable injected embryos). Note the reduced percentages of GFP positive embryos with the *Tg(1941-1117+ β-globin:eGFP)* and *Tg(967-1and1:eGFP)* constructs suggesting that both fragments are required for full mesenchymal expression (A). Note the even more reduced percentages obtained with smaller fragments *Tg(400-1and1:eGFP), Tg(876-680+ β-globin:eGFP), Tg(680-400+β-globin:eGFP)* (A). (**B-E**) Transient expression of *Tg(1941-1117and1:eGFP)* at 2 d.p.f. **(F-I)** Transient expression of *Tg(967-1and1:eGFP)* at 2 d.p.f. Neither fragment is capable of mimicking the expression of *Tg(2PΔepi:eGFP)***.** Note the very

small amount of reporter expressing mesenchymal cells (indicated by yellow arrowheads) (B, D-E, F, H-I). Brightfield (C, G), fluorescence (B, D, F, H), and brightfield/fluorescence merged images (E, I). A, Anterior; P, Posterior; D, Dorsal; V, Ventral. Scale bars: 200µm in A-E; 50µm in B-D, F-H.

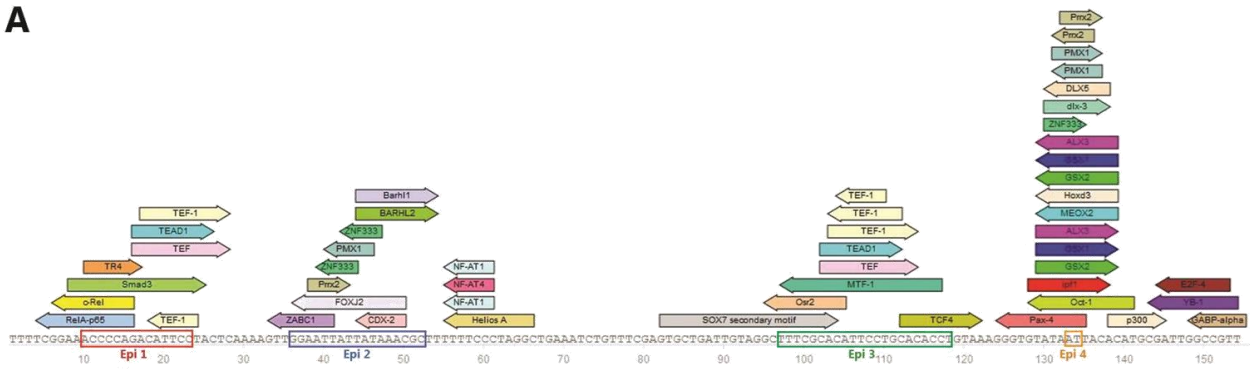

Figure 2.17. *In silico* analysis of the 150 b.p. Epi fragment for transcription factor binding domain identification. (A) All putative binding domains were identified via TRANSFAC transcription factor identification software. Basepair positions are indicated below the sequence. Epi sites 1-4 are indicated by colour coded boxes (A).

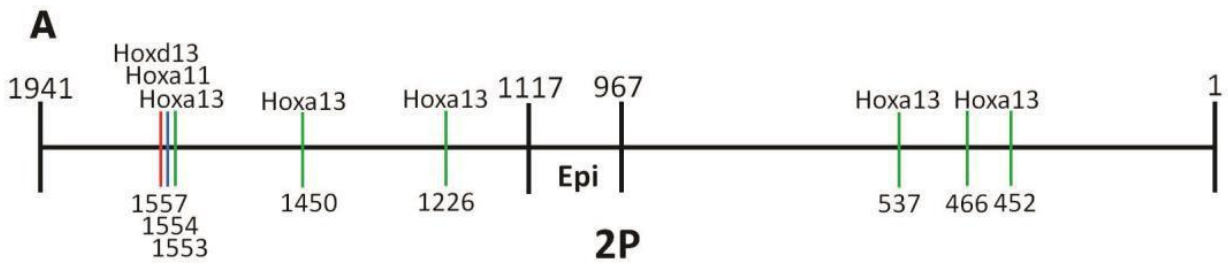

Figure 2.18. 2P fragment contains 6 putative hoxa13, 1 hoxa11, and 1 hoxd13 consensus binding domains. (A) Schematic representation of 2P fragment showing distribution of hoxa13, hoxa11 and hoxd13 putative binding domains. Hoxa13 binding domains are highlighted with a green line, hoxa11binding domains are highlighted with a blue line, and hoxd13 binding domains are highlighted with a red line. Basepair locations of each site are mentioned below. All putative binding domains were identified via TRANSFAC transcription factor identification software.

CHAPTER 3

Effects of fin fold mesenchyme ablation on fin development in zebrafish

3.1. Notes on Chapter

The present chapter has been published in PLOS ONE as per the following citation:

Lalonde RL & Akimenko MA. Effects of fin fold mesenchyme ablation on zebrafish fin development. PLoS ONE. 2018; 13(2): e0192500.

Author contributions

R.L.L. performed all experimental aspects of this paper, analysed the data, and wrote the paper. R.L.L. designed and created the protocols for long-term MTZ treatments on larval zebrafish. R.L.L. and M.A.A. conceived the project, reviewed and edited the manuscript.

Project Introduction & Objectives

Contributions of fin fold mesenchyme to larval and adult zebrafish fin development; implications for fin dermal bone loss

Fin fold mesenchyme has been shown to contribute to fin ray fibroblasts and osteoblasts suggesting their proper migration may be crucical for fin ray development. These cells may also be important for embryonic fin fold and actinotrichia maintenance as they express and secrete Actinodin proteins. Defects in fin fold mesenchyme migration have therefore been proposed as a mechanism of fin dermal bone loss during the fin-to-limb transition.

Objective: Observe the effects of fin fold mesenchyme ablation on actinotrichia, fin fold, and fin ray formation/maintenance

We predict in the absence of fin mesenchyme, actinotrichia, fin fold, and fin ray formation will be impaired. To test this, we used the NTR/MTZ system to selectively ablate fin fold mesenchyme throughout embryonic and larval development. We first examined the formation and maintenance of the fin fold and actinotrichia to shed light on the contributions of these cells to embryonic fin development. We then developed a system to partially ablate these cells until late larval stages to observe the effects on fin ray formation.

3.2. Abstract

The evolution of the tetrapod limb involved an expansion and elaboration of the endoskeletal elements, while the fish fin rays were lost. Loss of fin-specific genes, and regulatory changes in key appendicular patterning genes have been identified as mechanisms of limb evolution, however their contributions to cellular organization and tissue differences between fins and limbs remains poorly understood. During early larval fin development, *hoxa13a/hoxd13a*-expressing fin fold mesenchyme migrate through the median and pectoral fin along actinotrichia fibrils, non-calcified skeletal elements crucial for supporting the fin fold. Fin fold mesenchyme migration defects have previously been proposed as a mechanism of fin dermal bone loss during tetrapod evolution as it has been shown they contribute directly to the fin ray osteoblast population. Using the nitroreductase/metronidazole system, we genetically ablated a subset of *hoxa13a/hoxd13a*-expressing fin fold mesenchyme to assess its contributions to fin development. Following the ablation of fin fold mesenchyme in larvae, the actinotrichia are unable to remain rigid and the median and pectoral fin folds collapse, resulting in a reduced fin fold size. The remaining cells following ablation are unable to migrate and show decreased *actinodin1* mesenchymal reporter activity. Actinodin proteins are crucial structural component of the actinotrichia. Additionally, we show a decrease in *hoxa13a*, *hoxd13a*, *fgf10a* and altered *shha*, and *ptch2* expression during larval fin development. A continuous treatment of metronidazole leads to fin ray defects at 30dpf. Fewer rays are present compared to stage-matched control larvae, and these rays are shorter and less defined. These results suggest the targeted *hoxa13a/hoxd13a*-expressing mesenchyme contribute to their own successful migration through their contributions to actinotrichia. Furthermore, due to their fate as fin ray osteoblasts,

we propose their initial ablation, and subsequent disorganization produces truncated fin dermal bone elements during late larval stages.

3.3. Introduction

The evolution of limbs was a hallmark in vertebrate innovation. No longer restricted to aquatic environments, tetrapods rapidly radiated and conquered their new terrestrial niches (Ahlberg & Clack 2006; Ahlberg & Milner 1994; Daeschler et al. 2006). Fore- and hindlimbs evolved from the pectoral and pelvic fins, respectively, of lobe-finned sarcopterygian fish (George & Blieck 2011; Long et al. 2006; Shubin et al. 1997). The fossil record has yielded useful transitional tetrapod species to investigate changes in bone morphology crucial for the evolution of the limb from the sarcopterygian fish fin. Expansion and elaboration of the appendicular endochondral bone resulted in the three distinct limb regions common to all tetrapods: the stylopod, zeugopod, and the autopod (Ahlberg & Clack 2006; Schneider & Shubin 2013; Shubin et al. 2006). Simultaneously, the fin rays, present in all extant fish were gradually reduced before being completely lost from the tetrapod limb (Ahlberg & Clack 2006; Shubin et al. 2006). While gene regulation differences are being identified as mechanisms of limb evolution, more information is required to link the contributions of these regulatory differences to changes at the level of cellular organization and tissue patterning during this process.

By examining early fin and limb development we can identify diverging developmental or molecular processes that may have contributed to the expansion and reduction of appendicular endochondral and dermal bone, respectively. Early fin and limb outgrowth is initiated and maintained by an FGF feedback loop between the apical ectodermal ridge (AER) and the underlying mesenchyme (Grandel & Shulte-Merker 1998; Johnson & Tabin 1997; Lewandoski et al. 2000; Sun et al. 2002; Yano et al. 2012; Yano & Tamura 2013). During tetrapod limb

development, the AER is maintained relatively longer (E12.5 in the mouse forelimb) than in pectoral fin development resulting in sustained signalling FGF signalling (Guo et al. 2003; Lu et al. 2008). The contributions of long-term AER signalling on endochondral bone evolution have been previously proposed in Thorogood's Clock model (Thorogood 1991; Yano et al. 2012). During zebrafish pectoral fin development, the AER folds to form the apical fin fold as early as 36hpf (Grandel & Shulte-Merker 1998; Yano et al. 2012). Despite this morphological change, there is evidence suggesting components of AER-FGF signalling are maintained in fish pectoral fins despite the transition into apical fin fold (Tulenko et al. 2017; Yano & Tamura 2013). The fin fold is supported by two rows of fibrils known as actinotrichia, the first fin exoskeletal elements formed. Actinotrichia are made of collagen and actinodin (Duran et al. 2011; Géraudie 1977; Géraudie & Meunier 1980). The *actinodin* gene family (*actinodin 1–4*) (ZDB-GENE-030131-9105, ZDB-GENE-041105-2, ZDB-GENE-040724-185, ZDB-GENE-081022-5) which codes for structural proteins crucial for actinotrichia formation has been lost from the tetrapod genome during the fin-to-limb transition (Zhang et al. 2010). Beginning shortly after the onset of *actinodin* expression, actinotrichia fibrils form and support the pectoral fin fold as it extends distally (Duran et al. 2011; Géraudie 1977; Géraudie & Meunier 1980; Grandel & Shulte-Merker 1998). At this stage *actinodin* genes are expressed in the ectoderm at the border of the presumptive endochondral disk and fin fold (Lalonde et al. 2016; Zhang et al. 2010). At around 52hpf, *actinodin* expression begins in a second population of cells, referred here as fin fold mesenchyme, which migrate distally through the fin fold using the pre-existing actinotrichia as a scaffold (Lalonde et al. 2016; Wood & Thorogood 1984). This secondary activation of *actinodins* in the mesenchyme is proposed to contribute to the thickness and length of the pre-existing actinotrichia (Duran et al. 2011; Lalonde et al. 2016; Wood & Thorogood 1984).

Actinotrichia fibrils are also present in the median fin fold, which extends along the midline of the embryo from the 8th somite to the end of the trunk of the embryo, with *actinodin* expression starting at 24hpf (Abe et al. 2007; Kimmel et al. 1995; Zhang et al. 2010). In tetrapod limb development, no actinotrichia or fold forms. In the adult pectoral fin, the endochondral disc serves as a template for the proximal radial bones and novel cartilagenous condensations at the distal edge of the disc will ossify to become the distal radials (Grandel & Shulte-Merker 1998). The distal radials are linked to the dermal bone, calcified fin rays (lepidotrichia), which form via intramembranous ossification from fin fold mesenchyme (Grandel & Shulte-Merker 1998). The median fin fold will become the 3 unpaired fins of the adult zebrafish: dorsal, caudal and anal fins (Abe et al. 2007; Kimmel et al. 1995).

Early fin and limb patterning is regulated by the 5'*HoxA/D* (9–13) genes (Tarchini & Duboule 2006; Woltering et al. 2014; Zakany et al. 2004). Two distinct phases of *5'HoxA/D* expression are responsible for proximal and distal appendicular patterning, respectively (Ahn & Ho 2008; Freitas & Zhang 2007). Each phase is activated by regulatory sequences, called regulatory landscapes, found either 5' (Global control region) or 3' (Early limb control region) to the *HoxA* and *HoxD* gene clusters (Woltering et al. 2014). Late phase *5'HoxA/D* expression is activated in distal limb mesenchyme in tetrapods, whereas expression occurs in the distal cells of the endochondral disc, and the fin fold mesenchyme during fish fin development (Ahn & Ho 2008; Kherdjemil et al. 2016; Nakamura et al. 2016). 5'*Hox* regulatory data from the spotted gar and mouse, respectively, highlight a deep homology between distal fin and limb mesenchyme (Braasch et al. 2016; Gehrke et al. 2015; Leite-Castra J et al. 2016). In zebrafish, *hoxa13*-expressing mesenchymal cells migrate distally through the larval fin fold and contribute to adult fin dermal bone (Lee et al. 2013; Nakamura et al. 2016). Co-localization of *hoxa13* (ZDB-

GENE-990415-5, ZDB-GENE-980526-365) and *and1*, known autopod and fin fold markers respectively also supports a role of *hoxa13* during fin development in basal fish species (Tulenko et al. 2017). In mice, *Hoxa13*-expressing cells do not migrate and instead contribute to the endochondral bones of the autopod (Scotti et al. 2015). Several hypotheses propose fin fold mesenchyme migration defects may be a mechanism of fin dermal bone loss during limb evolution (Ahn & Ho 2008 ; Nakamura et al. 2016; Zhang et al. 2010). To that end, we set out to create fin fold mesenchyme defects in the zebrafish to assess the effects on larval fin development.

We utilized the nitroreductase/metronidazole (NTR/MTZ) system to specifically ablate a subset of *hoxa13a/hoxd13a*-expressing cells during fin development. Briefly, in the presence of the NTR enzyme, MTZ substrate is converted to a cytotoxic compound leading to the death of the NTR-expressing cells. Using regulatory elements specific for fin mesenchyme, we can drive NTR in transgenic fish and specifically ablate fin fold mesenchyme upon MTZ addition to the fish water, while not producing any bystander effects (Curado et al. 2008; Mathias et al. 2014). In order to ablate fin fold mesenchymal cells prior to and during migration within the median and pectoral fin folds, we utilized the previously characterized "*m-Inta11"* regulatory element (Kherdjemil et al. 2016). This regulatory element initiates antisense transcription at the *Hoxa11* exon 1 locus in mice, leading the distal repression of *Hoxa11* (MGI:96172). Using ChIP analysis, HOXA13 (MGI:96173) and HOXD13 (MGI:96205) have previously been shown to bind to this enhancer element in mice, and only *Hoxa13* -/- *Hoxd13* -/- double mutant mice show no activation of this enhancer element (single mutant mice show reduced enhancer activation) (Kherdjemil et al. 2016). Furthermore, transgenic reporter zebrafish lines: *Tg(m-Inta11-β-globin:eGFP)* show reporter activation within the *hoxa13a* expression domain in the median and

pectoral fins, further confirming a regulatory link between HOXA13 and the *m-Inta11* enhancer (Kherdjemil et al. 2016).

In the present study, we show that the ablation of fin fold mesenchymal cells during median and pectoral fin development results in fin fold collapse and actinotrichia defects. In addition, we observed endoskeletal disc reduction in the pectoral fin bud, as well as shifts in expression profiles of several key fin patterning genes. This suggests fin fold mesenchyme is crucial for the maintenance of actinotrichia and the fin fold during larval development. In addition, sustained metronidazole exposure for 30 days leads to fin ray defects in the pectoral fins at late larval stages, accompanied with a premature calcification in the proximal regions of the anterior-most fin rays compared to stage-matched controls. We propose that fin fold mesenchyme ablation, compounded by the lack of larval fin fold and actinotrichia maintenance, and distal reduction in *hoxa13a/hoxd13a* expression results in pectoral fin dermal bone defects.

3.4. Results

Subset of *hoxa13a/hoxd13a*-expressing cells are specifically ablated in *Tg(Inta11:NTR)* larvae following metronidazole treatment

To ablate fin fold mesenchyme in the median and pectoral fin fold, we utilized the previously characterized "*m-Inta11"* regulatory element (Kherdjemil et al. 2016) inserted upstream of the human *β-globin* minimal promoter to generate the *Tg(m-Inta11-β-globin:YFP-NTR)* transgenic line, thereafter named *Tg(Inta11:NTR*). We previously showed that the *m-Inta11-β-globin* regulatory elements drive transgene reporter expression in the *hoxa13a*-expressing fin fold mesenchyme of the pectoral fin buds (Fig. 3.1E and (Kherdjemil et al. 2016)). Here we show that the transgenic reporter zebrafish line *Tg(m-Inta11-β-globin:eGFP)* also expresses the reporter gene in *hoxa13a*-expressing fin fold mesenchyme of the median fin (Fig

3.1A and 3.1I). To ensure NTR expression is consistent with the previously described *Tg(m-Inta11-β-globin:eGFP)* transgenic line, we produced another transgenic line: *Tg(m-Inta11-β-globin:mCherry)* to show co-localization of YFP and mCherry within the fin fold mesenchyme (Fig. 3.1C and 3.1D). Despite evidence that both HOXA13 and HOXD13 bind to this enhancer in mice, we propose Hoxa13a as the main contributor to *m-Inta11* activation in the median fin fold. Neither *hoxa13b*, nor *hoxd13a* (ZDB-GENE-990415-119) are expressed in the median fin fold at 60hpf (Fig. 3.1K and 3.1L), however we acknowledge Hoxa13b or Hoxd13a may still be contributing to enhancer activation due to protein persistence or a delay in reporter activity following binding. In the pectoral fin fold *hoxa13b* and *hoxd13a* expression extends more proximally in the endoskeletal disc regions of the pectoral fin at 72hpf, not consistent with *Tg(m-Inta11-β-globin:eGFP)* reporter expression nor *hoxa13a* expression (Fig. 3.1E–3.1H). *Tg(m-Inta11-β-globin:eGFP)* larvae do show more eGFP-positive fin fold mesenchyme in the posterior half of the pectoral fin fold (Fig. 3.1E), comparable to *hoxd13a* transcript localization (Fig. 3.1H), suggesting Hoxd13a is likely contributing to enhancer activation in this region. Where therefore propose the *m-Inta11-β-globin* regulatory elements show activity in a subset of *hoxa13a/hoxd13a*-expressing cells in the pectoral fin, and *hoxa13a* only-expressing mesenchymal cells in the median fin fold. The *Tg(Inta11:NTR)* transgenic line recapitulates the previously described *Tg(m-Inta11-β-globin:eGFP)* transgenic line (Fig. 3.1B).

Treatments of larvae with metronidazole were initiated at the onset of *Inta11:NTR* transgene expression, designed to encompass the peak of *hoxa13a/hoxd13a*-expressing cell migration in each fin. For median fin analysis “larval 1” treatment is performed spanning from 30-60hpf, and for pectoral fin analysis “larval 2” treatment is performed spanning from 52-72hpf (Fig. 3.9). Each experiment consists of one experimental group: *Tg(Inta11:NTR)* larvae treated

with MTZ (Inta11: NTR + MTZ) and two control groups: WT larvae treated with MTZ (WT + MTZ), and *Tg(Inta11:NTR)* larvae treated with DMSO alone (Inta11: NTR—MTZ)(Fig 2A–2C). To ensure our system can specifically and consistently ablate fin fold mesenchyme in larval zebrafish we examined YFP expression in the median fin fold. Following "Larval 1" metronidazole (MTZ)-treatment, (Fig. 3.2D and Fig. 3.9) *Tg(Inta11*: *NTR)* larvae show a drastic decrease in YFP expression in the median fin fold at 72hpf (Fig. 3.2C and 3.2F), compared to untreated transgenic larvae (Fig. 3.2B and 3.2E). The median fin fold of WT (non-transgenic) larvae that received MTZ developed normally (Fig. 3.2A). To confirm the loss of YFP expression is indicative of cell death, a TUNEL assay was performed. Following "Larval 1" treatment (Fig. 3.2D and Fig. 3.9), all MTZ-treated *Tg(Inta11*: *NTR)* larvae showed TUNEL-positive cells in the median fin fold at 72hpf (Fig. 3.2I) (n = 16/16). Control fish groups present single TUNEL-positive cells in 1–2 larvae at 72hpf (Fig. 3.2G and 3.2H). Consistently, *hoxa13a*, and *hoxd13a* expression is reduced in both the median and pectoral fins following MTZ-mediated ablation (see below). Altogether, these results confirm that treatment with metronidazole of the *Tg(Inta11:NTR)* transgenic line specifically ablates a subset of *hoxa13a/hoxd13a*-expressing fin fold mesenchyme.

Morphological and migratory defects of the pectoral and median fin fold mesenchyme in *Tg(Inta11:NTR)* larvae following metronidazole treatment

To facilitate visualization of the fin fold mesenchyme defects following metronidazole treatments, *Tg(Inta11*: *NTR)* zebrafish were outcrossed to *Tg(m-Inta11-β-globin:eGFP)*, resulting in decreased ablation efficiency and higher number of surviving fin fold mesenchymal cells (Figs. 3.1F and 3.3A–X). For pectoral and median fin analysis, larvae were treated according to "larval 2", and "larval 1" treatments, respectively (Fig. 3.9). At 60hpf,

mesenchymal cells begin to migrate in the fin fold of the pectoral fin of untreated *Tg(Inta11*: *NTR)* larvae (Fig. 3.3A–C). In contrast, no actively migrating cells are present in the pectoral fins of treated *Tg(Inta11*: *NTR)* larvae (Fig. 3.3D-F), indicating a delay in migration. At 72hpf, untreated *Tg(Inta11:NTR)* larvae have actively migrating fin fold mesenchyme in proximal-posterior region of the pectoral fin fold, with several cells extending distally (Fig. 3.3G–I). MTZ-treated larvae show reduced fin fold mesenchyme migration and cells are less elongated (more rounded) in shape (Fig. 3.3J-L). Similar observations can be made for the median fin fold. At 60 and 72hpf, untreated larvae show actively-migrating fin fold mesenchyme through the median fin (Fig. 3.3M-O and 3.3S-U). Cells are elongated and branched in shape. In contrast, treated larvae display clusters of mesenchymal cells in the fin fold surrounding the trunk region that have failed to initiate migration (Fig. 3.3P–R and 3.3V–X). Furthermore, cells are rounded and unbranched in shape. These results show that following metronidazole treatment, mesenchymal cells in *Tg(Inta11*: *NTR)* larvae transition from an elongated, branched morphology to a rounded, unbranched morphology (a characteristic of dying cells) and subsequently fail to migrate properly.

Actinotrichia defects and fin fold collapse in pectoral and median fins of *Tg(Inta11:NTR)* following metronidazole treatment

We propose that the observed decrease in median and pectoral fin fold size is due to fin fold collapse resulting from actinotrichia defects. At 72hpf, both the median and pectoral fins of MTZ-treated *Tg(Inta11*: *NTR)* larvae show signs of fin fold collapse (Fig. 3.4B, 3.4F and 3.4J) when compared to untreated controls (Fig. 3.4A, 3.4E and 3.4I). This was seen following “larval 1” or “larval 2” treatments. At closer magnification, fins of treated individuals show disorganized actinotrichia in the pectoral fin, with bending that is parallel to the fin fold collapse

(Fig. 3.4F). In order to observe actinotrichia structure in both the median and pectoral fin, we performed immunohistochemistry for Collagen type II, which has previously been shown to label actinotrichia during larval development (Duran et al. 2011) (Fig. 3.5). At 72hpf, actinotrichia of MTZ-treated larvae are unable to remain rigid, and bend within the fin fold (Fig. 3.5D–F and 3.5J–L). This correlates with fin fold collapse along the entire edge of the pectoral and median fin fold (Fig. 3.5D–F and 3.5J–L). The actinotrichia do not remain parallel to one another, consistently revealing gaps between the fibrils. Furthermore, there is an apparent unbundling of Collagen II stained strands (Fig. 3.5D and 3.5J). Fin fold migration defects can also be observed using DAPI staining, however cell mesenchyme morphology is not as evident. Fin fold mesenchyme nuclei mimic cell shape but the extent of cellular elongation is not visible, precluding the use of DAPI staining for cell displacement measurements. Fin fold mesenchyme of MTZ-treated larvae clustered near endoskeletal disk of the pectoral fin, and the trunk region anterior to the median fin (Fig. 3.5E, 3.5F, 3.5K and 3.5L). Untreated larvae show straight, rigid actinotrichia throughout the median and pectoral fin fold, with visible fin fold mesenchyme migration (Fig 3.5A–C and 3.5G–I). Fin fold mesenchyme produce and secrete actinodin proteins, and we propose their ablation results in a failure to maintain the actinotrichia fibres and in the subsequent collapse of the fin fold. To maintain ablation effects until 7dpf, a secondary metronidazole treatment, “larval 3”, from 72hpf -7dpf, is required to suppress fin fold mesenchyme regeneration following “larval 1 & 2” treatments (Fig. 3.9 and 3.12). At 7dpf, MTZ-treated *Tg(Inta11:NTR)* larvae continue to show severe collapse of the fin fold and actinotrichia defects in the pectoral fin (Figs. 3.4D, 3.4H and 3.5P–R) compared to untreated larvae (Fig. 3.5C, 3.5G and 3.5M–O), following a combination of “larval 2”+ “larval 3” treatments (Fig. 3.9). The actinotrichia are still unable to remain parallel and bend at the distal tip

of the fin fold. The most severe defects are at the anterior and posterior regions where the actinotrichia bend inward correlating with fin fold collapse along the anterior-posterior axis (Fig. 3.5P). Untreated larvae show rigid parallel actinotrichia throughout the pectoral fin fold (Fig. 3.5M–O). DAPI staining reveals two-fold defects in surviving fin fold mesenchyme migration: migrating cells are now restricted centrally having converged inward from anterior-posterior fin fold collapse, and many cells show improper orientation that seems to correlate with the actinotrichia defects (Fig. 3.5P–R). Many cells appear to elongate along several different axes within the fin fold compared to untreated larvae that show cell elongation restricted to the proximal-distal axis (Fig. 3.5Q, 3.5R, 3.5N and 3.5O). At 7dpf, MTZ-treated *Tg(Inta11:NTR)* larvae continue to show a reduction in size of the median fin fold compared to untreated control larvae, (Fig. 3.4L and 3.4K) following "larval 1" and "larval 3" treatments (Fig. 3.9). Actinotrichia defects are also observed in the median fin of MTZ-treated *Tg(Inta11:NTR)* larvae (Fig. 3.4J–L and 3.5V–X) compared to control larvae (Fig. 3.4I, 3.4K and 3.5S–U). Similar to observations in the pectoral fin, fin fold mesenchymal cells appear to elongate along different axes compared to untreated larvae (Fig. 3.5W, 3.5X, 3.5T and 3.5U). Median fin fold defects are ameliorated in treated larvae at 7dpf, (Fig. 3.4L) when compared to 72hpf median fins (Fig. 3.4J). We believe median fins trend towards a complete reversal of the 72hpf phenotype (Fig. 3.4J) due to incomplete median fin fold mesenchyme ablation. This aspect will be addressed in the discussion.

Metronidazole-treated, *Tg(Inta11:NTR)* larvae show defects in median fin fold mesenchyme migration, a reduction in median and pectoral fin fold size and a reduction in endoskeletal disc size

Following MTZ-mediated ablation of fin fold mesenchyme in *Tg(Inta11:NTR)*, we observed severe median fin fold collapse and reduced overall size (Fig. 3.2C). In order to quantify these median fin fold defects, we measured fin fold length and height, as well as overall median fin fold mesenchyme cell displacement (Fig. 3.6A–E). Cell displacement was measured as a proportion of total median fin fold length (trunk to distal tip), and recorded as a percentage. All measurements are therefore relative to the size of the fin fold, eliminating any bias for a general impairment of fin fold growth. Following "Larval 1" or "Larval 3" treatments, median fins of all groups were examined at 48, 60, 72hpf and 7dpf. MTZ-treated *Tg(Inta11:NTR)* animals display significantly reduced median fin fold mesenchymal cell displacement from 48 to 72hpf compared to both control groups (Fig. 3.6C). At 48hpf, the median fin fold length and height of MTZ-treated *Tg(Inta11:NTR)* larvae display no difference compared to controls (Fig. 3.6D and 3.6E). However significant reductions are observed starting at 60hpf and the defects are maintained through 7dpf (Fig. 3.6D and 3.6E). To ensure the effects were not limited to the median fin, we measured the area of the distal pectoral fin fold and endoskeletal disc (Fig. 3.6F–I). Following "Larval 2" or "larval 3" treatments, the distal pectoral fin fold area is significantly reduced MTZ-treated *Tg(Inta11:NTR)* larvae at 72hpf compared to both groups of control larvae and the defect is maintained until 7dpf (Fig. 3.6J). To measure the endoskeletal disc area, *Tg(Inta11:NTR)* fish were outcrossed with *Tg(Kr19)* transgenic fish (Fig. 3.6G and 3.6I), where KillerRed is expressed in the endoskeletal disk, among other regions (Teh et al. 2010). At 7dpf, MTZ-treated *Tg(Inta11:NTR)* larvae show a decrease in endoskeletal disc size compared to control larvae (Fig. 3.6J). These results show that following metronidazole treatment, cells targeted for ablation in *Tg(Inta11*: *NTR)* larvae show significant defects in their migration. MTZ-

treated *Tg(Inta11:NTR)* fish also show a reduction in the size of the median and pectoral fin folds, as well as of the endoskeletal disc.

Altered gene expression profiles in the median and pectoral fin of *Tg(Inta11:NTR)* larvae following metronidazole treatment

In order to observe the consequences of fin fold mesenchyme ablation on gene expression and interpret the subsequent morphological defects, we performed whole mount *in situ* hybridization for several genes which play important roles in fin (and limb) development (Fig. 3.7 and Fig. 3.10). As a subset of *hoxa13a/hoxd13a*-expressing cells are targeted for ablation, we first confirmed lower distal transcript levels of *hoxa13a* in the median and pectoral fins of MTZ-treated *Tg(Inta11:NTR)* at 60- and 72hpf (Fig. 3.7B and 3.7D) compared to control larvae (Fig. 3.7A and 3.7C and Fig. 3.10) and decreased *hoxd13a* expression in the distal pectoral fin fold and disc at 72hpf (Fig. 3.7F) compared to control larvae (Fig. 3.7E and Fig. 3.10). There is no change in *hoxd13a* expression in the proximal disc regions (Fig. 3.7F). No visible change in expression is observed for *hoxa13b*, and *hoxa11b* (ZDB-GENE-990415-4) in the pectoral fins of MTZ-treated *Tg(Inta11*: *NTR)* larvae at 72hpf (Fig. 3.10). The domains of expression for *hoxa13b* and *hoxa11b* extend more proximally, outside the region targeted for ablation, and therefore the unaffected high levels of proximal transcripts may be masking the decreases in the distal domain. No change in *and1* ectodermal expression is visible by *in situ* hybridization (Fig. 3.10). Although a decrease in mesenchymal expression of *and1* is expected, it may be hidden by ectodermal expression of the same gene. The larval fin has *and1* expression in the fin fold ectoderm and mesenchyme. To show a decrease in *and1* in the mesenchyme, we outcrossed *Tg(Inta11:NTR)* fish with the *and1* mesenchymal reporter line: *Tg(2PΔEpi:mCherry)* (Lalonde et al. 2016). The regulatory elements "2PΔEpi" contain multiple mesenchymal-specific enhancers,

and the endogenous *and1* promoter (Lalonde et al. 2016). Following metronidazole treatment, double transgenic larvae show fewer mCherry-positive cells in the pectoral 72hpf compared to untreated controls, indicating lower *and1* expression (Fig. 3.7G–J).

Expression of 5'*hox*A/D genes has been previously shown to be required for activation and maintenance of *Shh* expression during mouse limb development (Kmita et al. 2005; Sheth et al. 2013). In MTZ-treated *Tg(Inta11:NTR)* larvae, both *shha* (ZDB-GENE-980526-166), and its receptor *ptch2* (ZDB-GENE-980526-44) display a smaller domain of expression along the proximal-distal axis of the posterior endoskeletal disc at 72hpf, as well as a slight anterior expansion (Fig. 3.7L and 3.7N) when compared to control larvae (Fig. 3.7K, 3.7M and 3.10). No difference in the expression of *hhip* (ZDB-GENE-030131-4827), coding for a shha antagonist, is observed in the pectoral fins of MTZ-treated *Tg(Inta11:NTR)* larvae compared to controls at 72hpf (Fig. 3.10). Altered SHH signalling via decreased 5'*Hox* transcripts has previously been associated with decreased endoskeletal disc proportions (Sakamoto et al. 2009), and thus supports reduced endoskeletal disc size observed in MTZ-treated *Tg(Inta11:NTR)* larvae at 7dpf (Fig. 3.6J).

AER-FGF signalling in tetrapod limb development relies on feedback loops with SHH and 5'HOX signalling (Laufer et al. 1994; Niswander et al. 1994; Rodriques et al. 2017; Sheth et al. 2013). We therefore wished to determine if changes in expression of *fgf8a* (ZDB-GENE-990415-72), and *fgf10a* (ZDB-GENE-030715-1) are observed in MTZ-treated *Tg(Inta11*: *NTR)* larvae. At 72hpf, treated larvae show a clear decrease in *fgf10a* expression in the median fin fold compared to control larvae (Fig. 3.7O, 3.7P and 3.10). Treated larvae show a slight decrease in *fgf10a* transcripts in the posterior fold mesenchyme of pectoral fins compared to controls (Fig 7Q, 7R and 3.10). Despite a decrease in *fgf10a* expression, no change in *fgf8a* expression is

observed at 72hpf in pectoral fins of treated larvae compared to controls (Fig. 3.10). Decreased AER-FGF signalling has been associated with decreased endochondral bone elements, and therefore may also be causing the endoskeletal disc reduction observed in treated *Tg(Inta11:NTR)* larvae at 7dpf (Fig. 3.6J) (Lewandoski et al. 2000; Mariani et al. 2008; Niswander et al. 1994). The ablation of fin fold mesenchyme in *Tg(Inta11:NTR)* larvae following metronidazole treatment results in decreased *hoxa13a* and *hoxd13a* transcripts in the distal median and pectoral fins. We propose this decrease in overall 5'*hoxA/D* transcripts may result in a decrease in fgf signalling, possibly followed by a decrease in downstream shha signalling, and can account for the reduction in endoskeletal disc size observed in Inta11: NTR + MTZ larvae at 7dpf.

Actinotrichia defects, fin fold collapse, and fin ray defects in pectoral fins of *Tg(Inta11:NTR)* fish during late larval stages following metronidazole treatment

In order to observe the effects of fin fold mesenchyme ablation on the development of lepidotrichia (fin ray), we established a protocol for rearing zebrafish larvae in metronidazole until 30dpf (Fig. 3.9 Fig). We initially proposed examining the formation of caudal fin rays as these were observed as early as 12dpf in treated *Tg(Inta11:NTR)* individuals. Following a "juvenile 4" treatment (Fig. 3.9), *Tg(Inta11:NTR)* larvae did not show any caudal fin ray defects at 20dpf (n = 4, 7.4% survival rate (Fig. 3.9)). As the defects observed at 7dpf for pectoral fin appeared more pronounced than those in the median fin at the same stage (Fig. 3.4), we decided to extend the treatment to observe the effects on pectoral fin ray formation. Due to developmental delays in treated *Tg(Inta11:NTR)* larvae (Fig. 3.11), we decided to raise this group of fish until 30dpf, when fin ray formation was initiated. "Juvenile 5" treatment was devised in order to decrease rates of mortality in the MTZ-treated group (Fig. 3.9). Following

alcian blue and alizarin red staining for cartilage and bone respectively, zebrafish were staged based on three criteria: standard length, cartilaginous disc decomposition, and calcification of spinal cord and ribs (Fig. 3.8 and 3.11). At 30dpf, all treated *Tg(Inta11:NTR)* larvae have pectoral fin defects (n = 7) (Fig. 3.8C, 3.8F and 3.8I), and the three most developed larvae display pectoral fin ray defects (n = 3) (Fig. 3.8F and 3.8I). At developmental stage 6.4mm, MTZ-treated *Tg(Inta11:NTR)* larvae continue to display fin fold collapse and actinotrichia defects (n = 4) (Fig. 3.8C) compared to stage-matched controls (Fig. 3.8A and 3.8B). Initial formation of the anterior most rays does not appear delayed in 6.4mm treated larvae compared to controls (Fig. 3.8A–C). At length 6.8, and 7.2mm, treated larvae show several key differences with control larvae: the larvae have two missing posterior rays at each stage (5, and 6 compared to 7, and 8 respectively). The rays are shorter (Fig. 3.8L) and less distally defined; the interray zones are poorly defined, and the proximal fin ray regions show premature calcification in the anterior most rays (Fig. 3.8F, 3.8I and 3.8L). Control larvae have longer fin rays (Fig. 3.8J and 3.8K) that have distinct distal tips, with clearly defined interray zones (Fig. 3.8D-E, 3.8G-H, and 3.8J-K). No calcification is observed in any control larvae at these developmental stages (Fig. 3.8D-E, 3.8G-H, and 3.8J-K). The poorly defined interray zones of treated larvae (Fig. 3.8F, 3.8I and 3.8L) are comparable to the less developed posterior fin rays in the control larvae (Fig. 3.8D-E, 3.8G-H, and 3.8J-K). By comparing treated *Tg(Inta11:NTR)* larvae at 7.2mm (Fig. 3.8I and 3.8L) to less developed control larvae (WT + MTZ, 6.8mm; untreated, 6.9mm) (Fig. 3.8D and 3.8E), we can remove the possibility that these defects are simply due to a delay in fin ray development. At 30dpf, treated transgenic larvae continue to show no defects in caudal fin rays (n = 7, 13.5% survival rate (Fig. 3.9) compared to controls (Fig. 3.11). However, a small percentage of larvae in each treatment group display unrelated major caudal fin deformities (Fig.

3.11). The number of fish with caudal fin deformities is displayed in the bottom right corner of each panel and is presented as a fraction over total observed fish (Fig. 3.11). These results show that a sustained daily metronidazole treatment can sufficiently ablate the fin fold mesenchyme to produce pectoral fin ray defects at 30dpf. Thus, we are able to show that defects in larval fin fold mesenchyme, through genetic ablation, can produce truncated dermal bone elements in adult pectoral fins.

3.5. Discussion

Implications for the fin-to-limb transition

We have shown that, following metronidazole treatment, we can consistently and efficiently ablate fin fold mesenchyme in *Tg(Inta11:NTR)* larval zebrafish. Furthermore, the apoptotic nature of cell ablation was confirmed via TUNEL assay. This population of cells has been shown to express multiple 5'*hox* genes, including *hoxa13a*, *hoxa13b*, *hoxd13a*, and *hoxa11b* (Ahn & Ho 2008) and *actinodin* genes (Lalonde et al. 2016; Zhang et al. 2010). Enhancer, cell lineage-tracing and knockout data have also proposed a deep homology between fin fold mesenchyme in teleost and presumptive autopod mesenchyme of tetrapods (Braasch et al. 2016; Gehrke et al. 2015; Nakamura et al. 2016; Scotti et al. 2015). In fact, fin mesenchyme migration failure has been proposed as a mechanism of fin dermal bone loss during limb evolution (Ahn & Ho 2008; Nakamura et al. 2016). Actinotrichia are crucial for proper fin fold mesenchyme migration, and thus seem to be an obvious target to disrupt migration (Duran et al. 2011; Zhang et al. 2010; Wood & Thorogood 1984). We have previously explored the possibilities of *actinodin* loss/change in regulation as mechanisms of actinotrichia defects and subsequent loss of dermal bone in fins of tetrapods (Lalonde et al. 2016; Zhang et al. 2010).

Our data show that fin fold mesenchyme survival is crucial for fin fold and actinotrichia maintenance. Following ablation, the larval median and pectoral fin folds collapse and disorganized actinotrichia are observed. The actinotrichia are no longer able to support the fin fold. They are unable to remain rigid, and bend parallel to the collapsed fin fold region (Fig. 3.5). It appears that fin fold mesenchymal cells contribute to their own successful migration, likely through their contributions to structural components of the actinotrichia (Duran et al. 2011; Lalonde et al. 2016; Zhang et al. 2010). Indeed, we show that *and1* reporter expression in the mesenchyme is decreased using the *Tg(2PΔEpi:mCherry)* transgenic line, demonstrating lower *and1* activity (Fig. 3.7G–J). At the same time, previous studies have also proposed that *hoxa13* contributes to pectoral fin fold formation (Tulenko et al. 2017). Thus, *hoxa13a/hoxa13b* double mutants display a reduced larval pectoral fin fold size (Nakamura et al. 2016). Although *Tg(Inta11:NTR)*larvae do show reduced transcripts for *hoxa13a*, levels of *hoxa13b* do not appear to be affected, suggesting the mechanisms of fin fold reduction (ie. actinotrichia defects) differ from that occurring in *hoxa13a/hoxa13b* double mutants. No fin fold defects are observed in single mutant larvae (*hoxa13a -/-* or *hoxa13b -/-*) nor in *hoxd13a* mutant larvae (Nakamura et al. 2016). In addition, despite similar reductions in size, pectoral fin fold morphology appears to differ in *hoxa13a/hoxa13b* double mutants compared to *Tg(Inta11:NTR)*larvae following ablation. The pectoral fin folds of treated *Tg(Inta11:NTR)*larvae show a characteristic distal "peak" as the actinotrichia bend (Fig. 3.4 and 3.5), which is absent in *hoxa13a/hoxa13b* double mutants. Finally, no effect is described in the median fin fold of *hoxa13a/hoxa13b* double mutants (Nakamura et al. 2016). Additional work is required to investigate the contributions of *5'hox* to the larval fin fold.

To assess the effects of prolonged fin fold mesenchyme ablation on later larval fin ray formation, we developed a protocol to treat the larvae until 30dpf. Through sustained metronidazole treatments, we were able to show pectoral fin ray defects at 30dpf (6.8–7.2mm) in *Tg(Inta11:NTR)*larvae. These larvae have lower fin ray numbers, which are shorter and less distally defined compared to stage-match control larvae (Fig. 3.8). Fin fold mesenchyme has been shown to contribute to both fibroblast and osteoblast lineages (Lee et al. 2013; Nakamura et al. 2016). To assess the contributions of fin fold mesenchyme Nakamura et al. used a "late-phase" *hoxa13* enhancer to drive the Cre recombinase enzyme in their lineage-tracing experiments. Since the *lnta11* regulatory element used in the present study is activated by Hoxa13a & Hoxd13a, fin fold mesenchymal cells that show *Inta11:NTR* transgene expression would also contribute to the osteoblast lineage. We propose a loss or disorganization of osteoblasts can account for the mispatterning of the fin rays in *Tg(Inta11:NTR)* larvae following metronidazole treatment. Proteoglycans are known to be involved in the organization of endochondral and intramembranous bone extracellular matrix. They actively regulate collagen fibrillogenesis and are secreted by differentiating and mature osteoblasts (Gori et al. 2001; Lamoureux et al. 2007). In *Tg(Inta11:NTR)* fish, alcian-blue stained proteoglycans appear dispersed through the adult fin fold rendering the interray tissue and distal fin ray regions undefined (Fig. 3.8F, 3.8I and 3.8L). In control larvae, the presumptive fin ray definition appears to be due to condensation of alcian blue-stained proteoglycans (Fig. 3.8-E, 3.8G-H and 3.8J-K). An analysis of osteoblast markers is necessary to provide conclusive evidence for a loss or disorganization of osteoblasts, however due to limited sample number, further analysis was not possible. These results provide evidence that larval fin fold mesenchyme defects can produce a

truncation in late larval pectoral fin rays and may have potential implications for the loss of fin dermal bone in tetrapods.

In contrast to pectoral fin ray defects, no caudal fin ray defects were observed (Fig. 3.11). We showed that at 7dpf, median fin fold defects are ameliorated compared to 72hpf in *Tg(Inta11:NTR)* following metronidazole treatment suggesting an early reversal of the severe larval median fin fold phenotype. We propose several explanations for this observation. First, transgenic zebrafish frequently display variable transgene expression between individuals and this may have resulted in inconsistent ablation (Roberts et al. 2014). This contingency, combined with higher relative numbers of fin fold mesenchymal cells in the median fin (Fig. 3.1F and 3.1J), could result in a reduced effect in the median fins compared to the pectoral fins. Second, in order to avoid metronidazole toxicity at 72hpf, "larval1" treatment spanned from 30-60hpf and may have missed a key developmental period from 60-72hpf important for long-term median fin fold maintenance. Finally, fin fold mesenchyme ablation may simply yield a more severe and prolonged effect in the pectoral fin due to differences in patterning and morphology. In fact, transitional tetrapods maintained caudal fin rays for millions of years following the loss of dermal bone in paired appendages (Clack 2009) suggesting the caudal fin may have been less susceptible to the mechanisms of fin dermal bone loss ie. fin fold mesenchyme defects.

Implications for fin development

Following fin fold migration defects, a shift in cell fate from dermal to endochondral bone progenitors has been proposed as a mechanism for simultaneous dermal reduction and endochondral expansion (Nakamura et al. 2016). We have shown dermal bone reductions following fin fold mesenchyme ablation at 30dpf; however no effects are observed in the presumptive proximal and distal radials (Fig. 3.8). We recognize that cell ablation methods are

not ideal to test any hypotheses of fin fold mesenchyme shifts in cell fate. We are not differentially allocating these cells to the proximal regions of the pectoral fin, we are simply lowering the number of cells that properly migrate and contribute to adult dermal bone. We therefore do not predict an expansion of endochondral bone, simply a reduction in fin dermal bone (fin ray defects).

*Tg(Inta11:NTR)*larvae show decreased endoskeletal disc size at 7dpf following metronidazole treatment, which is in contradiction with a hypothesis of endochondral bone expansion during limb evolution (Freitas et al. 2012; Nakamura et al. 2016; Yano & Tamura 2013). We propose that disc size reductions are a secondary effect of the fin fold mesenchyme ablation. As shown by *in situ* hybridization, lower amounts of distal transcripts are present for *hoxa13a*, and *hoxd13a* (Fig. 3.7A–F). While *hoxa13b* and *hoxa11b* are expressed in the ablated population of cells, their expression patterns extend much more proximally in the pectoral fin, outside the zone of ablation. This may account for the absence of obvious decreases in distal expression, as many *hoxa13b/hoxa11b*-expressing cells are not affected (Fig. 3.10). Overall, we provide evidence for a global decrease in 5'*hox* transcripts, which has been linked to decreased FGF signalling and endochondral bone size. Decreased FGF signalling between the apical ectodermal ridge and underlying limb mesenchyme results in reduced endochondral bone during limb development in mice (Lewandoski et al. 2000; Mariani et al. 2008; Niswander et al. 1994). We show decreased levels of transcripts for *fgf10a* (Fig. 3.7O–R), however levels of *fgf8a* transcripts are unaffected (Fig. 3.10). Lower levels of *fgf10a* expression may be due to ablation of *fgf10a*–expressing cells or lowered 5'Hox signalling. Finally, the change in expression of *shha* and *ptch2* highlight the reduced endoskeletal disc proportions (Fig. 3.7K–N). Altered *shha* expression may be due to lower transcript levels of *fgf10a* or simply an effect of the disc size

reduction itself. Feedback loops between 5'Hox, FGF and HH signalling are well-documented (Laufer et al. 1994; Niswander et al. 1994; Rodriques et al. 2017; Sheth et al. 2013).

In contrast to decreased presumptive endochondral bone elements at 7dpf, *Tg(Inta11:NTR)*larvae show earlier dermal bone calcification in the proximal regions of the anterior-most fin rays at 30dpf following metronidazole treatment. This suggests increased osteoblast activity in this zone. At 30dpf, we show high levels of YFP-expressing cells in the proximal fin fold mesenchyme and anterior-most fin rays in the pectoral fin (Fig. 3.12), indicative of sustained or reactivated *hoxa13a/hoxd13a* expression in these regions. We have previously shown that *m-Inta11* regulatory element is activated by Hoxa13 and Hoxd13 in mice (Kherdjemil et al. 2016). We propose that increased osteoblast activity may be due to altered FGF-signalling in response to the reactivation of *hoxa13a* /*hoxd13a* during fin fold mesenchyme regeneration. An analysis of osteoblast markers is necessary to provide conclusive evidence for increased osteoblast activity, however due to limited sample number, further analysis was not possible. *5'Hox* signalling has been shown to contribute to *Fgf10* signalling in mice (Sheth et al. 2013). In addition, FGF-signalling has been linked to the induction of osteoblast/chondrocyte differentiation, and the promotion of intramembranous bone ossification (Martin 1998; Mercader 2007; Su et al. 2014).

Nitroreductase/Metronidazole system for long-term cell ablation

The nitroreductase/metronidazole system was devised as a tool for analysing developmental and regenerative processes following cell-specific ablation (Curado et al. 2008). Unfortunately, the regenerative capabilities of zebrafish fins make long-term sustained cell ablation difficult. We, and others, show that the NTR/MTZ system is efficient at specifically ablating cells of interest in short-term experiments (Mathias et al. 2014). At 3dpf, we observed

nearly complete fin fold mesenchyme ablation in the median fin fold. If metronidazole is removed however, a secondary wave of YFP-expressing fin fold mesenchyme appears within 48 hours (Fig. 3.12). To assess the effects of fin fold mesenchyme ablation on fin ray formation, we therefore had to maintain metronidazole exposure during the entire course of development. At high concentrations or following prolonged exposure times, metronidazole is toxic and can induce non-specific effects (Mathias et al. 2014). We therefore utilised a more efficient triple mutant variant of nitroreductase in order to reduce treatment length/concentration and minimize metronidazole toxicity (Mathias et al. 2014). Furthermore, to promote survival of larvae, metronidazole concentrations were reduced as development progresses and 6 hour rotifer baths/feeding breaks were provided daily (Fig. 3.9). Despite all these measures, *Tg(Inta11:NTR)* larvae had extremely low survival rates (13.5%) at 30dpf (Fig. 3.9) and experienced severe developmental delays (Fig. 3.11) following a "juvenile 5" treatment. No caudal fin ray defects were observed in the surviving larvae and only modest pectoral fin ray defects were produced. High levels of YFP-expressing cells were present in the caudal fin and in the proximal regions of the pectoral fins of MTZ-treated *Tg(Inta11:NTR)* larvae at 30dpf. These observations highlight regeneration of the fin fold mesenchyme despite the sustained metronidazole treatment (Fig. 3.12). "Juvenile 4" and juvenile 3" treatments, with minimal increases in metronidazole concentration, result in more severe developmental delays and complete lethality of *Tg(Inta11:NTR)* larvae prior to 30dpf (Fig. 3.9). WT larvae exposed to metronidazole also show impaired survival following a "juvenile 3" treatment (Fig. 3.9). In summary, it seems the metronidazole concentrations required for survival *Tg(Inta11:NTR)* larvae to 30dpf are insufficient to maintain complete fin fold mesenchyme ablation. Therefore, metronidazole toxicity and the regenerative properties of zebrafish decrease the usefulness of this system for

long-term cell ablation of *hoxa13a/hoxd13a*-expressing fin fold mesenchyme. The difficulties of raising zebrafish in metronidazole are worsened by the existence of an additional secondary pattern of YFP-expressing cells in the lower digestive tract of *Tg(Inta11:NTR)*larvae (Fig. 3.9). These cells do express *hoxa13a*, as confirmed by whole mount *in situ* hybridization (Fig. 3.9), and are therefore also subject to cell ablation. The ablation of *hoxa13a*-expressing cells in the lower digestive tract likely contributed to developmental delays and decreased survival of MTZ-treated *Tg(Inta11:NTR)* larvae.

In conclusion, we show that ablation of fin fold mesenchyme results in actinotrichia defects and collapse of the median and pectoral fin folds in zebrafish larvae. Using a sustained 30 day metronidazole treatment, we are also able to produce pectoral fin ray defects. We propose that the ablation of mesenchymal cells results in a failure to maintain the actinotrichia, likely due to a decrease in total actinodin proteins, and subsequent collapse of the fin fold. Impaired migration of any surviving or regenerating fin fold mesenchyme results in a lower number of presumptive osteoblasts that are also less organized, thus creating defects in fin ray length, number and definition. In addition, 7dpf larvae show a reduction in endoskeletal disc size, while 30dpf larvae show earlier calcification in the proximal regions of the fin rays. We propose that these phenotypes are long term effects from the initial cell ablation and subsequent regeneration.

3.6. Methods

Animal care

All fish are bred and raised in the D' Iorio, University of Ottawa, zebrafish facility. Wild-type zebrafish stock has been bred in the laboratory for several years. The fish facility is maintained at 28°C, with a photo-period of 14 h of light and 10 h of darkness (Westerfield 2000). Animal care and experiments were certified by the Canadian Council on Animal Care and licensed under the

Ontario Animals for Research Act. Zebrafish larvae were anesthetized and euthanized using tricaine. Approved protocol number: BL-1851.

Plasmid construction

All cloning and subcloning was performed following standard procedures (Sambrook & Russell 2001). The original vector used was *pEGFP-N1*. The CMV regulatory regions were removed and Tol2 arms were inserted between the *AseI* and *NheI* (left arm) and *AflII*(right arm).

The human beta-globin minimal promoter was isolated from the *p1230* vector, amplified, and inserted in the BamHI, and AgeI sites using the following primers:

FW 5' GGATCCCTGGGCATAAAAGTCAG 3'

Rev 5' ACCGGTTCTGCTTCTGGAAGGCT 3'

m-Inta11 element was inserted at the XmaI site according to (Kherdjemil et al. 2016).

The YFP-NTR transgene was amplified from the pBK 2xNRSE-2xzHB9-5xUAS-TagYFP-T2A-NTR plasmid and inserted into the AgeI and NotI sites using the following primers:

FW 5' ACCGGTATGGTTAGCAAAGGCGAGG

Rev 5' GCGGCCGCTTACACCTCTGTCAGGGTGA

Microinjection in Zebrafish embryos and transgenic Zebrafish

Constructs (final concentration of 100ng/μL) are co-injected with transposase RNA (final concentration of 50ng/μL) mixed with RNAse-free water and 0.5% phenol red in one cell-stage zebrafish embryos.

Transgenic lines were identified via fluorescence microscopy and the expression patterns were confirmed with 3 lines. The transgenic line with the brightest YFP expression was used for experiments.

Treatments

For “Larval 1–3” treatments (Fig. 3.9), larvae were raised in petri dishes with 50 embryos in 25ml of treatment solution (E3 media + MTZ/1%DMSO). For “larval 3” treatment (Fig. 3.9), solutions were changed daily and larvae were raised in the incubator with no light cycle. Larvae were not fed. Larvae displaying non-specific defects at 7dpf from MTZ toxicity (heart edema, shortened trunk) were consistently omitted from analysis across treatment groups.

For “juvenile 1–5” treatments (Fig. 3.9), larvae were transferred to 1L tanks at 5dpf. Each 1L tank housed two ~450ml mesh bottom baskets containing 12–13 larvae. Mesh bottom baskets could be lifted and easily transferred to new 1L during treatment changes without harming the larvae. Treatment solution (Water + MTZ/1%DMSO) was changed daily, and larvae were raised at 28°C, with a photo-period of 14 h of light and 10 h of darkness (Westerfield 2000). Larvae were fed Gemma75 food once daily from 6-10dpf, twice daily from 10-15dpf, and Gemma150 four times daily from 16-30dpf.

For “juvenile 1–2” treatments (Fig. 3.9), one third of the treatment solution was a concentrated rotifer bath.

For “juvenile 3–5” treatments (Fig. 3.9), larvae were transferred to a rotifer bath (1/3 concentrated rotifers, 2/3 water) for 6 hours a day to facilitate feeding then returned to the treatment solution (Water + MTZ/1%DMSO). From 16dpf onward, larvae were simply transferred to water for 6 hours daily instead of the rotifer bath.

All treatments are made with 1% DMSO.

TUNEL assay

Embryos were fixed in 4%PFA O/N at 4°C. Following rehydration in PBST, embryos were permeabilized by digestion with 25mg/µl proteinase K in PBS for 20min at RT. Embryos were then post-fixed for 20min in 4%PFA and washed 5X in PBST, 5 min each wash. Following

washes, embryos were permeabilized using fresh 0.1% sodium citrate in PBST for 15min at RT, and then washed 3X in PBST, 5 min each wash. TUNEL reaction mix was added according the manufacturer's instructions (Roche Cat#12156792910) and incubated for 2hours at 37°C in the dark. Following TUNEL reaction, embryos were washed 3X in PBS for 5 min each wash.

***In situ* hybridization**

In situ hybridization on whole-mount embryos was performed as previously described (Thisse & Thisse 2008). Digoxigenin-labelled antisense RNA probes were generated using the following cDNAs: *and1* (2,383 base pairs (bp) (Zhang et al. 2010), *hoxd13a*(793bp, (Zhang et al. 2010)), *shha* (2.5kb, (Smith et al. 2008)]), *fgf10a*(1.6kb; kindly provided by I. Belmonte), *fgf8a*(1.5kb; (Zhang et al. 2010)), *hoxa13a*(500 bp; Addgene 36463, (Ahn & Ho 2008)), *hoxa13b* (700 bp; Addgene 36568, (Ahn & Ho 2008)), *hoxa11b* (800 bp; Addgene 36466, (Ahn & Ho 2008)), *ptch2*(1.15 kb; (Laforest et al. 1998)) and *hhip*(2 kb;).

hhip cDNA was amplified using the following primers:

FW 5'ATGAAGCATTTGAAATTTGTGCT

Rev 5'GTCTTTCTCACCGTCCCCTT

Immunohistochemistry (IHC)

Embryos were fixed in 4%PFA O/N at 4°C, and then stored in methanol. From methanol, larvae are permeabilized in acetone at -20°C for 20 min. No proteinase K treatment is required. Following 2X5min washes in PBST, larvae are placed in blocking solution for 3 hours (10% calf serum, 0.5% TritonX100 in PBS) and then incubated in primary antibody overnight (Primary Antibody: mouse anti-Collagen II (II-II6B3, 1:100 dilution in blocking, Developmental Studies Hybridoma Bank). Following 4X10min PBST washes, larvae are incubated in secondary antibody (Secondary Antibody: Alexa Fluor Goat anti-Mouse 488, 1:500 in PBST, Life

technologies) for 3 hours at room temperature. Larvae are then washed 4X10min in PBST, with the first wash containing DAPI (1:10 000) stain.

Transgenic fish

***Tg(Kr19)*transgenic line**

Transgene is integrated 32,151 bp downstream of ENSDARG00000078279, and at a second unknown integration site. Kr19 fish show membrane-tethered KillerRed expression in the choroid plexus and endoskeletal disc cells, among other regions (Teh et al. 2010).

Bone and cartilage staining

Following O/N fixation in 4%PFA at 4°C, 20-30dpf larvae were stained using the "Two-color acid-free" method previously described (Walker & Kimmel 2007). 60mM $MgCl_2$ was used for alcian blue stain.

Fin measurements

Adobe Photoshop CS6 was used to take the fin measurements. Each fin is measured 5 times, and the 3 median values are then averaged for a single value per fin. 7dpf median fins and pectoral fins were dissected off and imaged using the stereoscopic microscope. Median fin photos from 48-72hpf were taken whole-mount using the dissection scope. The position of migrating cells in the median fin fold is visualized using highly contrasted brightfield images. The distal most cell is used to measure the distance migrated. The pectoral fin was precluded for cell migration measurements as these cells are not visible without fin dissection. Fin mounting further creates difficulties regarding mesenchymal cell visibility due to their subsequent flattened morphology.

3.7. Acknowledgments

We thank Dr. Mumm for providing the pBK 2xNRSE-2xzHB9-5xUAS-TagYFP-T2A-NTR plasmid, and Samuel MacDonnell for creating the *Tg(m-Inta11-β-globin:mCherry)* transgenic

line. We also thank Dr. Marc Ekker and Dr. Qingming Qu for their critical reading of the manuscript. This work is supported by the Natural Sciences and Engineering Research Council of Canada (#155817–2012 & #429427–2012) to M.-A.A.

3.8. Figures

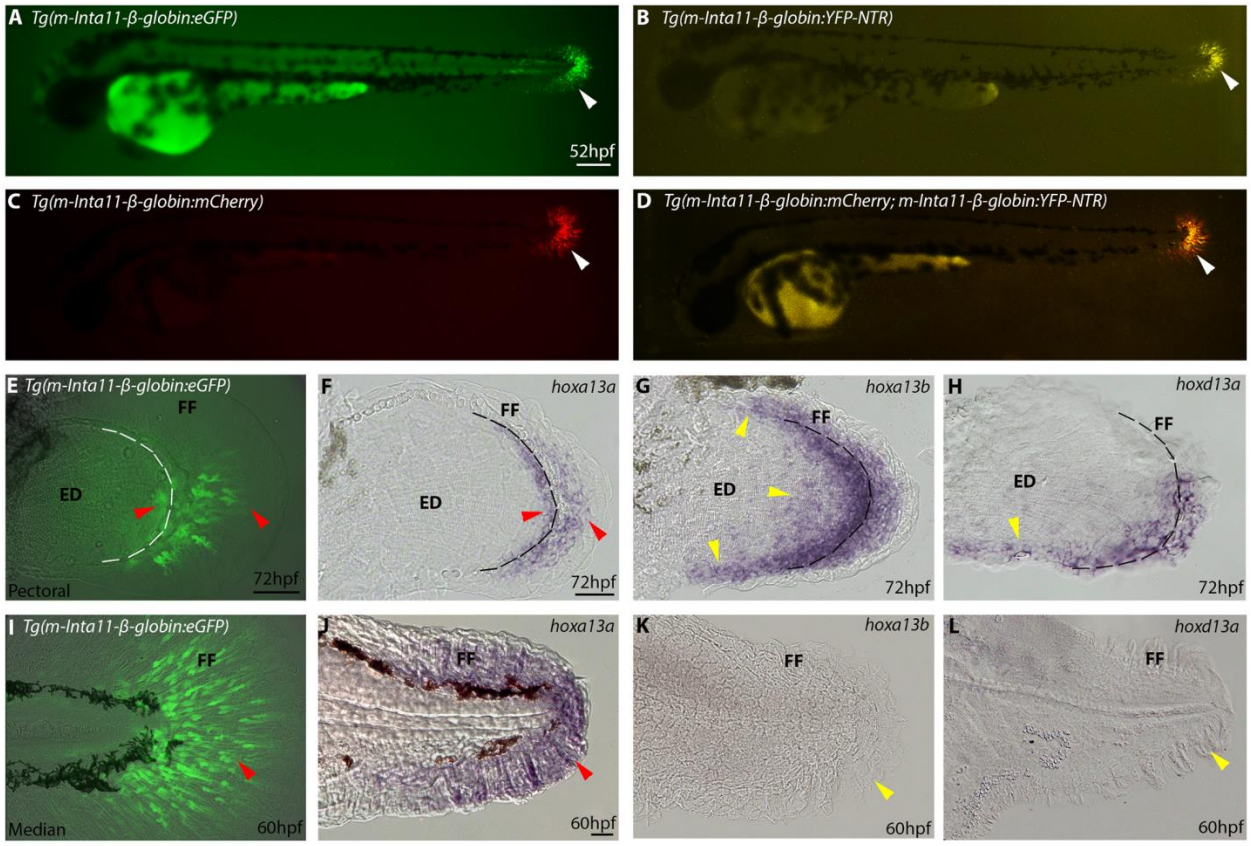

Figure 3.1. Nitroreductase (NTR) in *Tg(Inta11:NTR)* is expressed in subset of *hoxa13a/hoxd13a*-expressing mesenchyme of pectoral fin fold and *hoxa13a*-only expressing mesenchyme of the median fin fold.

(A-D) Whole mount view of transgenic lines using the "*m-Inta11-β-globin*" regulatory elements at 52hpf. **(E-H)** Pectoral fin dissections showing reporter, *hoxa13a*, *hoxa13b*, and *hoxd13a* expression in the fin fold mesenchyme at 72hpf. **(I-L)** Median fin dissections showing reporter, *hoxa13a*, *hoxa13b*, and *hoxd13a* expression in the fin fold mesenchyme at 60hpf. At 52hpf, transgene (*eGFP*, *mCherry*, *YFP-NTR*) expression is visible in the migrating mesenchyme of the median fin fold using the "*m-Inta11-β-globin*" regulatory elements (white arrow) (A-D). Double transgenic fish *Tg(m-Inta11-β-globin:mCherry; m-Inta11-β-globin:YFP-NTR)* show

colocalization of mCherry and YFP expressing cells in the median fin fold (D). Reporter expression is present in the migrating mesenchyme within the pectoral fin fold, as well as cells located at the distal edge of the endoskeletal disc (red arrow) (E), recapitulating a subset of *hoxa13a/hoxd13a*-expressing cells (F). *hoxa13b*, and *hoxd13a* expression extends proximally within the endoskeletal disk and this region does not correlate with reporter expression (yellow arrows) (G, H). Dotted line represents limit between fin fold and endoskeletal disc (F-H). Reporter expression is present in the migrating mesenchyme within the median fin fold (red arrow) (I), recapitulating endogenous *hoxa13a* expression (J). No *hoxa13b* or *hoxd13a* expression is visible in the median fin at 60hpf (yellow arrows) (K, L). Brightfield (F-H, J-L), fluorescence (A-D), and brightfield/fluorescence merged images (E, I K). ED, Endoskeletal disc; FF, Fin fold. Scale bars: 200μm in A-D; 50μm in E-G, I-L; 30μm in H.

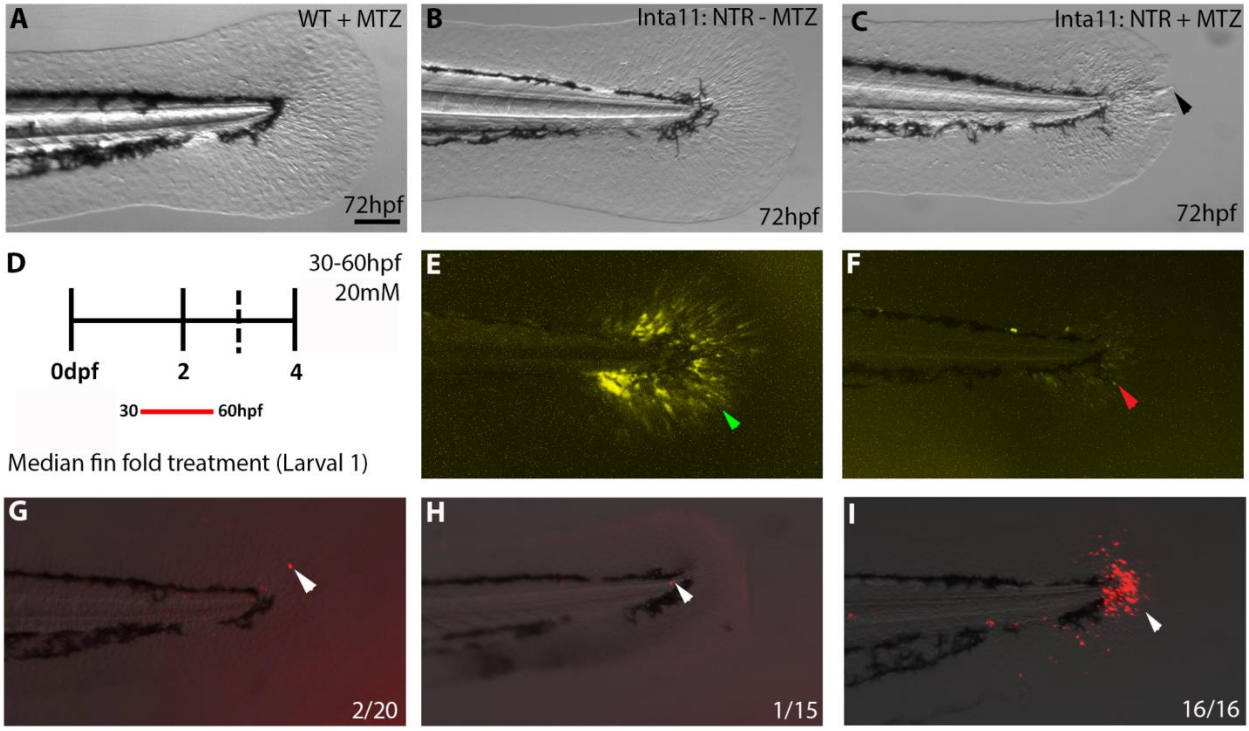

Figure 3.2. Subset of *hoxa13a/hoxd13a*-expressing cells specifically ablated in *Tg(Inta11:NTR)*fish following metronidazole treatment.

(A-C, E-I) Median fin fold of 72hpf larvae from 3 treatment groups (2 control, 1 experimental), YFP expression levels and TUNEL assay are shown. **(D)** Schematic of "Larval 1" treatment, larvae are exposed from 30-60hpf. Median fin morphology unaffected in treatment control groups (WT + MTZ, Inta11: NTR—MTZ) (A, B) compared to Inta11: NTR + MTZ (C). Inat11: NTR + MTZ larvae show median fin fold collapse (black arrow) (C). YFP expression drastically reduced in Inta11: NTR + MTZ larvae (red arrow) (F), when compared to Inta11: NTR—MTZ (green arrow) (E). A small percentage of treated control larvae (10% and 6.66%) display single TUNEL-positive cells in the median fin fold (white arrow) (G, H). All treated Inta11: NTR + MTZ larvae (n = 16) show TUNEL-positive cells in the median fin fold (white arrow) (I).

Brightfield (A—C), fluorescence (E, F), and brightfield/fluorescence merged images (G-I). Scale bars: 100µm in A-C, E-I.

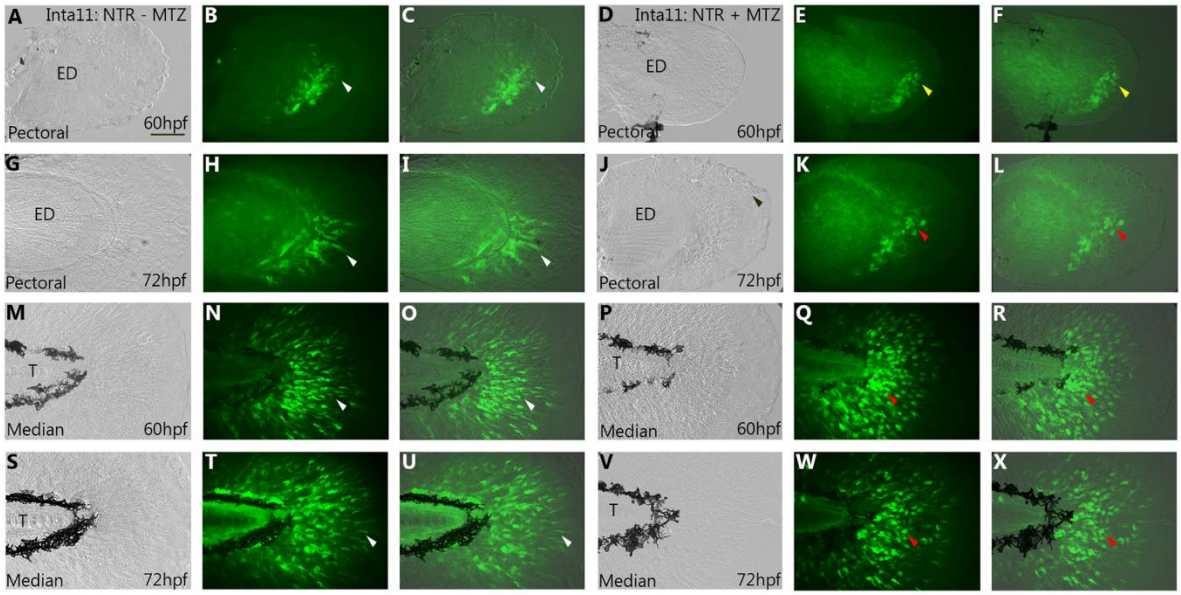

Figure 3.3. Morphological and migratory defects of the pectoral and median fin fold mesenchyme in *Tg(Inta11:NTR)* larvae following metronidazole treatment.

(A-J) Pectoral and **(M-W)** median fin of 60, and 72hpf Inta11: NTR + MTZ and Inta11: NTR—MTZ larvae outcrossed with *Tg(Inta11-β-globin:eGFP)* transgenic larvae. At 60hpf, Inta11: NTR—MTZ show the beginning of fin fold migration in the pectoral fin (white arrow) (A-C). Migration is absent/delayed in the pectoral fin of the Inta11: NTR + MTZ group (yellow arrow) (D-F). At 72hpf, Inta11: NTR + MTZ larvae display reduced fin fold mesenchyme migration in the pectoral fin (J-L) compared to the control (G-I). Fin fold mesenchyme are less elongated/branched and are clustered close to the endoskeletal disk (red arrow) (J-L), compared to control pectoral fins (white arrow) (G-I). At 60, and 72hpf median fin fold mesenchyme of Inta11: NTR + MTZ larvae cluster next to the trunk, and are more round and less elongated/branched (red arrow) (P-R, V-X), compared to control larvae (white arrow) (M-O, S-U). Brightfield (A, D, G, J, M, P, S, V), fluorescence (B, E, H, K, N, Q, T, W), and

brightfield/fluorescence merged images (C, F, I, L, O, R, U, X). ED, Endoskeletal disc; T, Trunk. Scale bars: 50µm in A-X.

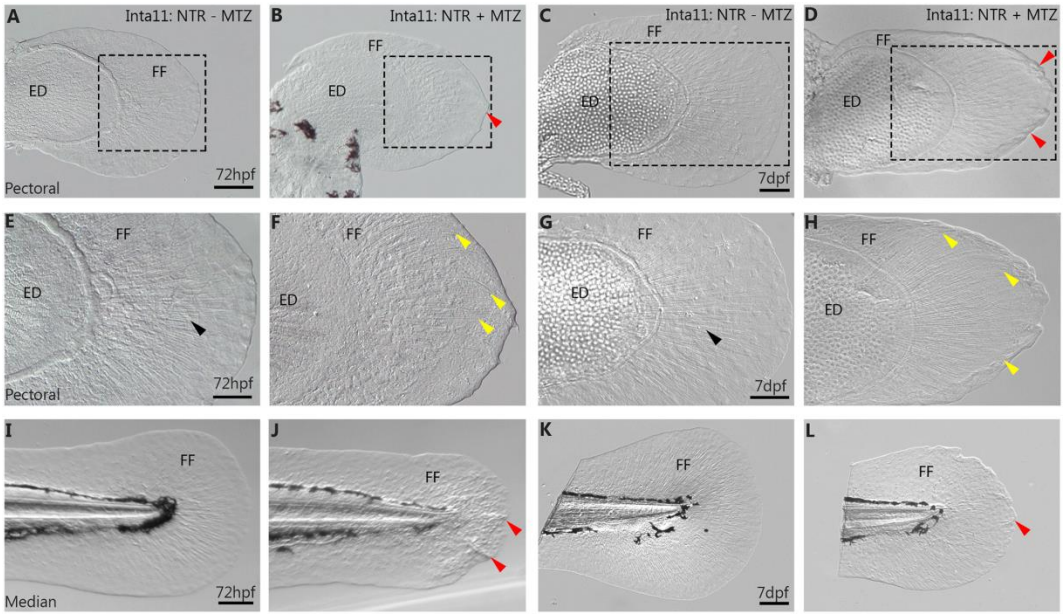

Figure 3.4. Fin fold collapse in 72hpf, 7dpf pectoral and median fins of *Tg(Inta11:NTR)* following metronidazole treatment.

(A-H) Pectoral and **(I-L)** median fins of Inta11: NTR + MTZ and Inta11: NTR–MTZ control larvae at 72hpf and 7dpf. Inta11: NTR + MTZ larvae display pectoral fin fold collapse at 72hpf (B, F) and 7dpf (D, H), compared to Inta11: NTR—MTZ (A, C, E, G). Note the collapse of the fin fold (red arrows) (B, D). Panels E-H are magnifications of dotted box in panels A-D. Note the appearance of bending actinotrichia fibrils (yellow arrows) in Inta11: NTR + MTZ larvae (F, H) compared to straight actinotrichia (black arrows) in the Inta11: NTR—MTZ larvae (E, G). Inta11: NTR + MTZ larvae display major median fin fold defects at 72hpf (J) compared to Inta11: NTR—MTZ larvae (I). Note the collapse of the fin fold (red arrows) (J). By 7dpf, Inta11: NTR + MTZ larvae continue to show a reduction in median fin fold size compared to Inta11: NTR—MTZ larvae (K), however defects are ameliorated compared to Inta11: NTR + MTZ

larvae at 72hpf (J, L). Note the minor folding of distal tip of the median fin (red arrow) (L). ED, Endoskeletal disc; FF, Fin fold. Scale bars: 100µm in A-D, F, H, I-L; 50µm in E, G.

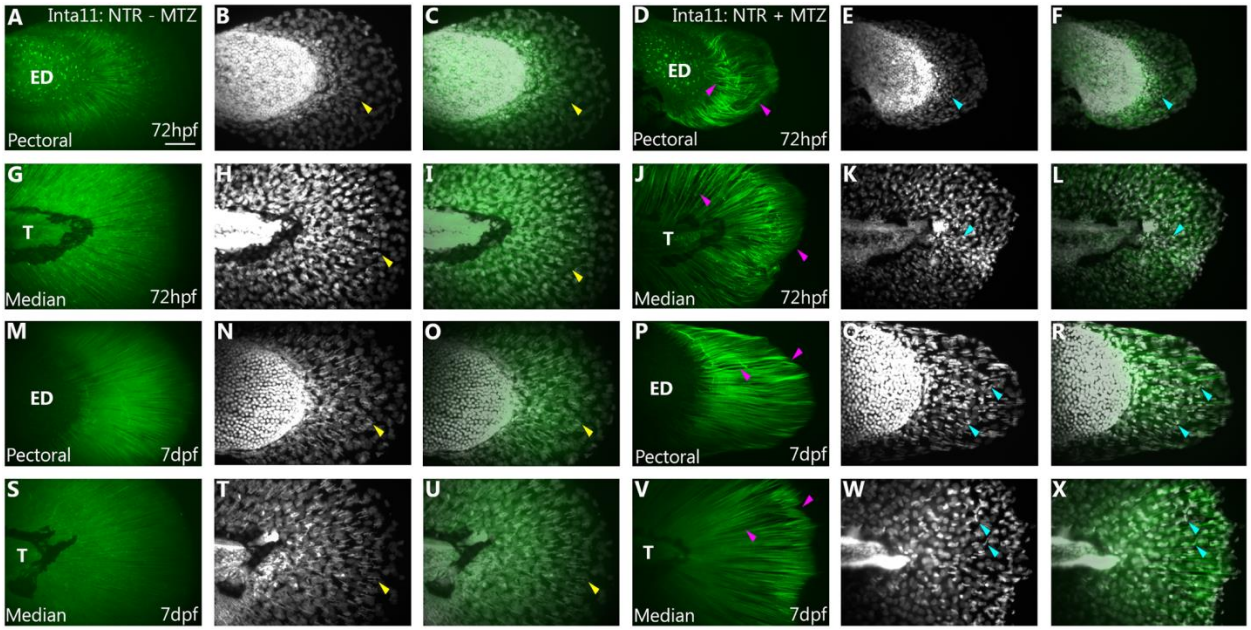

Figure 3.5. Actinotrichia defects in 72hpf, 7dpf pectoral and median fins of *Tg(Inta11:NTR)* following metronidazole treatment.

Collagen II Immunostaining of **(A-F, M-R)** pectoral and **(G-L, S-X)** median fins of Inta11: NTR + MTZ and Inta11: NTR–MTZ control larvae at 72hpf and 7dpf. At 72hpf, and 7dpf untreated larvae show rigid, parallel actinotrichia throughout the pectoral and median fin fold (A, C, G, I, M, O, S, U), with DAPI staining revealing proper fin fold mesenchymal cell migration (Yellow arrow) (B, H, N, T). Note the fin fold mesenchyme elongate along the proximal distal axis, aligning with the actinotrichia (Yellow arrow) (B-C, H-I, N-O, T-U). At 72hpf, and 7dpf, actinotrichia of MTZ-treated larvae are unable to remain rigid and bend within the fin fold (Purple arrow) (D, F, J, L, O, R, V, X). This correlates with fin fold collapse. The actinotrichia are unable to remain parallel to one another, creating gaps within the fin fold (D, F, J, L, O, R, V, X). Note the apparent unbundling of Collagen II stained strands at 72hpf (Purple arrow) (D, J).

At 72hpf, DAPI staining reveals fin fold mesenchyme cluster next to the pectoral fin endoskeletal disc and the trunk region proximal to the median fin fold (Teal arrow) (E, K), having failed to migrate correctly. At 7dpf, surviving fin fold mesenchyme fails to migrate correctly (Teal arrow) (Q, W). In the pectoral fin, migration is restricted to the central region of the fin fold (Teal arrow) (Q) and in both the pectoral and median fin, these cells display elongation along various different axes, correlating with actinotrichia defects (Teal arrow) (P-R, V-X). Collagen II staining (A, D, G, J, M, P, S, V), DAPI (B, E, H, K, N, Q, T, W) and merged (C, F, I, L, O, R, U, X) images are presented. ED, Endoskeletal disc, T, Trunk Scale bars: 50μm in A-X.

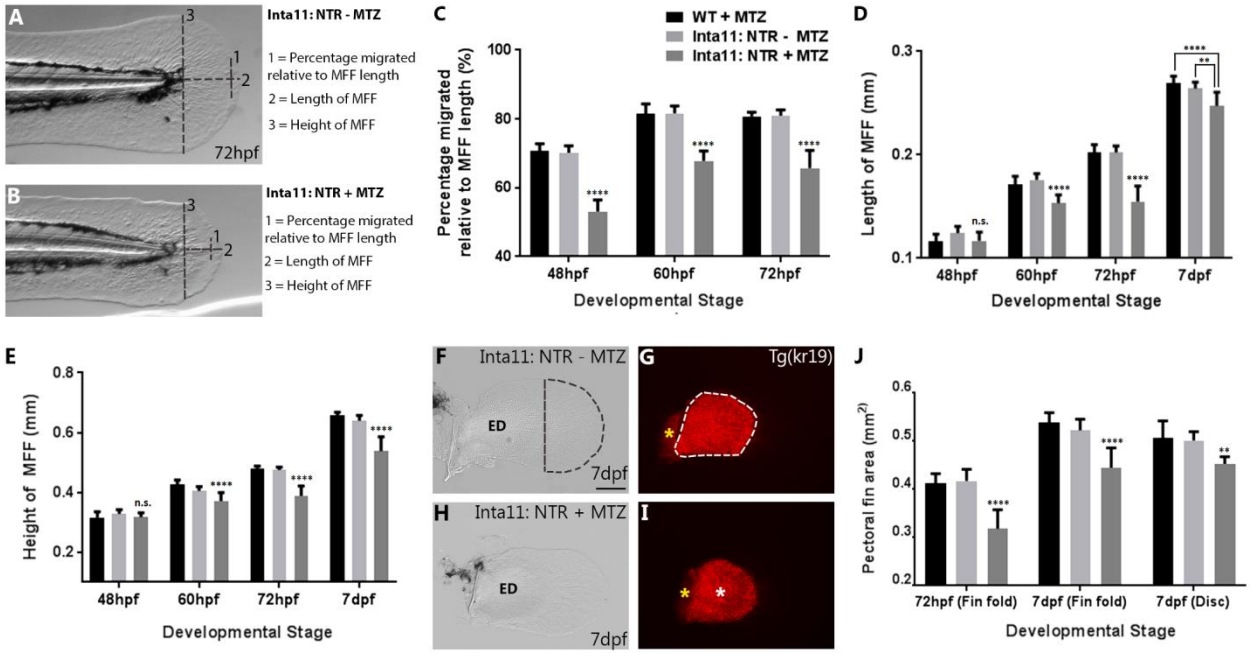

Figure 3.6. Metronidazole-treated *Tg(Inta11:NTR)* larvae show defects in median fin fold mesenchyme migration, a reduction in median and pectoral fin fold size and a reduction in endoskeletal disc size.

(A-B) Schematic of median fin fold measurements. **(C-E, J)** Graphs displaying measurements of median fin mesenchyme displacement (%), median fin fold width (mm) and height (mm), and pectoral fin fold and endoskeletal disc area (mm^2). **(F-G)** Inta11: NTR—MTZ and **(H-I)** Inta11: NTR + MTZ pectoral fin at 7dpf outcrossed with *Tg(kr19)* to highlight endoskeletal disc. Fin fold mesenchyme cell displacement is represented as a percentage displaced relative to the overall fin fold length (trunk to distal tip) (Measurement 1), length of median fin fold is measured from trunk to distal tip (measurement 2), and height of median fin fold is measured from dorsal to ventral tips at the trunk (measurement 3) (A-B). Inta11: NTR + MTZ larvae display a reduction in median fin fold mesenchyme cell displacement at 48, 60, and 72hpf

compared to control larvae (C). Inta11: NTR + MTZ larvae show a reduction in median fin fold width and height at 60, 72hpf, and 7dpf compared to control larvae (D, E). No difference is observed for either measurement at 48hpf (D, E). Inta11: NTR + MTZ larvae show a decrease in pectoral fin fold area at 72hpf, and 7dpf, as well as a reduction in endoskeletal disc size at 7dpf (J). Example of Inta11: NTR—MTZ (F, G) and Inta11: NTR + MTZ (H, I) pectoral fin used for distal fin fold, endoskeletal disc measurements. Region used for measurement is indicated by dotted line (F, G). Note the decreased disc size in the Inta11: NTR + MTZ pectoral fin (white asterisks) (I). Scapulocoracoid not included in the disc area measurements (yellow asterisks) (G, I). All bar values are an average of 10 measurements (n = 10 fins) with standard deviation indicated, with the exception of endoskeletal disc size (J). Endoskeletal disc values are based on measurements of 5, 5, and 8 fins (n = 5 fins, n = 5 fins, n = 8 fins) for treatment controls and Inta11: NTR + MTZ larvae respectively. Standard one-way ANOVA was performed. Each mean was compared against both other means. Tukey's correction was applied. No statistically relevant difference was ever detected between treatment controls (WT + MTZ, Inta11: NTR—MTZ). Inta11: NTR + MTZ P-values (asterisks) are representative of comparisons with both treatment controls, with the exception of median fin fold width at 7dpf, where unique P-values are indicated for comparisons with each control (D). Brightfield (A-B, F, H), fluorescence (G, I). P-values: ** P = 0.001>0.005, **** P = <0.0001. ED, Endoskeletal disc; MFF, Median fin fold. Scale bars: 100μm (F-I).

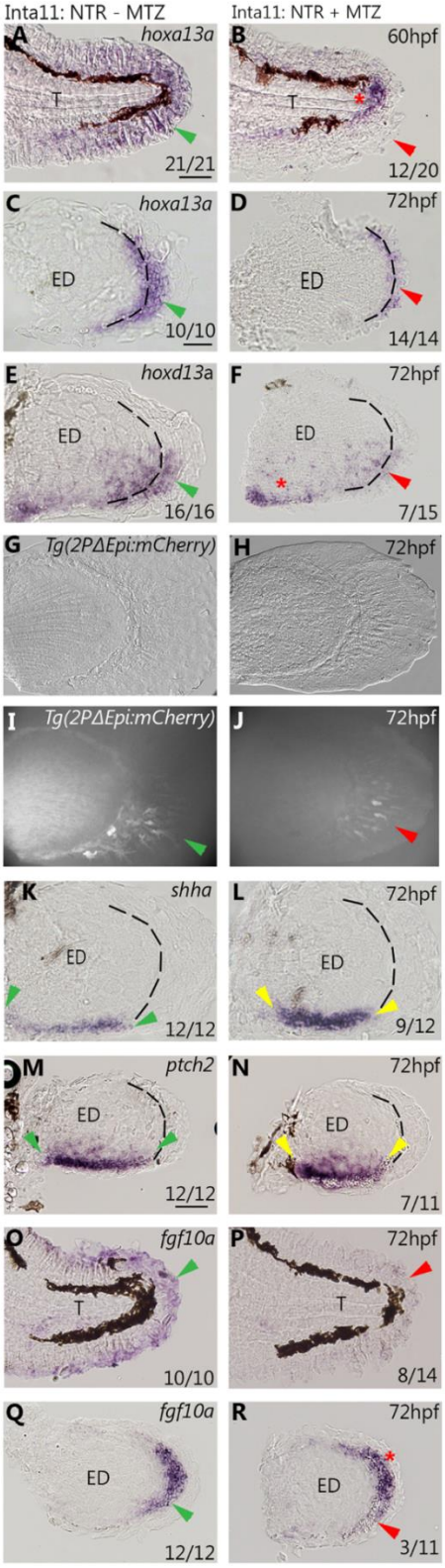
Inta11: NTR - MTZ
Inta11: NTR + MTZ
A
hoxa13a
T
21/21
B
60hpf
T
12/20
C
hoxa13a
ED
10/10
D
72hpf
ED
14/14
E
hoxd13a
ED
16/16
F
72hpf
ED
7/15
G
Tg(2PΔEpi:mCherry)
H
72hpf
I
Tg(2PΔEpi:mCherry)
J
72hpf
K
shha
ED
12/12
L
72hpf
ED
9/12
M
ptch2
ED
12/12
N
72hpf
ED
7/11
O
fgf10a
T
10/10
P
72hpf
T
8/14
Q
fgf10a
ED
12/12
R
72hpf
ED
3/11

Figure 3.7. *Altered gene expression profiles in the median and pectoral fin of Tg(Inta11:NTR)* larvae following metronidazole treatment.

(A-N) *in situ hybridization* and *and1* reporter data showing gene expression profiles in the median and pectoral fin at 60, and 72hpf in Inta11: NTR—MTZ and Inta11: NTR—MTZ larvae. Inta11: NTR—MTZ are present in the left panels (A, C, E, G, I, K, M, O, Q) and Inta11: NTR + MTZ are present in the right panels (B, D, F, H, J, L, N, P, R). Inta11: NTR + MTZ show a decrease in distal *hoxa13a* expression (red arrow) in the median fin at 60hpf (B), and in the pectoral fin at 72hpf (D) compared to Inta11: NTR—MTZ (green arrow) (A, C). Note unaltered *hoxa13a* expression in the trunk region of Inta11: NTR + MTZ (red asterisks) (B). Inta11: NTR + MTZ show a decrease in distal *hoxd13a* expression (red arrow) in the pectoral fin at 72hpf (F) compared to Inta11: NTR—MTZ larvae (green arrow) (E). Note unaltered *hoxd13a* expression in the proximal disc region of Inta11: NTR + MTZ larvae (red asterisks) (F). Inta11: NTR + MTZ double transgenic larvae show decreased *and1* reporter activity (red arrow) (J) in the pectoral fin compared to Inta11: NTR—MTZ double transgenic larvae (Red arrow) (I) at 72hpf. Brightfield (G-H) and fluorescent (I-J) images are included. Inta11: NTR + MTZ larvae show an increased anterior-posterior, and decreased proximal–distal expression domain of both *shha* and its receptor *ptch2* in the pectoral fin at 72hpf (yellow arrows) (L, N) compared to Inta11: NTR—MTZ larvae (green arrow) (K, M). Inta11: NTR + MTZ show a decrease in distal/distal posterior *fgf10a* expression at 72hpf, in the median and pectoral fin respectively (red arrows) (P, R) compared to Inta11: NTR—MTZ larvae (green arrows) (O, Q). Note unaltered expression of *fgf10a* in the anterior pectoral fin mesenchyme of Inta11: NTR + MTZ larvae (red asterisks) (N). Dotted lines indicate fin fold and disk boundary (C-F, K-N, Q-R)). Probe or reporter line is indicated in the top right corner of each panel in the left column, age is indicated in the top right

corner of each panel in the right column (A-R). Number of larvae displaying gene expression pattern, for *in situ* hybridization data, are indicated in the bottom right corner of each panel (A-F, K-R). WT-MTZ+DMSO images are contained in Fig. 3.9 and show similar expression profiles to Inta11: NTR—MTZ larvae (A, C, E, K, M, O, Q). ED, Endoskeletal disc; T, Trunk. Scale bars: 100µm in A, B, K, L; 50µm in I, J, M, N; 30µm in C-H.

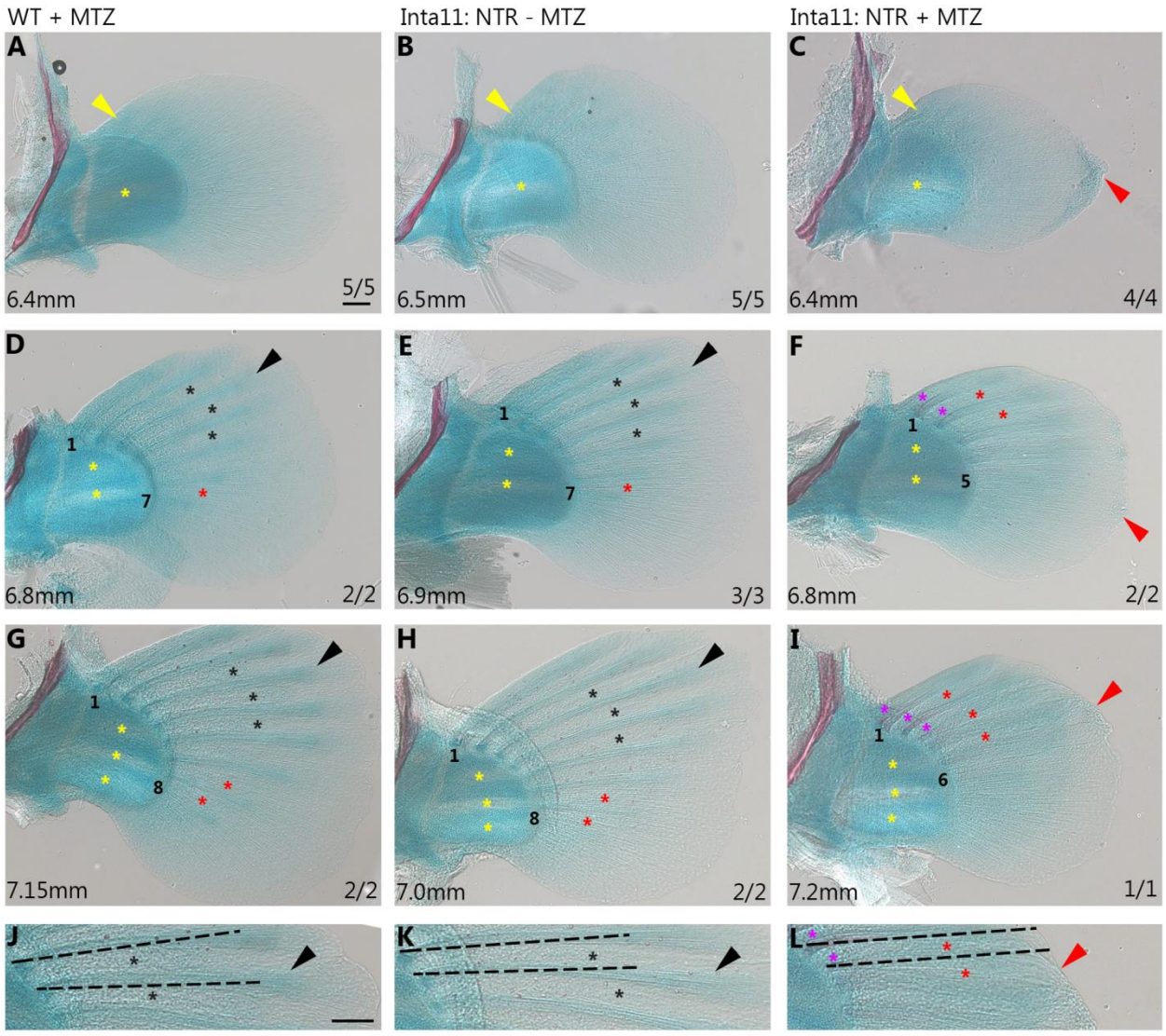

Figure 3.8. Actinotrichia defects, fin fold collapse, and fin ray defects in pectoral fins of *Tg(Inta11:NTR)* fish during late larval stages following metronidazole treatment.

(A-L) Cartilage and bone stained pectoral fins of WT-MTZ+DMSO, Inta11:NTR—MTZ, and Inta11: NTR + MTZ larvae at three standard lengths (6.4, 6.8, and 7.2mm). At standard length 6.4mm, Inta11: NTR + MTZ larvae continue to show fin fold collapse (red arrow), and actinotrichia disorganization (C), compared to control larvae (A-B). Decomposition of disc cartilage matrix between presumptive proximal radials 2 and 3 has started (yellow asterisks) (A-C). Note, the initial stages of anterior-most lepidotrichia formation are not affected in the Inta11:

NTR + MTZ larvae (C), compared to control larvae (A-B) (yellow arrows). At standard lengths 6.8mm and 7.2mm, Inta11: NTR + MTZ larvae have a reduced number of visible lepidotrichia compared to control larvae (D-I). Anterior-most and posterior-most visible rays have been numbered. Inta11: NTR + MTZ larvae continue to have minor collapse of the fin fold (red arrows) (F, I, L). Control larvae have clearly defined interray zones (black asterisks) and distal ray regions (black arrow) (D-E, G-H, J-K). Inta11: NTR + MTZ larvae have poorly defined interray zones (red asterisks) (F, I, L) similar to less developed rays in control larvae (red asterisks) (D-E, G-H) and the distal tips of the fin rays are nearly indiscriminate from the surrounding regions of the fin fold (F, I, L). Inta11: NTR + MTZ larvae show premature proximal fin ray calcification (purple asterisks) in the anterior rays (F, I, L) which is absent in control larvae (D-E, G-H, J-K). Estimate of fin ray length reduction highlighted with dotted line (J-L). As distal tip of fin rays are undefined in Inta11: NTR + MTZ, length measurements were not possible. Dotted lines span from proximal edge of fin ray to the distal edge of the fin fold at fin rays 2, and 3 (L). Identical length lines are then superimposed over control fin rays 2 and 3 (J, K) to show discrepancy in length. Disc matrix decomposition has started between presumptive proximal radials 1 and 2 (yellow asterisks) (D-F) at 6.8mm in length, and presumptive proximal radials 3 and 4 (yellow asterisks) at 7.2mm in length (G-I). All Inta11: NTR + MTZ larvae are 30dpf, and staged matched control larvae were selected based on three different staging criteria (standard length, spinal cord/rib calcification progress, and stages of endoskeletal disc cartilage matrix decomposition). Scale bars: 100μm in A-L.

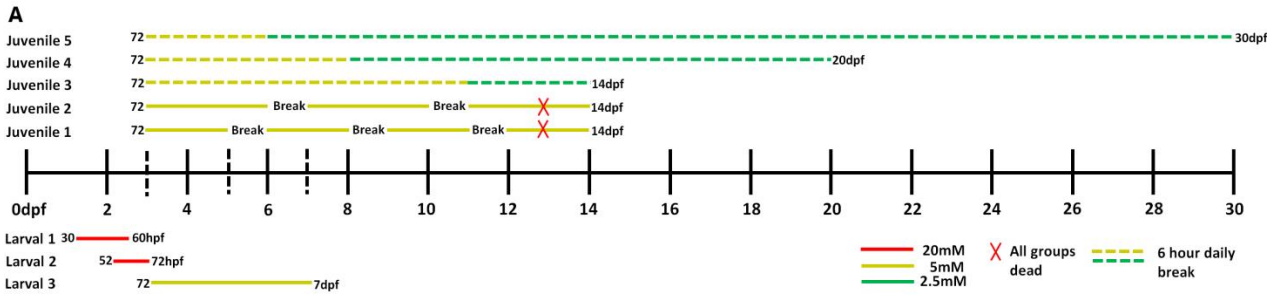

B

Survival Rate	Treatment	Day 11	Day 14	Day 20	Day 30
Juvenile 3	Inta11: NTR – DMSO	100%	100%	N/A	N/A
	WT – MTZ+DMSO	85%	50%	N/A	N/A
	Inta11: NTR – MTZ+DMSO	30%	0%	N/A	N/A
Juvenile 4	Inta11: NTR – DMSO	100%	100%	100%	N/A
	WT – MTZ+DMSO	-	-	-	N/A
	Inta11: NTR – MTZ+DMSO	85%	15%	7.4%	N/A
Juvenile 5	Inta11: NTR – DMSO	100%	95%	94%	N/A
	WT – MTZ+DMSO	94%	94%	94%	N/A
	Inta11: NTR – MTZ+DMSO	87.5%	54%	37.5%	13.5%

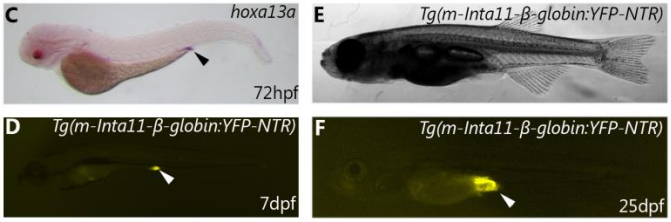

Figure 3.9. Schematic of larval and juvenile treatments, including survival rate of "juvenile 3–5" treatments.

(A-B) All metronidazole treatments tested, including survival rates in "juvenile 3–5" treatments. **(C)** Secondary expression pattern of *hoxa13a*, YFP-NTR in digestive tract. "Larval 1–3" treatments used for all stats in Fig 6 (A). "Juvenile 1–2" treatments resulted in completely lethality at 13dpf of all treatment groups (A). "Juvenile 3–5" treatments included 6-hour daily breaks (A), however only "juvenile 5" treatment resulted in some Inta11: NTR + MTZ survival (13.5%) by 30dpf (B). WT + MTZ and Inta11: NTR—MTZ showed no difference in survival rate at 20dpf using "juvenile 5" treatment (B), and larvae were not raised to 30 dpf as they developed faster than Inta11: NTR + MTZ. Secondary expression pattern of NTR in digestive tract at 7dpf (white arrow) (D), consistent with *hoxa13a* expression during early larval development (black arrow) (C). Digestive tract YFP-NTR expression maintained throughout late larval development (25dpf) (white arrow) (E-F). Brightfield (C, E), fluorescence (D, F).

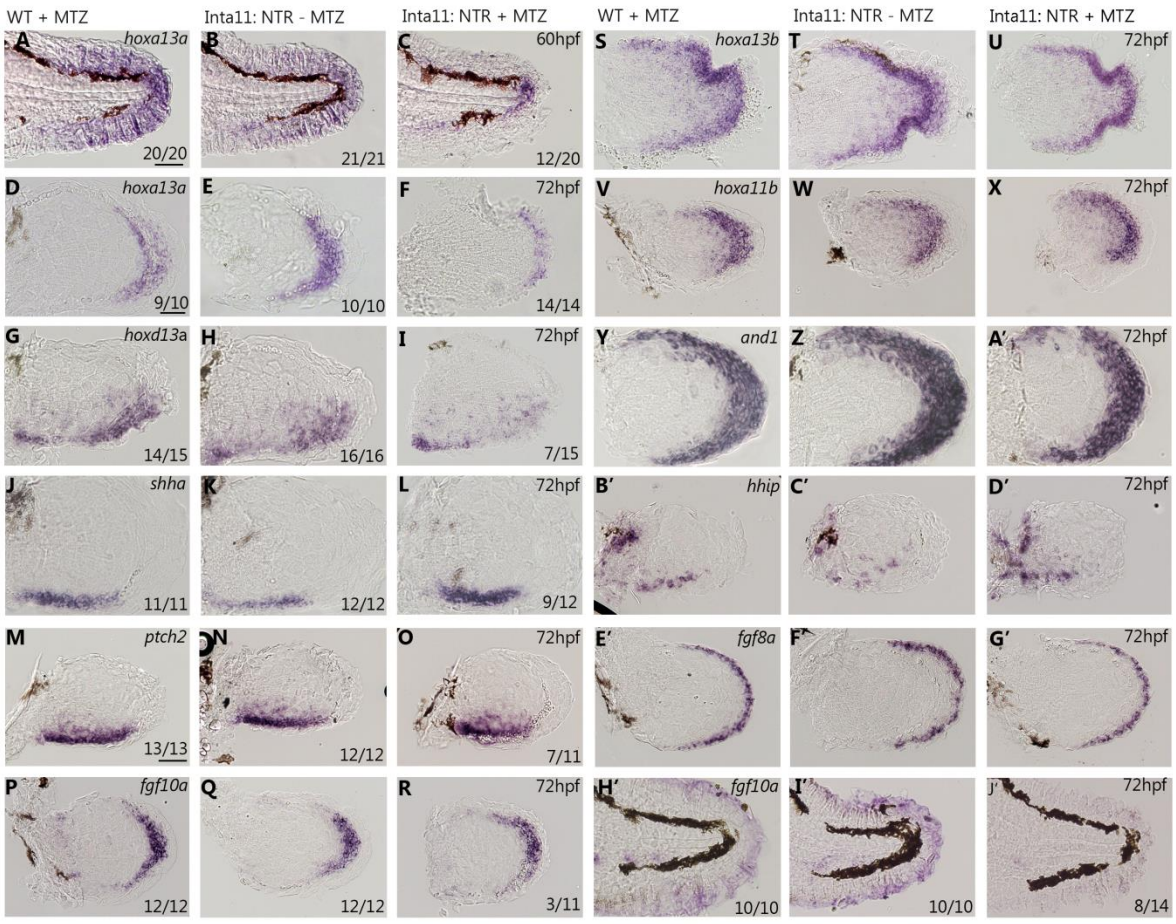

Figure 3.10. *Altered gene expression profiles in the median and pectoral fin of Tg(Inta11:NTR)* larvae following metronidazole treatment.

(A-J') Whole-mount *in situ* hybridization data showing altered, and unaltered gene expression profiles in the median and the pectoral fins of WT + MTZ, Inta11: NTR—MTZ, and Inta11: NTR + MTZ larvae. Inta11: NTR + MTZ larvae show altered gene expression patterns for *hoxa13a*, *hoxd13a*, *shha*, *ptch2*, and *fgf10a* as indicated in Fig 3.6 (A-R, H'-J'). WT—MTZ+DMSO larvae are included (A, D, G, J, M, P, H'). Inta11: NTR + MTZ show no difference in gene expression for *hoxa13b*, *hoxa11b*, *and1*, *hhip*, and *fgf8a* in the pectoral fin at 72hpf compared to control larvae (S-G'). Probe is indicated in the top right corner of each panel in the 1st, and 4th column (A, D, G, J, M, P, S, V, Y, B', E', H'), age is indicated in the top right

corner of each panel in the 3rd, and 6th column (C, F, I, L, O, R, U, X, A', D', G', J'). Number of larvae displaying gene expression pattern is indicated in the bottom right corner of each panel (A-R, H'-J'). Probes with no difference in gene expression do not have a value for number of larvae (C-G'), however each *in situ* hybridization experiment had 10–15 larvae per treatment group. Scale bars: 100µm in A-C, H'-J'; 50µm in M-R, V-X, B'-G'; 30µm in D-L, S-U, Y-A'.

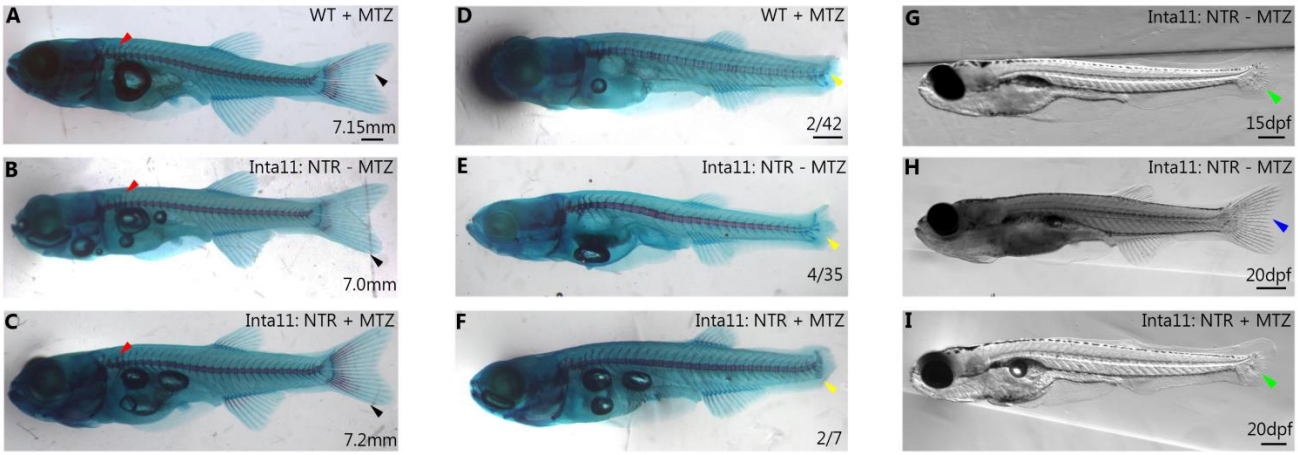

Figure 3.11. Absence of caudal fin defects in *Tg(Inta11:NTR)*larvae at 30dpf following metronidazole treatment, small percentage of larvae display major unrelated caudal fin defects in all treatment groups. Developmental delays in *Tg(Inta11:NTR)*larvae following metronidazole treatment.

(A-C) Whole-mount view of larvae used for Fig 3.8G–8L. **(D-F)** Example of major caudal defects present in all treatment groups. **(G-I)** Comparison of larvae development between Inta11: NTR—MTZ and Inta11: NTR + MTZ. At 30 dpf, Inta11: NTR + MTZ larvae do not show caudal fin ray defects (black arrow) (A) compared to control larvae (black arrows) (B-C). Calcification of entire spinal cord and first 3–4 ribs (red arrow) used for stage matching between treatment groups. Standard length present in bottom right corner (A-C). Pectoral fins were dissected and imaged for Fig 3.8G–8L. All treatment groups (WT + MTZ, Inta11: NTR—MTZ, Inta11: NTR + MTZ) have a small percentage of larvae with major unrelated caudal fin defects (Yellow arrow) (D-F). Number of larvae with phenotype present in bottom right corner of each panel (D-F). Inta11: NTR + MTZ larvae show >5 day developmental delay at 20dpf (I). Inta11: NTR—MTZ larvae at 15dpf (G), and 20dpf (H) shown as comparison. Beginning of caudal fin ray formation detected in 15dpf Inta11: NTR—MTZ (G), and 20dpf Inta11: NTR + MTZ larvae

(I) (Green arrow). All caudal fin rays present at 20dpf in Inta11: NTR—MTZ larvae (blue arrow) (H). Scale bars: 50μm in A-C, D-F, H; 30μm in G, I.

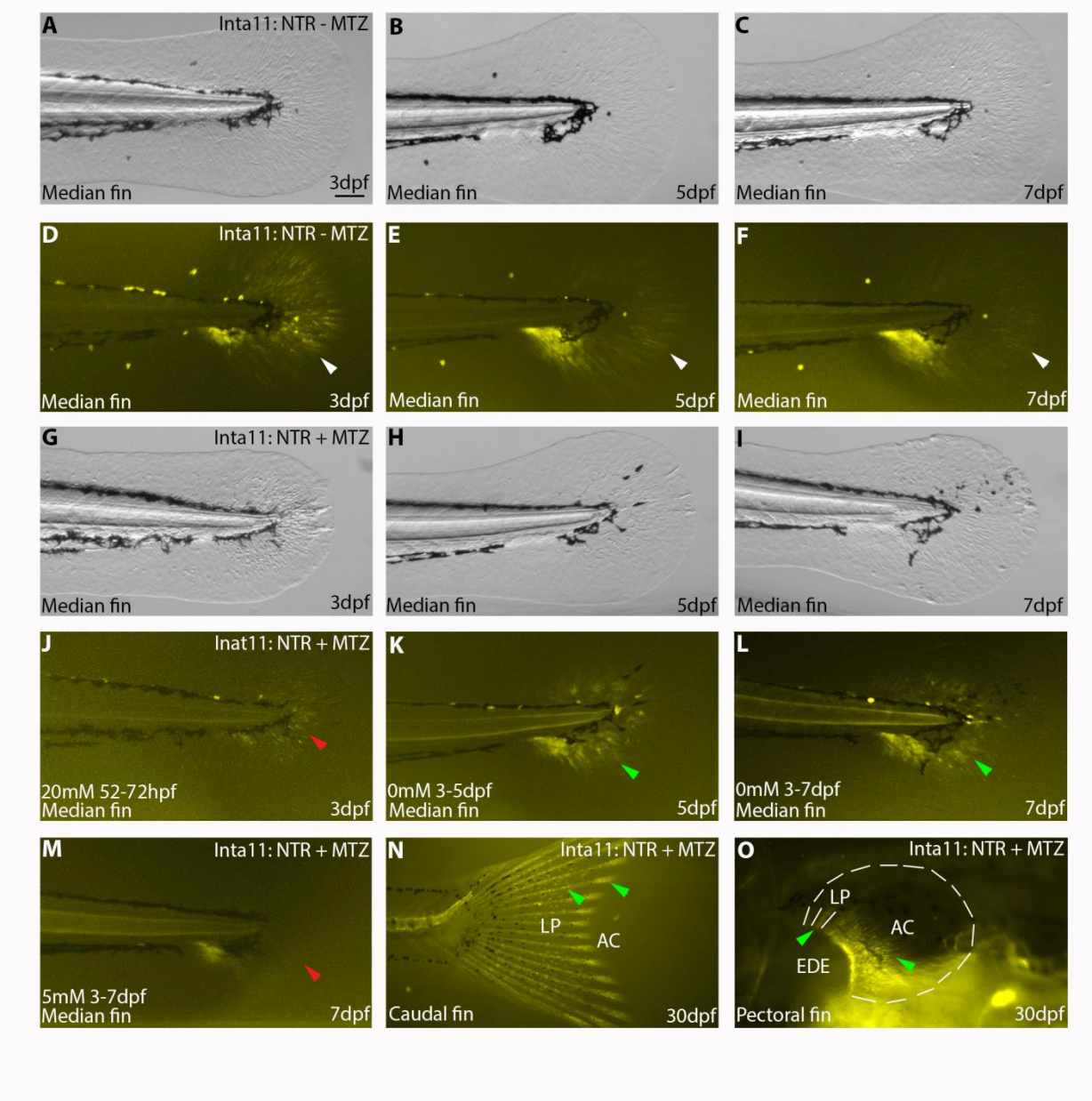

Figure 3.12. Fin fold mesenchyme regeneration in *Tg(Inta11:NTR)*larvae following metronidazole treatment, incomplete ablation YFP-expressing cells in caudal and pectoral fin of *Tg(Inta11:NTR)* larvae at 30dpf.

(A-M) Comparison of YFP-NTR expression in the median fin from 3-7dpf in Inta11: NTR—MTZ, I Inta11: NTR + MTZ, where treatment is halted at 3dpf, and Inta11: NTR + MTZ where treatment is maintained until 7dpf. **(N-O)** Levels of YFP-NTR expression in Inta11: NTR + MTZ at 30dpf. Inta11: NTR—MTZ larvae show highest levels of YFP-NTR expression in the

median fin fold at 3dpf (white arrow) (A, D). YFP-NTR expression levels decline by 5dpf (white arrow) (B, E) and 7dpf (white arrow) (C, F) in Inta11: NTR—MTZ larvae. Following ablation, YFP-NTR expression is nearly absent in Inta11: NTR + MTZ larvae at 3dpf (red arrow) (G, J). If left untreated, a new wave of YFP-NTR-expressing cells are initiated in the proximal fin regions surrounding the trunk by 5dpf (green arrow) (H, K), and continue distal migration at 7dpf (green arrow) (I, L). If treatment is maintained in Inta11: NTR + MTZ until 7dpf, we continue to ablate YFP-NTR expressing cells (red arrow) (M). Note panel M is representative of "larval 3" treatment (Fig. 3.9), "juvenile 5" treatment requires 6-hour daily breaks and modified concentrations for larvae survival (S4 Fig). By 30dpf, Inta11: NTR + MTZ show high levels of YFP-NTR expression in both the caudal (N) and pectoral fin (O) indicating fin fold mesenchymal is constantly being regenerated. In the caudal fin, YFP-NTR expressing cells are along the entire proximal-distal length of the lepidotrichia (green arrow) (LP) and concentrated at the distal tip where the actinotrichia (AC) are present (green arrow) (N). In the pectoral fin, YFP-NTR expressing cells are only present in the proximal portions of the lepidotrichia and actinotrichia (green arrows), immediately adjacent to the endoskeletal elements (O). Border of the pectoral fin is highlighted by dotted line (O). Brightfield (A-C, G-I), fluorescence (D-F, J-O). AC, actinotrichia; EDE, Endoskeletal Elements; LP, lepidotrichia. Scale bars: 100μm in A-M.

CHAPTER 4

Evolution of *Hoxa11* regulation in vertebrates is linked to the pentadactyl state

4.1. Notes on Chapter

The present chapter has been published in Nature as per the following citation:

Kherdjemil Y, Lalonde RL, Sheth R, Dumouchel A, de Martino G, Pineault KM et al. Evolution of Hoxa11 regulation in vertebrates is linked to the pentadactyl state. Nature. 2016; 539(7627): 89–92.

Author contributions

R.L.L. cloned all of the zebrafish reporter constructs (*hoxa11a/b*) to test for the presence of an intronic enhancer, microinjected all zebrafish and mouse constructs and screened for positive transient embryos. R.L.L. raised and screened injected embryos to obtain transgenic lines, and performed basic analysis on these lines. R.L.L. performed *in situ* hybridization analysis in an attempt to identify antisense transcripts in the zebrafish, as well as for *hoxa11a/b, hoxa13a/b* and *hoxd13a*. R.L.L. compared the enhancer activity of the mouse intron during median and pectoral fin development to the expression profiles of *hoxa11a/b, hoxa13a/b* and *hoxd13a* to assess the possible roles of these genes during enhancer activation in mice. R.L.L. provided initial analysis of all fish data and all fish experiments were performed by R.L.L. under the supervision of M.-A.A.. Y.K. and M.K. conceived the study and analysed the data. Y.K. designed and conducted all mouse experiments with the help of R.S. for the generation of the mouse lines. R.S. performed the ChIP–seq experiments. A.D. provided technical help for the mouse experiments. G.M. performed preliminary experiments related to Figs 4.2a and 4.3c, e. D.M.W. and K.M.P provided *Hoxa11*$^{eGFP/eGFP}$ embryos. H.S.S. provided the HOXA13 and HOXD13 antibodies. M.K. wrote the paper. All authors commented on the manuscript.

Project Introduction & Objectives

Mechanisms of *Hoxa11* distal repression; contribution to the evolution of the pentadactyl state

Previous functional studies in mice have highlighted the contributions of *5'HoxA/D* genes to limb endochondral bone patterning. Furthermore, changes in regulation of *5'HoxA/D* genes have been implicated in endochondral bone evolution during the fin-to-limb transition. During limb development *Hoxa11* and *Hoxa13* have non-overlapping complementary expression domains. *Hoxa13* is expressed in the presumptive autopod, and *Hoxa11* is restricted to more proximal limb regions. In zebrafish, *hoxa11b* and *hoxa13a/b* have overlapping domains of expression suggesting *Hoxa11* distal repression may be a tetrapod-specific novelty. Modulation of *Hoxa11* activity may have had consequences for endochondral bone evolution during the fin-to-limb transition.

Objective: Identify the molecular mechanisms and contributions of *Hoxa11* distal repression during mouse limb development and determine this system exists in bony fish

A previous study has idenfied the existence of antisense long non-coding RNAs (lncRNA) at the *Hoxa11* locus in mice which show perfectly complementary expression with *Hoxa11* duing limb development. The *Hoxa11* antisense lncRNAs completely overlap with *Hoxa13* expression in the autopod. We predict that *Hoxa11* distal repression may be linked to Hoxa13-mediated activation of antisense lncRNAs at the *Hoxa11* locus. We therefore investigated the excistance of *cis*-acting regulatory elements at the *Hoxa11* locus responsible for lncRNA activation in mice. To determine if this system is unique to tetrapods, we also tested for the presence of antisense lncRNAs and *cis*-acting regulatory elements at the *hoxa11a* and *hoxa11b* locus in zebrafish. Finally, we performed functional analysis of *Hoxa11* distal repression in mice to determine the effects on limb development.

4.2. Abstract

The fin-to-limb transition represents one of the major vertebrate morphological innovations associated with the transition from aquatic to terrestrial life and is an attractive model for gaining insights into the mechanisms of morphological diversity between species (Shubin et al. 2009). One of the characteristic features of limbs is the presence of digits at their extremities. Although most tetrapods have limbs with five digits (pentadactyl limbs), palaeontological data indicate that digits emerged in lobed fins of early tetrapods, which were polydactylous[2]. How the transition to pentadactyl limbs occurred remains unclear. Here we show that the mutually exclusive expression of the mouse genes *Hoxa11* and *Hoxa13*, which were previously proposed to be involved in the origin of the tetrapod limb (Coates et al. 2002; Davis et al. 2007; Metscher et al. 2005; Sakamoto et al. 2009; Shubin et al. 2009; Sordino et al. 1996), is required for the pentadactyl state. We further demonstrate that the exclusion of *Hoxa11* from the *Hoxa13* domain relies on an enhancer that drives antisense transcription at the *Hoxa11* locus after activation by HOXA13 and HOXD13. Finally, we show that the enhancer that drives antisense transcription of the mouse *Hoxa11* gene is absent in zebrafish, which, together with the largely overlapping expression of *hoxa11* and *hoxa13* genes reported in fish (Ahn & Ho 2008; Davis et al. 2007; Metscher et al. 2005; Sakamoto et al. 2009; Sordino et al. 1996), suggests that this enhancer emerged in the course of the fin-to-limb transition. On the basis of the polydactyly that we observed after expression of *Hoxa11* in distal limbs, we propose that the evolution of *Hoxa11* regulation contributed to the transition from polydactyl limbs in stem-group tetrapods to pentadactyl limbs in extant tetrapods.

4.3. Main

Several studies provided evidence for the implication of Hox genes in the fin-to-limb transition (Freitas et al. 2007; Freitas et al. 2012; Shubin et al. 1997; Sordino et al. 1995; Wagner & Chiu 2001; Woltering et al. 2014), notably *Hoxa13* and *Hoxd13* (*Hox13* hereafter), which are required for digit morphogenesis (Sordino et al. 1995; Freitas et al. 2007; Freitas et al. 2012; Fromental-Ramain et al. 1996; Woltering et al. 2014). Comparison of their expression pattern in fin and limb buds revealed a significant expansion of the *Hox13* domain in distal limbs (Schneider & Shubin 2013) and engineered enlargement of the *Hoxd13* domain in fish resulted in more chondrogenic tissue forming distally as well as fin fold reduction (Freitas et al. 2012)—that is, morphological changes associated with the fin-to-limb transition. It was thus proposed that the evolution of *Hox13* regulation has likely been instrumental to the emergence of the limb characteristic feature, that is, the digits (Freitas et al. 2012; Sordino et al. 1995). In mice, this regulation relies on a series of remote transcriptional enhancers (Berlivet et al. 2013; Montavon et al. 2011), and although a subset of these enhancers exists in fish (Gehrke et al. 2015), the expansion of the *Hox13* domain in limb was probably associated with the emergence of tetrapod-specific enhancers during the fin-to-limb transition (Freitas et al. 2007; Freitas et al. 2012; Sordino et al. 1995; Woltering et al. 2014). Another notable difference is the mutually exclusive expression of *Hoxa11* and *Hoxa13* in tetrapod limbs, contrasting with their largely overlapping expression in fins (Ahn & Ho 2008; Davis et al. 2007; Metscher et al. 2005; Sakamoto et al. 2009; Sordino et al. 1996). Two hypotheses have been put forward to explain how *Hoxa11* gets proximally restricted in tetrapod limbs. One hypothesis suggested a *Hoxa13*-dependent repression of *Hoxa11* in the presumptive autopod (Sheth et al. 2014; Wagner & Chiu 2001; Woltering et al. 2014), whereas the second proposed that antisense transcription at the *Hoxa11*

locus prevents expression of the gene distally (Hsieh-Li et al. 1995; Leite-Castro et al. 2016; Potter & Branford 1998), but the functional importance of the mutually exclusive expression of *Hoxa11* and *Hoxa13* in tetrapod limbs is unknown.

Previous chromatin conformation analyses revealed that, in distal limbs, 5′ *HoxA* genes (that is, *Hoxa9* to *Hoxa13*) are grouped within a chromatin sub-topological domain (sub-TAD) interacting with sub-TADs containing distal limb enhancers (Berlivet et al. 2013). Yet, although *Hoxa10* and *Hoxa13* are both expressed distally, *Hoxa11* expression is proximally restricted (Fig. 4.1a–c), suggesting that *Hoxa11* is part of the distal limb regulatory landscape, but a specific, yet unknown, mechanism prevents its expression distally (Sheth et al. 2014; Woltering et al. 2014). To test this possibility, we first took advantage of a mouse line in which the *Hoxa11* gene is replaced by a PGK-neomycin resistance cassette (Small & Potter 1993), which we used as a reporter transgene. We found neomycin expression in distal limbs (Fig. 4.1d), indicating that *Hoxa11* proximal restriction is linked to specific feature(s) of the gene itself. We next analysed the putative implication of antisense long non-coding RNAs previously identified at the *Hoxa11* locus (Hsieh-Li et al. 1995; Potter & Branford 1998) and robustly expressed in the distal limb bud (Hsieh-Li et al. 1995) (Fig. 4.1e). Among the distinct *Hoxa11* antisense transcripts (*Hoxa11as*, also known as *Hoxa11os*), two initiate upstream of the *Hoxa11* gene and are thus non-overlapping with *Hoxa11* (*Hoxa11as-a*; Fig. 4.1e) and the other two initiate within *Hoxa11* exon 1 (*Hoxa11as-b*; Fig. 4.1f). Notably, only *Hoxa11as-b* expression pattern is mutually exclusive with *Hoxa11* expression domain (Fig. 4.1f, compare with Fig. 4.1b). To test whether antisense transcription overlapping with *Hoxa11* exon 1 prevents *Hoxa11* expression distally, we took advantage of the $Hoxa11^{eGFP}$ mutant line, which lacks *Hoxa11as-b* start sites as the enhanced green fluorescent protein (eGFP) coding sequence replaces most of *Hoxa11* exon 1

(Nelson et al. 2008). This mutation disrupted antisense transcription normally initiating 3′ to *Hoxa11* promoter (Fig. 4.5a, b) while *gfp* expression driven by the *Hoxa11* promoter was present both in the proximal and distal domains (Fig. 4.1g). By contrast, ectopic expression of *Hoxa11as-b* in the entire limb had no effect on *Hoxa11* expression (Fig. 4.5c–e), thereby excluding a *trans*-acting effect of *Hoxa11as-b* on *Hoxa11* expression. Together, our data suggest that *Hoxa11* distal repression is due to the antisense transcription event or the antisense *Hoxa11as-b* transcripts acting in *cis*.

Previous mapping of active enhancers in distal limbs (Berlivet et al. 2013) (referred to as 'digit' enhancers hereafter) uncovered a putative 'digit' enhancer embedded in *Hoxa11* intron. We thus proposed that this enhancer might control *Hoxa11as-b* expression. We first tested the transcriptional enhancer activity of this DNA region in transgenic embryos and confirmed its ability to act as a transcriptional enhancer in distal limbs (Fig. 4.2a). Next, we generated mutant mice lacking this enhancer ($Hoxa11^{\Delta Int/\Delta Int}$; Fig. 4.6) to examine its potential implication in *Hoxa11as-b* expression. Analysis of antisense transcription in $Hoxa11^{\Delta Int/\Delta Int}$ limbs showed no detectable expression of *Hoxa11as-b* in the most distal cells (Fig. 4.2b, c), indicating that in these cells, the identified enhancer is required for antisense transcription overlapping with *Hoxa11* exon 1. Some *Hoxa11as-b* expression remained in proximal cells of the presumptive handplate (presumptive carpal region; Fig. 4.2c), which suggests that additional *cis*-regulatory element(s) trigger antisense transcription in these cells. Notably, the deletion of the enhancer abrogating *Hoxa11as-b* expression in the most distal cells also resulted in ectopic expression of *Hoxa11* in the presumptive digits (Fig. 4.2d, e). The gain-of-sense transcription in $Hoxa11^{eGFP/eGFP}$ distal limbs (Fig. 4.1g) indicates that it is not the intronic regulatory region per

se but *Hoxa11as-b* expression or the antisense transcription event that represses *Hoxa11* expression distally.

Analysis of the enhancer sequence revealed several putative binding sites for HOXA13, the expression of which occurs in digit progenitor cells (Scotti et al. 2015) and is required in conjunction with HOXD13 for digit morphogenesis (Fromental-Ramain et al. 1996). Chromatin immunoprecipitation followed by high-throughput sequencing (ChIP–seq) indicated that, in distal limb cells, HOXA13 as well as HOXD13 bind to the identified enhancer (Fig. 4.7a). Moreover, transcription assay in 293T cells shows that HOXA13 has a positive effect on the enhancer activity (Fig. 4.7b). Together, these results raised the possibility that distal *Hoxa11* antisense transcription relies on HOX13. We thus analysed *Hoxa11* antisense transcription in the *Hoxa13;Hoxd13* allelic series. We used the probe recognizing all antisense transcripts such that expression in the proximal limb, where *Hox13* genes are not expressed, served as internal control. We found that although antisense transcription is barely modified in single mutants (Fig. 4.8), it markedly decreases in the $Hoxa13^{-/-}Hoxd13^{+/-}$ mutant (Fig. 4.3c, compare to Fig. 4.3a), and is completely abrogated in $Hoxa13^{-/-}Hoxd13^{-/-}$ distal limbs (Fig. 4.3e). Analysis of the distal-specific antisense transcripts (*Hoxa11as-b)* confirmed that distal antisense transcription requires HOX13 function (Fig. 4.9). Importantly, concomitant with the abrogation of antisense transcription, *Hoxa11* expression was gained distally (Fig. 4.3d–f, compare with Fig. 4.3b) consistent with the requirement of antisense transcription for *Hoxa11* proximal restriction.

To assess the functional significance of the HOXA13/D13-mediated repression of *Hoxa11*, we investigated the phenotypic outcome of distal *Hoxa11* expression. Although the deletion of the enhancer driving antisense transcription results in *Hoxa11* expression in distal limbs, the deletion extends up to the exon 1–intron boundary, thereby precluding the use of this

mutant line to assess the phenotype resulting from distal *Hoxa11* expression. We thus generated a *Hoxa11* conditional gain-of-function allele (*Rosa26*^{Hoxa11}; Fig. 4.10) to express *Hoxa11* ectopically and distally. We found that embryos carrying the *Rosa26*^{Hoxa11} allele and either *Hoxa13:Cre* (Scotti et al. 2015) or *Prx1*:*Cre* (Logan et al. 2002) have limbs with extra digits (Fig. 4.3g, h), including postaxial extra digits (arrow in Fig. 4.3h and Fig. 4.11). While some variations in the digit phenotype were observed among individuals, all homozygous mutants analysed were polydactylous (Fig. 4.11c–e). Increased expression of *Hoxd11* in the presumptive autopod in the absence of *Hoxd13* also resulted in polydactyly, whereas a similar gain of *Hoxd10* or *Hoxd12* had no effect on digit number (Kmita et al. 2002). These data raise the possibility that the formation of extra digits upon ectopic expression of *Hoxa11* or *Hoxd11* distally reflects the divergence between *Hoxa11*/*Hoxd11* targets and those of the other 5′ *HoxA/D* genes. Notably, the evidence that *Hoxa11* expression in the distal limb results in the formation of extra digits indicates that the proximal restriction of *Hoxa11* expression is required for the pentadactyl state.

In contrast to the mutually exclusive *Hoxa11* and *Hoxa13* pattern in tetrapod limbs, *hoxa11* and *hoxa13* gene expression is largely overlapping in zebrafish fins (Ahn & Ho 2008; Davis et al. 2007; Metscher et al. 2005; Sakamoto et al. 2009; Sordino et al. 1996) (Fig. 4.12) as well as in other teleosts (Takamatsu et al. 2007) (the medaka *Oryzias latipes*) and in fish models of both chondrichthyans (Sakamoto et al. 2009) (*Scyliorhinus canicula*) and basal actinopterygians (Davis et al. 2007) (*Polyodon spathula*). The HOXA13/D13-mediated repression of *Hoxa11* identified in distal limb cells was thus probably implemented after the separation of actinopterygians and chondrichthyans, during the evolution of vertebrates towards tetrapod species. Consistent with this hypothesis, no *hoxa11* antisense transcription has been reported in fish (Leite-Castro et al. 2016; Ulitsky et al. 2011) (Fig. 4.13). Moreover, sequence comparison of

the mouse *Hoxa11* intron showed robust conservation among tetrapods, whereas considerably weaker sequence conservation was observed with fish *hoxa11* orthologues (Fig. 4.4a). To examine whether the lack of *hoxa11* antisense transcription in fish could be due to the absence of a distal enhancer within *hoxa11* intron, we tested the zebrafish *hoxa11a* and *hoxa11b* intronic sequences for potential enhancer activity using transgenic reporter assays in both zebrafish and mice. Neither the *hoxa11a* nor *hoxa11b* intron was capable of triggering expression of a reporter gene in fin nor in mouse limb buds (Table 4.1), indicating that there is no distal enhancer in *hoxa11a* nor *hoxa11b* intron. By contrast, when we tested the transcriptional activity of the mouse *Hoxa11* intron in zebrafish, the analysis of four stable transgenic lines revealed that the mouse *Hoxa11* intron was able to drive reporter gene expression in the pectoral fin mesenchyme (Fig. 4.4b, c). At 60 hours post-fertilization (hpf), eGFP-positive cells were present at the distal rim of the endoskeletal disc and migrating into the fin fold (Fig. 4.4b) and by 72 hpf most eGFP-positive cells were found in the fin fold mesenchyme (Fig. 4.4c). The expression of the reporter transgene was reminiscent of *hoxa13a* expression at 60 hpf (Fig. 4.4d) and 72 hpf (Fig. 4.4e), indicating that the mouse enhancer in *Hoxa11* intron was active in the *Hoxa13* domain also in zebrafish. Together, our data indicate that all the transcription factors required for the activity of the mouse enhancer are present in zebrafish fins, and that the enhancer driving *Hoxa11* antisense transcription does not exist in the intron of the zebrafish *hoxa11a* and *hoxa11b* genes. We therefore propose that the emergence of the enhancer triggering *Hoxa11* antisense transcription, and thus distal repression of *Hoxa11*, occurred in the course of evolution towards tetrapod species.

In summary, our work reveals that the mutually exclusive expression of *Hoxa11* and *Hoxa13* in tetrapods is associated with the emergence of a transcriptional enhancer in *Hoxa11*

intron, which upon HOXA13/D13-dependent activation, triggers antisense transcription and thereby prevents *Hoxa11* expression distally. On the basis of the evidence that this HOX13-mediated regulation of *Hoxa11* probably emerged during the fin-to-limb transition and the polydactyly resulting from distal expression of *Hoxa11* in mice, we propose that the evolution of *Hoxa11* regulation has contributed to the transition from polydactyly in stem-group (extinct) tetrapods to pentadactyly in extant tetrapods.

4.3. Methods

No statistical methods were used to predetermine sample size.

Mouse lines

Hoxa11^{Neo}, *Hoxa11*^{eGFP}, *Hoxa13null* (*Hoxa13*^{Str}) and *Hoxd13null* (*Hoxd13*^{lacZ}) mouse lines were previously described (Fromental-Ramain et al. 1996; Kmita et al. 2000; Nelson et al. 2008; Small & Potter 1993).

Rosa^{Hoxa11} knock-in allele was constructed as followed: PacI-AscI fragment from pBTG (Addgene plasmid 15037) (Murtaugh et al. 2003) was inserted into the previously described *Rosa26* targeting vector (Soriano 1999) pROSA26Am1 (Addgene plasmid 15036) (Cong et al. 2013). The mouse *Hoxa11* cDNA was inserted at the SmaI site within the MCS. The vector was linearized by SwaI digest prior electroporation into embryonic stem (ES) cells. After double selection using G418 and DTA negative selection, 96 ES cell clones were analysed by Southern blot for homologous recombination. Two independent clones were injected into blastocysts obtained from C57BL/6J mice, subsequently implanted into pseudo-pregnant females. After germline transmission of the *Rosa*^{Hoxa11} allele, mice and embryos were genotyped by Southern blot (a scheme with restriction sites and probes used is presented in Fig. 4.10) and PCR. The following PCR primers were used: fw_wt : 5′-GCAATACCTTTCTGGGAGTTCT-3′, rev_wt :

5′-TCGGGTGAGCATGTCTTTTAATC-3′, rev_flox : 5′-TTCAATGGCCGATCCCATATT-3′, rev_del : 5′-AGGTTGGAGGAGTAGGAGTATG-3′. Wild-type band: 384 bp, flox band: 881 bp, del band: 583 bp. The moderate transcription resulting from the *Rosa26* promoter allowed for *Rosa26*^{Hoxa11} expression at a level comparable to the *Hoxa11* gain observed in our series of mutants.

Hoxa11$^{\Delta Int}$ mouse line was generated through pronuclei injection of single-guide RNAs (sgRNAs). We used the CRISPR (http://crispr.mit.edu/) platform to design sgRNAs flanking the region to delete. Complementary strands were annealed, phosphorylated and cloned into the BbsI site of pX330 CRISPR/Cas9 vector (Addgene plasmid 42230) (Cong et al. 2013). SgInt1_fw : 5′-CACCGACTCCCCTTTCATAAAGCCC-3′; SgInt1_rev : 5′-AAACGCGCTTTATGAAAGGGGAGTC-3′; SgInt2_fw : 5′-CACCGAGCAACAGGCGAGTTTGCGC-3′; SgInt2_rev : 5′-AAACGCGCAAACTCGCCTGTTGCTC-3′. Mice and embryos were genotyped by Southern blot (a scheme with restriction sites and probe used is presented in Extended Data Fig. 2) as well as PCR. The Southern blot probe corresponds to the ScaI-HpaI fragment in the 3′ untranslated region (UTR) of the *Hoxa11* gene. Primers used for PCR genotyping, fw: 5′-GGCCACCTAAGGAAGGAGAG-3′; rev: 5′-GGCTCCGGTGCGTATAAAG-3′

Three *Prx1-Hoxa11as* transgenic lines were derived from three distinct founders obtained from pronuclear injection of the *Prx1-Hoxa11as* transgene. The *Prx1-Hoxa11as* transgene carries the *Prx1* promoter upstream of the mouse *Hoxa11as* (GenBank: U20367.1 and U20366.1) and the SV40 polyadenylation sequence was inserted downstream *Hoxa11as*. Embryos were genotyped by PCR using DNA from the amniotic membrane and the following pair of primers: fw: 5′-CTTTCTCTCTGGCTCTGATG-3′ and rev: 5′-GACAAGAACGCCGAGAA-3′ (for U20367.1)

or fw: 5′-GTCCGAGGAAAAGGAGGTAG-3′ and rev: 5′-GCTCCTCTAACATGTATTTG-3′ (for U20366.1).

All mice were of mixed background (C57BL/6 X 129).

The Tg(*m-Inta11-LacZ*) transgene was generated by subcloning the mouse *Hoxa11* intron upstream of the *Hbb* (β-globin) minimal promoter and a LacZΔCpG NLS reporter. The *H19* insulator was inserted upstream of the *Hoxa11* intron. Tg(*m-Inta11-LacZ*) embryos were produced by pronuclear injection.

Whole-mount *in situ* hybridization, X-gal staining, skeletal preparations and imaging

For skeletal preparation, newborn mice were processed using the standard alcian blue alizarin red staining protocol (Sheth et al. 2012) ($n = 10$ for each genotype).

Whole-mount *in situ* hybridizations were performed using previously described protocol (Scotti & Kmita 2012) and probes protocol (Scotti & Kmita 2012) (*gfp* (Mattar et al. 2008), *Neo*, *Hoxa11*, *Hoxa13*). Embryos were genotyped prior *in situ* hybridization (no blinding). *Hoxa11as* probes were generated using limb cDNA and the following primers: fw 5′-AGAGGCGCTGAGGAGCCTTCTC-3′ and rev 5′-GGCCGCTGTGGACACTAGCATATACC-3′ (probe A); fw 5′-CCTTCTCGGCGTTCTTGTC-3′ and rev 5′-GGCATACTCCTACTCCTCCAACCT-3′ (probe B).

X-gal staining was performed using standard protocol (Scotti & Kmita 2012). Embryos were genotyped after X-gal staining (which results in blinding test).

All mouse specimens were imaged using the Leica DFC450C camera. For each experiment, a minimum of three embryos per genotype was used as we considered that reproducible staining/expression patterns with three distinct embryos of the same genotype are significant. The experiments shown were repeated at least twice. We did not use the randomization method.

Subcloning of zebrafish *hoxa11a/b* intron and microinjections in zebrafish embryos

The zebrafish *hoxa11a* (713 bp; gene ID 58061, NCBI) and *hoxa11b* (747bp; gene ID 30382, NCBI) introns were amplified from zebrafish genomic DNA using the following primers: *hoxa11a* intron: fw 5′-GAATTCAACAGTAAGTACGAGCTCAAC-3′; rev 5′-GGTACCACCTAAATGTAAATACACGT-3′; *hoxa11b* intron: fw 5′-GAATTCCAGCGGCAGCAGCAGTACGT-3′; rev 5′-GGTACCCCGTGTCTTTTGTCCATCTAA-3′.

The zebrafish *hoxa11a* and *hoxa11b* and the mouse *Hoxa11* introns were sub-cloned into the pEGFP-N1 vector (CLONTECH Laboratories, Inc.) in which the CMV promoter upstream of eGFP was replaced with the human *HBB* minimal promoter using the following primers: fw 5′-GGATCCCTGGGCATAAAAGTCAG-3′, rev 5′-ACCGGTTCTGCTTCTGGAAGGCT-3′. This vector also contains the Tol2 arms to increase transgenesis efficiency. For screening purposes, a heart marker (*cmlc2*:*mCherry* (Yelon et al. 1999)) was added to zebrafish Tg(*z-Inta11a-eGFP*) and Tg(*z-Inta11b-eGFP*) constructs. All constructs were microinjected in one-cell stage wild-type zebrafish embryos at a concentration of 100 ng μl^{-1} together with 50 ng μl^{-1} transposase mRNA.

Generation of zebrafish transgenic lines

Primary injected zebrafish (P_1) are raised until 3 months of age, and then are screened for transgenic progeny (F_1). P_1 fish are crossed with wild-type fish and the embryos are screened at 2 days post-fertilization (dpf). Owing to lack of fin fold eGFP expression in the Tg(*z-Inta11a-eGFP; cmlc2:mCherry*), Tg(*z-Inta11b-eGFP; cmlc2:mCherry*) injected fish, embryos were screened for the presence of the *cmlc2*:*mCherry* heart marker and genotyped to confirm the presence of the *hoxa11a/b intron:eGFP* elements. The following primers were used for

genotyping: *hoxa11a*: fw 5′-GGTACCACCTAAATGTAAATACACGT-3′, rev (eGFP) 5′-GTCCTCCTTGAAGTCGATGC-3′; *hoxa11b*: fw 5′-GGTACCCCGTGTCTTTTGTCCATCTAA-3′, rev (eGFP) 5′-GTCCTCCTTGAAGTCGATGC-3′.

Three transgenic lines for Tg(*m-Inta11-eGFP*) were obtained to confirm the expression pattern. A fourth line containing the *cmlc2:mCherry* heart marker was also created. To confirm the *Hbb* minimal promoter does not drive tissue-specific expression alone, a transgenic line Tg(*HBB:eGFP; cmlc2:mCherry*) was also created and genotyped using the following primers: *Hbb*: fw 5′-GGATCCCTGGGCATAAAAGTCAG-3′, rev (eGFP) 5′-GTCCTCCTTGAAGTCGATGC-3′.

Zebrafish *in situ* hybridization

In situ hybridization on whole-mount embryos was performed as previously described (Thisse & Thisse 2008). Digoxigenin-labelled antisense RNA probes were generated using the following cDNAs: *hoxa13a* (500 bp; Addgene 36463), *hoxa13b* (700 bp; Addgene 36568), *hoxa11b* (probe 1 (Fig. 4.12c, d); 800 bp; Addgene 36466). For *hoxa11a/b* antisense/sense RNA probes (Fig. 4.13a, b), *hoxa11a* (713 bp; Gene ID 58061, NCBI) and *hoxa11b* (747 bp; gene ID 30382, NCBI) partial cDNAs (exon 1) were obtained by PCR with reverse transcription from total RNA of 24–48 hpf embryos using the following primers: *hoxa11a* exon 1: fw 5′-ATGATGGATTTTGACGAAAGGGTT-3′, rev 5′-TGTTCCCACCGCTAGTTTTTTCCT-3′; *hoxa11b* exon 1: fw 5′-ATGATGGATTTTGATGAGCGGGTA-3′, rev 5′-TGCTGCTGCCGCTGAATTTATCTT-3′.

For accurate comparison, *hoxa11a* and *hoxa11b* sense and antisense probes, respectively, are identical in length and were transcribed using the same RNA polymerase. *In situ* hybridizations were also performed in parallel with identical staining times.

Transfection and gene expression analysis

293T cells (ATCC) were transfected using lipofactamine. Cells (800,000) were plated in 6-well plates. Cells were checked for mycoplasma contamination using Venor GeM Mycoplasma Detection Kit (MP0025 SIGMA). A total of 2 μg of DNA (250 ng reporter plasmid, 250 ng effector plasmid or empty expression vector), 25ng of mCherry expression vector as internal control and 1.45 μg carrier pBSK plasmid was used for each transfection. All transfections were performed in duplicates. Then, 24 h after transfection, the medium was changed and 48 h after transfection, cells were processed for RNA extraction. Reporter gene expression was normalized to internal control mCherry ($n = 3$). Gene expression (*Hoxa11*) was measured in dissected E11.5 forelimb buds of the $Rosa^{Hoxa11}$ knock-in embryos that were stored in RNA later before RNA extraction ($n = 4$).

RNA extraction was done using RNAeasy Plus mini kit (Qiagen 74134). cDNA synthesis was performed using M-MuLV reverse transcriptase (NEB) and a mix of random primers and oligo-dT on 1ug of total RNA. Quantitative real-time-PCR was performed with cDNA and the SYBR Green kit (applied biosystems) using the following primers: fw 5′-AGGAGAAGGAGCGACGG-3′ and rev 5′-GGTATTTGGTATAAGGGCAGCG-3′ (*Hoxa11*); fw 5′-CTTTGTCAAGCTCATTTCCTGG-3′ and rev 5′-TCTTGCTCAGTGTCCTTGC-3′ (*Gapdh*); fw 5′-TTGACCTAAAGACCATTGCACTTC-3′ and rev 5′-TTCTCATGATGACTGCAGCAAA-3′ (*Tbp*); fw 5′-GCCTACAACGTCAACATCAAG-3′ and

rev 5′-GCGTTCGTACTGTTCCAC-3′ (mCherry); fw 5′-GACCCTGAAGTTCATCTGCA-3′ and rev 5′-CCGTCGTCCTTGAAGAAGA-3′ (*gfp*).

Study approval

All mice experiments described in this article were approved by the Animal Care Commitee of the Institut de Recherches Cliniques de Montréal (protocols 2011-39 and 2014-14) and zebrafish experiments were approved by uOttawa Animal Care Committee (protocol BL-2317-R1).

4.4. Author Contributions

Y.K. and M.K. conceived the study and analysed the data. Y.K. designed and conducted all mouse experiments with the help of R.S. for the generation of the mouse lines. All fish experiments were performed by R.L.L. under the supervision of M.-A.A. R.S. performed the ChIP–seq experiments. A.D. provided technical help for the mouse experiments. G.M. performed preliminary experiments related to Figs 2a and 3c, e. D.M.W. and K.M.P provided *Hoxa11*$^{eGFP/eGFP}$ embryos. H.S.S. provided the HOXA13 and HOXD13 antibodies. M.K. wrote the paper. All authors commented on the manuscript.

Acknowledgements

We thank Q. Zhu and L. Lian from the IRCM transgenic core facility for the ES cell work and production of transgenic mouse lines. We are particularly grateful to A. Kania for critical reading of the manuscript as well as laboratory members for insightful discussions and sharing reagents. This work was supported by the Canadian Institute for Health Research (MOP-115127) and the Canada Research Chair program to M.K. (RCHS0192), the Natural Sciences and Engineering Research Council of Canada (155817-2012) to M.-A.A. and Shriners Hospital Research grant 85400 to H.S.S. Y.K. was supported by a fellowship from the Molecular Biology program of the Université de Montréal and the IRCM fellowship Michel-Bélanger. R.S. was supported by a

post-doctoral fellowship from the Canadian Institute for Health Research. D.M.W. and K.M.P. were supported by NIH NIAMS AR061402, with K.M.P. additionally supported by NIH T32 DE007057.

4.6. Figures

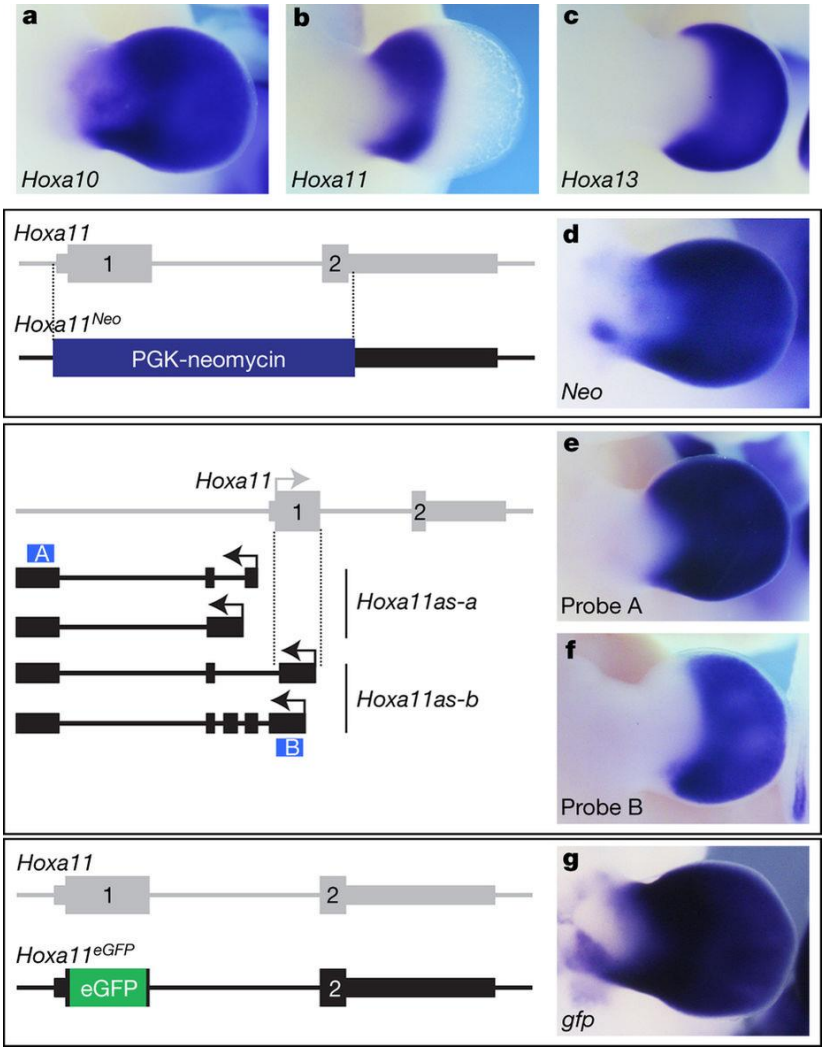

Figure 4.1. The proximal restriction of *Hoxa11* is linked to antisense transcription at the *Hoxa11* locus.

a–**c**, Expression of *Hoxa10* (**a**), *Hoxa11* (**b**) and *Hoxa13* (**c**) in wild-type limb bud from embryonic day (E) 11.5 mouse. **d**, Replacement of the *Hoxa11* gene with the PGK-neomycin cassette (*Hoxa11*^{Neo}; scheme to the left), results in neomycin expression both in the proximal and distal domains. **e**, **f**, Expression of all antisense transcripts (**e**) and antisense transcripts overlapping with *Hoxa11* exon 1 (**f**) in E11.5 wild-type limb. Schemes of the antisense transcripts and the probes used (blue boxes) are on the left. Note that the antisense transcripts

overlapping with *Hoxa11* exon 1 (*Hoxa11as-b*) are distally restricted (**f**), reminiscent of *Hoxa13* expression (**c**) and mutually exclusive with the *Hoxa11* pattern (**b**). **g**, Deletion of the antisense transcript start sites in *Hoxa11* exon 1, via replacement of most of exon 1 with the eGFP coding sequence (*Hoxa11*^{eGFP}; scheme to the left) and expression of *gfp* under the control of the *Hoxa11* promoter (right). Original magnification, ×31.5 (for all images).

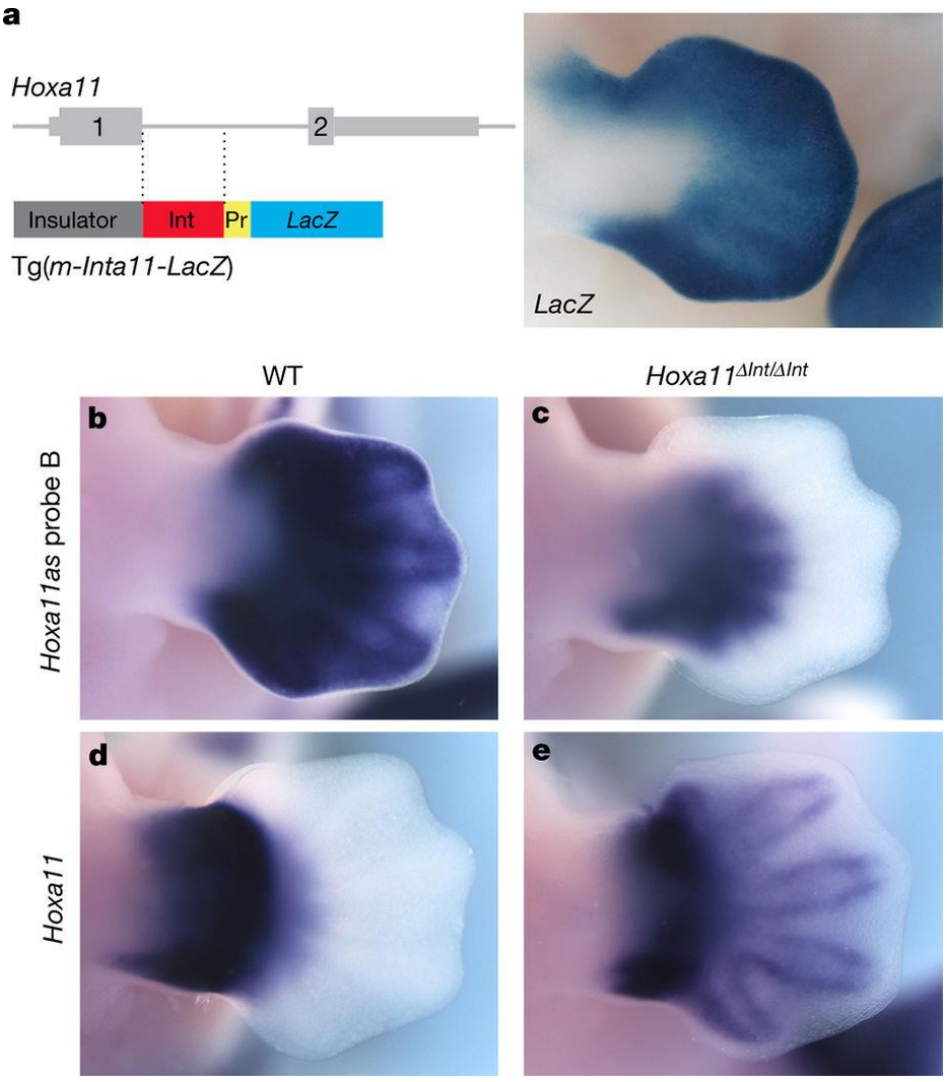

Figure 4.2. Deletion of the distal enhancer in *Hoxa11* intron results in impaired antisense transcription and gain of sense transcription in distal cells.

a, Left, scheme of the Tg(*m-Inta11-LacZ*) transgene carrying the predicted distal enhancer (Int, red box). Right, X-gal staining of E12.5 transgenic embryos ($n = 5$). **b**–**e**, Expression of *Hoxa11as-b* (**b**, **c**) and *Hoxa11* (**d**, **e**) in wild-type (WT; **b**, **d**) and $Hoxa11^{\Delta Int/\Delta Int}$ (**c**, **e**) mouse limbs at E12.5. Note that based on the observed gain of *Hoxa11* expression, other regulatory input(s) could be implicated in *Hoxa11* regulation in distal cells. Pr, minimal promoter. Original magnification, ×31.5 (for all images).

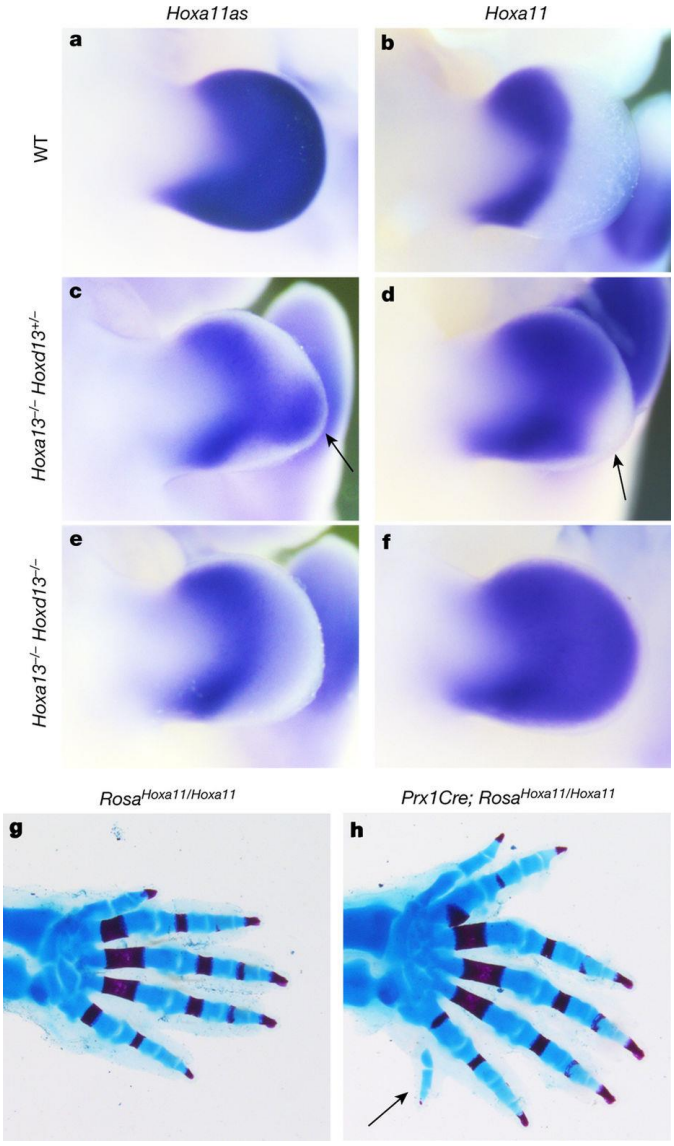

Figure 4.3 *Hox13* inactivation disrupts *Hoxa11* antisense transcription in distal cells and distal *Hoxa11* expression results in the formation of supernumerary digits.

a–**f**, *Hoxa11as* (probe A) (**a**, **c**, **e**) and *Hoxa11* (**b**, **d**, **f**) expression in E11.5 limb buds from wild-type (**a**, **b**), *Hoxa13*$^{-/-}$ *Hoxd13*$^{+/-}$ (**c**, **d**) and *Hoxa13*$^{-/-}$ *Hoxd13*$^{-/-}$ (**e**, **f**) mouse embryos. Arrows in **c** and **d** show the group of cells still expressing *Hoxa11as* in *Hoxa13*$^{-/-}$*Hoxd13*$^{+/-}$ limbs (**c**), which corresponds to distal cells in which *Hoxa11* expression is not gained (**d**). **g**, **h**, Skeleton of *Rosa*$^{Hoxa11/Hoxa11}$ (**g**) and *Prx1Cre*; *Rosa*$^{Hoxa11/Hoxa11}$ (**h**) distal forelimb at postnatal day 0 (P0). Anterior is up. Original magnification, ×31.5 (**a**–**f**) and ×20 (**g**, **h**).

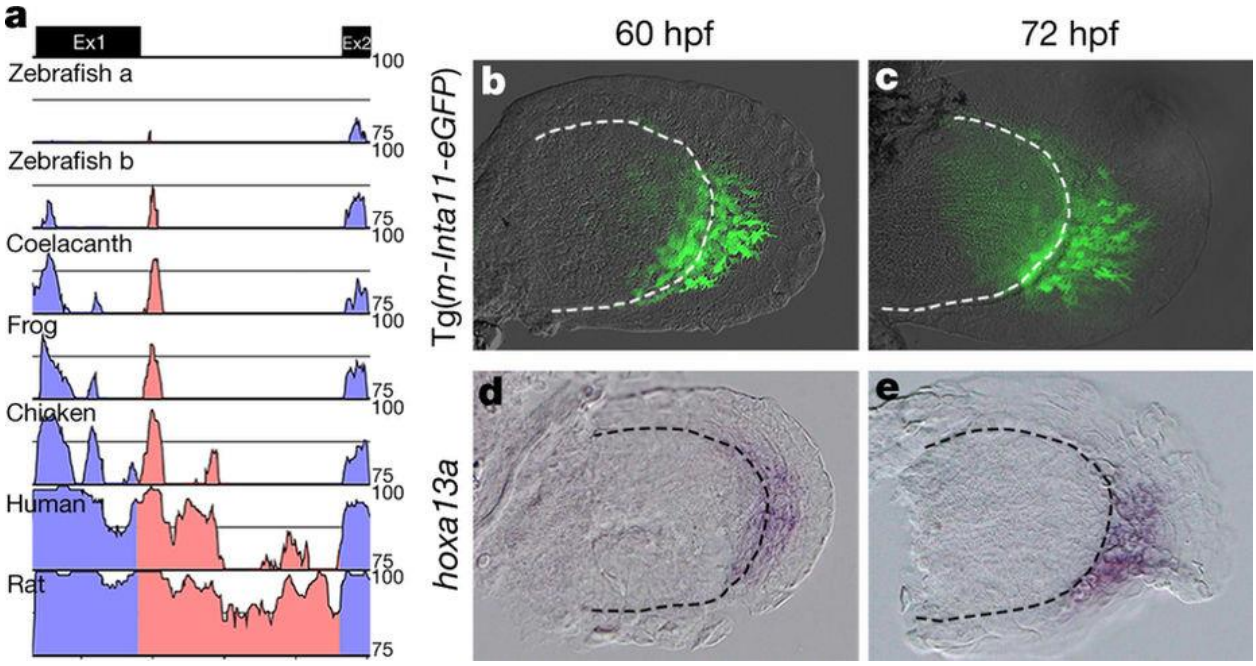

Figure 4.4. The mouse *Hoxa11* antisense enhancer is functional in distal fins.

a, mVISTA sequence conservation plot of the mouse *Hoxa11* intron (red) with tetrapod (rat, human, chicken and frog) and fish representatives (coelacanth and zebrafish). Ex1, exon 1; Ex2, exon 2. Note that zebrafish has two *hoxa11* genes expressed in developing fins, *hoxa11a* and *hoxa11b*. **b**, **c**, GFP expression in fin buds of Tg(*m-Inta11-eGFP*) transgenic zebrafish embryos at 60 hpf (**b**) and 72 hpf (**c**), revealing the enhancer activity of the mouse *Hoxa11* intron in fish. Note the filopodia-like protrusions in GFP^{+} mesenchymal cells suggestive of a migration towards the fin fold. **d**, **e**, *hoxa13a* expression in developing fins at 60 hpf (**d**) and 72 hpf (**e**). Original magnification, ×400.

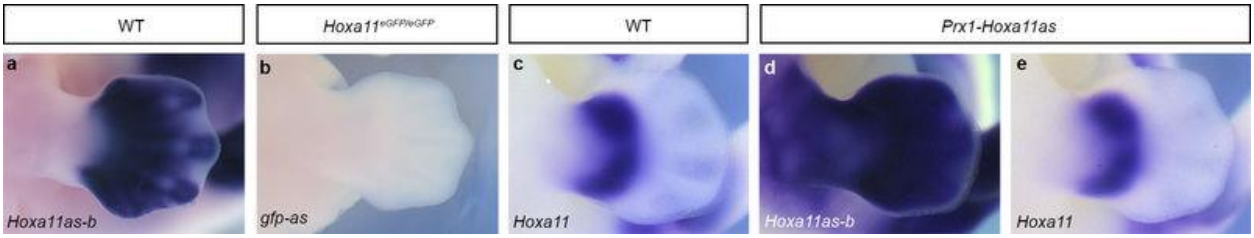

Figure 4.5 Absence of antisense transcription 3′ to the *Hoxa11* promoter in the *Hoxa11*$^{eGFP/eGFP}$ limb and evidence that *Hoxa11as-b* transcripts produced in *trans* have no effect on *Hoxa11* expression.

a, **b**, Detection of *Hoxa11as-b* transcripts in wild-type limb buds at E12.5 (**a**), and whole-mount *in situ* hybridization to detect *gfp* antisense transcripts in *Hoxa11*$^{eGFP/eGFP}$ limb buds at E12.5 (**b**). **c**–**e**, *Hoxa11* expression in wild-type limb buds (**c**), and *Hoxa11as-b* (**d**) and *Hoxa11* (**e**) expression in *Prx1-Hoxa11as* limb buds. Original magnification, ×31.5.

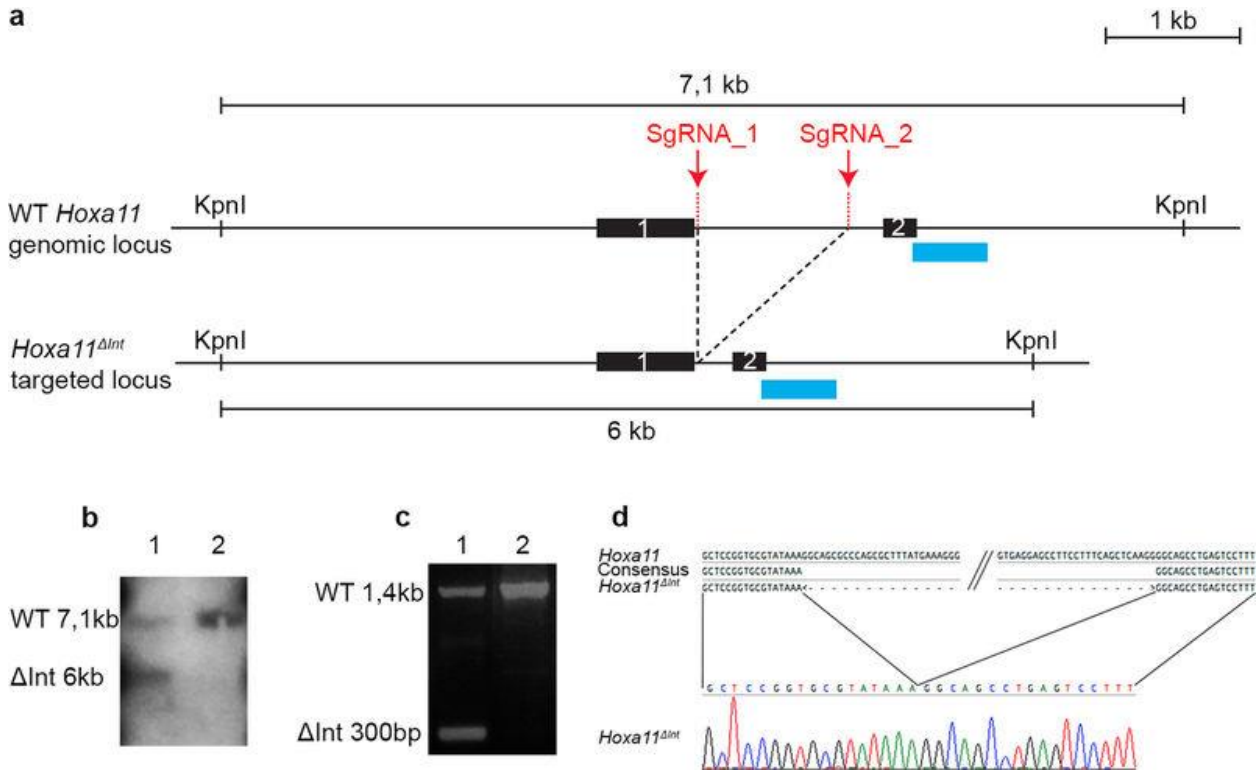

Figure 4.6. Deletion of the distal enhancer in *Hoxa11* intron using CRISPR-Cas9.
a, Scheme of the wild-type and targeted (*Hoxa11*$^{\Delta Int}$) loci. Sites targeted by the single-guide RNAs (sgRNA_1 and sgRNA_2) for the CRISPR-Cas9-mediated deletion of the distal enhancer. The blue rectangles indicate the position of the DNA probe used to confirm the deletion by Southern blot in **b**. **b**, Lane 1 shows the 6-kb KpnI band resulting from the CRISPR-Cas9-mediated deletion. Lane 2 was loaded with wild-type DNA. **c**, PCR reaction using a forward primer located upstream of sgRNA_1 and a reverse primer located downstream sgRNA_2 shows the presence of a 300 bp (ΔInt 300 bp) fragment expected for the *Hoxa11*$^{\Delta Int}$ allele. **d**, The sequence of the 300-bp PCR fragment confirms the CRISPR-Cas9-mediated deletion of the *Hoxa11* intronic region containing the distal enhancer (only the sequence encompassing the deletion breakpoints is shown).

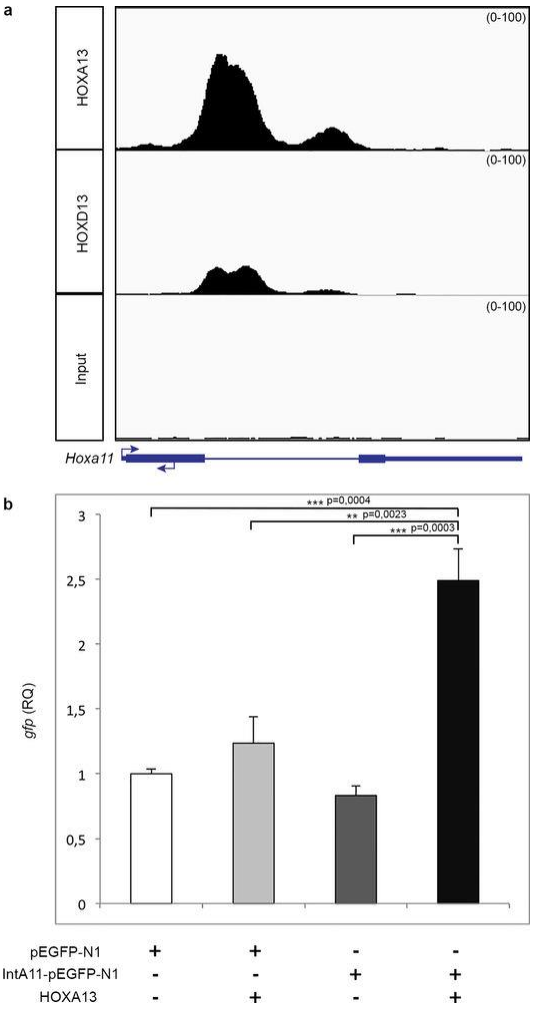

Figure 4.7. The distal enhancer located in the *Hoxa11* intron is bound by HOXA13 and HOXD13 in distal limb cells and its activity is increased by HOXA13 in 293T cells.

a, Integrative genomics viewer (IGV) screenshot showing HOXA13 and HOXD13 ChIP–seq data at the *Hoxa11* locus. These ChIP–seq data were obtained using chromatin from distal forelimb buds of wild-type E11.5 mouse embryos (R. Sheth *et al*., manuscript submitted). **b**, Transfection assay shows HOXA13 dependent activation of *Hoxa11* intron driving reporter gene expression. Two-tailed Tukey's multiple comparisons test was performed. Error bars indicate s.d ($n = 3$). RQ, relative quantification.

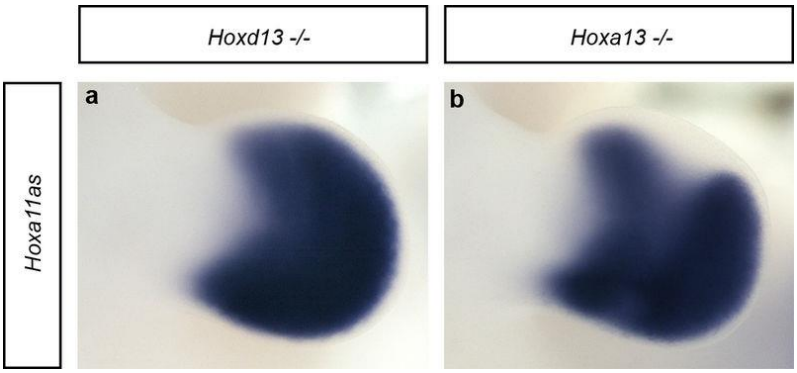

Figure 4.8. Individual inactivation of *Hoxa13* or *Hoxd13* is not sufficient to fully abrogate antisense transcription in distal limbs.

a, **b**, Whole-mount *in situ* hybridization, using probe A (see Fig. 1) to detect all antisense transcripts, on *Hoxd13*$^{-/-}$ (**a**) and *Hoxa13*$^{-/-}$ (**b**) mouse limb buds at E11.5. Antisense transcription in distal limbs remains robust in both mutants but a clear reduction is seen in the distal *Hoxa13*$^{-/-}$ limbs. Original magnification, ×31.5.

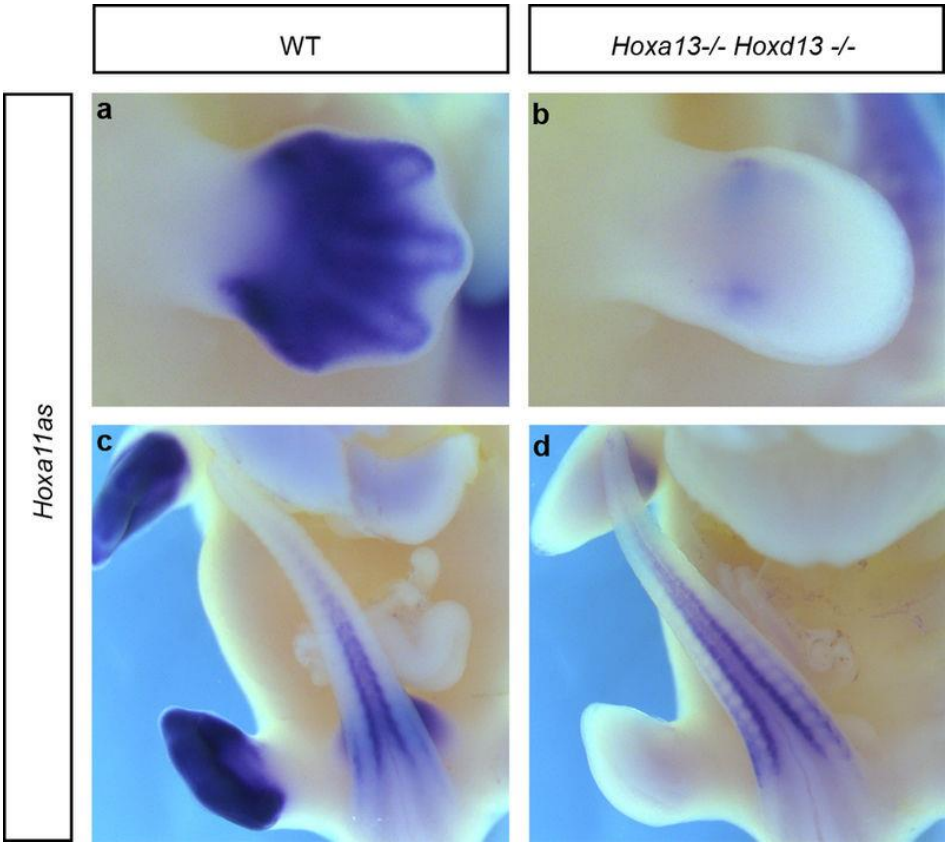

Figure 4.9. Inactivation of both *Hoxa13* and *Hoxd13* disrupts antisense transcription overlapping with the *Hoxa11* exon 1.

a–**d**, *Hoxa11as-b* expression (probe B in Fig. 1) in limb buds (**a**, **b**) and tail buds (**c**, **d**) from wild-type (**a**, **c**) and $Hoxa13^{-/-}$ $Hoxd13^{-/-}$ (**b**, **d**) E12.5 mouse embryos. Whole-mount *in situ* hybridization shows that *Hoxa11as-b* expression in tail buds (internal control) is similar in both the wild-type (**c**) and double-mutant (**d**) embryos, whereas there is almost no expression remaining in $Hoxa13^{-/-}$ $Hoxd13^{-/-}$ limb buds (**b**). Original magnification, ×31.5.

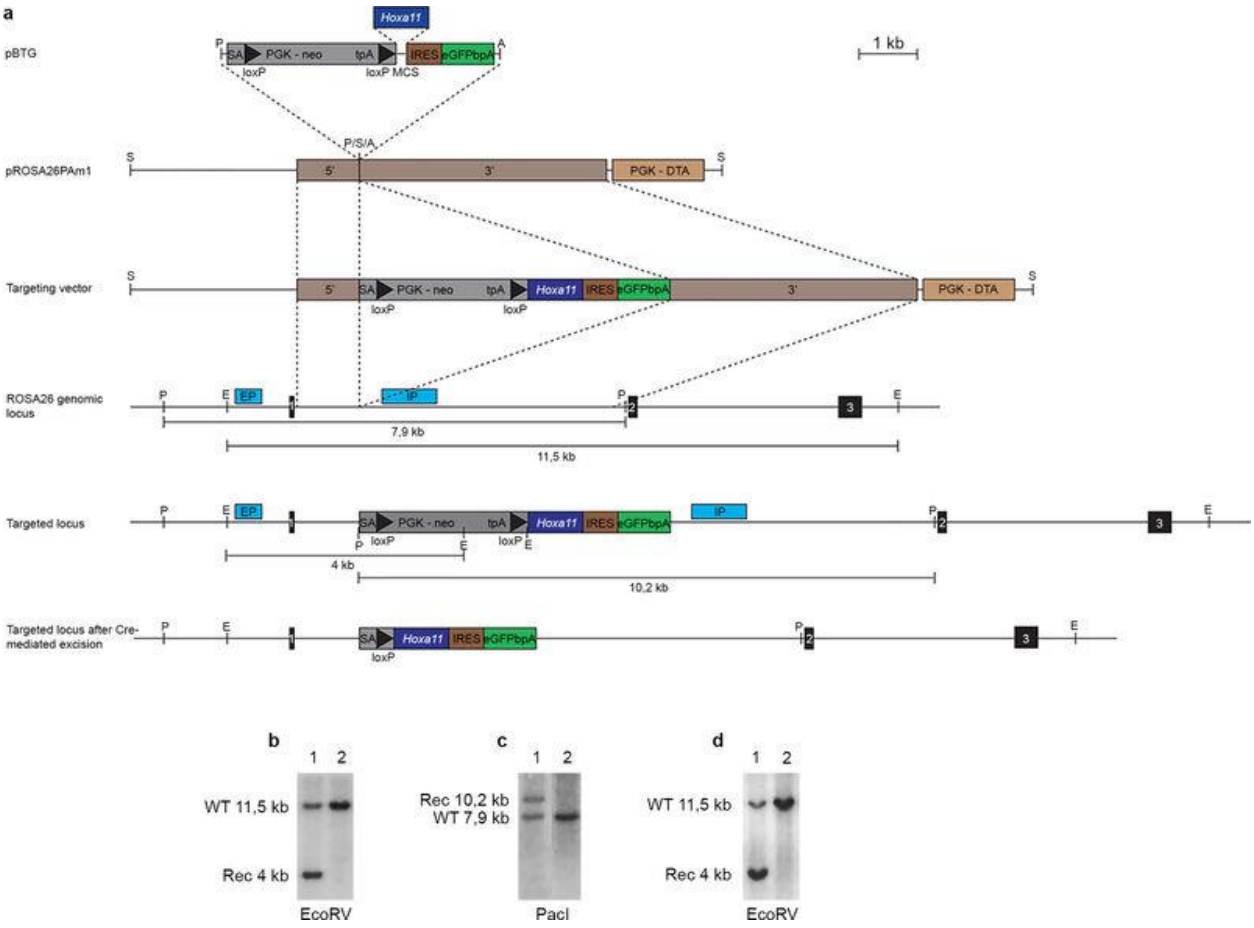

Figure 4.10. Generation of the *Rosa*^{Hoxa11} knock-in mouse line.

a, Targeting of the endogenous *Rosa26* locus (top three lines). The wild-type *Rosa26* locus is shown below (middle). Regions used as homologous arms for the recombination in ES cells are indicated by brown rectangles labelled 5′ and 3′, respectively. Scheme of the targeted locus after homologous recombination in ES cells and after Cre-mediated recombination is shown at the bottom. The position of the internal (IP) and external (EP) probes and restriction sites used for Southern blot analysis are indicated on both the wild-type and targeted locus. **b**, **c**, Southern blots of ES cells clones using the internal probe (**b**) and external probe (**c**) to detect the targeted allele (lane 1). **d**, Southern blot of wild-type (lane 2) and heterozygous (lane 1) mice. A, AscI; E, EcoRV; P, PacI; S, SwaI.

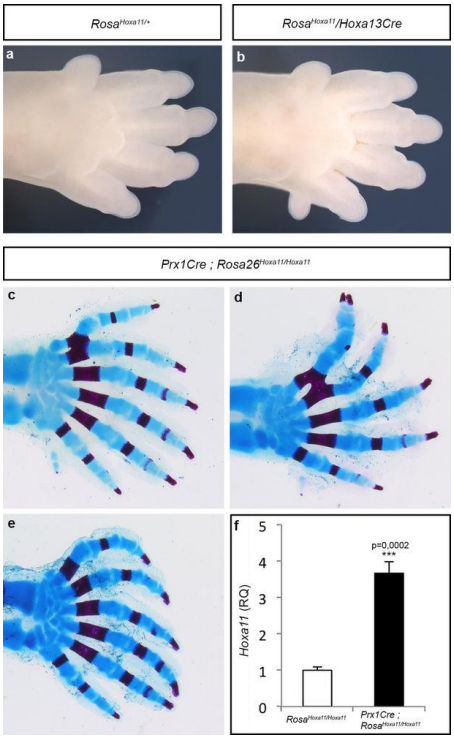

Figure 4.11. The conditional gain of *Hoxa11* using the *Hoxa13Cre* allele results in the formation of supernumerary digits.

a, **b**, Autopod of *Rosa*$^{Hoxa11/+}$ (**a**) and *Rosa*^{Hoxa11} *Hoxa13Cre* (**b**) at E15.5. Anterior is up. The *Rosa26* locus and *Hoxa13Cre* allele being on the same chromosome (Chr6), the gain-of-function phenotype was assessed with only one copy of the *Rosa*^{Hoxa11} allele. **c**–**e**, Autopod skeletons of *Prx1Cre*; *Rosa*$^{Hoxa11/Hoxa11}$ mice at P0 from four distinct mutants (anterior is up). The number of digits varies from 6 to 7, with often a small post-axial extra-digit (posterior). The extra-digit phenotype is fully penetrant upon Cre-activation of two copies of the *Rosa*^{Hoxa11} allele ($n = 10$). Original magnification, ×20.**d**, Quantification of *Hoxa11* expression level by quantitative reverse transcriptase PCR (RT–qPCR) on RNA extracted from E11.5 forelimb, relative to both *Gapdh* and *Tbp* mRNA of *Prx1Cre*; *Rosa*$^{Hoxa11/Hoxa11}$ embryos. Two-tailed *t*-test was performed. Error bars indicate s.d ($n = 4$).

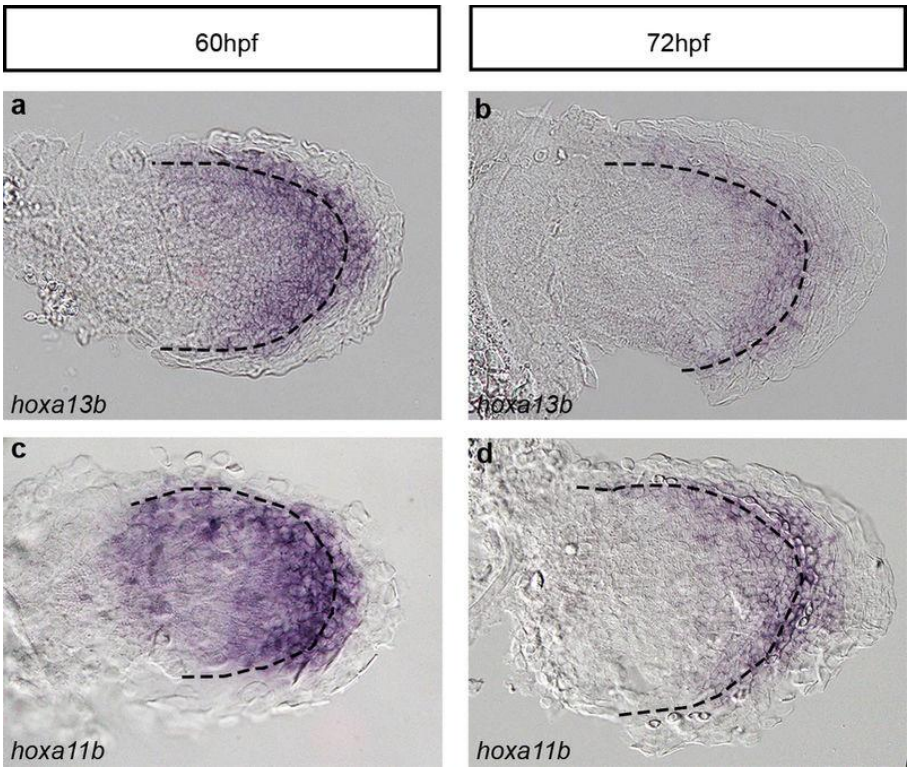

Figure 4.12. *hoxa11* and *hoxa13* are expressed in overlapping domains in zebrafish fins.

a–**d**, Expression of *hoxa13b* (**a**, **b**) and *hoxa11b* (**c**, **d**) in zebrafish fins at 60 hpf (**a**, **c**) and 72 hpf (**b**, **d**). Dotted lines indicate the boundary between the endochondral disc and the fin fold. Original magnification, ×400.

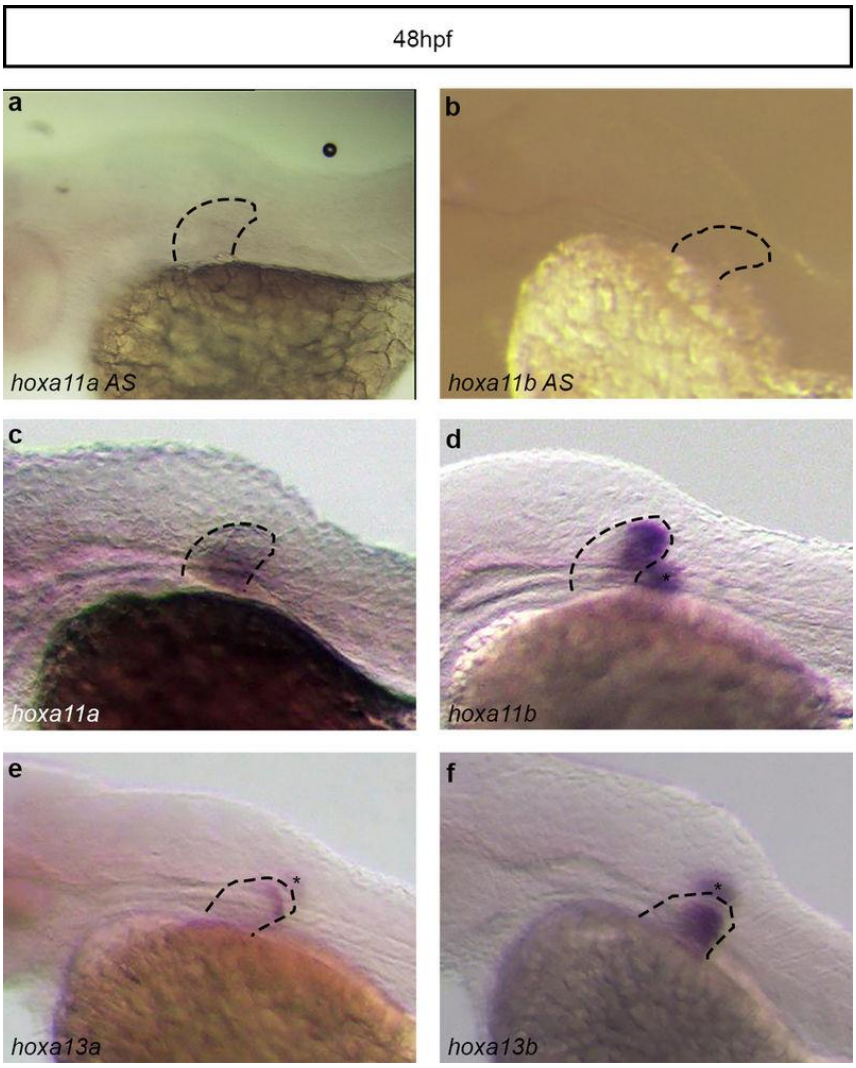

Figure 4.13. Absence of antisense transcription at the *hoxa11a* and *hoxa11b* loci in zebrafish fins.

a, **b**, Whole-mount *in situ* hybridization with probes designed to detect putative antisense transcription at *hoxa11a* (**a**) and *hoxa11b* (**b**). **c**–**f**, No antisense transcription is detected, whereas expression of *hoxa11a* (**c**), *hoxa11b* (**d**), *hoxa13a* (**e**) and *hoxa13b* (**f**) is observed in zebrafish fins at the same stage. Asterisks correspond to the staining from the fin on the other side of the embryo. Original magnification, ×63.

Table 4.1. Summary of transient transgenic embryos analysed

Zebrafish stable lines for Tg(*z-Inta11a-eGFP; cmlc2:mCherry*); Tg(*z-Inta11b-eGFP; cmlc2:mCherry*) were also generated and three genotyped F_1 embryos per line were analysed and confirmed for the absence of *gfp* expression. For Tg(*m-Inta11-eGFP; cmlc2:mCherry*), four distinct transgenic lines were also generated and analysed.

Zebrafish Transient Transgenics	
Construct	% of eGFP positive fish
Tg(*HBB:eGFP*)	0% (n=74)
Tg(*z-Inta11a-eGFP*)	0% (n=105)
Tg(*z-Inta11b-eGFP*)	1.19% (n=84)
Tg(*m-Inta11-eGFP*)	91.9% (n=123)
Tg(*HBB:eGFP; cmlc2:mCherry*)	1.25% (n=94)
Tg(*z-Inta11a-eGFP; cmlc2:mCherry*)	0% (n=200)
Tg(*z-Inta11b-eGFP; cmlc2:mCherry*)	0% (n=300)
Tg(*m-Inta11-eGFP; cmlc2:mCherry*)	88.9% (n=53)
Mouse Transient Transgenics	
Construct	% of eGFP positive embryos (# eGFP positive / # genotyped positive)
Tg(*z-Inta11a-eGFP*)	0% (n=0/10)
Tg(*z-Inta11b-eGFP*)	0% (n=0/7)

CHAPTER 5

Discussion

5.1. Notes on Chapter

This discussion chapter is adapted from a review paper titled: Contributions of *5'HoxA/D* regulation to *actinodin* evolution and the fin-to-limb transition. This review has been submitted to the "International Journal of Developmental Biology".

Author contributions

R.L.L. wrote the review and Dr. Marie-Andrée Akimenko and Dr. Qingming Qu provided critical insight.

5.2. Introduction

The evolution of the tetrapod limbs from paired fish fins involved drastic changes to the appendicular dermal and endochondral skeleton (Ahlberg & Clack 2006; Long et al. 2006; Shubin et al. 1997; Shubin et al. 2006; Schneider and Shubin 2013). The fin dermal skeleton of extant teleosts, consisting of the calcified lepidotrichia fin rays and collagenous actinotrichia fibrils, is completely absent in tetrapod limbs (Ahlberg & Clack 2006; Grandel & Schulte-Merker 1998; Mari-Beffa and Murciano 2010; Shubin et al. 2006; Tamura et al. 2008; Yano & Tamura 2013). The limb proximal endochondral skeleton has been reduced to a single bone, referred to as the stylopod and the distal-most endochondral skeleton expanded and elaborated to form the autopod, a structure unique to the tetrapod limb (Ahlberg & Clack, 2006, Shubin et al. 2006; Schneider and Shubin 2013). Modulation of 5*'HoxA/D* genes have been consistently linked to endochondral skeletal changes during the fin-to-limb transition, including the evolution of the autopod (Freitas et al 2012; Leite-Castro et al. 2016; Kherdjemil et al. 2016; Kherdjemil & Kmita 2017; Paço & Freitas 2017; Tanaka 2016; Yano & Tamura 2013). We have also uncovered evidence that modulation in *5'HoxA/D* activity may have had implications for the loss of the dermal skeleton (Lalonde et al. 2016). The *actinodin* genes code for structural proteins in the actinotrichia fibrils, and the loss of this gene family during tetrapod evolution is proposed to have contributed to the loss of fin dermal bone (Duran et al. 2011; Lalonde et al. 2016; Zhang et al. 2010). Specifically, it has been shown that actinotrichia defects disrupt proper larval fin fold mesenchyme migration, a population of cells that contribute directly to the dermal lepidotrichia fin rays (Nakamura et al. 2016; Zhang et al. 2010). Failure of these cells to migrate correctly has been proposed as a mechanism for fin dermal bone loss and through a change in cell fate, the expansion of the limb endochondral skeleton (Ahn & Ho 2008; Lalonde & Akimenko 2018;

Nakamura et al. 2016). We uncovered evidence that modulation of *5'HoxA/D* activity may have had consequences for *actinodin* regulatory evolution as well. A powerful tool for uncovering evidence of regulatory conservation or divergence during the fin-to-limb transition is to perform fish-tetrapod transgenic swap experiments, where *cis*-acting regulatory elements (CREs) are tested for activity between species (Gehrke & Shubin 2016; Gordon & Ruvinsky 2012). This discussion will first highlight *5'HoxA/D* and *actinodin* enhancer transgenic swap experiments that provide evidence for regulatory conservation and divergence between fish and tetrapods. The next section will provide a summary of experimental data testing the morphological implications of *5'HoxA/D* and *actinodin* regulatory evolution on fin and limb evolution. Finally, this discussion will also serve to illustrate some of the advantages and disadvantages of using zebrafish to study the molecular and morphological changes during the fin-to-limb transition. Where relevant, the discussion includes additional projects and future directions that are directly linked to the work in my main chapters.

5.3. Regulatory Conservation and the Autopod Debate

It has long been debated whether the autopod represents a distinct *de novo* structure that evolved during the fin-to-limb transition or whether it is a modification on pre-existing distal fish fin structures (Shubin et al. 2006; Shubin & Alberch 1986; Sordino et al. 1995; Woltering et al. 2010; Woltering et al. 2014). Due to major morphological differences between distal fish fin elements and the tetrapod autopod, these structures tend to not be considered homologous in a classical sense (Grandel & Schulte-Merker 1998; Mari-Beffa and Murciano 2010; Tamura et al. 2008; Yano & Tamura 2013). Fish fin rays are dermal bone formed through intramembranous ossification, while the tetrapod autopod consists entirely of endochondral bone (Grandel & Schulte-Merker 1998; Mari-Beffa and Murciano 2010; Tamura et al. 2008; Yano & Tamura

2013). Advances in the fields of molecular and developmental biology have revealed a deep homology between distal fin structures and the autopod (Davis 2013; Fromental-Ramain et al. 1996; Nakamura et al. 2016; Schneider & Shubin 2013; Scotti et al. 2015; Shubin et al. 1997; Zakany & Duboule. 2007). Deep homology describes the evolutionary relationship of two structures that develop through shared genetic regulatory networks, even when they are morphologically and phylogenetically distinct (Shubin et al. 2009). This section will summarize *5'HoxA/D* and *actinodin1* fin/limb enhancers that show conserved regulatory activity when tested using transgenic swap experiments between different fish species and mice (Gehrke & Shubin 2016; Gordon & Ruvinsky 2012).

Fish (Donor) to Mouse (Host)

We have previously identified and described *cis*-acting regulatory elements that drive *actinodin1* (*and1*) expression in the ectoderm and mesenchyme, known respectively as "Epi" and "2PΔEpi" (Lalonde et al. 2016, Chapter II). Despite the disappearance of the *actinodin* (*and*) genes from the tetrapod genome, the *and1* ectodermal fin fold enhancer "Epi" shows conserved regulatory activity in the presumptive autopod ectoderm of the mouse (Lalonde et al. 2016). This represents to date the only fin fold ectodermal enhancer that has been tested in mice, and supports homology between the fin fold ectoderm and the autopod ectoderm. These results are also unique as the "Epi" enhancer represents regulatory elements that are no longer found in the tetrapod genome (Lalonde et al. 2016). Using *in silico* analysis, a putative binding domain for tcf proteins has been identified within the "Epi" enhancer. This protein family represents a good candidate for "Epi" activation as multiple *tcf* genes are expressed in the fin fold ectoderm of zebrafish and the autopod ectoderm of mice, and *tcf7* GFP enhancer trap zebrafish mutants show

median and pectoral fin defects, with GFP localizing in the fin fold ectoderm (Gray et al. 2004; Nagayoshi et al. 2008).

Multiple fish late-phase *5'hoxA/D* enhancers that show activity in the zebrafish fin fold mesenchyme also show regulatory conservation in the presumptive autopod mesenchyme. These results have been extensively covered in other reviews (Gehrke & Shubin 2016; Paço & Freitas 2017; Pieretti et al. 2015), and support homology between fish larval fin fold mesenchyme and the autopod mesenchyme of tetrapods. Briefly, the orthologous late-phase *hoxD* enhancer "Island I" from the spotted gar and coelacanth; the orthologous late-phase *hoxD* enhancer "CsB" from the spotted gar and the skate; and the orthologous late-phase *hoxA* enhancer "e16" from the spotted gar all show conserved functionality when tested in the mouse (Amemiya et al. 2013; Gehrke et al. 2015; Schneider et al. 2013). The spotted gar Island I, and e16 enhancers are active in the zebrafish distal fin fold mesenchyme, while CsB drives reporter activity more proximally, aligning with their activity in the mouse.

Mouse (Donor) to Fish (Host)

A *cis*-acting regulatory element has been previously identified and described located within the intron of the mouse *Hoxa11,* titled "m-Inta11", that shows activity in the presumptive autopod during mouse limb development (Kherdjemil et al. 2016; Kherdjemil & Kmita 2017; Chapter IV). This regulatory element has been shown to be a tetrapod-specific innovation during the fin-to-limb transition (Kherdjemil et al. 2016; Kherdjemil & Kmita 2017) and the functional consequences of this enhancer during limb evolution will be extensively covered in the next two sections of this discussion. ChIP experiments have shown both HOXA13, and HOXD13 preferentially bind to this regulatory element during mouse limb development, and *Hoxa13* (-/-)*/Hoxd13* (-/-) double knockout mice show loss of enhancer activity (Kherdjemil et al. 2016).

When tested in zebrafish, this enhancer is able to drive reporter expression in the distal fin fold mesenchyme, specifically within a subpopulation of *hoxa13a/b*- and *hoxd13a*-expressing cells (Fig. 5.1), providing further evidence to a homology between distal fin mesenchyme and presumptive autopod mesenchyme (Kherdjemil et al. 2016; Lalonde & Akimenko 2018). Zebrafish possess two *Hoxa13* paralogs (*hoxa13a,* and *hoxa13b*), and a single *Hoxd13* gene (*hoxd13a*). The expression of *hoxa13a* and *hoxa13b* extend more anteriorly in the distal fin fold mesenchyme compared with m-Inta11 enhancer activity, suggesting at least one Hoxa13 protein (Hoxa13a or Hoxa13b) and Hoxd13a may independently bind and are required to activate this enhancer (Fig. 5.1A-F). Another possibility is that activation of this enhancer is dose-dependent. Several developmental processes, including digit patterning, are regulated in a dose-dependent manner by multiple 5'HoxA/D proteins (Zakany et al. 1997). The zebrafish *hoxa13a* and *hoxa13b* paralogs also show differential expression during pectoral fin development (Fig. 5.1C) (Ahn & Ho 2008, Lalonde & Akimenko 2018). Interestingly, m-Inta11 is not activated in the proximal-posterior endoskeletal disc and fin fold regions that co-express *hoxa13b* and *hoxd13a*, providing additional evidence that all three Hox13 proteins (Hoxa13a, Hoxa13b, and Hoxd13a) may be required for m-Inta11 activation in the pectoral fin. Alternatively, differential enhancer activating capacities may exist between Hoxa13 paralogs in zebrafish (Fig. 6C).

Mouse late-phase *HoxD* enhancers "Island I, II, IV" also show conserved activity in the limb presumptive autopod and the zebrafish distal fin. All three regulatory elements drive reporter expression in the distal fin fold mesenchyme, in addition to more proximal fin regions (Gehrke et al. 2015).

Nonhomology: Fish unpaired fins and tetrapod tails

The *and1* ectodermal enhancer "Epi" and mouse "m-Inta11" regulatory elements are functional in both the pectoral and median fin folds during larval zebrafish development; however show no activity in mouse tails. An important distinction being that "m-Inta11" is active in the somites of the proximal tail region; and *Tg(2P:LacZ)* does show ectopic tail expression (Lalonde et al. 2016; Kherdjemil et al. 2016). The tetrapod tail is an extension of the vertebral column, and shares no aspect of homology with fish unpaired fins, which arise from the fish larval median fin fold (Sallan 2016). Early tetrapods retained tail fin rays after the loss of pectoral and pelvic fin rays however were eventually lost during terrestrialization (Clack 2009; Markey & Marshall 2007). As the autopod is proposed to have evolved from modified pre-existing distal fin elements, we expect and observe conserved regulatory activity between these structures. Late-phase 5'*hoxA/D* enhancer activity within the median fin fold of zebrafish was not discussed in previously cited publications, however would be useful for investigating differential *5'hoxA/D* activity between the paired and unpaired fins (Braasch et al. 2015; Gehrke et al. 2015; Schneider et al. 2013). Differential *5'hoxA/D* expression between fins could shed light on the individual roles of these genes during fin development and during the evolution of paired from unpaired fins (Freitas et al. 2006).

5.4. Regulatory divergence: Zebrafish to Tetrapods

Although an initial conserved genetic regulatory system underlies both fin and limb development, it is also known that major differences in fin/limb morphology are supported by diverging regulatory strategies (Freitas et al 2012; Leite-Castro et al. 2016; Paço & Freitas 2017; Yano & Tamura 2013). This section will first discuss instances of tetrapod-specific *cis*- and *trans*-regulatory evolution that has been linked to changes in *5'HoxA/D* and *actinodin* expression

during limb evolution. We will also summarize evidence that the expression pattern of *hoxd13a* in the pectoral fin of zebrafish may represent a derived state in teleost fish.

Novel regulatory elements: Tetrapod-specific Innovations

Changes in 5`*HoxA/D* regulation have consistently been linked to morphological changes during limb evolution, and yet the exact mechanism responsible for such regulatory changes often remains elusive. One recent exception being the identification of the novel tetrapod limb enhancer: "m-Inta11" or mouse *Hoxa11* intronic enhancer (Kherdjemil et al. 2016; Kherdjemil & Kmita 2017). This regulatory element is activated by HOXA13 and HOXD13 in the distal limb mesenchyme of mice, and shows conserved functionality in distal fin fold mesenchyme of zebrafish (as discussed in section I) (Fig. 5.1, 5.2A-B, Fig. 5.4). In tetrapods, the "m-Inta11" enhancer drives the expression of long non-coding RNAs at the *Hoxa11* exon 1 locus, resulting in the repression of *Hoxa11* from the distal limb bud domain where *Hoxa13* and *Hoxd13* are expressed (Fig. 5.2B). In zebrafish, *hoxa11b* distal expression overlaps with the expression of paralogs *hoxa13a, hoxa13b,* and partially with *hoxd13a* and no enhancers were identified in the *hoxa11a,* and *hoxa11b* intronic regions (Ahn & Ho 2008**;** Kherdjemil et al. 2016) (Fig. 5.2A). The "m-Inta11" regulatory element therefore represents a novel tetrapod-specific enhancer that can be directly linked to changes in regulation of *Hoxa11* during limb evolution. The morphological consequences of *Hoxa11* distal repression during limb evolution will be covered in section III.

Mouse late-phase *HoxD* enhancers Island II, III, IV, and CsC may also represent novel tetrapod enhancers that contributed to changes in regulation of *5'HoxD* genes. Using sequence alignment, only Island III was found to be conserved in the spotted gar genome (Gehrke et al. 2015; Gonzalez et al. 2007). When the putative "Island III" enhancer, and orthologous "Island

II", and "Island IV" regions from the spotted gar were tested in zebrafish, they were not able to drive reporter expression in the pectoral fin suggesting they may not exist in fish. However, it should be noted that the activity of these elements was only observed in primary injected fish with mosaic transgene integration. It may be beneficial to observe these elements in stable transgenic lines with the addition of eye/heart markers (*cryaa*, *cmlc2*) for screening purposes (for example, see methods in Kherdjemil et al. 2016). Furthermore, only 3 of 7 mouse late-phase *HoxA* enhancers (e10, e13, and e16) were identified by sequence conservation in spotted gar, with only "e16" being tested for activity in zebrafish. Importantly, absence of sequence conservation is not sufficient enough evidence that these enhancers do not exist in fish. The zebrafish Island I enhancer was not identified from sequence alignments, yet this element was shown to drive reporter expression in the distal pectoral fin fold mesenchyme (Gehrke et al. 2015).

***actinodin* regulatory evolution**

The *actinodin* genes, which code for the structural component of actinotrichia fibrils, were lost during the fin-to-limb transition. We have previously proposed that changes in *actinodin* regulation contributed to the loss of this gene family from the tetrapod genome (Lalonde et al. 2016). The potential contributions of *actinodin* loss/downregulation will be discussed in section III. As mentioned in section I, the ectodermal *actinodin1* enhancer "epi" shows conserved functionality in the tetrapod autopod ectoderm. In contrast, the mesenchymal *and1* enhancer "2PΔEpi", which drives expression in the zebrafish pectoral and median fin fold mesenchyme, is not functional in the mouse highlighting the possibility that changes in regulation occurred during the fin-to-limb transition (*trans* evolution in tetrapods) (Lalonde et al. 2016). Strong evidence suggests that mesenchymal *actinodin1* activation may be dependent on

one or more 5'HoxA/D proteins. Firstly, the "2PΔEpi" regulatory element contains five Hoxa13 putative binding sites, as well as one site for Hoxd13 and Hoxa11 each (Lalonde et al. 2016). When testing this element for enhancer activity, we see a drastic decrease in its ability to drive reporter expression when a putative binding site for Hox proteins, termed "Mes 1", has been removed (Fig. 5.3). Finally, "2PΔEpi" drives reporter expression in the pectoral fin in a manner identical to that of "m-Inta11", which is activated by Hoxa13a and Hoxd13a (Fig. 5.2A, 5.6). We therefore propose that 5'*HoxA/D* regulatory changes during the fin-to-limb transition may have also had consequences on the expression of *actinodin1* in the mesenchyme. Additionally, we know two mesenchymal enhancers exist and are required simultaneously to recapitulate the full expression pattern observed using "2PΔEpi" (Lalonde et al. 2016). We are in the process of identifying this second enhancer, and have identified its potential location to within 150bp. It is therefore possible either or both mesenchymal enhancer elements have experienced a change in regulation during limb evolution (*trans* evolution in tetrapods). Within this region, there is a putative binding domain for Prrx1. From published literature, we know *prrx1a* and *prrx1b* are expressed in the fin fold mesenchyme, and reporter lines for both genes show enhancer activity in these cells (Hernández-Vega & Minguillón 2011).

Due to the phylogenetic distance between zebrafish and mice, the *trans* machinery of the host (mouse) may not be able to decode the donor (zebrafish) *cis* sequence (Gehrke & Shubin 2016; Gordon & Ruvinsky 2012). This process is called Developmental Systems Drift (DSD) and suggests that the inability of "2PΔEpi" to drive reporter expression in the mouse limb autopod may not be due to the intrinsic lack of activity of the enhancer, but due to *cis* and *trans* coevolution in zebrafish (Gehrke & Shubin 2016; Gordon & Ruvinsky 2012; True and Haag 2001) (Fig. 5.5). The zebrafish ``2PΔEpi`` may have experienced sequence divergence (relative

to more basal ray-finned fish) (*cis* evolution), paired with transcription factor modulation (*trans* evolution), that render it unrecognizable to the tetrapod orthologous transcription factors (*cis trans* coevolution). Therefore limited conclusions and interpretations can be drawn when testing the functionality of "2PΔEpi" in mice. There are multiple teleost 5'*hoxA/D* enhancers that are not functional when tested in mice, including the zebrafish and pufferfish orthologous "CsB" and the zebrafish orthologous "Island I" regulatory elements (Gehrke et al. 2015; Woltering et al. 2014). In contrast, when the spotted gar orthologous "CsB" and "Island I" were tested in mice, they showed conserved regulatory activity with their mammalian counterparts, as summarized in section I (Gehrke et el. 2015). The spotted gar is a more basal ray-finned fish, whose lineage split off prior to the teleost-specific whole genome duplication. The spotted gar genome is believed to have experienced less sequence divergence compared to zebrafish due to its unduplicated state, and therefore the *trans* machinery of the host (mouse) is able to decode the *cis* enhancer sequences of the donor (Braasch et al. 2016). To support a change in *actinodin1* mesenchymal regulation during the fin-to-limb transition, the spotted gar orthologous "2PΔEpi" regulatory element should be identified and tested for functionality in the zebrafish and mouse (Fig. 5.5). To date, sequence analysis has not revealed any conserved putative enhancers upstream of *actinodin1* in the spotted gar (Lalonde et al. 2016), however due to the expression of *actinodin* and the presence of actinotrichia in this species, a *cis*-acting regulatory element should exist (Tulenko et al. 2016).

"**Posteriorization" of *hoxd13a*: A teleost-specific modification**

Autopod evolution has been linked to an expansion of late-phase 5'*HoxD* expression in tetrapods, particularly *Hoxd13* (Sordino et al. 1995). Late- or second-phase *5'HoxD* expression is governed by a regulatory landscape on the centromeric side (5') of the cluster called the global

control region (GCR) and patterns distal limb and fin structures (Tarchini & Duboule 2006; Zakany et al. 2004). It has been shown that zebrafish may lack or display only a partial second-phase of *hoxd13a* expression, supporting the notion that 5'*HoxD* expansion may be linked to autopod evolution (Ahn & Ho 2008; Woltering & Duboule 2010). More recent expression analysis across a phylogenetically broad range of fish species, however, has concluded fish have a definite second phase of *5'HoxD* expression during fin development; however there appears to be species-specific variation in the degree of this second phase (Paço & Freitas 2017). Therefore, while it is generally accepted that the evolution of the autopod involved tetrapod-specific 5*'HoxD* regulatory modulation, the absence of or partial late-phase *hoxd13a* expression in zebrafish may represent a derived modification in teleosts. This portion will summarize enhancer data that supports this hypothesis.

Firstly, the zebrafish orthologous late-phase *hoxD* enhancer "Island I" shows differential activity when compared to the spotted gar or mouse version (Fig. 5.6). All three "Island I" elements were tested for reporter activity in zebrafish (Gehrke et al. 2015). At 55 hours post fertilization (hpf), the zebrafish "Island I" is restricted to the posterior half of the pectoral fin fold while the spotted gar "Island I" extends much more anteriorly (Fig. 5.6). Similarly, the mouse "Island I" shows more anterior activity in the pectoral fin at 48hpf compared to the zebrafish version (Gehrke et al. 2015) (Fig. 5.6). Late phase *5'HoxA/D* expression occurs uniquely in the distal fin fold mesenchyme starting around 60hpf (Ahn & Ho 2008). By 72hpf, the pectoral fin fold has significantly elongated compared to 55hpf, and much more fin fold mesenchyme have invaded the fold (Grandel & Schulte-Merker 1998; Mari-Beffa and Murciano 2010). Therefore, these elements should be observed at 72hpf to get a more accurate picture of their late-phase activity in the distal pectoral fin fold. Finally, the zebrafish "Island I" enhancer is not functional

in mice providing evidence of teleost-specific enhancer sequence divergence (Gehrke et al. 2015). It should also be noted that the zebrafish "Island I" enhancer was not detectable by sequence conservation and therefore the amplified region might not contain all elements within the spotted gar and mouse "Island I".

Next, both "m-Inta11" and "2PΔEpi" enhancers show stronger activity in the posterior pectoral fin fold mesenchyme (Kherdjemil et al. 2016; Lalonde et al. 2016) (Fig. 5.2A, 5.4). The "m-Inta11" enhancer is activated by Hoxa13a and Hoxd13a, and due to the overlapping domains of activity, we believe "2PΔEpi" element is regulated similarly in the zebrafish pectoral fin (Fig. 5.4). The regulatory consequence of "m-Inta11" activity in the tetrapod lineage is distal repression of *Hoxa11* (Kherdjemil et al. 2016). Therefore we predict the activity of "m-Inta11" to overlap with *Hoxa11* when this enhancer element evolved. In zebrafish, the expression of *hoxa11b* extends much more anteriorly compared to the activity of "m-Inta11" (Lalonde & Akimenko 2018), and we predict this is due to the derived "posteriorization" of *hoxd13a* (Fig. 5.2A). Similarly, despite actinotrichia being present in the entire pectoral fin fold, "2PΔEpi" activity is posteriorly restricted and this may again be due to the derived expression pattern of *hoxd13a* (Lalonde et al. 2016) (Fig. 5.2A). Changes in mesenchymal *actinodin1* regulation in zebrafish may have yielded no functional consequences, as other *actinodin* paralogs can compensate (Zhang et al. 2010). The expression of *actinodin* was observed in paddlefish fins, a basal actinopterygian, and appears to extend to the anterior fin fold mesenchyme; however the study does not distinguish between ectodermal and mesenchymal expression in their conclusions (Tulenko et al. 2016).

5.5. Morphological consequences during fin and limb evolution

The past section summarized major advances in identifying potential regulatory changes during limb evolution; however the most exciting discoveries are able to link changes at a molecular level to functional consequences at a morphological level. This section will first highlight the evidence linking the "m-Inta11" element to the evolution of the "pentadactyl" or 5-digit state, in tetrapods, followed by a summary of experimental data predicting the potential implications of *actinodin* changes during the fin-to-limb transition, and finally will discuss the implications of 5'*HoxA/D* modulation during both fin and limb evolution.

***Hoxa11* distal repression & the pentadactyl state in tetrapods**

The regulatory consequences of "m-Inta11" evolution within the tetrapod lineage were covered in section II. Briefly, this regulatory element contributes to the active repression of *Hoxa11* from the presumptive autopod mesenchyme during limb development (Kherdjemil et al. 2016; Kherdjemil & Kmita 2017). To determine the functional consequences of *Hoxa11* distal repression on limb evolution, a *Hoxa11* conditional gain-of-function allele ($Rosa^{Hoxa11}$) was used to ectopically express *Hoxa11* in the presumptive autopod mesenchyme. All homozygous gain-of-function mutants displayed polydactylous limbs, an ancestral state, providing evidence that the distal repression of *Hoxa11* during the fin-to-limb transition contributed to the evolution of "pentadactyl" or 5-digit state in tetrapods (Kherdjemil et al. 2016; Kherdjemil & Kmita 2017). In addition, "m-Inta11" deletion mutants and *Hoxa13 -/- Hoxd13 -/-* loss-of-function mutants express *Hoxa11* in the distal limb bud, further confirming the regulatory consequences of "m-Inta11" activity during limb development (Fig. 5.2C). Finally, the functionality of "m-Inta11" in zebrafish (as discussed in section I) reveals the elements required for activation, including HOXA13/HOXD13 proteins, were conserved in the common ancestor of tetrapods and bony fish (Kherdjemil et al. 2016). The repression of *Hoxa11* from the distal limb domain may have also

had consequences for *actinodin* regulation. In Section II, we summarized the supporting evidence that *and1* is regulated by one or more 5'HoxA/D proteins, including Hoxa11b (Lalonde et al. 2016; Lalonde, unpublished data). During limb evolution, the absence of *Hoxa11* in the distal fin/limb region could have resulted in a loss of mesenchymal *actinodin* activity, supporting the hypothesis that regulatory changes during the fin-to-limb transition are responsible for the lack of functionality of "2PΔEpi" in mice (Lalonde et al. 2016). To confirm a regulatory link between Hoxa11b and *actinodin1* mesenchymal activation, we propose crossing zebrafish *hoxa11b* loss-of-function mutants with the *actinodin1* mesenchymal reporter line: *Tg(2PΔEpi:eGFP)*, and looking for a loss of reporter activity in the pectoral fin (Lalonde, unpublished data). We have created *hoxa11a, hoxa11b,* and *hoxd11a* mutants using the CRISPR/Cas9 system and are currently in the process of being analysed. Single mutants for *hoxa11b* will also be useful for testing the loss of distal *hoxa11b* during pectoral fin development, partially mimicking the distal repression of *Hoxa11* during mouse limb development as discussed in the previous paragraph. Zebrafish possess two *hoxa11* paralogs: *hoxa11a,* and *hoxa11b,* with only *hoxa11b* being expressed in the distal fin mesenchyme. We predict that although we have produced *hoxa11b* loss-of-function mutants, *hoxa11a* may be able to compensate in non-fin regions as they have similar expression patterns. Triple *hox11* mutants (*hoxa11a, hoxa11b,* and *hoxd11a*) are currently being analysed and are part of collaborative project to complement studies which created *Hoxa11-/-; Hoxd11-/-* mutant mice (Davis et al. 1995). Recent research has already compared triple *hox13* zebrafish mutants (*hoxa13a, hoxa13b,* and *hoxd13a*) to previous *Hoxa13 -/-; Hoxd13 -/-* mutant mice to support a deep homology between fish fin rays and the tetrapod autopod (Nakamura et al. 2016).

Loss/downregulation of *actinodin* genes and appendicular dermal bone loss in tetrapods

The *actinodin* gene family codes for structural proteins in the actinotrichia fibrils (Zhang et al. 2010). Actinotrichia are considered the first exoskeletal elements formed during fin development, and support the larval fin fold while simultaneously directing the distal migration of mesenchymal cells through the fold (Grandel & Schulte-Merker 1998). Actinotrichia and dermal fin rays (lepidotrichia) are absent in tetrapods. Experimental evidence suggests actinotrichia are crucial for larval fin fold development, and for proper fin ray formation due to their involvement in proper fin fold mesenchyme migration. Fin fold mesenchyme has been shown to directly contribute to fin ray fibroblast and osteoblast populations (Lee et al. 2013; Nakamura et al. 2016). It is therefore proposed that actinotrichia defects, through changes in *actinodin* expression, may have contributed to the loss of fin rays during the fin-to-limb transition (Zhang et al. 2010; Lalonde et al. 2016).

Morpholino-mediated knockdown of *actinodin1* & *actinodin2* leads to an absence of actinotrichia, impaired fin fold development and defects in fin fold mesenchyme migration (Zhang et al. 2010). Knockdown of either paralog individually yields no actinotrichia defects, highlighting their ability to compensate for one another. No functional analysis has been performed on the shorter *actinodin* paralogs *and3/4;* however their expression patterns are similar to *and1/2* during larval fin development (Zhang et al. 2010). Due to the transient nature of mopholino oligonucleotides, the impact of actinotrichia defects on fin ray formation is unknown. Loss-of-function *actinodin* mutants are required to observe how fin ray development proceeds in the absence of actinotrichia. We are therefore in the process of making *actinodin* loss-of-function mutants for all four *actinodin* paralogs (*and1-4)* (Lalonde unpublished data, Qu unpublished data). Based on the morpholino data, it may only be necessary to create double *and1/2* mutants to disrupt proper actinotrichia formation and fin fold mesenchyme migration.

Furthermore, if double *and1/2* mutants are embryonic lethal due to their expression in larval non-fin regions (Zhang et al. 2010), we propose mutating previously identified *and1* fin-specific regulatory elements (2P, mes1 and epi3) and crossing these fish with *and2* mutants (Lalonde et al. 2016). To date, I have identified three distinct mutants for *actinodin1* and *actinodin2* using the CRISPR/Cas9 system. Single heterozygous mutants for each paralog are being raised and can be bred to produce double homozygous mutants within two generations. If fin ray defects are observed in *actinodin* loss-of-function mutants this would support the hypothesis that the loss or downregulation of these genes may have contributed to fin dermal bone loss during the fin-to-limb transition.

To directly observe the effects of fin fold mesenchyme defects on fin ray formation, these cells were ablated during larval development using the nitroreductase/metronidazole (NTR/MTZ) system (Lalonde & Akimenko 2018; Mathias et al. 2014; Chapter III) . The ablation of these cells resulted in impaired larval fin fold development, actinotrichia defects, and defects during fin ray formation. The presence of fin ray defects supports the hypothesis that these cells are crucial for proper fin ray formation, and that mis-migration of these cells during the fin-to-limb transition may have contributed to the loss of dermal rays in fish (Lalonde et al. 2016; Nakamura et al. 2016; Ahn & Ho 2008). Fin fold mesenchyme defects may also have implications for *actinodin* expression and actinotrichia maintenance. As these cells migrate distally through the larval fin fold they secrete actinodin proteins, and it is thought that actinodin produced in the mesenchyme contributes to the thickness and length of the actinotrichia (Duran et al. 2011; Lalonde et al. 2016). Following ablation of these cells, mesenchymal *actinodin1* activity is decreased, actinotrichia defects occur, and surviving mesenchymal cells fail to migrate correctly (Lalonde & Akimenko 2018).

We have also tested mesenchymal cell ablation using the pro-apoptotic Caspase3 method of cell ablation (Mallet et al. 2002). Using the "2PΔEpi" regulatory element instead, we expressed the *Caspase3* gene in the fin fold mesenchyme, which will be processed *in vivo* to form active Caspase3 and initiate the apoptotic cascade. This eliminated the requirement for potentially toxic treatments, and avoided unwanted cell death in the lower digestive track. Using PCR on genomic extractions from F1 embryos, I identified three transgenic lines (*Caspase3*-positive embryos from 3 separate primary injected fish (P0)). F1 fish from each positively-identified P0 were raised; however no surviving F1 displayed pectoral or caudal fin defects (Line #1: 0/65, Line #2: 0/46, Line #3: 0/70) (Lalonde Unpublished). Additionally, a proportion of larvae from independent P0 crosses displayed craniofacial defects, and early lethality (7dpf) suggesting the Caspase3 activity may not have been limited to the fin fold mesenchyme.

Based on the phenotypes observed following fin fold mesenchyme ablation, it is proposed that these cells contribute to their own successful migration through their production and secretion of actinodin proteins. This concept raises the intriguing possibility that even minor changes in *actinodin* regulation during the fin-to-limb transition may have yielded drastic fin ray defects. Decreased *actinodin* expression would produce actinotrichia and mesenchymal cell migration defects, leading to less actinodin being secreted within the larval fin fold and more severe actinotrichia defects during the later stages of fin development. Ultimately, we predict fin fold mesenchyme would be extremely disorganized throughout fin development and would be unable to effectively form the adult fin rays. In addition to dermal bone loss during the fin-to-limb transition, fin fold mesenchyme migration defects have potential implications for endochondral bone expansion during autopod evolution and will be discussed in the following section (Ahn & Ho 2008; Lalonde & Akimenko 2018; Nakamura et al. 2016).

5'HoxA/D modulation during fin and limb evolution

During limb evolution the loss of fin dermal bone was preceded by modifications to the endoskeleton. The proximal anterior endoskeletal bone elements were lost (pro- and mesopterygium), and the distal endoskeletal bone elements became more expanded and elaborate to form the autopod. The tetrapod stylopod is considered to be homologous to the posterior most proximal bone elements in chondrichthyan and basal actinopterygian fish, the metapterygium (Onimaru et al. 2015; Tanaka 2016). In contrast, zebrafish possess highly reduced pectoral fin endochondral bone, having lost the metapterygium and the proximal-most pro- and mesopterygial bones (Mabee et al. 2004). The pro- and mesopterygial radials are retained. In section I, we summarized available enhancer data that reveals a deep homology between the tetrapod autopod and the distal fish regions. In section II, we discussed evidence of regulatory divergence, highlighting tetrapod-specific 5'*HoxA/D* regulatory innovations but also teleost-specific modifications. In this final section, we will summarize overexpression data, mutant models and cell ablation experiments that investigate the role of 5'*HoxA/D* regulatory changes in endochondral bone expansion during limb evolution. The repression of *Hoxa11* from the distal autopod region during limb development has already been covered and will be omitted from this part.

Although we have proposed that the absence or partial late phase *hoxd13a* expression in zebrafish may be a teleost-specific modification, it does not preclude the possibility that changes in 5*'HoxA/D* regulation during tetrapod evolution contributed to limb endochondral bone expansion (Paço & Freitas 2017). To assess the effects of *hoxd13a* modulation on endochondral bone formation, transient methods were used to overexpress *hoxd13a* in the zebrafish distal fin domain (Freitas et al. 2012). The group found that 40% of fish display properties consistent with

endochondral bone expansion and fin fold reduction (Freitas et al. 2012). Endochondral bone identity was confirmed using cartilage stains and chondrocyte markers and additional molecular markers were used to highlight a shift towards a "distal limb fate" (Freitas et al. 2012). Unfortunately due to the transient nature of these experiments, and high mortality rates among affected fish, analysis on radial and fin ray formation was not possible. It may be beneficial to revisit these experiments using stable transgenic lines incorporating other methods of inducible transgene expression (Akerberg et al. 2014; Knopf et al. 2010; Mosimann et al. 2011). Consistently, the ablation of *hoxa13a/hoxd13a*-expressing mesenchyme during larval development shows a decrease in expression of these genes and decreased endoskeletal disc size; further implicating *5'HoxA/D* genes during endochondral bone formation and evolution (Lalonde & Akimenko 2018). Although not investigated yet, modulation of 5'HoxA/D has also been linked to shifts in anterior-posterior positional identity and the loss of the proximal anterior bone elements (pro- and mesopterygium) during limb evolution (Onimaru et al. 2015; Tanaka 2016). Early fin and limb anterior-posterior patterning is in part established by opposing gradients of SHH and GLI3R (Hill et al. 2009; Litingtung et al. 2002; Prykhozhij & Neumann 2008). Increased transcript levels of *5'HoxA/D* during limb evolution would have promoted SHH-signaling and the conversion of GLI3 to GLI3R, leading to an expansion of posterior positional identify (Onimaru et al. 2015; Tanaka 2016).

Functional analysis of *hox13* genes (*hoxa13a, hoxa13b & hoxd13a*) in zebrafish has recently been performed using loss-of-function CRISPR mutants. Double (*hoxa13a, hoxa13b*) and triple (*hoxa13a, hoxa13b, hoxd13a*) homozygous mutants fail to form fin rays, and produced an increased number of distal radial bones (Nakamura et al. 2016). This phenotype represents a shift toward what is predicted to have occurred during the fin-to-limb transition: expanded

endochondral bone elements, and reduced dermal bone (Sordino et al. 1995; Tamura and Yano 2013; Tamura et al. 2008). And yet, we propose exercising caution when considering the implications of these mutants for the fin-to-limb transition. Evidently, tetrapods retained *Hoxa13* & *Hoxd13* during limb evolution with further evidence suggesting even an increase or expansion of expression (Freitas et al. 2012; Yano & Tamura 2008). It is therefore proposed that while the molecular mechanisms may not align with 5'*HoxA/D* regulatory changes during tetrapod evolution, the resulting morphology at a tissue level may mimic processes that occurred during the fin-to-limb transition (Nakamura et al. 2016). Specifically, it is thought *hox13* zebrafish mutants show defects in fin fold mesenchyme migration. In the previous section we discussed the implications of fin fold mesenchyme migration defects on dermal bone loss; however an additional hypothesis predicts that if these cells remain in the proximal fin domain, they may experience a shift in cell fate and contribute to endochondral bone instead (Ahn & Ho 2008; Lalonde & Akimenko 2018; Nakamura et al. 2016). Fin fold mesenchyme migration defects are not explored in *hox13* mutant fish, and should be considered a priority to determine the mechanisms of fin ray loss/distal radial expansion. While multiple fluorescent reporter lines are available that label fin fold mesenchyme, we recognize the time constraints of recreating *hoxa13/hox13b* homozygous mutants within transgenic reporter backgrounds (Kawakami 2007; Kherdjemil et al. 2016; Lalonde et al. 2016). As *hox13* loss-of-function zebrafish mutants do not recreate the expression of *Hoxa13* & *Hoxd13* in tetrapods, additional information is required to integrate these results with proposed with 5*'HoxA/D* regulatory changes during the fin-to-limb transition. To confirm a regulatory link between Hoxa13a/Hoxd13a and *actinodin1* mesenchymal activation, We propose crossing *hox13* loss-of-function mutants with the *actinodin1* mesenchymal reporter line: *Tg(2PΔEpi:eGFP)*, and looking for a loss of reporter

activity in the pectoral fin (Lalonde, unpublished data). Although we requested the *hox13* mutants for analysis they were not provided, therefore we are currently in the process of making *hoxa13a, hoxa13b,* and *hoxd13a* mutants using the CRISPR/Cas9 system (Qu unpublished).

In the *hoxd13a* overexpression study and the *hox13* loss-of-function zebrafish mutants, larval fin fold structure is observed by performing an *in situ* hybridization for *and1* (Freitas et al. 2012; Nakamura et al. 2016).We have previously discussed the inclusion of Hoxa13a & Hoxd13a as positive regulators of *and1* in the mesenchyme. While the results of *hoxd13a* overexpression (decreased *and1*) seem to dispute this conclusion, we would argue these results are not mutually exclusive and would like to highlight the importance of discussing tissue-specificity when investigating *actinodin1* expression (Freitas et al. 2012; Zhang et al. 2010). Fin fold ectodermal and mesenchymal *and1* expression begin at different stages of pectoral fin development, relying on distinct sets of transcription factors (Lalonde et al. 2016; Zhang et al. 2010). Conclusions using "global" *and1* fin transcript levels on whole mount samples may therefore be difficult to interpret. While *and1* expression is sufficient as a fin fold marker, examining tissue-specific changes using *and1* reporter lines could shed light on *actinodin* regulation by 5'HoxA/D proteins and the implications during the fin-to-limb transition (Lalonde et al. 2016; Lalonde & Akimenko 2018).

5.6. Discussion Conclusions

Combining regulatory data and functional analysis provides crucial insight into some of the molecular mechanisms that contributed to morphological changes during the fin-to-limb transition. Conserved regulatory strategies between fish and tetrapods highlight a deep homology between distal fin and limb structures, while diverging strategies illuminate instances of evolutionary novelty and trait loss (autopod and appendicular dermal bone, respectively). We

have highlighted how the zebrafish has remained a powerful model organism for performing transgenic swap experiments, however the derived nature of the genome and fin morphology limit interpretations regarding the fin-to-limb transition. Instead, it is becoming increasingly more common to study a phylogenetically broad range of fish species to draw conclusions regarding molecular and morphological change during limb evolution. The advances in fish genome availability and genome editing technology will serve as invaluable tools that will greatly facilitate future studies.

\

5.7. Figures

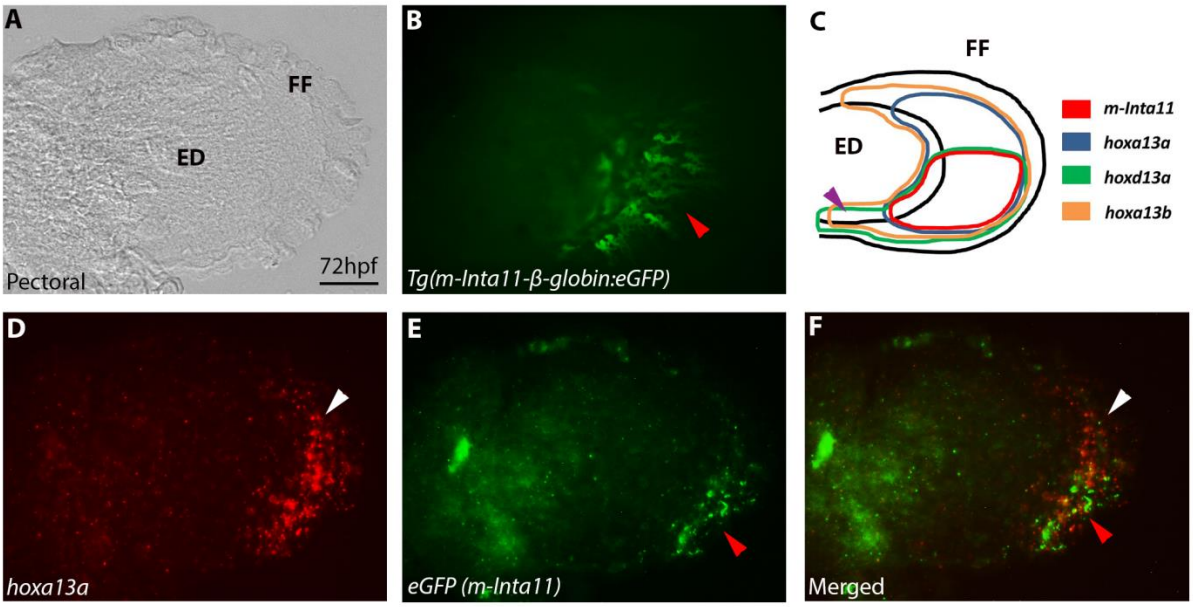

Figure 5.1. The"m-Inta11" regulatory element is active in a subpopulation of *hoxd13a- & hoxa13a*-expressing cells in the zebrafish pectoral fin at 72hpf. (A, D-F) Double fluorescent ISH for *hoxa13a, eGFP,* & **(B)** *Tg(m-Inta11:eGFP)* reporter activity in 72hpf pectoral fin. **(C)** Summary of expression patterns for *hoxa13a*, *hoxd13a*,*hoxa13b* and *m-Inta11* activity in 72hpf pectoral fin. The "m-Inta11" regulatory element drives expression in the posterior fin fold mesenchyme (red arrow): eGFP fluoresence (B) and eGFP transcripts are presented (E). The expression of *hoxa13a* extends to the anterior fin fold mesenchyme (white arrow) (D, F), outside the region where "m-Inta11" is active (red arrow) (E, F). The expression of *hoxd13a* is posteriorly restricted and partially mimics "m-Inta11" activity (C). The "m-Inta11" element is not active in the proximal-posterior endoskeletal disc and fin fold regions where *hoxd13a* , and *hoxa13b* are co-expressed (purple arrow) (C). Brightfield (A), fluorescent (B, D, E) and merged (F) images are present. ED = Endoskeletal disc, FF = Fin fold. Scale bar = 3µm.

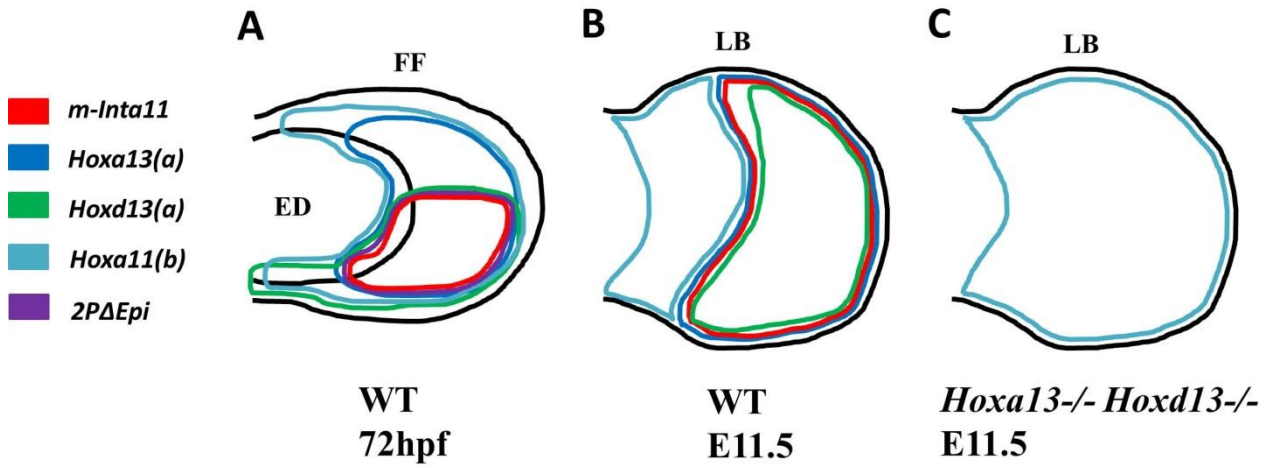

Figure 5.2. Expression patterns (*Hoxa13(a), Hoxd13(a), Hoxa11(b)*) and regions of enhancer activity (m-Inta11, 2PΔEpi) in 72hpf zebrafish pectoral fin, and E11.5 WT and *Hoxa13 -/- Hoxd13a -/-* mutant mouse forelimb bud. (A) 72hpf zebrafish pectoral fin, **(B)** E11.5 WT mouse forelimb bud, and **(C)** E11.5 *Hoxa13 -/- Hoxd13-/-* mutant mouse forelimb bud. Enhancers 2PΔEpi (purple) and m-Inta11 (red) show overlapping activity in a subpopulation of *hoxa13a/hod13a*-expressing cells (blue/green) in the zebrafish pectoral fin at 72hpf (A). Note *hoxa13a* expression expands more anteriorly (blue) and *hoxd13a* expression extends to the proximal-posterior disc and fin fold regions (green) (A). The expression of *hoxa11b* (turquoise) extends anteriorly outside the domain of activity of m-Inta11 (red) (A). In WT E11.5 limb buds, *Hoxa11* is restricted to the proximal domain due to m-Inta11 activity in the distal regions (turquoise) (B). The activity of m-Inta11 (red) overlaps completely with *Hoxa13* expression (blue) (B). Note *Hoxd13a* expression (green) does not completely overlap with *Hoxa13* (blue) and m-Inta11 activity (red) (B). m-Inta11 activity in the WT E11.5 limb bud is inferred through absence of distal *Hoxa11* transcripts (B). Enhancer activity was only observed

at E12.5 in transient transgenic mice (*Tg(m-Inta11:LacZ)*). In *Hoxa13 -/- Hoxd13 -/-* E11.5 limb buds, m-Inta11 shows no activity and *Hoxa11* is expressed in both the proximal and distal regions (turquoise) (C). Absence of m-Inta11 activity is inferred by the presence of *Hoxa11b* transcripts in the distal limb bud region (C). Note 2PΔEpi is not functional in WT or mutant limb buds (B, C). E = Embryonic day, ED = Endoskeletal disc, FF = Fin fold, hpf = hours post fertilization, LB = Limb bud, WT = Wild type.

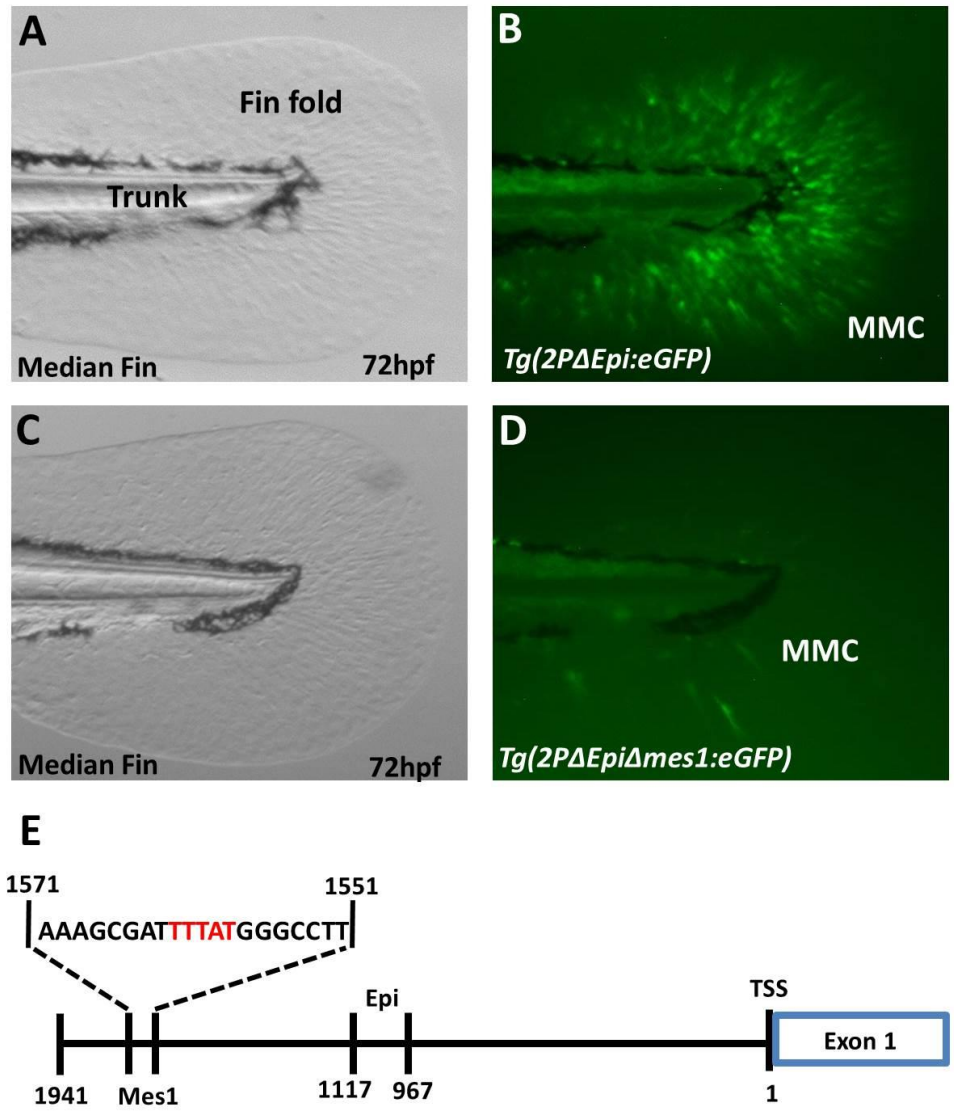

Figure 5.3. Enhancer activity of 2PΔEpi drastically reduced when putative binding site for Hox (mes1 site) removed. (A-D) Zebrafish median fins at 72hpf comparing eGFP reporter expression when driven by either 2PΔEpi or 2PΔEpiΔmes1 regulatory elements. **(E)** Schematic of *actinodin1* 1941bp region of the first non-coding exon. The 2PΔEpi regulatory element is able to drive reporter expression in the migrating mesenchymal cells of the median and pectoral fin folds (Median fin: A-B, Pectoral fin: Fig. 4B). Reporter expression is drastically reduced in the median fin when mes1 site is removed from the 2PΔEpi regulatory element (C-D). No eGFP-

positive cells are visible in the pectoral fin (data not shown). Mes1 site consists of a 20bp region containing the consensus Hox binding domain TTTAT (Red text) (E). 2PΔEpi regulatory contains the entire 1941bp fragment with Epi region removed (E). Two independent lines were obtained to confirmed the expression pattern of Tg(2PΔEpiΔmes1:eGFP). Brightfield (A, C) and fluorescent (B, D) images are displayed. MMC = Migrating mesenchymal cells, TSS = Transcription Start Site.

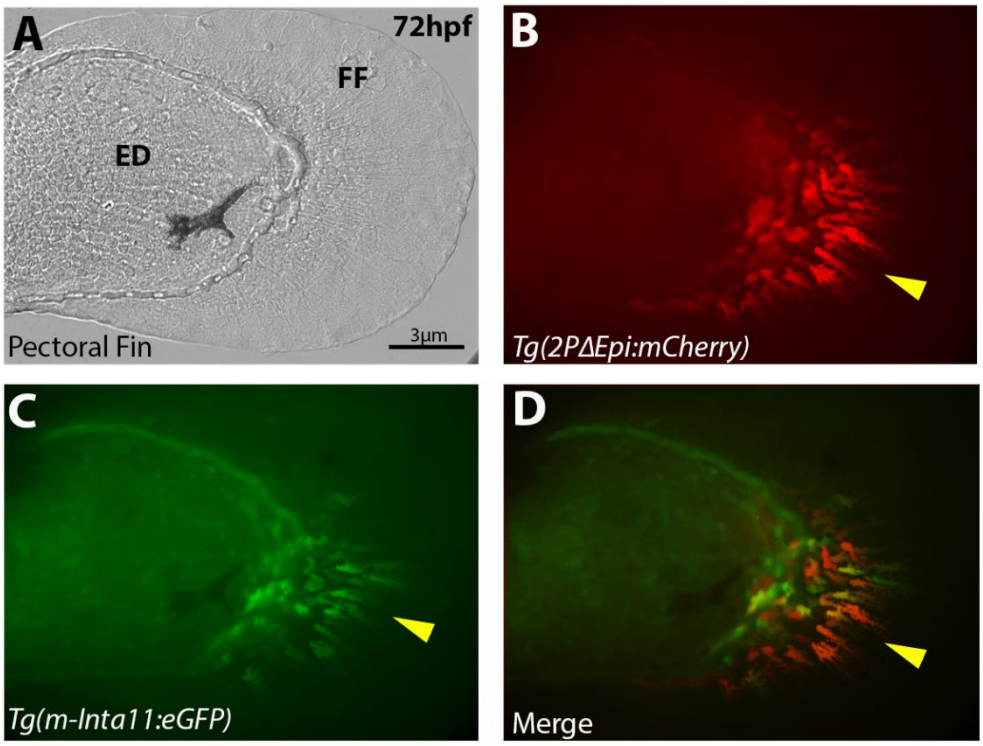

Figure 5.4. The "m-Inta11" & "2PΔEpi" enhancer elements display overlapping domains of activity in the zebrafish pectoral fin fold mesenchyme at 72hpf. (A-D) Zebrafish pectoral fin at 72hpf of *Tg(2PΔEpi:mCherry)* x *Tg(m-Inta11:eGFP)* double transgenic fish. Both regulatory elements drive overlapping reporter expression in posterior fin fold mesenchyme (yellow arrow) (B-D), providing evidence they may both be co-activated by Hoxa13a and Hoxd13a proteins. Note the absence of reporter activity in anterior fin fold mesenchyme (B-D). Due to inconsistencies within transgenic lines, individual cells contain variable amounts of eGFP and mCherry protein and accounts for the colour variation observed in different mesenchymal cells (D). Brightfield (A), Fluorescent (B, C), and merged (D) images are displayed. ED = Endoskeletal disc, FF = Fin fold. Scale bar = 3µm.

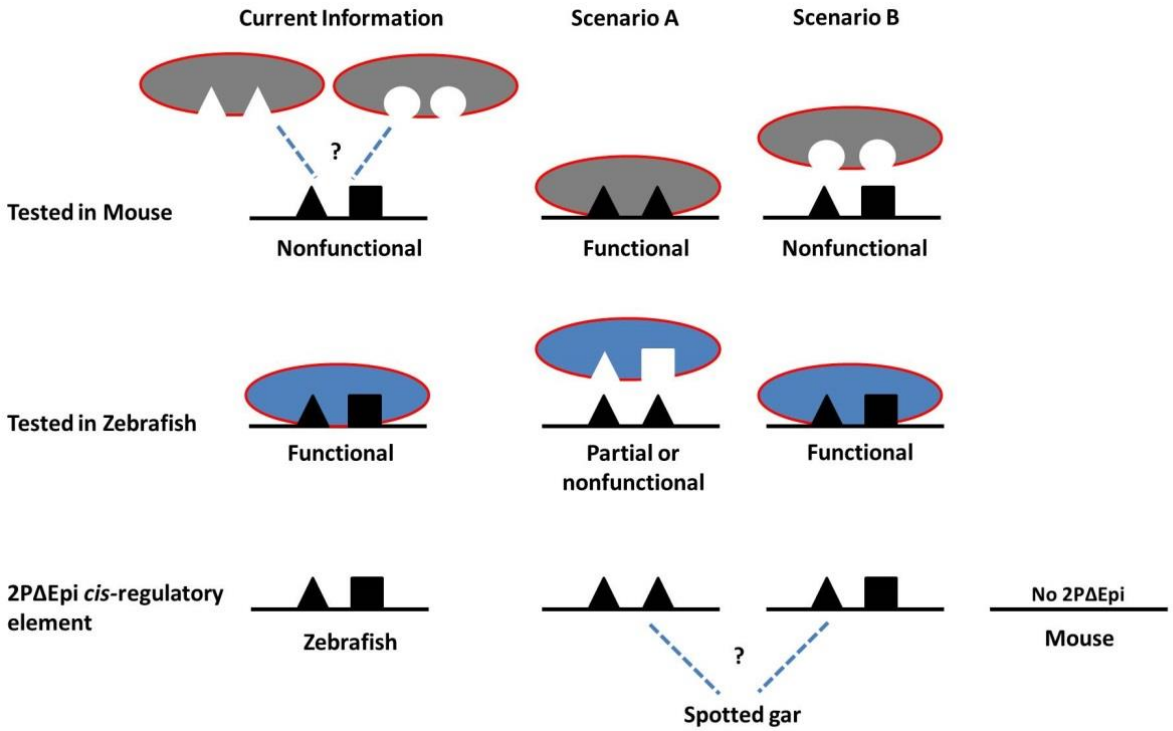

Figure 5.5. Orthologous spotted gar "2PΔEpi" regulatory element is required to support or contradict possibility of *trans actinodin* evolution in tetrapods during the fin-to-limb transition. Hypothetical scenarios if spotted gar orthologous "2PΔEpi" regulatory element is tested via transgenic swap experiments in the zebrafish and mouse. Current information represents experiments performed in Lalonde et al. 2016, where the zebrafish "2PΔEpi" element is not functional in the mouse. It is impossible to determine from these results if lack of enhancer functionality is due to changes to the *trans* environment in tetrapods, or *cis trans* coevolution in the zebrafish. In scenario A, the spotted gar orthologous "2PΔEpi" is functional in mice. From this result, we could conclude there is no evidence for *trans* evolution in tetrapods, and that the zebrafish has undergone *cis* and *trans* coevolution which the *trans* environment of the mouse is not able to decode. In this scenario, the gar element may be partially functional or nonfunctional when tested in the zebrafish. In scenario B, the spotted gar "2PΔEpi" element shows conserved functionality in zebrafish however is unable to function in the mouse. This result supports the

hypothesis that there was a change in regulation of *actinodin* due to *trans* evolution in tetrapods. If the spotted gar element is not functional in either zebrafish or mouse (not displayed), we could not conclude anything more than what is currently known.

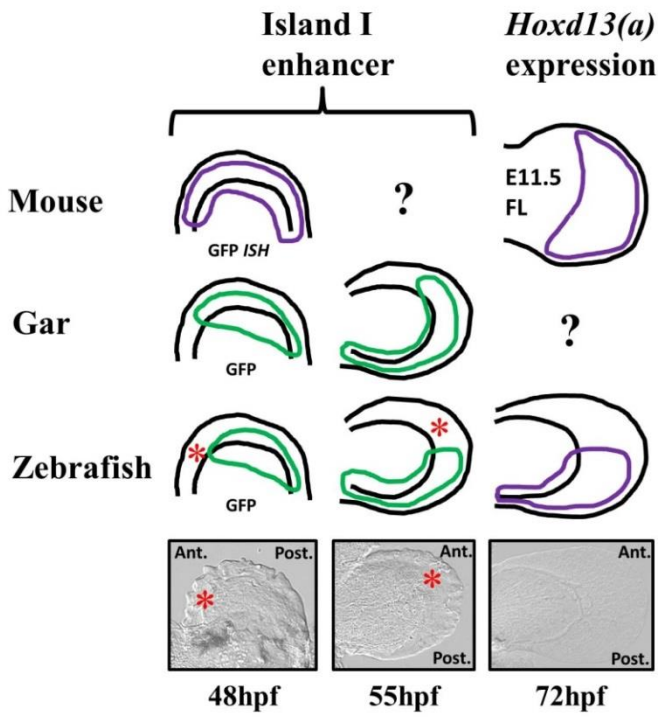

Figure 5.6. Orthologous gar and mouse Island I enhancers drive reporter expression in the anterior zebrafish pectoral fin. Mouse, gar, and zebrafish orthologous Island I enhancer activity at 48, and 55hpf in the zebrafish pectoral fin, and endogenous *Hoxd13(a)*expression in the mouse forelimb at E11.5 and the zebrafish pectoral fin at 72hpf. Mouse and gar Island I enhancer drive activity more anteriorly in the zebrafish pectoral fin compared to the orthologous zebrafish Island I (red asterisks). Endogenous *Hoxd13* expression extends to the anterior presumptive autopod at E11.5 in the mouse forelimb. Endogenous *hoxd13a* expression is absent from the anterior pectoral fin fold mesenchyme at 72hpf in the zebrafish. Mouse Island I enhancer activity at 55hpf, and endogenous *hoxd13* expression in the gar are unknown (Question mark). Donor organism indicated on the left. Brightfield representative pectoral fins shown below. Purple = *in situ* hybridization (ISH), green = GFP fluorescence. Schematic representation of Island I enhancer activity based on data from Gehrke et al. 2015. Ant. = Anterior, FL = Forelimb, Post. = Posterior.

CHAPTER 6

General Conclusions

The *actinodin* gene family was lost during the fin-to-limb transition. We propose that their diseappearance may have contributed to the loss of appendicular dermal bone and that changes in their regulation preceded their disappearance (Lalonde et al. 2016; Zhang et al. 2010). We have identified and characterized zebrafish *actinodin1 cis*-acting regulatory elements for fin ectoderm and fin mesenchyme expression. To test the functionality of these regulatory elements in tetrapods, we created a transgenic reporter mouse line. Despite the absence of this gene family in tetrapods, the ectodermal enhancer remains functional in the presumptive limb autopod, supporting a homology between distal fin and limb ectoderm. In contrast, the mesenchymal enhancer does not function in the limb mesenchyme supporting a possible change in *trans* regulation (*trans* evolution) during the fin-to-limb transition. The orthologous *actinodin1* regulatory elements from the spotted gar should be isolated and tested in tetrapods to further support this theory. We have also uncovered evidence that one or more 5'HoxA/D proteins may be regulating mesenchyme *actinodin1* expression, providing a possibility that *5'HoxA/D* regulatory changes during limb evolution may have also had consequences for *actinodin* evolution (Lalonde & Akimenko, submitted). A funtional analysis of the *actinodin* genes is currently underway using loss-of-function CRISPR/cas9 mutants. We predict in the absence of *actinodin* functionality, zebrafish will display actinotrichia and fin ray defects, supporting the hypothesis that the disappearance of these genes may have contributed to the loss of fin dermal bone during the fin-to-limb transition.

It is predicted that actinotrichia defects will have direct consequences for the migration of distal fin mesenchyme. Distal fin mesenchymes migrate through the fin fold along the actinotrifchia during embryonic and larval development and then differentiate into both fin ray fibroblast and osteoblast (Lee et al. 2013; Nakamura et al. 2016). It has been proposed that

defects in the migration of these cells could also be a mechanism of dermal bone loss during the fin-to-limb transition (Ahn & Ho 2008; Lalonde & Akimenko 2018; Nakamura et al. 2016). In fact, this hypothesis is not mutually exclusive with the potential contributions of the loss of the *actinodin* genes during limb evolution as transiently knocking down *actinodin1/2* leads to fin mesenchyme migration defects in larval zebrafish (Zhang et al. 2010). To mimic long-term distal fin mesenchyme defects and observe the effect on actinotrichia and fin ray formation, we ablated these cells throughout larval development using the nitroreductase/metronidazole system (Lalonde & Akimenko 2018). Following ablation, we observed severe fin fold and actinotrichia defects during early larval development, suggesting distal fin mesenchyme is crucial for proper fin fold and actinotrichia maintenance. Following sustained ablation up to 30dpf, we observed fewer fin rays that were shorter and less defined compared to control fish (Lalonde & Akimenko 2018). This result supports the hypothesis that distal fin mesenchyme defects can cause fin ray defects, and may be a mechanism of dermal bone loss during the fin-to-limb transition. Due to the limitations of metronidazole toxicity and the regenerative capabilities of the zebrafish, we only observed minor effects on fin ray formation at 30dpf. While our taCaspase3 methods of cell ablation were inconclusive, we predict our loss-of-function *actinodin* mutants will also display distal fin mesenchyme defects. These experiments will serve to strengthen a causal link between fin mesenchyme migration defects and fin ray defects.

We have highlighted how changes in regulation of the 5'HoxA/D genes may have had consequences on *actinodin* evolution. Fellow researchers have explored potential implications of these regulatory changes for proper fin fold mesenchyme migration as well. We have linked changes in the regulation of *Hoxa11*, specifically the distal repression of *Hoxa11*, during the fin-to-limb transition to the evolution of the pentadactly or 5-digit state. We uncovered evidence of a

tetrapod-specific Hoxa13/Hoxd13-dependent enhancer (m-Inta11) that drives antisense transcription at the *Hoxa11* locus during limb development, preventing *Hoxa11* sense transcripts from being produced (Kherdjemil et al. 2016). By inhibiting the activation of antisense transcripts, via the deletion of the enhancer, mice develop polydactylous limbs, a trait observed in extinct transitional tetrapods. Furthermore, we also showed m-Inta11 activity is functional in the distal fin mesenchyme of zebrafish supporting a homology with presumptive autopod mesenchyme in the limb (Kherdjemil et al. 2016). To test the functionality of *Hoxa11* distal repression during zebrafish fin development, we have produced *hoxa11b* loss-of-function mutants. We have also produced triple *hox11* (*hoxd11a*, *hoxa11a*, and *hoxa11b*) loss-of-function mutants to explore the role of these genes during fin development. As *Hox11* genes pattern the zeugopod (ulna & radius) in tetrapods, we may see no phenotype in the derived zebrafish fin due to lack of homologous structures (Davis et al. 1995).

The evolution of the tetrapod limb was a fundamental innovation that facilitated vertebrate terrestrial colonization and diversification, including our own species. Uncovering the modifications required in producing a limb provides amazing insight into our own human evolution. Overall, we have contributed to a better understanding of molecular and morphological changes that occurred during the fin-to-limb transition and the developmental mechanisms of fins and limbs. We believe our data furthers the field while introducing novel research questions and providing a platform for future exciting work.

REFERENCES

Abe G, Ide H, and Tamura K. Function of FGF signaling in the developmental process of the median fin fold in zebrafish. Developmental Biology. 2007; 304(1):355–366.

Ahlberg PE. Coelcanth fins and evolution. Nature. 1992; 358: 459.

Ahlberg PE, Clack JA, Blom H. The Axial skeleton of the Devonion tetrapod Ichthyostega. Nature. 2005; 437: 137-140.

Ahlberg PE, Clack JA. Paleontology: a firm step from water to land. Nature. 2006; 440(7085): 747-749.

Ahlberg P, and Milner A. The origin and early diversification of tetrapods. Nature. 1994; 368 (6471):507–514.

Ahn D, and Ho RK. Tri-phasic expression of posterior hox genes during development of pectoral fins in zebrafish: Implications for the evolution of vertebrate paired appendages. Developmental Biology. 2008; 322(1):220–233.

Akerberg AA, Stewart S and Stankunas K. Spatial and Temporal Control or Transgene Expression in Zebrafish. PLoS ONE. 2014; 9(3): e92217.

Albadri C, Del Bene F, Revenu C. Genome editing using CRISPR/Cas9-based knock-in approaches in zebrafish. Methods. 2017; 15(121-122): 77-85.

Amemiya CT, Alfoldi J, Lee AP, Fan S, Philippe H, Maccallum I, Braasch I et al. The African coelacanth genome provides insights into tetrapod evolution. Nature. 2013; 496(7445):311-316.

Anderson E, Peluso S, Lettice LA, Hill RE. Human limb abnormalities caused by disruption of hedgehog signaling. Trends Genet. 2012; 28: 364-373.

Badugu A, Kraemer C, Germann P, Menshykau D, Iber D. Digit patterning during limb development as a result of the BMP-receptor interaction. 2012; 2(991): 1-13.

Beanan MJ, Sargent TD. Regulation and function of Dlx3 in vertebrate development. Dev. Dyn. 2000; 218 (4): 545–553.

Berlivet S, Paquette D, Dumouchel A, Langlais D, Dostie J, Kmita M. Clustering of Tissue-specific sub-tads accompanies the regulation of HoxA genes in development limbs. PLOS genetics. 2013; 9(12): e1004018.

Bird NC, Mabee PM. Developmental morphology of the axial skeleton of the zebrafish, Danio rerio (Ostariophysi: Cyprinidae). Dev Dyn. 2003; 228(3): 337-357.

Boisvert CA, Mark-Kurik E, Ahlberg PE. The pectoral fin of *Panderichthys* and the origin of digits. Nature 2008; 456: 636–8.

Bouvet J. Differentiation and ultrastructure of the distal skeleton of the pectoral fin of the native trout (Salmo trutta fario L.). I. Differentiation and ultrastructure of the actinotrichia. Arch Anat Microsc Morphol Exp. 1974; 63(1): 79-96.

Braasch I, Gehrke AR, Smith JJ, Kawasaki K, Manousaki T, Pasquier J, Amores A et al. The spotted gar genome illuminates vertebrate evolution and facilitates human-teleost comparisons. Nature Genetics. 2016; 48:427-437.

Brookfield J. F. 2003 Gene duplications: the gradual evolution of functional divergence. Curr. Biol. 13, 229–230.

Burke AC, Nelson CE, Morgan BA, Tabin C. Hox genes and the evolution of vertebrate axial morphology. Development. 1995; 21(2): 333-346.

Capellini TD, Di Giacomo G, Salsi V, Brendolan A, Ferretti E, Srivastava D, Zappavigna V, Selleri L. Pbx1/Pbx2 requirement for distal limb patterning is mediated by the hierarchical control of Hox gene spatial distribution and Shh expression. Development. 2006; 133(11): 2263-2273.

Clack JA. Patterns and processes in the early evolution of the tetrapod ear. Development and Evolution of Hearing and Balance. 2002; 53(2): 251-264.

Clack JA. Devonian climate change, breathing, and the origin of the tetrapod stem group. Integr Comp Biol. 2007; 47(4): 510-523.

Clack JA. The Fish-Tetrapod Transition: New Fossils and Interpretations. Evolution: Education and Outreach. 2009; 2(2): 213–223.

Clark AJ, Iwobi M, Cui W, Crompton M, Harold G, Hobbs S, Kamalati T, Knox R, Neil C, Yull F, Gusterson B. Selective cell ablation in transgenic mice expressing E. Coli nitroreductase. Gene Therapy. 1997; 4: 101-110.

Coates MI, Clack JA. Polydactyly in the earliest known tetrapod limbs. Nature 1990;347:66–9.

Coates MI, Clack JA. Fish-like gills and breathing in the earliest known tetrapod. Nature 1991; 352: 234–6.

Coates MI. The origin of vertebrate limbs. Dev Suppl. 1994; 169-180.

Coates MI. The evolution of paired fins. Theory in Biosciences. 2003; 122(2-3); 266-287.

Coates MI, Cohn MJ. Fins, limbs and tails: outgrowths and axial patterning in vertebrate evolution. Bioessays. 1998; 20(5): 371-381.

Coates MI, Jeffery JE, Rut M. Fins to limbs: what the fossils say. Evol. Dev. 2002; 4: 390–401.

Cohn M, Izpisua-Belmonte, Abud H, Heath J, Tickle C. Fibroblast growth factors induce additional limb development from the flank of chick embryos. Cell. 1995; 24: 98-213.

Cole NJ, Currie P. Shaping muscle bioarchitecture for the fin to limb transition. Bioarchitecture. 2012; 2(3): 98-103.

Cong L. et al. Multiplex genome engineering using CRISPR/Cas systems. Science. 2013; 339: 819–823

Curado S, Anderson RM, Jungblut B, Mumm J, Schroeter E, Stainier DY. Conditional targeted cell ablation in zebrafish: a new tool for regeneration studies. Dev Dyn. 2007; 236(4): 1025-1035.

Daeschler EB, Shubin NH, and Jenkins FA. A devonian tetrapod-like fish and the evolution of the tetrapod body plan. Nature. 2006; 440(7085): 757–763.

Davis MC, Dahn RD, Shubin NH. An autopodial-like pattern of Hox expression in the fins of a basal actinopterygian fish. Nature. 2007; 447: 473–476.

Davis MC. The deep homology of the autopod: Insights from Hox Gene regulation. Integrative & Comparative Biology. 2013; 52(2): 224-232.

Davis AP, Witte DP, Hsieh-Li HM, Potter SS, Capecchi MR. Absence of radius and ulna in mice lacking hoax-11 and hoxd-11. Nature. 1995; 375: 791-795.

Dealy CN, Seghatoleslami MR, Ferrari D, Kosher RA. FGF-stimulated outgrowth and proliferation of limb mesoderm is dependent on syndecan-3. Developmental Biology. 1997; 184: 343-350.

Dehal P, Boore JL. Two Rounds of Whole Genome duplication in the ancestral vertebrate. PLOS biology. 2005; 3(10): e314.

De Smet R, Sabaghian E, Li Z, Saeys Y, Van de Peer Y. Coordinated Functional divergence of genes after genome duplication in Arabidopsis thaliana. Plant Cell. 2017; 29(11): 2786-2800.

Dewit J, Witten PE, Huysseune A. The Mechanism of Cartilage Subdivision in the Reorganization of the Zebrafish Pectoral fin Endoskeleton. J. Exp. Zoo. 2011; 316(8): 584-597.

Diogo R, Johnston P, Molnar JL, Esteve-Altava, B. Characteristic tetrapod musculoskeletal limb phenotype emerged more than 400 mya in basal lobe-finned fishes. Scientific reports. 2016; 6: 37592.

Doosey MH, Domke ND. Early Development of the Caudal Fin Skeleton of Capelin, Mallotus villosus (Osmeridae). Copeia. 2014; 2014(2): 355-365.

Doudna JA, Charpentier E. The new frontier of genome engineering with CRISPR-cas9. Science. 2014; 346(6213).

Duboule D. Temporal colinearity and the phylotypic progression: a basis for the stability of a vertebrate Bauplan and the evolution of morphologies through heterochrony. Development. 1994; 135-142.

Duran I, Marí-Beffa M, Santamaria JA, Becerra J, and Santos-Ruiz L. Actinotrichia collagens and their role in fin formation. Developmental Biology. 2011; 354(1): 160–172.

Ellies DL, Stock DW, Hatch G, Giroux G, Weiss KM, Ekker M. Relationship between the genomic organization and the overlapping embryonic expression patterns of the zebrafish dlx genes. Genomics. 1997; 45 (3):580–590.

Faro A, Boj SF, Ambrósio R, van den Broek O, Korving J, Clevers H. T-Cell 4 (tcf7l2) is the main effector of Wnt signalling during zebrafish intestine organogenesis. Zebrafish. 2009; 6 (1):59–68.

Feledy JA, Morasso MI, Jang SI, Sargent TD. Transcriptional activation by the homeodomain protein distal-less 3. Nucleic Acids Res. 1999; 27 (3):764–770.

Fernandez-Teran M, Piedra ME, Kathiriya IS, Srivastava D, Rodriguez-Rey JC, Ros MA. Role of dHAND in the anterior–posterior polarization of the limb bud: Implications for the Sonic hedgehog pathway. Development. 2000; 127:2133–2142.

Freitas R, Zhang G. Biphasic Hoxd gene expression in shark paired fins reveals an ancient origin of the distal limb domain. PLoS One. 2007; 2(1): e754.

Freitas R, Gomez-Marin C, Wilson JM, Casares F, Gomez-Skarmeta JL. Hoxd13 Contributions to the Evolution of Vertebrate Appendages. Developmental Cell. 2012; 23:1219–1229.

Fromental-Ramain C, et al. Hoxa-13 and Hoxd-13 play a crucial role in the patterning of the limb autopod. Development. 1996; 122: 2997–3011.

Gaj T, Gersbach CA, Barbas CF 3rd. ZFN, TALEN and CRISPR/CAS-based methods for genome engineering. Trends Biotechnol. 2013; 31(7): 397-405.

Galli A, Robay D, Osterwalder M, Bao X, Bénazet J-D, Tariq M, Paro R, Mackern S, Zeller R. Distinct rols of Hand2 in initiating polarity and posterior Shh Expression during the onset of mouse limb bud development. PLOS genetics. 2010; 6(4): e1000901.

Gehrke AR, Schneider I, de la Calle-Mustienes E, Tena JJ, Gomez-Marin C, Chandran M, et al. Deep conservation of wrist and digit enhancers in fish. Proceedings of the National Academy of Sciences of the United States of America. 2015; 112(3):803–808.

Gehrke AR, Shubin NH. Cis-regulator programs in the development and evolution of vertebrate paired appendages. Semin Cell Dev Biol. 2016; 57:31-39.

George D, and Blieck A. Rise of the earliest tetrapods: An early devonian origin from marine environment. PLoS One. 2011; 6(7).

Géraudie J. Initiation of actinotrichial development in early fin bud of fish, salmo. Journal of Morphology. 1977; 151(3):353–361.

Geraudie J, Meunier FJ. Elastoidin actinotrichia in coelacanth fins: A comparison with teleosts. Tissue and Cell. 1980; 12(4): 637-645.

Geraudie J, Meunier FJ. Structure and comparative morphology of camptotrichia of lungfish fins. Tissue and Cell. 1984; 16(2): 217-236

Géraudie J. Comparative Fine Structure of the Actinotrichia (Elastoidin) in Developing Teleost and Dipnoi Fish Fins. Biology of Invertebrate and Lower Vertebrate Collagens. 1985; 93: 451-455.

Gong Z, Ju B, Wan H. Green fluorescent protein (GFP) transgenic fish and their applications. Genetica. 2001; 111(1-3): 212-225.

Gonzalez F, Duboule D and Spitz F. Transgenic analysis of *Hoxd* gene regulation during digit development. Developmental Biology. 2007; 306(2): 847-859.

Gordon KL, Ruvinsky I. Tempo and mode in evolution of transcriptional regulation. PLoS Genet. 2012; 8(1): e1002432.

Gori F, Schipani E, Demay MB. Fibromodulin is expressed by both chondrocytes and osteoblasts during fetal bone development. J Cell Biochem. 2001; 82(1): 46–57.

Grandel H, and Schulte-Merker S. The development of the paired fins in the zebrafish, danio rerio. Mechanisms of Development. 1998; 79(1–2):99–120.

Gray PA, Fu H, Luo P, Zhao Q, Yu J, Ferrari A, Tenzen T et al. Mouse Brain Organization Revealed Through Direct Genome-Scale TF Expression Analysis. Science. 2004; 306(5705): 2255-2257.

Grégoire D, Kmita M. Recombination between inverted loxP sites is cytotoxic for proliferating cells and provides a simple tool for conditional cell ablation. PNAS. 2008; 105(38): 14492-14496.

Gross, J., Dumsha, B., 1958. Elastoidin – a 2-component member of the collagen class. Biochim. Biophys. Acta 28 (2), 268–270.

Guo Q, Loomis C, Joyner AL. Fate map of mouse ventral limb ectoderm and the apical ectodermal ridge. Developmental Biology. 2003; 264(1): 166–178.

Harfe BD, Scherz PJ, Nissim S, Tian H, McMahon AP, Tabin CJ. Evidence for an expansion-based temporal SHH gradient in specifying vertebrate digit identities.

Harfe BD. Keeping up with the zone of polarizing activity: New roles for an old signaling center. Developmental Dynamics. 2011; 240(5): 915-919.

Hayashi K, Ozawa E. Myogenic cell migration from somites is induced by tissue contact with medial region of the presumptive limb mesoderm in chick embryos. Development. 1995; 121: 661–669.

Heikinheimo M, Lawshe A, Shackleford G, Wilson D, MacArthur C. Fgf-8 expression in the post-gastrulation mouse suggests roles in the development of the face, limbs and central nervous system. Mch Dev. 1994; 48: 129-138.

Henderson LJ, Narasipura SD, Adarichev V, Kashanchi F, Al-Harthi L. Identification of novel T cell factor 4.TCF-4. binding sites on the HIV long terminal repeat which associate with TCF-4, beta-catenin, and SMAR1 to repress HIV transcription. J. Virol. 2012; 86(17): 9495–9503.

Hernandez-Vega A, Minguillon C. The Prx1 limb enhancers: targeted gene expression in developing zebrafish pectoral fins. Dev. Dyn. 2011; 240(8): 1977-1988.

Heude E, Shaikho S, Ekker M. The dlx5a/dlx6a genes play essential roles in the early development of zebrafish median fin and pectoral structures. PLoS One. 2014; 9(5): e98505.

Hill P, Gotz K, Ruther U. A SHH-dependent regulation of Gli3 is a significant determinant of anteriorposterior patterning of the limb bud. Developmental Biology. 2009; 328(2): 506-516.

Hirashima T, Iwasa Y, Morishita, Y. Distance between AER and ZPA is defined by feed-forward loop and is stabilized by their feedback loop in vertebrate limb bud. Bull. Math. Biol. 2008; 70: 438–59.

Hong SK, Levin CS, Brown JL, Wan H, Sherman BT, Huang da W, Lempicki RA, Feldman B. Pre-gastrula expression of zebrafish extraembryonic genes. BMC Dev. Biol. 2010; 10: 42.

Howe K, Clark MD, Torroja CF, Torrance J, Berthelot C, Muffato M, Collins JE et al. The zebrafish reference genome sequence and its relationship to the human genome. 2013; 496(7446): 498-503.

Hsieh-Li, H. M. *et al.* Hoxa 11 structure, extensive antisense transcription, and function in male and female fertility. Development. 1995; 121: 1373–1385.

Hwang WY, Fu Y, Maeder ML, Tsai SQ, Sander JD, Peterson RT, Yeh JR, Joung JK. Efficient genome editing in zebrafish using a CRISPR-Cas system. Nat Biotechnol. 2013; 31(3): 227-229.

Ibrahim DH, Hansen P, Rödelsperger C, Stiege AC, Doelken SC, Horn D, Jägen M, Janetzki C, Krawitz P, Leschik et al. Distinct global shifts in genomic binding profiles of limb malformation-associated HOXD13 mutations. Genome Res. 2013; 23(12): 2091–2102.

Johanson Z, Joss J, Boisvert CA, Ericsson R, Sutija M, Ahlberg PE. J Exp Zool B Mol Dev Evol. 2007 Dec 15; 308(6):757-68.

Johnson RL, and Tabin CJ. Molecular models for vertebrate limb development. Cell. 1997; 90(6):979–990.

Jonk LJC, Itoh S, Heldin C, Ten Dijke P, Kruijer W. Identification and functional characterization of a smad binding element.SBE. in the JunB promoter that acts as a transforming growth factor-beta, activin, and bone morphogenetic protein-inducible enhancer. J. Biol. Chem. 1998; 273(33): 21145–21152.

Jude E, Johanson Z, Kearsley A, Friedman M. Early evolution of the lungfish pectoral-fin endoskeleton: evidence from the middle Devonian (Giventian) Pentlandia macroptera. Earth Sci. 2014; 2(18): 1-15.

Kawai S, Yamauchi M, Wakisaka S, Ooshima T, Amano A. Zinc-finger transcription factor odd-skipped related 2 is one of the regulators in osteoblast proliferation and bone formation. J. Bone Miner. Res. 2007; 22(9): 1362–1372

Kawakami K. Tol2: a versatile gene transfer vector in vertebrates. Genome Biol. 2007; 8(S1): S7.

Kessel M, Gruss P. Homeotic transformations of murine vertebrae and concomitant alteration of Hox codes induced by retinoic acid. Cell. 1991; 67(1): 89-104.

Kherdjemil Y, Kmita M. Insights on the role of hox genes in the emergence of the pentadactyl groud state. Genesis. 2017; 56: e23046.

Kherdjemil Y, Lalonde RL, Sheth R, Dumouchel A, de Martino G, Pineault KM et al. Evolution of Hoxa11 regulation in vertebrates is linked to the pentadactyl state. Nature. 2016; 539(7627): 89–92.

Kimmel CB, Ballard WW, Kimmel SR, Ullmann B, and Schilling TF. Stages of embryonic-development of the zebrafish. Developmental Dynamics. 1995; 203(3):253–310.

King HM, Shubin NH, Coates MI, Hale ME. Behavioral Evidence for the Evolution of Walking and Bounding before terrestriality in sarcopterygian fishes. PNAS. 2011; 108(52): 21146-21151.

Kmita M, Fraudeau N, Hérault Y, Duboule D. Serial deletions and duplications suggest a mechanism for the collinearity of *Hoxd* genes in limbs. Nature. 2002; 420: 145–150.

Kmita M, Kondo T, Duboule D. Targeted inversion of a polar silencer within the HoxD complex re-allocates domains of enhancer sharing. Nat. Genet. 2000; 26: 451–454.

Kmita M, Tarchini B, Zakany J, Logan M, Tabin CJ, Duboule D. Early developmental arrest of mammalian limbs lacking HoxA/HoxD gene function. Nature. 2005; 435(7045): 1113-1116.

Knopf F. Schnabel K, Haase C, Pfeifer K, Anastassiadis K, Weidinger G. Dually inducible TetON systems for tissue-specific conditional gene expression in zebrafish. Proc. Natl. Acad. Sci. 2010; 107(46): 19933-19938.

Knosp WM, Saneyoshi C, Shou S, Bachinger HP, Stadler H. Elucidation, quantitative refinement, and in vivo utilization of the HOXA13 DNA binding site. J. Biol. Chem. 2007; 282(9): 6843–6853.

Konig D, Page L, Chassot B, Jazwinska A. Dynamics of actinotrichia regeneration in the adult zebrafish fin. Dev Biol. 2018; 433(2): 416-432.

Kraus P, Fraidenraich D, Loomis CA. Some distal limb structures develop in mice lacking Sonic hedgehog signaling. Mech. Dev. 2001; 100: 45–58.

Kronenberg HM. PTHrP and skeletal development. Ann. N.Y. Acad. Sci. 2006; 1068: 1-13.

Krumlauf R. Hox genes in vertebrate development. Cell. 1994; 78(2): 191-201.

Laforest L, Brown CW, Poleo G, Ge´raudie J, Tada M, Ekker M et al. Involvement of the Sonic hedgehog, patched1 and bmp2 genes in the patterning of the zebrafish dermal fin rays. Development. 1998; 125: 4175–4184.

Lalonde RL & Akimenko MA. Effects of fin fold mesenchyme ablation on zebrafish fin development. PLoS ONE. 2018; 13(2): e0192500.

Lalonde RL, Moses D, Zhang J, Cornell N, Ekker M, Akimenko MA. Differential *actinodin1* regulation in zebrafish and mouse appendages. Developmental Biology. 2016; 417(1):91–103.

Lam P, Kamei CN, Mangos S, Mudumana S, Liu Y, Drummond IA. Oddskipped related 2 is required for fin chondrogenesis in zebrafish. Dev. Dyn. 2013; 242(11): 1284–1292.

Lamoureux F, Braud'huin M, Duplomb L, Heymann D, Re´ dini F. Proteoglycans: key partners in bone cell biology. Bioessays. 2007; 29(8):758–771.

Laufer E, Nelson CE, Johnson RL, Morgan BA, Tabin C. Sonic hedgehog and Fgf-4 act through a signaling cascade and feedback loop to integrate growth and patterning of the developing limb bud. Cell. 994; 79:993–1003.

Lee RTH, Knapik EW, Thiery JP, Carney TJ. An exclusively mesodermal origin of fin mesenchyme demonstrates that zebrafish trunk neural crest does not generate ectomesenchyme. Development. 2013; 140: 2923-2932.

Leite-Castro J, Beviano V, Rodrigues PN, Freitas R. HoxA Genes and the Fin-to-Limb Transition in Vertebrates. Journal of Developmental Biology. 2016; 4(1): 10.

Lewandoski M, Sun X, and Martin G. Fgf8 signalling from the AER is essential for normal limb development. Nature Genetics. 2000; 26(4):460–463.

Li, J., Meng, X., Zong, Y., Chen, K., Zhang, H., Liu, J., Li, J., and Gao, C. Gene replacements and insertions in rice by intron targeting using CRISPR-Cas9. Nat. Plants. 2016; 2:16139.

Li N, Felber K, Elks P, Croucher P, Roehl HH. Tracking gene expression during zebrafish osteoblast differentiation. Dev. Dyn. 2009; 238(2): 459–466.

Li X-Y, Thomas S, Sabo PJ, Eisen MB, Stamatoyannopoulos JA, Biggin MD. The role of chromatin accessibility in directing widespread, overlapping patterns of Drosophila transcription factor binding.

Lidster K, Readman GD, Prescott MJ, Owen SF. International survey on the use and welfare of zebrafish *Danio rerio* in research. Journal of Fish Biology. 2017; 90(5): 1891-1905.

Litingtung Y, Dahn RD, Fallon JF, Chiang C. Shh and Gli3 are dispensable for limb skeleton formation but regulate digit number and identity. Nature. 2002; 418(6901): 979-983.

Logan, M. *et al.* Expression of Cre recombinase in the developing mouse limb bud driven by a Prxl enhancer. Genesis. 2002; 33: 77–80.

Long JA, Young GC, Holland T, Senden TJ, Fitzgerald EMG. An exceptional Devonian fish from Australia sheds light on tetrapod origins. 2006; 444: 199-202.

Lopez-Martinez A, Chang DT, Chiang C, Porter JA, Ros MA, Simandl BK, Beachy PA, Fallon JF. Limb-patterning activity and restricted posterior localization of the amino-terminal product of Sonic hedgehog cleavage. Current Biology. 1995; 5(7): 695-820.

Lu P, Yu Y, Perdue Y, Werb Z. The apical ectodermal ridge is a timer for generating distal limb progenitors. Development. 2008; 135: 1395-1405.

Mabee PM, Noordsy M. Development of the paired fins in the paddlefish, *Polyodon spathula*. Journal of Morphology. 2004; 261(3): 334–344.

Maccabe AB, Gasseling MT, Saunders Jr. JW. Spatiotemporal distribution of mechanisms that control outgrowth and anteroposterior polarization of the limb bud in the chick embryo. Mechanisms of Ageing and Development. 1973; 2: 1-12.

Mackie EJ, Ahmed YA, Tatarczuch L, Chen K-S, Mirams M. Endochondral ossification: How cartilage is converted into bone in the developing skeleton. The Intl. Journal of Biochem & Cell Biol. 2008; 40(1): 46-62.

Mallet VO, Mitchell C, Guidotti JE, Jaffray P, Fabre M, Spencer D, Arnoult D, Kahn A, Gilgenkrantz H. Conditional cell ablation by tight control of caspase-3 dimerization in transgenic mice. Nat Biotechnol. 2002; 20:1234–1239.

Mari-Beffa M, Murciano C. Dermoskeleton morphogenesis in zebrafish fins. Dev Dyn. 2010; 239(11): 2779-2794.

Mariani F, Ahn CP, Martin GR. Genetic Evidence that FGFs have an instructive role in limb proximal-distal patterning. Nature. 2008; 453: 401–405.

Markey MJ, Marshall CR. Terrestrial-style feeding in a very early aquatic tetrapod is supported by evidence from experimental analysis of suture morphology. PNAS. 2007; 104(17):7134-7138.

Martin P. Tissue patterning in the developing mouse limb. Int J Dev Biol. 1900; 34(3): 323-336.

Martin GR. The roles of FGFs in the early development of vertebrate limbs. Genes & Dev. 1998; 12:1571–1568.

Mathias JR, Zhang Z, Saxena MT, Mumm JS. Enhanced Cell-Specific Ablation in Zebrafish Using Triple Mutant of Escherichia Coli Nitroreductase. Zebrafish. 2014; 11(2): 85–97.

Mattar, P. *et al.* Basic helix-loop-helix transcription factors cooperate to specify a cortical projection neuron identity. Mol. Cell. Biol. 2008; 28: 1456–1469.

Matys V, Kel-Margoulis OV, Fricke E, Liebich I, Land S, Barre-Dirrie A, Retuer I, Chekmenev D, Krull M, Hornischer K, Voss N, Stegmaier P, Lewicki Potapov B, Saxel H,

Kel AE, Wingender E. TRANSFAC and its module TRANSCompel: transcriptional gene regulation in eukaryotes. Nucleic Acids Res. 2006; 34 (Database issue), D108–D110.

Mercader N. Early steps of paired fin development in zebrafish compared with tetrapod limb development. Development, Growth, and Differentiation. 2007; 49(6):421–437.

Metscher, B. D., Takahashi, K., Crow, K., Amemiya, C., Nonaka, D. F. & Wagner, G. P. 2005. Expression of *Hoxa-11* and *Hoxa-13* in the pectoral fin of a basal ray-finned fish, *Polyodon spathula*: implications for the origin of tetrapod limbs. *Evol. Dev*. **7**, 186–195.

Montavon, T. *et al.* A regulatory archipelago controls Hoix genes transcription in digits. Cell. 2011; 147: 1132–1145,

Mosimann C, Kaufman CK, Li P, Pugach EK, Tamplin OJ, Zon LI. Ubiquitous transgene expression and Cre-based recombination driven by the ubiquitin promoter in zebrafish. Development. 2011; 138(1): 169-177.

Muller F, Chang B, Albert S, Fischer N, Tora L, Strahle U. Intronic enhancers control expression of zebrafish sonic hedgehog in floor plate and notochord. Development. 1999; 126(10): 2103–2116.

Murakami Y, Tanaka M. Evolution of motor innervation to vertebrate fins and limbs. Developmental Biology. 2011; 355(1): 164-172.

Murtaugh LC, Stanger BZ, Kwan KM, Melton DA. Notch signaling controls multiple steps of pancreatic differentiation. Proc. Natl Acad. Sci. USA. 2003; 100: 14920–14925.

Nagayoshi S, Hayashi E, Abe G, Osato N, Asakawa K, Urasaki A, Horikawa K, Ikeo K, Takeda H, And Kawakami K. Insertional mutegenesis by the Tol2 transposon-mediated enhancer trap approach generated mutations in two developmental genes: tcf7 and synembryn-like. Development. 2008; 135(1):159-169.

Nakamura T, Gehrke A, Lemberg J, Szymaszek J, Shubin NH. Digits and fin rays share common developmental histories. Nature. 2016; 537(7619): 225–228.

Nelson LT, Rakshit S, Sun H, Wellik DM. Generation and expression of a Hoxa11eGFP targeted allele in mice. Dev. Dyn. 2008; 237: 3410–3416.

Neto A, Mercader N, Luis Gomez-Skarmeta J. The osr1 and osr2 genes act in the pronephric anlage downstream of retinoic acid signaling and upstream of wnt2b to maintain pectoral fin development. Development. 2012; 139(2): 301–311.

Nikaido et al. Coelacanth genomes reveal signatures for evolutionary transition from water to land. Genome res. 2013; 23: 1740-1748.

Nishidate M, Nakatani Y, Kudo A, Kawakami A. Identification of novel markers expressed during fin regeneration by microarray analysis in medaka fish. Dev. Dyn. 2007; 236(9): 2685–2693.

Nishiyama A, Xin L, Sharov AA, Thomas M, Mowrer G, Meyers E, Piao Y, Mehya S, Yee S, Nakatake Y., et al. Uncovering early response of gene regulatory networks in ESCs by systematic induction of transcription factors. Cell Stem Cell. 2009; 5(4): 420-433.

Niswander L, Anderson KV. Hopeful monsters and morphogens at the beach. Nature Cell Biology. 2002; 4:E259-E262.

Niswander L. Jeffrey S, Martin GR, Tickle C. A positive feedback loop coordinates growth and patterning in the vertebrate limb. Nature. 1994; 371(6498): 609-612.

Niswander L, Tickle C, Vogel A, Booth I, Martin GR. FGF-4 replaces the apical ectodermal ridge and directs outgrowth and patterning of the limb. Cell. 1993; 75(3): 579-587.

Nulens R, Scott L, Herbin M. An updated inventory of all known specimens of coelacanth, latimeria. 2010; 3.

Nusslein-Volhard C, Dahm R. Zebrafish : A practical approach. New York: Oxford University Press. 2002:303p.

Onimaru K, Kuraku S, Takagi W, Hyodo S, Sharpe J, Tanaka M. A shift in anterior-posterior positional information underlies the fin-to-limb evolution. eLife. 2015; 4:e07048.

Ohuchi H, Nakagawa T, Yamamoto A, Araga A, Ohata T, Ishimaru Y, Yoshioka H, Kuwana T, Nohno T, Yamasaki M, Itoh N and Noji S. The mesenchymal factor, FGF10, initiates and maintains the outgrowth of the chick limb bud through interaction with FGF8, an apical ectodermal factor. Development. 1997; 124*:* 2235 -*2244.*

Ortega N, Behonick DJ, Werb Z. Matrix remodeling during endochondral ossification. Trends Cell Biol. 2004; 14(2): 86-93.

Paco A, Freitas R. Hox D genes and the fin-to-limb transition: Insights from fish studies. Genesis. 2017; 56(1): e23069.

Padhi BK, Joly L, Tellis P, Smith A, Nanjappa P, Chevrette M, Ekker M, Akimenko M-A. Screen for genes differentially expressed during regeneration of the zebrafish caudal fin. Dev. Dyn. 2004; 231 (3):527–541.

Patton JT, Kaufman MH. The timing of ossification of the limb bones, and growth rates of various long bones of the fore and hind limbs of the prenatal and early postnatal laboratory mouse. J. Anat. 1995; 186(Pt 1): 175-185.

Pieretti J, Gehrke AR, Schneider I, Adachi N, Nakamura T and Shubin NH. Organogenesis in deep time: A problem in genomics, development, and paleontology. PNAS. 2015; 112(16): 4871-4876.

Potter SS, Branford WW. Evolutionary conservation and tissue-specific processing of Hoxa 11 antisense transcripts. Mamm. Genome. 1998; 9: 799–806.

Prud'homme B, Gompel N, Carroll SB. Emerging principles of regulatory evolution. PNAS. 2007; 104 (suppl 1): 8605-8612.

Prykhozhij SV, Neumann CJ. Distinct roles of Shh and Fgf signaling in regulating cell proliferation during zebrafish pectoral fin development. 2008; 9: 91.

Rai K, Sarkar S, Broadbent TJ, Voas M, Grossman KF, Nadauld LD, Dehghanizadeh S, Hagos FT, Li Y, Toth RK, Chidester S, Bahr TM, Johnson WE, Sklow B, Burt R, Cairns BR, Jones DA. DNA demethylase activity maintains intestinal cells in an undifferentiated state following loss of APC. Cell. 2010; 142 (6): 930–942.

Rath D, Amlinger L, Rath A, Lundgran M. The CRISPR-cas immune system: Biology, mechanisms and applications. Biochimi. 2015; 117: 119-128.

Riddle RD, Johnson RL, Laufer E, Tabin C. Sonic hedgehog mediates the polarizing activity of the ZPA. Cell. 1993; 75(7): 1401-1416.

Robert B, Lallemand Y. Anteroposterior patterning in the limb and digit specification: Contribution to mouse genetics. Dev. Dyn. 2006; 235: 2337-2352.

Roberts JA, Miguel-Escalada I, Slovik KJ, Walsh KT, Hadzhiev Y, Sanges R, Stupka E, Marsh EK, Balciuniene J, Balciunas D, Muller F. Targeted transgene integration overcomes variability of position effects in zebrafish. Development. 2014; 141(3): 715-724.

Robledo RF, Rajan L, Li X, Lufkin T. The Dlx5 and Dlx6 homeobox genes are essential for craniofacial, axial, and appendicular skeletal development. Genes Dev. 2002; 16(9): 1089–1101.

Romer AS. Tetrapod limbs and early tetrapod life. Evolution. 1958; 12(3): 365-369.

Ruta M, Wagner PJ, Coates MI. Evolutionary patterns in early tetrapods. I. Rapid initial diversification by decrease in rates of character change. Proc Biol Sci. 2006; 273(1598): 2107-2111.

Sagai T, Hosoya M, Mizushina Y, Tamura M, Shiroishi T. Elimination of long-range cis-regulatory module causes complete loss of limb-specific Shh expression and truncation of the mouse limb. Development. 2005; 132(4): 797-803.

Sakamoto K, Onimaru K, Munakata K, Suda N, Tamura M, Ochi H, Tanaka M. Heterochonic shift in Hox-mediated activation of Sonic hedgehog leads to morphological changes during fin development. PLoS ONE. 2009; 4(4): e5121.

Sallan L. Fish `tails` result from outgrowth and reduction of two separate ancestral tails. Curr Biol. 2016; 26(23):R1224-R1225.

Salsi V, Vigano MA, Cocchiarella F, Mantovani R, Zappavigna V. Hoxd13 binds in vivo and regulates the expression of genes acting in key pathways for early limb and skeletal patterning. Dev. Biol. 2008; 317(2): 497-507.

Sambrook J, Russell DW. Molecular Cloning: A Laboratory Manual (3rd edition). Cold Spring Harbour laboratory Press. 2001.

Sander JD, Joung JK. CRISPR-Cas system for editing, regulating, targeting genomes. Nat Biotechnol. 2014; 32(4): 347-355.

Santamaria JA, Santos Ruiz L, Becerra. An Antiserum against ceratotrichia (selachia) recognizes actinotrichia in teleost regenerating fins. Int. J. Dev. Biol. 1996; 40: S175-S176.

Sastry LVS, Ramachan Lk. Protein components of elastoidin. Biochim. Biophys. Acta. 1965; 97(2): 281.

Saunders JW Jr. The proximo-distal sequence of origin of the parts of the chick wing and the role of the ectoderm. J. Exp. Zoology. 1948; 108(3): 363-403.

Saunders Jr. JW. Developmental control of three-dimensional polarity in the avian limb. Annals of the New York Academy of Sciences. 1972; 193(1): 29-42.

Scherz PJ, McGlinn E, Nissim S, Tabin CJ. Extended exposure exposure to Sonic hedgehog is required for patterning the posterior digits of the vertebrate limb. Dev Biol. 2007; 308(2): 343-354.

Schneider I, Shubin NH. The origin of the tetrapod limb: from expeditions to enhancers. Trends Genetics. 2013; 7:419–416.

Scotti M, Kherdjemil Y, Roux , Kmita M. A *Hoxa13*:Cre Mouse strain for Conditional Gene Manipulation in Developing Limb, Hindgut, and Urogenital System. Genesis. 2015; 53(6): 366–376.

Scotti M & Kmita M. Recruitment of 5′ *Hoxa* genes in the allantois is essential for proper extra-embryonic function in placental mammals. Development. 2012; 139(4): 731–739.

Shen W-F, Rozenfeld S, Lawrence JH, Largman C. The Abd-B-like Hox homeodomain proteins can be subdivided by the ability to form complexes with Pbx1a on a novel DNA target. J. Biol. Chem. 1996l 272(13): 8198–8206.

Sheth, R., Bastida, M. F., Kmita, M. & Ros, M. "Self-regulation," a new facet of *Hox* genes' function. Dev. Dyn. 2014; 243(1): 182–191.

Sheth R, Barozzi I, Langlais D, Osterwalder M, Nemec S, Hanqian L, Carlson H et al. Distal limb patterning requires modulation of cis-regulatory activities by HOX13. Cell Reports. 2016; 17(11): 2913-2926.

Sheth R, Grégoire D, Dumouchel A, Scotti M, Pham JM, Nemec S et al. Decoupling the function of Hox and Shh in developing limb reveals multiple inputs of Hox genes on limb growth. Development. 2013; 140(10): 2130–2138.

Sheth R, Marcon L, Bastida MF, Junco M, Qintana L, Dahn R, Kmita M, Sharpe J, Ros MA. Hox genes regulate digit patterning by controlling the wavelength of a Turing-Type mechanism. Science. 2012; 338(6113): 1476-1480.

Shubin NH and Alberch P. A Morphogenetic Approach to the Origin and Basic Organization of the Tetrapod Limb. Evolutionary Biology. 1986; 20(1):319-387.

Shubin NH, Daeschler EB, Coates MI. The early evolution of the tetrapod humerus. Science. 2004; 304: 90-93.

Shubin NH, Daeschler EB, Jenkins JA Jr. The pectoral fin of Tiktaalik roseae and the origin of the tetrapod limb. Nature. 2006; 440(7085): 764-771.

Shubin NH, Daeschler EB, Jenkins JA Jr. Pelvic girdle and fin of Tiktaalik roseae. PNAS. 2014; 111(3): 893-899.

Shubin NH, Tabin C, and Carroll S. Fossils, genes and the evolution of animal limbs. Nature. London. 1997; 388(6643):639–648.

Shubin N, Tabin C & Carroll S. Deep homology and the origins of evolutionary novelty. Nature. 2009; 457(7231): 818–823.

Singh PP, Arora J, Isambert H. Identification of ohnolog originating from whole genome duplication in early vertebrates based on synteny comparison across multiple genomes.

Small KM & Potter SS. Homeotic transformations and limb defects in *Hox A11* mutant mice. Genes Dev. 1993; 7(12A): 2318–2328.

Smith M, Hickman A, Amanze D, Lumsden A, Thorogood P. Trunk neural crest origin of caudal fin mesenchyme in the zebrafish Brachydanio rerio. Proc. R. Soc. 1994; 256(1346):137–145.

Smith A. et al. Gene expression analysis on sections of zebrafish regenerating fins reveals limitations in the whole-mount in situ hybridization method. Developmental Dynamics. 2008; 237: 417–425.

Sontheimer EJ, Barrangou R. The bacterial origin of CRISPR genome-editing revolution. Human Gene Therapy. 2015; 26(7).

Sordino P, van der Hoeven F and Duboule D. *Hox* gene expression in teleost fins and the origin of vertebrate digits. Nature. 1995; 375:678-681.

Sordino P, Duboule D & Kondo T. Zebrafish *Hoxa* and *Evx-2* genes: cloning, developmental expression and implications for the functional evolution of posterior *Hox* genes. Mech. Dev. 1996; 59(2): 165–175.

Soriano P. Generalized *lacZ* expression with the ROSA26 Cre reporter strain. Nat. Genet. 1999; 21(1): 70–71.

Spitz F, Gonzalez F, Duboule D. A global control region defines a chromosomal regulatory landscape containing the HoxD cluster. Cell. 2003; 113(3): 405-417.

Standen EM, Du TY, Larsson HCE. Developmental plasticity and the origin of tetrapods. Nature. 2014; 513: 54-58.

Sumiyama K, Ruddle FH. Regulation of Dlx3 gene expression in visceral arches by evolutionarily conserved enhancer elements. Proc. Natl. Acad. Sci. USA. 2003; 100(7): 4030–4034.

Summerbell D, Lewis JH, Wolpert L. Positional information in chick limb morphogenesis. Nature. 1973; 244: 492–96.

Summerbell D. A quantitative analysis of the effect of excision of the AER from the chick limb-bud. J. Embryol. Exp. Morphol. 1974; 32(3): 651-660.

Sun X, Mariani FV, Martin GR. Functions of FGF signalling from the apical ectodermal ridge in limb development. Nature. 2002; 418(6897):501–508.

Su N, Jin M, Chen L. Fole of FGF/FGFR signalling in skeletal development and homeostasis: learning from mouse models. Bone Research. 2014; 2: e14003.

Suzuki T. How is digit identity determined during limb development?. Development, Growth, and Differentiation. 2013; 55(1): 130-138.

Takamatsu N. *et al.* Duplicated *Abd-B*class genes in medaka *hoxAa* and *hoxAb* clusters exhibit differential expression patterns in pectoral fin buds. Dev. Genes Evol. 2007; 217(4): 263–273.

Tamura K, Yonei-Tamura S, Yano T, Yokoyama H, Ide H. The autopod: Its formation during limb development. Development, Growth & Differentiation. 2008; 50(S1):S177-S187.

Tanaka EM, Gann AAF. Limb Development: The budding role of FGF. Current Biology. 1995; 5(6): 594-597.

Tanaka M. Fins into limbs: Autopod acquisition and anterior elements reduction by modifying gene networks involved 5`Hox, Gli3, and Shh. Dev Biol. 2016; 413(1): 1-7.

Tarchini B & Duboule D. Control of *HoxD* Genes' Collinearity during Early Limb Development. Dev Cell. 2006; 10(1): 93-103.

Taylor JS, Braasch I, Frickey T, Meyer A, Van de Peer Y. Genome duplication, a trait shared by 22,000 species of ray-finned fish. Genome Res. 2003; 13(3): 382-390.

Teh C, Chudakoc DM, Poon K-L, Mamedov IZ, Sek J-Y, Shidlovsky K, Lukyanov S, Korzh V. Optogenetic *in vivo* cell manipulation in KillerRed-expressing zebrafish transgenics. BMC Developmental Biology. 2010; 10:110.

te Welscher P, Fernandez-Teran M, Ros MA, Zelle R. Mutual genetic antagonism involving GLI3 and dHAND prepatterns the vertebrate limb bud mesenchyme prior to SHH signaling. Genes Dev. 2002; 16(4): 421-426.

Thisse C. & Thisse B. High-resolution in situ hybridization to whole-mount zebrafish embryos. Nature Protocols. 2008; 3: 59–69.

Thorogood P. The Development of the Teleost Fin and Implications for our Understanding of Tetrapod Limb Evolution. Developmental Patterning of the Vertebrate Limb. Hinchliffe, Hurle Summerbell Eds. 1991; 347–354.

Tickle C, Eichele G. Vertebrate Limb Development. Annu. Rev. Cell Biol. 1994; 10: 121-152.

Tickle C. Patterning systems – from one end of the limb to the other. Dev. Cell. 2003; 4(4): 449–458.

True JR, Haag ES. Developmental system drift and flexibility in evolutionary trajectories. Evol Dev. 2001; 3(2): 109-119.

Tulenko FJ, Augustus GJ, Massey JL, Sim SE, Mazan S, Davis MC. HoxD expression in the fin-fold compartment of the basal gnathostomes and implications for paired appendage evolution. Scientific Reports. 2016; 6: 22720.

Tulenko FJ, Massey JL, Holmquist E, Kiqundu G, Thomas S, Smith SME et al. Fin-fold development in paddlefish and catshark and implications for the evolution of the autopod. Proceedings of the Royal Society: Biol Sci. 2017; 284(1855).

Ulitsky I, Shkumatava A, Jan CH, Sive H & Bartel DP. Conserved function of lincRNAs in vertebrate embryonic development despite rapid sequence evolution. Cell. 2011; 147(7): 1537-1550.

van den Boogaart JGM, Muller M, Osse JWM. Structure and function of the median finfold in larval teleosts. J. Exp. Biol. 2012; 215(14): 2359–2368.

Venkatesh B, Lee AP, Vydianathan R, Maurya AK, Lian MM, Swann JB, Ohta Y et al. Elephant shark genome provides unique insights into gnathstome evolution. Nature. 2014; 505: 174-179.

Vorobyeva EI, Schultze HP. Description and Systematics of panderichthyid fishes with comments on their relationship to tetrapods. In: Schultze H-P, Trueb L, editors. Origins of the higher groups of tetrapods. Ithaca: Comstock; 1991. p. 68–109.

Wagner GP & Chiu CH. The tetrapod limb: a hypothesis on its origin. J. Exp. Zool. 2001; 291(3): 226–240.

Walker MB, Kimmel CB. A two-colour acid-free cartilage and bone stain for zebrafish larvae. Biotech Histochem. 2007; 82(1): 23–28.

Wakahara T, Kusu N, Yamauchi H, Kimura I, Konishl M, Miyake A, Itoh N. Fibin, a novel secreted lateral plate mesoderm signal, is essential for pectoral fin bud initiation in zebrafish. Dev. Biol. 2007; 303(2): 527–535.

Wanek N, Muneoka K, Holler-Dinsmore G, Burton R, Bryant SV. A staging system for mouse limb development. J. Exp Zoology. 1989; 249(1): 41-49.

Wang B, Fallon JF, Beachy PA. Hedgehog-regulated processing of Gli3 produces an anterior/posterior repressor gradient in the developing vertebrate limb. Cell. 2000; 100(4): 423-434.

Wang Y, Lorenzi I, Georgiev O, Schaffner W. Metal-responsive transcription factor-1.MTF-1. selects different types of metal response elements at low vs. high zinc concentration. Biol. Chem. 2004; 385(7): 623–632.

Warren IA, Ciborowski KL, Casadei E, Hazlerigg DG, Marting S, Jordan WC, Sumner S. Extensive local gene duplication and functional divergence among paralogs in Atlantic Salmon. Genome Biol Evol. 2014; 6(7): 1790-1805.

Webb AE, Sanderford J, Frank D, Talbot WS, Driever W, Kimelman D. Laminin α5 is essential for the formation of the zebrafish fins. Dev. Biol. 2007; 311(2): 369–382.

Westerfield M. The Zebrafish Book. A Guide for the Laboratory Use of Zebrafish, Danio rerio (4th Edition).University of Oregon Press, Eugene. 2000.

Wiley EO, Fuiten AM, Doosey MH, Lohman BK, Merkes C, Azuma M. The caudal skeleton of the zebrafish, *Danio* rerio from a phylogenetic Perspective: A polyural Interpretation of homologous structures. Copeia. 2015; 103(4): 740-750.

Wittkopp PJ, Haerum BK, Clark AG. Evolutionary changes in cis and trans gene regulation. Nature. 2004; 430(6995): 85-88.

Woltering JM, Duboule D. The origin of digits: expression patterns versus regulatory mechanisms. Dev Cell. 2010; 18(4): 526-532.

Woltering JM, Noordermeer D, Leleu M, and Duboule D. Conservation and divergence of regulatory strategies at hox loci and the origin of tetrapod digits: E1001773. PLoS Biology 2014; 12(1).

Wood A, and Thorogood P. An analysis of in-vivo cell migration during teleost fin morphogenesis. Journal of Cell Science. 1984; 66:205–222.

Wyngaarden LA, Vogeli KM, Ciruna BG, Wells M, Hadjantonakis A-K, Hopyan S. Oriented cell motility and division underlie early limb bud mophogenesis. Development. 2010; 137(15): 2551-2558.

Xu B, Wellik DM. Axial Hox9 activity establishes the posterior field in the developing forelimb. Proc Natl Acad Sci. 2011; 108(12): 4888-491.

Yano T, and Tamura K. The making of differences between fins and limbs. Journal of Anatomy. 2013; 222(1):100–113.

Yano T, Abe G, Yokoyama H, Kawakami K, and Tamura K. Mechanism of pectoral fin outgrowth in zebrafish development. Development. 2012; 139(16):2916–2925.

Yelon D, Horne SA & Stainier DY. Restricted expression of cardiac myosin genes reveals regulated aspects of heart tube assembly in zebrafish. Dev. Biol. 1999; 214(1): 23–37.

Zakany J, Duboule D. The role of Hox genes during vertebrate limb development. Curr Opin Genet Dev. 2007; 17(4): 359-366.

Zakany J, Fromental-Ramain C, Warot X, Duboule D. Regulation of number and size of digits by posterior *Hox* genes: A dose-dependent mechanism with potential evolutionary implications. PNAS. 1997; 94(25): 13695-13700.

Zakany J, Kmita M, Duboule D. A dual role for Hox genes in limb anterior-posterior asymmetry. Science. 2004; 304(5677): 1669–1672.

Zerucha T, Ekker M. Distal-less-related homeobox genes of vertebrates: evolution, function, and regulation. Biochem. Cell. Biol. – Biochim. Biol. Cell. 2000; 78(5):593–601.

Zeller R, Lopez-Rios J, Zuniga A. Vertebrate limb bud development : moving towards integrative analysis of organogenesis. Nat. Rv. Genet. 2009; 10: 845-858.

Zhang J, Wagh P, Guay D, Sanchez-Pulido L, Padhi BK, Korzh V et al. Loss of fish actinotrichia proteins and the fin-to-limb transition. Nature. 2010; 466(7303):234–237.